Analysis and improvement of GNSS navigation message demodulation performance in urban environments

Marion Roudier

THÈSE

En vue de l'obtention du

DOCTORAT DE L'UNIVERSITÉ DE TOULOUSE

Délivré par :

Institut National Polytechnique de Toulouse (INP Toulouse)

Discipline ou spécialité :

Signal, Image, Acoustique et Optimisation

Présentée et soutenue par :

Mme MARION ROUDIER

le vendredi 16 janvier 2015

Titre :

DEFINITION DE SIGNAUX ET DE TECHNIQUES DE TRAITEMENT INNOVANTS POUR LES FUTURS SYSTEMES GNSS

Ecole doctorale :

Mathématiques, Informatique, Télécommunications de Toulouse (MITT)

Unité de recherche :

Laboratoire de Traitement du Signal et des Télécommunications - LTST, à l'ENAC

Directeur(s) de Thèse :

M. OLIVIER JULIEN

MME MARIE LAURE BOUCHERET

Rapporteurs :

M. EMMANUEL BOUTILLON, UNIVERSITE DE BRETAGNE SUD

M. MARCO LUISE, UNIVERSITA DI PISA

Membre(s) du jury :

M. EMMANUEL BOUTILLON, UNIVERSITE DE BRETAGNE SUD, Président

M. AXEL GARCIA PENA, ECOLE NATIONALE DE L'AVIATION CIVILE, Membre

M. CHARLY POULLIAT, INP TOULOUSE, Membre

M. CHRISTOPHER HEGARTY, THE MITRE CORPORATION BEDFORD, Membre

M. MATTEO PAONNI, IPSC, Membre

Mme MARIE LAURE BOUCHERET, INP TOULOUSE, Membre

M. OLIVIER JULIEN, ECOLE NATIONALE DE L'AVIATION CIVILE, Membre

Abstract

Global Navigation Satellite Systems (GNSS) are increasingly present in our everyday life. New users are emerging with further operational needs implying a constant evolution of the current GNSS systems. A significant part of the new applications are found in environments with difficult reception conditions such as urban areas, where there are many obstacles such as buildings or trees. Therefore, in these obstructed environments, the signal emitted by the satellite is severely degraded. The signal received by the user has suffered from attenuations, as well as refractions and diffractions, making difficult the data demodulation and the user position calculation.

GNSS signals being initially designed in an open environment context, their demodulation performance is thus generally studied in the associated AWGN propagation channel model. But nowadays, GNSS signals are also used in degraded environments. It is thus essential to provide and study their demodulation performance in urban propagation channel models.

Nevertheless, GNSS modernization with new signals design such as GPS L1C or Galileo E1 OS, takes into account these new obstructed environments constraints. Since they have been designed especially for urban propagation channels [1], they are expected to have better demodulation performance compared with current GNSS signals. It is thus particularly interesting to firstly provide their demodulation performance in urban environments (not available in the literature) and secondly to compare it with the new GNSS signal designed in this PhD research context. In this way, their performance could be used as a benchmark for the future signals design.

However these modernized signals are not yet available for this moment (for example, GPS L1C is expected to be operational over the entire constellation in 2026). It is thus essential to provide and study their demodulation performance in urban environments through simulations.

It is in this context that this PhD thesis is related, the final goal being to improve GNSS signals demodulation performance in urban areas, proposing a new signal.

In order to be able to provide and study GNSS signals demodulation performance in urban environments, a simulation tool has been developed: SiGMeP for 'Simulator for GNSS Message Performance'. It allows simulating the entire emission/reception GNSS signal chain in urban environment getting away from dependence of real signals availability, controlling the simulation parameters and testing new configurations.

Existing and modernized signals demodulation performance has thus been computed with SiGMeP in urban environments. Since the classical way to compute and represent GNSS signals demodulation performance assumes an AWGN propagation channel model, and since the urban environments are really different from the AWGN channel, this classical method is not satisfactory in our urban context.

Thus, in order to represent GNSS signals demodulation performance faithfully to reality, a new methodology more adapted to the user environment is proposed. It is based on the fundamental characteristics of a GNSS system, as well as on the urban environment impact on the received signal analysis. GNSS signals demodulation performance is thus provided in urban environments thanks to this new methodology, and compared with the classic methodology used in the AWGN case.

Then, to improve GNSS signals demodulation performance in urban environments, many strategies are possible. However, the research axis of this thesis focuses on the 'Channel Coding' aspect. It is thus this field which will be privileged to improve GNSS signals demodulation performance in urban environments.

Each message, in addition to containing the useful information, carries redundant information, which is in fact the channel coding result, applying to the useful information. The message thus needs to be decoded at the reception. In order to decode the transmitted useful information, the receiver computes a detection function at the decoder input. But the detection function used in classic receivers corresponds to an AWGN propagation channel. This dissertation thus proposes an advanced detection function which is adapting to the propagation channel where the user is moving. This advanced detection function computation considerably improves demodulation performance, just in modifying the receiver part of the system.

Finally, in order to design a new signal with better demodulation performance in urban environments than one of existing and future signals, a new LDPC channel code profile has been proposed, optimized for a CSK modulation in an AWGN channel for iterative decoding. Indeed, the CSK modulation is a promising modulation in the spread spectrum signals world, which permits to free from limitations in terms of data rate implied by current GNSS signals modulations. Moreover, LDPC codes belong to the modern codes family, the first being able to approach the channel capacity. They thus represent promising achievable performance.

Résumé

Les systèmes de navigation par satellites sont de plus en plus présents dans notre vie quotidienne. De nouveaux utilisateurs émergent, avec des besoins différents, ce qui implique une évolution constante des systèmes de navigation par satellites actuels. La majorité de ces nouveaux besoins concernent des applications en environnement urbain. Dans ce type d'environnement très obstrué, le signal reçu par l'utilisateur a subit des atténuations ainsi que des réfractions/diffractions, ce qui rend difficile la démodulation des données et le calcul de position de l'utilisateur.

Les signaux de navigation par satellites étant initialement conçus dans un contexte d'environnement dégagé, leurs performances de démodulation sont donc généralement étudiées dans le modèle de canal de propagation AWGN associé. Or aujourd'hui ils sont utilisés aussi en environnements dégradés. Il est donc indispensable de fournir et d'étudier leurs performances de démodulation dans des modèles de canal de propagation urbain.

C'est dans ce contexte que s'inscrit cette thèse, le but final étant d'améliorer les performances de démodulation des signaux GNSS en milieux urbains, en proposant un nouveau signal.

Afin de pouvoir fournir et analyser les performances de démodulation des signaux de navigation par satellite en milieux urbains, un outil de simulation a été développé dans le cadre de cette thèse : SiGMeP pour « Simulator for GNSS Message Performance ». Il permet de simuler la chaine entière d'émission/réception d'un signal de navigation par satellites et de calculer ses performances de démodulation en milieu urbain.

Les performances de démodulation des signaux existants et modernisés ont donc été calculées avec SiGMeP en environnement urbain. Afin de représenter au mieux ces performances pour qu'elles soient le plus réalistes possibles, une nouvelle méthode est proposée dans ce manuscrit. Elle se base sur les caractéristiques fondamentales d'un système de navigation par satellites, ainsi que sur l'analyse de l'impact d'un environnement urbain sur le signal reçu. Les performances de démodulation des signaux en environnement urbains sont donc fournies à travers cette nouvelle méthodologie, et comparer à la méthodologie classique utilisée dans le cas AWGN.

Ensuite, pour améliorer ces performances de démodulation des signaux de navigation par satellites, plusieurs stratégies sont envisageables. Cependant, l'axe de recherche de cette thèse est centré sur l'aspect « codage canal ». C'est donc ce domaine d'étude qui sera privilégié.

Chaque message, en plus de contenir l'information utile, transporte de l'information redondante, qui est en fait le résultat du codage canal appliqué sur l'information utile. Ainsi à la réception, le message de navigation doit être décodé, afin que le récepteur retrouve l'information utile transmise. Pour décoder l'information utile transmise, le récepteur calcule une fonction de détection à l'entrée du

décodeur. Or la fonction de détection utilisée dans les récepteurs classiques correspond à un modèle de canal AWGN. Ce manuscrit propose donc une fonction de détection avancée, qui s'adapte au canal de propagation dans lequel l'utilisateur évolue, ce qui améliore considérablement les performances de démodulation, en ne modifiant que la partie récepteur du système.

Enfin, dans le but de concevoir un nouveau signal avec de meilleures performances de démodulation en environnement urbain que celles des signaux existants ou futurs, un nouveau codage canal de type LDPC a été optimisé pour une modulation CSK. En effet, la modulation CSK est une modulation prometteuse dans le monde des signaux de type spectre étalé, qui permet de se débarrasser des limitations en termes de débit de données qu'impliquent les modulations actuelles des signaux de navigation par satellites. Ainsi, la conception d'un code LDPC optimisé pour un signal de navigation par satellite modulé en CSK a été examinée.

Acknowledgements

J'aimerais tout d'abord remercier les personnes qui m'ont permis de faire cette thèse : Christophe Macabiau qui me l'a proposée, et Damien Kubrak qui m'a convaincue de le faire (et tous les autres que j'ai interrogés sans retenue, et qui, avec leurs réponses très sincères m'ont également bien aidée dans mon choix).

Ensuite bien sûr je remercie mes encadrants : Axel Garcia-Pena, qui au quotidien m'a aidée, expliquée (parfois plusieurs fois la même chose, et sans jamais s'énerver…), soutenue et comprise, Olivier Julien, qui même très occupé a toujours su trouver du temps pour moi, pour m'orienter, me corriger, me conseiller (et pas uniquement sur le sujet de la thèse), et Charly Poulliat qui m'a accompagnée dans ce monde nouveau des « Comm Num », qui m'a énormément appris, même si l'on ne s'est pas vus très souvent finalement. Merci de ne pas m'avoir abandonnée, surtout ce weekend du 11 novembre dont je me souviendrai très longtemps ! Merci également à Marie-Laure Boucheret.

Je tiens également à remercier les financeurs de cette thèse : Thales Alenia Space et le CNES. Merci à Lionel Ries et Thomas Grelier d'avoir suivi l'avancement de mon travail. Et c'est avec grand plaisir que l'aventure continue avec le CNES !

I also gratefully acknowledge my three reviewers: Emmanuel Boutillon, Marco Luise and Christopher Hegarty for reviewing my thesis, and in addition Matteo Paonni, for attending my defense.

Je remercie aussi très chaleureusement le laboratoire SIGNAV de l'ENAC. C'est en partie grâce aux gens formidables de ce laboratoire que j'en suis là aujourd'hui. Et merci à tous mes collègues grâce à qui l'ambiance a été si bonne : Jérémy (tous les deux dans la même galère …), Anaïs (ma compère de footing, bon d'accord il n'y en a pas eu beaucoup… et surtout de potins !), Antoine (ses chemises, son humour, et son attachant décalage), Rémi (plus qu'un collègue, merci pour les vraies discussions…), Ludovic (mon co-bureau et mon co-légumes !), Kevin (qui me faisait très peur quand il travaillait comme un fou sur la rédaction de sa thèse, je m'étais dit : moi jamais ça ! Mais oui bien sûr…), Jimmy (mon frère breton, vive le beurre salé !), Enik, Alexandre, Christophe, Paul, les petits nouveaux Alizé, Giuseppe, Quentin, J-B… C'est avec un gros pincement au cœur que je vous quitte.

Et pour finir merci à ma famille. Merci à mes parents de m'avoir toujours soutenue, c'est grâce à vous si j'en suis là, tant logistiquement que moralement. Merci pour votre dévouement, pour votre confiance, et pour m'avoir toujours poussée. Merci aussi à ma petite sœur, sans qui je ne serai pas

celle que je suis. Et bien évidemment merci à Cyril. Je ne nous ai pas rendu la vie facile avec mes études, et même si physiquement on a souvent été séparés, depuis le début tu es là, et ça a énormément compté. Merci d'être toi, tu m'as rendu la vie tellement plus facile… Merci.

Table of Contents

List of Figures

List of Tables

Abbreviations

ADC Analog to Digital Converter
APP A Posteriori Probability
AWGN Additive White Gaussian Noise
BER Bit Error Rate
BICM Bit Interleaved Coded Modulation
BOC Binary Offset Carrier
BP Belief-Propagation
bps bits per second
BPSK Binary Phase-shift keying
CBOC Composite Binary Offset Carrier
CDDS Commercial Data Distribution Service
CED Clock and Ephemeris Data
CEDER Clock and Ephemeris Data Error Rate
CIR Channel Impulse Response
CN Check Node
CNAV Civil NAVigation
CRC Cyclic Redundancy Check
CSI Channel State Information
CSK Code Shift Keying
DLR German Aerospace Center
DS-SS Direct Sequence Spread Spectrum
EGNOS European Geostationary Navigation Overlay Service
ER Error Rate
EXIT EXtrinsic-Information-Transfer
FLL Frequency-locked loop
GIOVE Galileo In-Orbit Validation Element
GNSS Global Navigation Satellites System
GPS L1 C/A: GPS L1 Coarse/Acquisition
IF Intermediate Frequency

IRA Irregular Repeat Accumulate
LDPC Low-Density Parity-Check
LLR Log Likelihood Ratio
LMS Land-Mobile Satellite
LNA Low Noise Amplifier
LOS Line-Of-Sight
LSB Least Significant Bits
LSR Linear Shift Register
MAP Maximum A Posteriori
MBOC Multiplexed Binary Offset Carrier
ML Maximum Likelihood
MSB Most Significant Bits
OS Open Service
pdf Probability Density Function
PLL Phase-Locked Loop
PRN Pseudo Random Noise
REP Repetition
RF Radio Frequency
RIMS Ranging Integrity Monitoring Stations
SBAS Satellite-Based Augmentation System
SiGMeP Simulator for GNSS Message Performance
SISO Soft Input Soft Output
SNR Signal to Noise Ratio
SoL Safety of Life
SPA Sum-Product Algorithm
SPC Single Parity Check constraint
sps symbols per second
TI Integration Time
TOI Tile Of Interval
TOW Time Of Week
TTFF Time To First Fix
UTC Coordinated Universal Time
VCO Voltage-Controlled Oscillator
VN Variable Node
WAAS Wide Area Augmentation System

Chapitre 1: PhD Introduction

1.1 Background and Motivation

Global Navigation Satellite Systems (GNSS) are increasingly present in our everyday life. The interest of new users with further operational needs implies a constant evolution of the current GNSS systems. A significant part of the new applications are found in environments with difficult reception conditions such as urban or indoor areas. In these obstructed environments, the received signal is severely impacted by obstacles which generate fast variations of the received signal's phase and amplitude that are detrimental to both the ranging and demodulation capability of the receiver. One option to deal with these constraints is to consider enhancements to the current GNSS systems, where the design of an innovative signal more robust than the existing ones to distortions due to urban environments is one of the main aspects to be pursued. A research axis to make a signal more robust, which was already explored, is the design of new modulations adapted to GNSS needs that allows better ranging capabilities even in difficult environments [2][3]. However, other interesting axes remain to be fully explored such as the channel coding of the transmitted useful information: users could access the message content even when the signal reception is difficult.

GNSS signal channel coding has considerably evolved since the first emitted GNSS signal GPS L1 C/A, of which the channel coding was extremely simplistic. This channel code is an extended Hamming code (32, 26). In fact, the receiver can only detect errors but it is not able to correct them. In 2005, with the appearance of the second civilian signal GPS L2C specifically designed to meet commercial needs [1], and from the SBAS signals previously designed, a more advanced channel code was implemented. Two encoders in serial are used, the outer channel code being a cyclic code called CRC-24Q and the inner channel code being a (171, 133, R = ½) convolutional code. This code represents a major innovation concerning the GNSS signals channel coding since for the first time, it is able to detect and correct errors. In parallel, the European GNSS is being developed: Galileo. Channel codes implemented on Galileo signals are the same than for GPS L2C, but tail bits are added to transform the convolutional encoded stream into ended encoded words, which simplifies the decoding process [4]. Moreover, interleavers are introduced for the first time, using the temporal diversity to efficiently counteract the multiple bursts of errors, which often occur in urban environments [5]. Then, the design of GPS L1C marks another spectacular step towards channel coding improvement. However GPS L1C is not yet broadcast, it will be emitted by the new generation of GPS III satellites, for which the launching in expected to begin in 2016 [1]. But the future and modernized GPS L1C signal specially designed to improve mobile GPS reception in cities and other challenging environments [1], promises high performance, with its two irregular (1200,600) and (548,274) LDPC channel codes. For the first time in GNSS a modern code is used, able to provide near-optimum AWGN performance [5] (contrary to classical channel codes previously implemented).

1.2 Thesis Objectives

The objective of this PhD thesis consists thus in improving the GNSS signals demodulation performance in urban environments with the channel coding theory field being the main research aspect to follow. Moreover, the objective of this work consists in using all the conducted analysis and proposed improvements in order to design a new GNSS signal which would be able to outperform the current GNSS signals in challenging environments (from the demodulation performance point of view). Since GPS L1C is the signal obtaining the best demodulation performance, this signal will be used as a benchmark all along this work.

In order to be able to meet the objectives of this PhD thesis, it is necessary to be able to compute GNSS signals demodulation performance in urban environments. However, the use of real measurements to compute the demodulation performance cannot be considered as an option. First, GPS L1C signal is not yet available; it is thus not possible to compute its real demodulation performance. Second, since the final purpose of this work is to design a new GNSS signal with high performance, the only practical solution to test the new designed signal demodulation performance consists in conducting simulations which faithfully represent the entire communication chain. In addition, a simulator easily allows testing new algorithms and new configurations. Therefore, a software simulator able to model the entire GNSS signal emission/reception chain must be developed to finally provide the demodulation performance in urban environments. The first part of this PhD thesis thus consists in developing this simulator based on the preliminary work of A. Garcia-Pena for its PhD thesis in 2010 [4].

An important part of this simulator concerns the propagation channel modeling. The aim is to find a Land-Mobile Satellite propagation channel model which simulates an urban environment, applicable for the GNSS context and feasible in practice. A refined state-of-the-art about this needs thus to be conducted. Then, the propagation channel models should be implemented into the software simulator.

Once the simulator will be completely developed, the first work is to provide the current GNSS signals demodulation performance in urban environments because without these results, we will not be able to evaluate our work aiming to improve this performance. Few works have been done on this issue [4][6], it is thus interesting to add contributions to this literature. Since the study of GNSS signals demodulation performance in urban environments differs from the analysis in open environments, the classical methodology used to compute and represent it in AWGN propagation channel models is not adapted. It thus necessary to propose a new way of representing the GNSS signals demodulation performance, adapted to urban environments.

Then, the PhD thesis is entirely concentrated around the GNSS signals demodulation performance improvement in urban environments. The first part of this work concerns the receiver optimization. The classical detection function at the decoder input considered an AWGN channel. Since we are interested by urban environments, this classical detection function is not anymore adapted. The detection function mathematical expression thus needs to be derived considering an urban propagation channel, according to different propagation channel knowledge levels.

The second part of the GNSS signals demodulation performance improvement in urban environments is dedicated to a new signal design. For this new designed signal, an innovative and promising modulation for the GNSS field will be investigated: the CSK modulation, associated with LDPC channel coding. The LDPC channel code profile will be optimized for the CSK modulation in an

AWGN channel for an iterative decoding using the EXtrinsic Information Transfer (EXIT) charts analysis and asymptotic optimization method.

1.3 Thesis Original Contributions

The main contributions presented in this thesis are the following:

- Development of a software simulator in C language, able to realistically model the entire GNSS signal emission/reception chain in urban environments.
- Provision of the GPS L1C signal demodulation performance in an urban environment with the classical method, for a wideband propagation channel model: the DLR model.
- Development of an innovative method specially adapted to provide the GNSS signals demodulation performance in urban environments and representative to reality.
- Provision of the GPS L1C signal demodulation performance in an urban environment with the new method.
- Derivation of the detection functions at the decoder input in an urban environment for a GNSS signal, considering perfect CSI knowledge, statistical CSI knowledge and no CSI knowledge.
- Adaptation of an advanced method allowing the detection function computation adaptation to any kind of user reception environment, to a GNSS signal, without any CSI knowledge, improving the demodulation performance compared with the classical detection function use only in modifying a part of the receiver process.
- Provision of the CSK demodulator EXIT charts in an AWGN propagation channel model, according to different bits per CSK symbols.
- Optimization of a LDPC code profile for a CSK-modulated signal and iterative decoding in an AWGN propagation channel model, thanks to the EXIT charts analysis and asymptotic optimization method.

The articles published along this dissertation are listed below.

- M. Roudier, T. Grelier, L. Ries, A. Garcia-Pena, O. Julien, C. Poulliat, M.-L. Boucheret, and D. Kubrak, “GNSS Signal Demodulation Performance in Urban Environments,” in *Proceedings of the 6th European Workshop on GNSS Signals and Signal Processing*, Munich, Germany, 2013.
- M. Roudier, A. Garcia-Pena, O. Julien, T. Grelier, L. Ries, C. Poulliat, M.-L. Boucheret, and D. Kubrak, “New GNSS Signals Demodulation Performance in Urban Environments,” in *Proceedings of the 2014 International Technical Meeting of The Institute of Navigation*, San Diego, California, 2014.
- M. Roudier, C. Poulliat, M.-L. Boucheret, A. Garcia-Pena, O. Julien, T. Grelier, L. Ries, and D. Kubrak, “Optimizing GNSS Navigation Data Message Decoding in Urban Environment,” in *Proceedings of the 2014 IEEE/ION Position Location and Navigation Symposium of The Institute of Navigation*, Monterey, California, 2014.

- M. Roudier, A. Garcia-Pena, O. Julien, T. Grelier, L. Ries, C. Poulliat, M.-L. Boucheret, and D. Kubrak, "Demodulation Performance Assessment of New GNSS Signals in Urban Environments," in *Proceedings of the 2014 ION GNSS+ of The Institute of Navigation*, Tampa, Florida, 2014.

1.4 Thesis Outline

This PhD dissertation is organized as follows.

Chapter 1 contains the motivation, objective and original contributions of the thesis and a brief description of the PhD thesis dissertation.

Chapter 2 provides the state-of-the-art review. The chapter begins by describing the current GNSS signals through their time evolution, paying special attention to their implemented channel code. Then the LDPC encoding and decoding are explained since the new GNSS signal design will be based on this type of channel code. Finally, the urban propagation channel models implemented into the simulator are detailed.

Chapter 3 describes the software simulator which has been developed for this PhD thesis, justifies the mathematical models implemented by the simulator and analyses the impact of the simulator parameters on the simulation time with respect to the simulated demodulation performance.

Chapter 4 provides the GPS L1C signal demodulation performance in urban environment. The classical way of representing GNSS signals demodulation performance considers an AWGN propagation channel model. Since urban propagation channel models are really different from the AWGN model, it is necessary to adapt the way of representing the performance to the propagation channel. In this sense, an innovative method is proposed, using the GNSS specificities in urban environments in order to provide demodulation performance results representative of reality. This new method has been applied to GPS L1C.

Chapter 5 addresses the improvement of GNSS signals demodulation performance in urban environments by only optimizing the receiver data processing block, and more specifically, the detection function. Indeed, the classical detection function at the GNSS receiver decoder input has been derived considering an AWGN channel. Since we are interested by urban environments, the detection function mathematical expression needs to be derived considering an urban channel. Thus, the detection function is derived for a GNSS signal in an urban propagation channel according to different levels of the propagation channel knowledge referred as Channel State Information (CSI): perfect CSI, statistical CSI and no CSI. These detection functions mathematical expressions have then be tested with the simulator and compared with the classical detection function results.

Chapter 6 establishes the first steps in the design of a high-demodulation performance GNSS signal in urban environments. A LDPC code profile is optimized for a CSK-modulated signal in an AWGN propagation channel for iterative decoding, with the aim of then testing it in urban environments. The optimization process has been conducted using the EXtrinsic Information Transfer (EXIT) charts analysis and asymptotic optimization method.

Finally, **Chapter 7** summarizes the PhD thesis work and proposes suggestions for future works.

Chapitre 2: PhD Thesis Work Contextualization

The challenge of this PhD thesis consists in analysing and improving the GNSS signals performance in the particular propagation channel involved by urban environments. This chapter thus establishes a preliminary basis to understand the research axis followed during this PhD thesis. It presents and describes the main aspects which will be then used, starting with the GNSS signals evolution history, then with the description of the most high-performance channel code which protects the GNSS navigation message against potential errors due to the urban channel: the LDPC coding, and finishing with the presentation of both urban propagation channel models chosen to be used to simulate a GNSS user urban environment.

The main research axis of this PhD thesis being the Channel Coding domain, this contextualization chapter begins with the GNSS signals description mainly through the channel coding temporal evolution. The main mass-market GNSS signals being GPS L1 C/A, GPS L2C, Galileo E1 OS and GPS L1C, they will be described in section 2.1, together with SBAS signals. This section will help understand the PhD thesis challenges.

In this first section, it will be seen that the most highly developed and the latest designed channel code implemented in GNSS signals is the LDPC code of GPS L1C. LDPC coding has thus been particularly investigated during this thesis. Section 2.2 thus presents the LDPC encoding as well as the LDPC decoding processes.

In order to be able to compute and analyse the GNSS signals demodulation performance in an urban propagation channel even before these signals are broadcast, a simulator has been developed. The propagation channel modeling is the key element of the simulator. It has to be correctly modeled in order to obtain a faithful representation of the environment impact on the received signal. This is the purpose of section 2.3 which presents two urban propagation channel models usable for GNSS signals.

2.1 GNSS Signals Description and Evolution

In this section, GNSS signals for mass-market applications of two major GNSS will be covered: GPS signals from the United States, and Galileo signals from the European Union. The signals description is made through a temporal evolution beginning by GPS L1 C/A which is the first ever GNSS signal, emitted since 1978.

From 1995, since some GPS applications required higher accuracy and integrity than brought by the GPS L1 C/A signal (such as civil aviation), a new augmentation system has been developed by the USA to increase the GPS capacity. This augmentation system is based on ground stations which compute some errors corrections and geostationary satellites which send the corrections to GNSS users based on the same signal modulation as GPS satellites. This new system is referred to as

Satellite-Based Augmentation System (SBAS). The United States system WAAS (Wide Area Augmentation System) became operational in 2003 [1], and the European system EGNOS (European Geostationary Navigation Overlay Service) in 2009 [7]. It is interesting to describe the SBAS signals in this section, as the protection of the SBAS message was clearly enhanced compared to the protection of the GPS L1 C/A message. The EGNOS signal will thus be described (but the WAAS system operates in the same way).

Then, in 1999, a GPS signals modernization program was set up [8], providing two additional civil GPS signals: GPS L2C firstly launched in 2005 and GPS L5 in 2010 [1]. Since GPS L5 is dedicated to safety-of-life use applications which are not specifically targeted in this PhD thesis; and since GPS L2C and GPS L5 present many similitudes regarding message coding, only GPS L2C will be described in this section.

Finally, in 1998, the European Union decided to design and develop its own GNSS: Galileo [8]. In order to test the system, two satellites have been preliminary launched: GIOVE A and GIOVE B, for Galileo In-Orbit Validation Element. On 7 May 2008, the first Galileo signal was emitted [7]. Several Galileo signals exist: E1 Open Service (OS) is the equivalent of the existing GPS L1C or GPS L2C civil signals (although with clear differences) in the sense that it will be widely used by mass-market applications, Galileo E5a and E5b are more related to GPS L5 signal, and Galileo E6 Commercial Service (CS) was designed for commercial applications implying paid access. The Galileo E1 OS signal will thus be described in this section.

Finally, a new generation of civil GPS signals is under development, referred to as GPS L1C. It is the last designed GNSS signal, which is expected to be launched in 2016 with GPS III. This section thus ends with the GPS L1C signal description.

2.1.1 GPS L1 C/A

GPS L1 Coarse/Acquisition (C/A) is the first emitted GNSS signal. However it is the only GPS civil signal broadcast by the full GPS constellation still will continue to be broadcast in future. Nevertheless, its channel code capacity is very limited.

2.1.1.1 Signal Structure

The GPS L1 C/A signal is composed of three components [9]:

- A carrier:

  The carrier frequency L_1 is used to transmit the signal with a BPSK modulation.

- The NAV navigation message $D(t)$:

  The message consists of a low-flow data stream with a rate of 50 bits per second. Each bit lasts thus 20 ms and is represented by a 1 or a -1.

- The PRN code $C_{PRN}(t)$:

  The spreading code is a Pseudo-Random Noise (PRN) sequence of 1023 chips, repeated every 1 ms, used to spread the signal spectrum. It gives a rate of 1.023 Mchips per second. Each satellite emits a different PRN code to be differentiated by the receiver.

The navigation message *D(t)* is first multiplied by the PRN code $C_{PRN}(t)$. The resulting signal is then modulated by the carrier. The process is described by the block diagram of Figure 1.

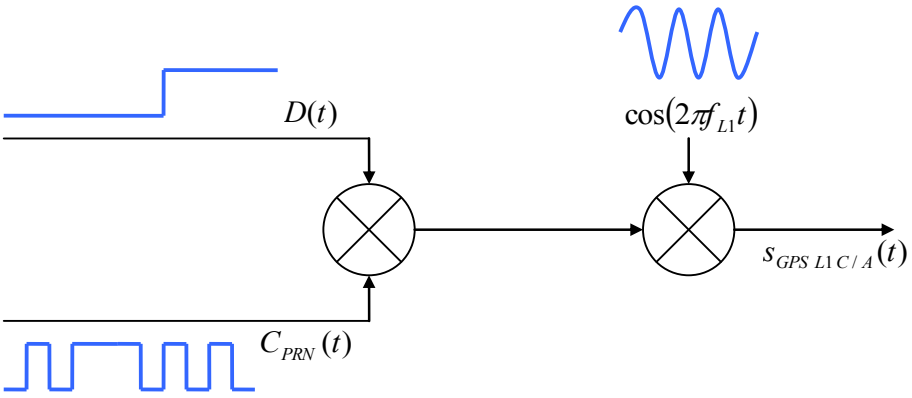

Figure 1: GPS L1 C/A signal modulation block diagram

The simplified mathematical expression of GPS L1 C/A can thus be written as equation (2.1).

$$s_{GPS\ L1\ C/A}(t) = D(t)\ C(t)\ cos\left(2\pi f_{L_1} t\right) \tag{2.1}$$

where:

- $D(t)$ is the NAV data stream,
- $C(t)$ is the PRN code,
- $f_{L_1} = 1575.42\ MHz$ is the carrier frequency.

2.1.1.2 Navigation Message Structure

The GPS L1 C/A navigation message is called NAV message. A complete message is composed of 25 frames which form one super-frame. Each frame is divided into 5 subframes. Each subframe is divided into 10 words. And one word is composed of 30 bits, as it is described in Figure 2 [9].

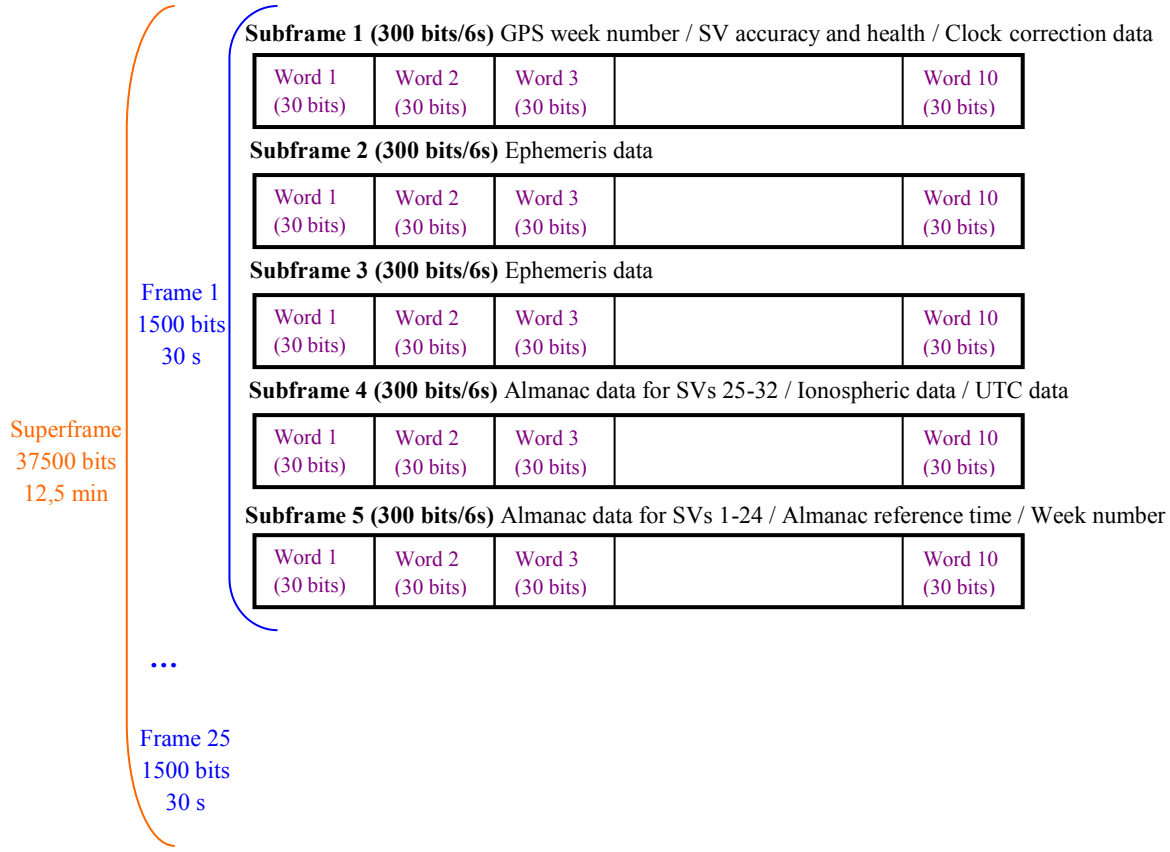

Figure 2: GPS L1 C/A navigation message general structure

Subframes 4 and 5 typically remain unchanged during one super-frame. It means its information remains the same in frames 1 to 25. Subframes 1, 2 and 3 contain the Clock error corrections and Ephemeris Data (CED), the essential demodulated data to compute the user position. These particular data remain unchanged during 2 hours.

Each word contains 24 bits dedicated to information and the remaining 6 bits are parity bits as it is described in Figure 3. The channel code is applied over each word.

Figure 3: GPS L1 C/A navigation message word structure

2.1.1.3 Channel Coding

Each word belonging to the GPS L1 C/A navigation message is encoded by an extended Hamming code (32, 26). A Hamming code is a particular linear block code, (32, 26) meaning that there are 26 data bits, encoded into 32 bits. It is known (see Figure 3) that one word is composed of 30 bits (whereas there are 32 encoded bits) of which 24 are data bits, whereas there should be 26 input bits to the Hamming encoder. The 2 missing input bits are in fact the last 2 bits of the previous code word.

They are placed at the beginning of the next code word, the first 26 bits are used as input bits, the coding process is applied and the 2 first bits are finally deleted (see Figure 4).

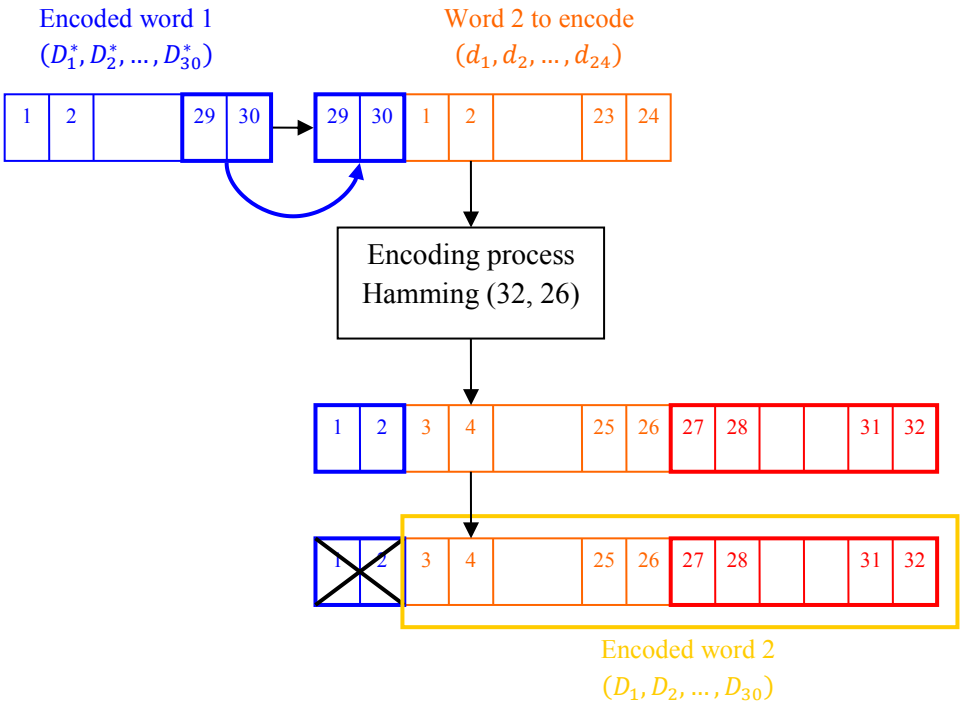

Figure 4: GPS L1 C/A channel coding description

The Hamming (32, 26) encoding is not systematic. The 26 information bits are all transformed by the Hamming process. The 30 encoded symbols are deduced from Figure 5.

Table 20-XIV. Parity Encoding Equations

$D_1 = d_1 \oplus D_{30}^*$
$D_2 = d_2 \oplus D_{30}^*$
$D_3 = d_3 \oplus D_{30}^*$
•
•
•
•
$D_{24} = d_{24} \oplus D_{30}^*$
$D_{25} = D_{29}^* \oplus d_1 \oplus d_2 \oplus d_3 \oplus d_5 \oplus d_6 \oplus d_{10} \oplus d_{11} \oplus d_{12} \oplus d_{13} \oplus d_{14} \oplus d_{17} \oplus d_{18} \oplus d_{20} \oplus d_{23}$
$D_{26} = D_{30}^* \oplus d_2 \oplus d_3 \oplus d_4 \oplus d_6 \oplus d_7 \oplus d_{11} \oplus d_{12} \oplus d_{13} \oplus d_{14} \oplus d_{15} \oplus d_{18} \oplus d_{19} \oplus d_{21} \oplus d_{24}$
$D_{27} = D_{29}^* \oplus d_1 \oplus d_3 \oplus d_4 \oplus d_5 \oplus d_7 \oplus d_8 \oplus d_{12} \oplus d_{13} \oplus d_{14} \oplus d_{15} \oplus d_{16} \oplus d_{19} \oplus d_{20} \oplus d_{22}$
$D_{28} = D_{30}^* \oplus d_2 \oplus d_4 \oplus d_5 \oplus d_6 \oplus d_8 \oplus d_9 \oplus d_{13} \oplus d_{14} \oplus d_{15} \oplus d_{16} \oplus d_{17} \oplus d_{20} \oplus d_{21} \oplus d_{23}$
$D_{29} = D_{30}^* \oplus d_1 \oplus d_3 \oplus d_5 \oplus d_6 \oplus d_7 \oplus d_9 \oplus d_{10} \oplus d_{14} \oplus d_{15} \oplus d_{16} \oplus d_{17} \oplus d_{18} \oplus d_{21} \oplus d_{22} \oplus d_{24}$
$D_{30} = D_{29}^* \oplus d_3 \oplus d_5 \oplus d_6 \oplus d_8 \oplus d_9 \oplus d_{10} \oplus d_{11} \oplus d_{13} \oplus d_{15} \oplus d_{19} \oplus d_{22} \oplus d_{23} \oplus d_{24}$

Where

$d_1, d_2, \dots, d_{24}$ are the source data bits;

the symbol $\star$ is used to identify the last 2 bits of the previous word of the subframe;

$D_{25}, D_{26}, \dots, D_{30}$ are the computed parity bits;

$D_1, D_2, \dots, D_{29}, D_{30}$ are the bits transmitted by the SV;

$\oplus$ is the "modulo-2" or "exclusive-or" operation.

Figure 5: GPS L1 C/A encoding process [9]

The decoding process could be the classical one used for a Hamming code, but a simpler algorithm is proposed by [9].

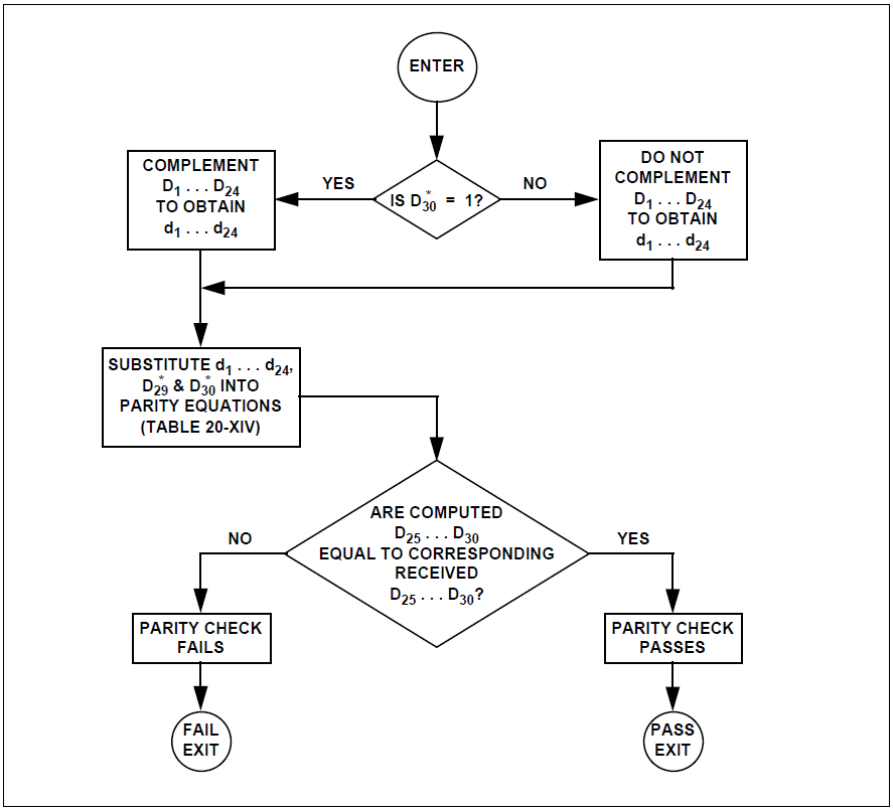

Figure 6: GPS L1 C/A decoding process proposed by [9]

2.1.1.4 Conclusion

The GPS L1 C/A signal is protected by a very minimalist channel code, approaching the demodulation performance of an uncoded BPSK modulated signal [10].

2.1.2 SBAS Signals

Several SBAS systems exist or are under development around the world such as EGNOS in Europe, WAAS in the United States, MSAS in Japan, GAGAN in India or SDCM in Russia. They are shown in Figure 7.

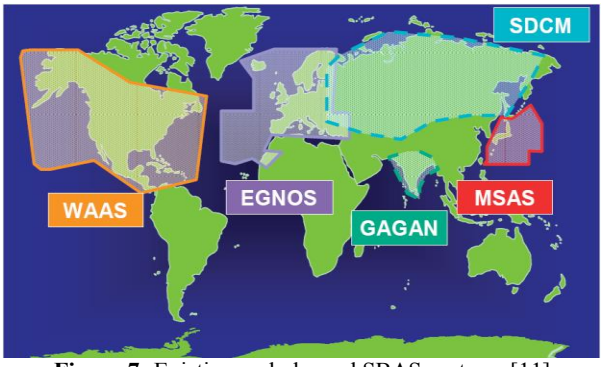

Figure 7: Existing and planned SBAS systems [11]

The next subsection details the case of EGNOS signals, but similar SBAS systems have already been commissioned by the US (WAAS) and Japan (MSAS), and EGNOS signals have been designed according to the same standard [11].

EGNOS provides corrections and integrity information to GPS signals over Europe. It consists of 3 geostationary satellites for the space segment and a network of stations for the ground segment. The EGNOS system provides 3 services [11]: an Open Service (OS), freely available to the public in Europe since 2009, a Safety of Life service (SoL) available since 2011 and dedicated to support Civil Aviation applications and a Commercial Data Distribution Service (CDDS) provided a paying service.

The EGNOS OS and SoL signals have the same structure [11][12], described below. The SBAS signals are very close to the GPS L1 C/A in terms of modulation (same PRN code length and chipping rate), but a great advance has been made on the channel encoding, which will inspire the next GNSS signals design.

2.1.2.1 Signal Structure

The SBAS signal is composed of three components, by the same way than the GPS L1 C/A signal described before and illustrated in Figure 1:

- A carrier:

  The carrier frequency L_1 is used to transmit the signal

- The augmentation message $D(t)$**:**

  The message consists of a 250 bps data stream with channel encoding resulting in 500 sps stream. Thus each symbol lasts 2 ms.

- The PRN code $C_{PRN}(t)$:

  The spreading code is a PRN sequence of 1023 chips, belonging to the same length-1023 Gold code family as the GPS L1 C/A-codes.

2.1.2.2 Navigation Message Structure

Each message consists of 250 bits: 8 bits of preamble, 6 bits of message type identifier, 212 bits of data and 24 parity bits, as it is described in Figure 8 [13].

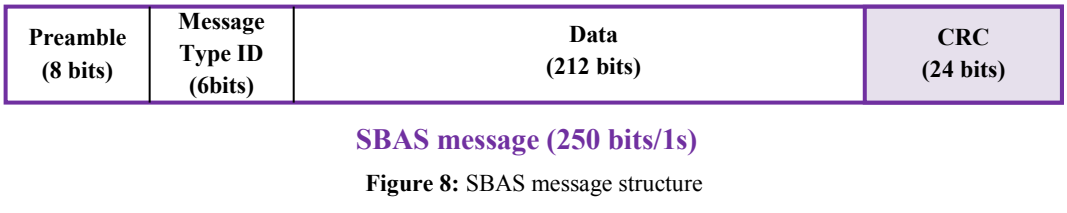

Figure 8: SBAS message structure

The message is then encoded by a rate ½ channel coder (see Annex B for more details about the channel code rate), resulting in 500 bits in 1 second.

2.1.2.3 Channel encoding

The SBAS message is encoded by two encoders in a serial form (see Annex B for concatenated codes details). The outer channel code is a cyclic code called CRC-24Q and the inner channel code is a convolutional code (171, 133, R = ½).

The CRC-24Q adds 24 bits to the 226 data bits and the convolutional code transforms these 250 data bits into 500 coded bits. Figure 9 depicts the channel encoding process.

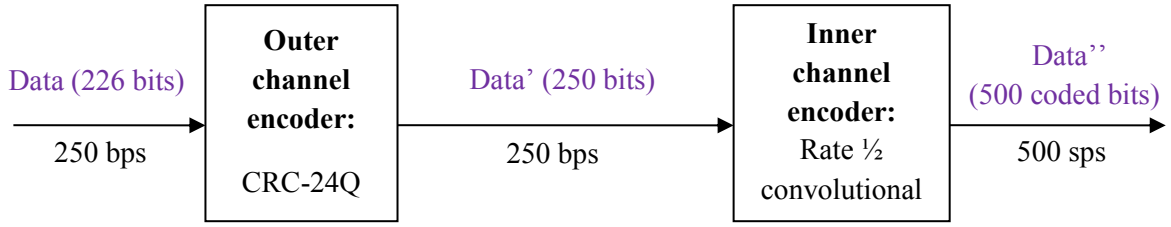

Figure 9: SBAS channel encoding description

2.1.2.3.1 Outer Code: CRC-24Q

The CRC-24Q is a cyclic code. The encoder generates a sequence of 24 bits from the sequence of 226 data bits through the computation process of equation (2.2) [9].

$$c(X) = m(X)X^{24} + r(X) \tag{2.2}$$

where:

- $c(X)$: the CRC-24Q coded word Data',
- $m(X)$: the data word,
- $r(X) = \frac{m(X)X^{24}}{g(X)}$: the remainder,
- $g(X) = \sum_{i=0}^{24} g_i X^i$: the generator polynomial,
- $g = (g_0\ g_1 \dots\ g_{24}) = (1100111100110010011000011)$.

2.1.2.3.2 Inner Code: Convolutional (171, 133, R = ½)

The inner channel encoder uses the convolutional code (171, 133, R = ½), which means that each data' bit is encoded into two coded bits via the encoder of Figure 10. The polynomial generators are equal to $171_{\text{octal}} = 001\ 111\ 001_{\text{binary}}$ and $133_{\text{octal}} = 001\ 011\ 011_{\text{binary}}$.

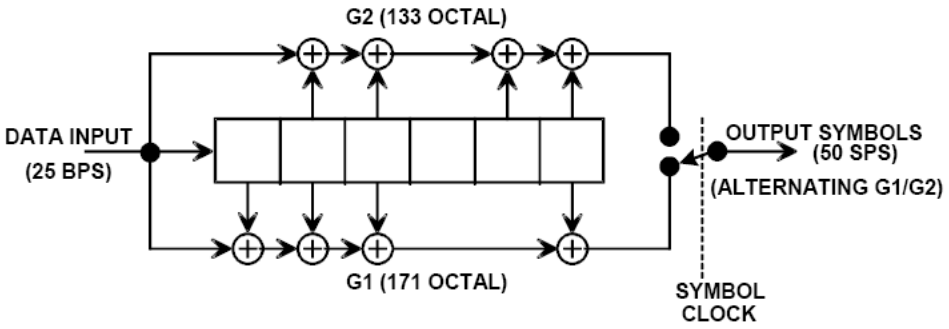

Figure 10: SBAS convolutional encoder [9]

2.1.2.4 Conclusion

The SBAS signal is thus really similar to the GPS L1 C/A signal, but its channel code is really enhanced. This enhanced channel encoding will then be used for most signals of the next generation.

2.1.3 GPS L2C

GPS Civilian L2 (L2C) belongs to the generation of modernized GNSS signals. It was designed in order to improve the civilian GPS services, offering an easy access to dual frequency to civilian users. The first satellite transmitting GPS L2C has been launched in 2005 but the CNAV message (GPS L2C navigation message) has only been emitted since 2014 [1]. Its channel code (convolutional code) is more advanced than GPS L1 C/A and used for most current GNSS signals (such as SBAS, GPS L5 and Galileo signals). Moreover, several other characteristics such as the use of a dataless (or pilot) component, differentiate it from the GPS L1 C/A signal described before.

2.1.3.1 Signal Structure

The GPS L2C signal is composed of four components [9]:

- A carrier:

  The carrier frequency L_2 is used to transmit the signal with a BPSK modulation.

- The CNAV navigation message $D_c(t)$:

  The Civil NAVigation data (CNAV) $D_c(t)$ is a 25 bps data stream with channel encoding resulting in 50 sps stream. Thus each symbol lasts 20 ms.

- A Civilian Moderate length PRN code $CM(t)$:

  It is a sequence of 10 230 chips, repeated every 20 ms. It gives a rate of 511.5 Kchips per second.

- A Civilian Long length PRN code $CL(t)$:

  It is a sequence of 767 250 chips, repeated every 1500 ms. It gives a rate of 511.5 Kchips per second too. Such a long PRN code exhibits excellent auto- and cross-correlation properties.

Each data symbol (20 ms) is multiplied by the CM sequence (20 ms). Then the resulting sequence CM' is time-multiplexed with the CL code: between each CM'' code chip, a CL code chip is placed.

Finally, a sequence with a rate of 511.5*2 = 1023 Kchips per second is generated. Figure 11 illustrates the multiplexing technique.

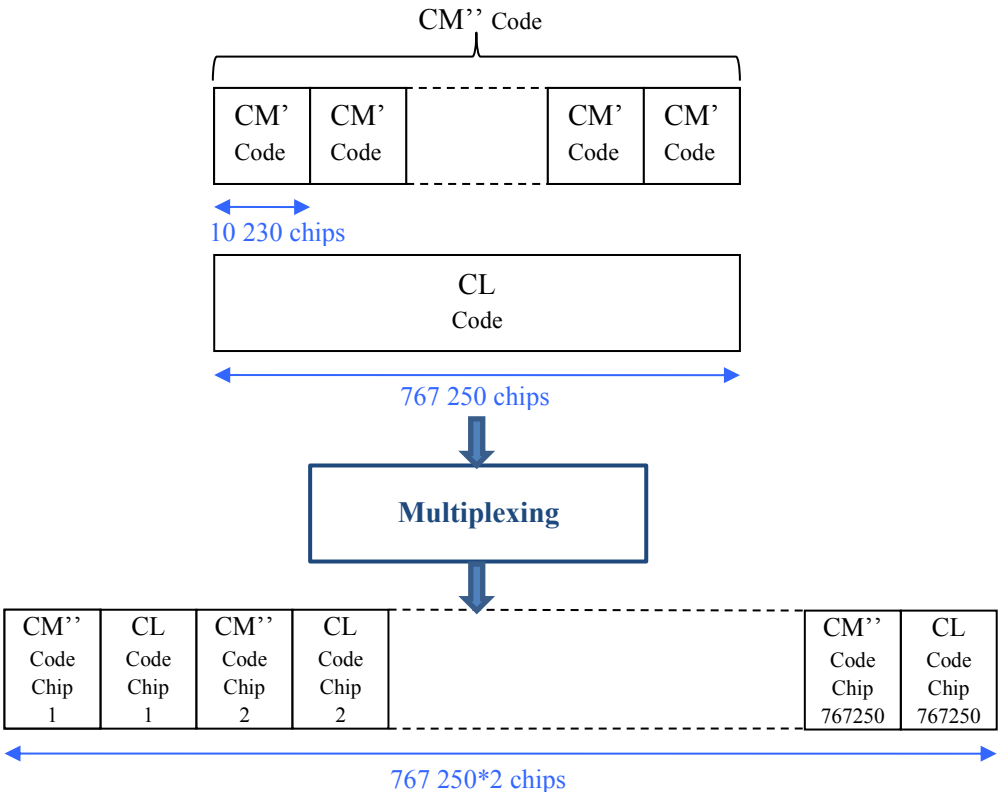

Figure 11 : Multiplexing process for CM and CL PRN codes

Following the multiplexing, the resulting component is modulated by the carrier, as it is described in Figure 12.

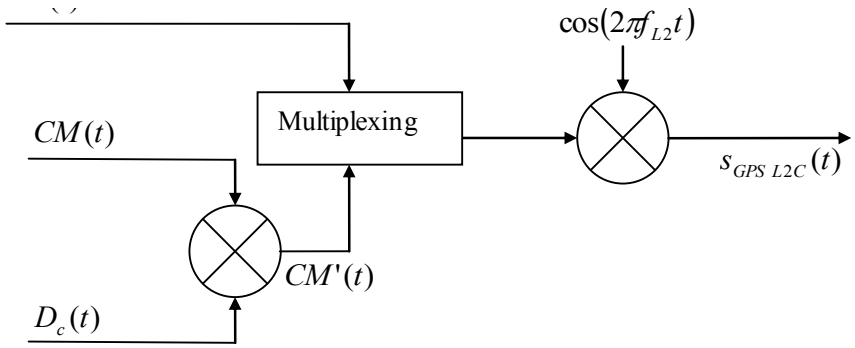

Figure 12: GPS L2C signal modulation block diagram

The signal thus has two distinct components:

- A data component which carries the CNAV data,

- A pilot component with no data which is used for ranging purposes. With a pilot signal, since the phase ambiguity due to the data bits sign is not a problem anymore, the carrier phase can be tracked thanks to a true PLL instead of a Costas loop, improving the tracking threshold by 6 dB (in terms of equivalent C/N_0) [14]. Being able to track in a more robust way the carrier phase means that it could also be possible to demodulate the data (on the data component) even at low C/N_0 or in more difficult environments.

It is thus possible with the GPS L2C signal to use the data component to demodulate the data, and to use the pilot component to track the signal. The resulting simplified mathematical expression of GPS L2C can thus be written as equation (2.3).

$$s_{GPS\ L2C}(t) = [D(t)\ CM(t) \oplus CL(t)]\ cos\left(2\pi f_{L_2} t\right) \tag{2.3}$$

where:

- $D(t)$ is the CNAV data stream,
- $\oplus$ is the multiplexing operator,
- $f_{L_2} = 1227.60\ MHz$ is the carrier frequency.

2.1.3.2 Navigation Message Structure

The CNAV data at 25 bps forms messages composed of 300 bits: 276 data bits and 24 Cyclic Redundancy Check (CRC) bits. Each message begins by 8 bits of preamble, followed by 6 bits representing the PRN number of the transmitting satellite (to reduce the problems of cross-correlation resulting in the tracking of the wrong signal), 6 bits representing the message type and 17 bits representing the Time Of Week (TOW) [9]. The remaining data bits differ from one message type to another. They are used to provide particular information, according to the message type. The general message structure is illustrated in Figure 13.

Figure 13: GPS L2C navigation message general structure

Each message type carries specific information. Table 1 describes the different message types and their content [9]. CED information is contained in message types 10, 11 and 30's.

The messages are broadcast arbitrarily, but sequenced to provide optimum user performance. Message types 30's, 10 and 11 shall be emitted at least once every 48 seconds. All other messages shall be broadcast in-between, not exceeding the maximum broadcast interval showed in Table 1.

Table 1: The GPS L2C navigation message types [9]

Word type	Data type	Maximum broadcast intervals
10 and 11	Ephemeris	48 sec
30's	Clock correction parameters	48 sec
30	Clock correction parameters + inter-Signal correction, ionospheric correction	288 sec
31	Clock correction parameters + reduced almanac	20 min
12	Reduced almanac	20 min
37	Clock correction parameters + Midi almanac	120 min
32	Clock correction parameters + Earth Orientation Parameters	30 min
33	Clock correction parameters + UTC	288 sec
34	Clock correction parameters + Differential correction	30 min
13 and 14	Differential correction	30 min
35	GPS/GNSS Time Offset, satellite clock correction parameters	288 sec
36	Text, satellite clock correction parameters	As needed
15	Text	As needed

2.1.3.3 Channel Coding

The GPS L2C navigation message is encoded by two encoders in a serial form, exactly like SBAS signals described before. The outer channel code is a cyclic code called CRC-24Q and the inner channel code is a convolutional code (171, 133, R = ½), see sections 2.1.2.3.1 and 2.1.2.3.2 for more details.

The CRC-24Q adds 24 bits to the 276 data bits and the convolutional code transforms these 300 data bits into 600 coded bits. Figure 14 depicts the channel encoding process.

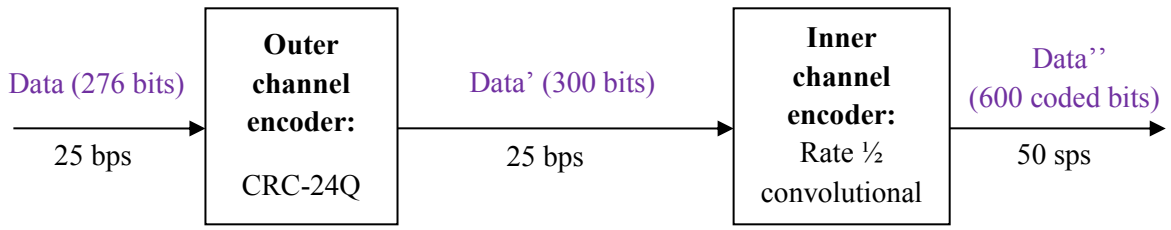

Figure 14: GPS L2C channel encoding description

2.1.3.4 Conclusion

The GPS L2C signal presents several innovations in its design compared with the GPS L1 C/A signal:

- A pilot component:

This is a real innovation in GNSS signal design, allowing the use of a true PLL instead of a Costas loop required in presence of data bits. The substitution of a Costas loop by a PLL involves a tracking threshold gain equal to 6 dB. However, since the GPS L2C signal is split in a data and pilot component with a 50/50% power share, it implies that the real tracking gain in comparison with GPS L1 C/A is equal to 3 dB [14]. Moreover, the use of a short code on the data channel

allows a faster acquisition, and the use of a long code on the pilot channel allows for better correlation properties [14].

- A better channel code:

This convolutional channel code has been firstly implemented on the SBAS signals [14]. This more advanced channel code induces a data recovery threshold gain equal to 5 dB [14]. Moreover, the lower data rate improves of 3 dB this gain, but since the data component power is reduced by 3 dB compared with L1 C/A, these contributions cancel each other.

- A more compact and flexible navigation message.

The GPS L5 signal is very similar, but the data rate is twice higher and the data and pilot signal components are put in quadrature contrary to GPS L2C where they are just time-multiplexed.

2.1.4 Galileo E1 OS

Galileo E1 OS is a civilian signal intended for mass-market and safety-critical services. It is meant to be the equivalent of the GPS L1 C/A signal. It includes modulation innovations such as the use of Binary Offset Carrier modulations. Its channel code is the same than GPS L2C and L5 signals, but innovations have been implemented, through the addition of tail bits and block interleaving.

2.1.4.1 New modulation: BOC

In this modernized GNSS signal, a new modulation has been implemented: the use of Binary Offset Carrier (BOC) modulations.

The BOC modulation is generally noted as BOC(p,q), where p refers to the sub-carrier frequency and q to the spreading code frequency by this way [15]:

$$\begin{cases} f_{sc} = p\ 1.023\ MHz \\ f_C = q\ 1.023\ MHz \end{cases} \tag{2.4}$$

More precisely, Galileo E1 OS and GPS L1C will implement a specific derivation of the BOC modulation that is compliant with the so-called Multiplexed BOC (MBOC) (6,1,1/11). This MBOC is defined in the Power Spectral Density (PSD) domain as a mix of BOC(1,1) and BOC(6,1) modulations. $\frac{10}{11}^{\text{th}}$ of the signal power is associated to a BOC(1,1) modulation and $\frac{1}{11}^{\text{th}}$ of the signal power is associated to a BOC(6,1) modulation [16]. The actual Galileo E1 OS signal implements the MBOC PSD in a specific way, using a Composite BOC CBOC(6,1,1/11). It means that each ranging code is modulated by a weighted combination of a BOC(1,1) and BOC(6,1) subcarriers.

2.1.4.2 Signal Structure

Galileo E1 OS is separated into two channels: the data channel which supports data and the pilot channel which is free of data. It is composed of [17]:

- A carrier:

The carrier frequency E_1, which is equal to the L1 frequency, is used to transmit the signal with a CBOC(6,1,1/11) modulation.

- The I-NAV navigation message $D_{E1\text{-}B}(t)$:

The message consists of a low-flow data stream with a rate of 125 bits per second, encoded with a convolutional code of rate ½. It provides finally an encoded data stream with a rate of 250 sps. Each bit lasts thus 4 ms and is represented by a 1 or a -1.

- The data channel PRN code $C_{E1\text{-}B}(t)$:

$C_{E1\text{-}B}(t)$ is a PRN sequence of 4092 chips. It lasts 4 ms. The associated rate is thus equal to 1.023 Mchips per second.

- The pilot channel PRN code $C_{E1\text{-}C}(t)$:

$C_{E1\text{-}C}(t)$ is a PRN sequence of 25*4092 chips. It lasts 100 ms. The associated rate is thus equal to 1.023 Mchips per second too.

- The sub-carriers $sc_{E1\text{-}Y,a}(t)$ and $sc_{E1\text{-}Y,b}(t)$:

Sub-carriers are used to apply the CBOC(6,1,1/11) modulation, as it is illustrated in Figure 15.

The data channel PRN code is multiplied by the data stream and the resulting component is modulated by the two subcarriers, each affected by a coefficient, $\alpha = \sqrt{\frac{10}{11}}$ and $\beta = \sqrt{\frac{1}{11}}$. In parallel, the pilot channel PRN code is modulated by the subcarriers too. Both channels are then added and modulated by the carrier. The process is depicted by Figure 15.

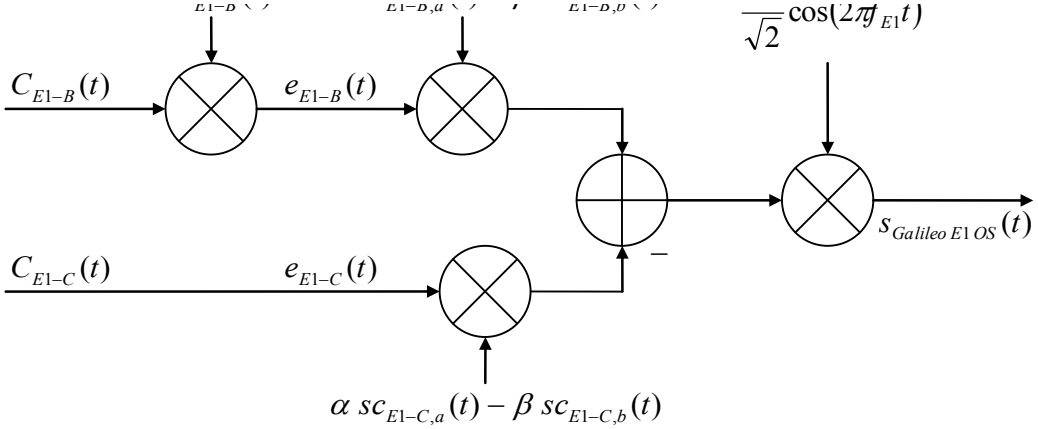

Figure 15 : Galileo E1 OS signal modulation block diagram

The mathematical expression corresponding to Figure 15 is developed in equation (2.5).

$$s_{Galileo\ E1\ OS}(t) = \frac{1}{\sqrt{2}}\left[e_{E1-B}(t)\left(\alpha\ sc_{E1-B,a}(t) + \beta\ sc_{E1-B,b}(t)\right) - e_{E1-C}(t)\left(\alpha\ sc_{E1-C,a}(t) - \beta\ sc_{E1-C,b}(t)\right)\right]cos(2\pi f_{E1}t) \quad (2.5)$$

where:

- $e_{E1-B}(t) = C_{E1-B}(t)D_{E1-B}(t)$,
- $C_{E1-B}(t)$: the PRN code of the data channel,
- $D_{E1-B}(t)$: the I-NAV data stream,
- $e_{E1-C}(t) = C_{E1-C}(t)$,
- $C_{E1-C}(t)$: the PRN code of the pilot channel,
- $sc_x(t) = sgn\{sin(2\pi f_{sc,x}t)\}$: the subcarrier,
- $f_{sc,E1-y,a} = 1.023\ MHz$ the rate of the sub-carriers $sc_{E1-B,a}(t)$ and $sc_{E1-C,a}(t)$,
- $f_{sc,E1-y,a} = 6.138\ MHz$ the rate of the sub-carriers $sc_{E1-B,b}(t)$ and $sc_{E1-C,b}(t)$,
- $\alpha = \sqrt{\frac{10}{11}}$ and $\beta = \sqrt{\frac{1}{11}}$: the coefficients for the CBOC(6,1,1/11) modulation,
- $f_{E_1} = 1575.42\ MHz$: the carrier frequency.

2.1.4.3 Navigation Message Structure

Three types of navigation message structure exist for Galileo: F/NAV (freely accessible navigation), I/NAV (integrity navigation) and C/NAV (commercial navigation). The navigation message type depends on the signal as it is detailed in Table 2.

Table 2: Galileo navigation message types

Message type	Component
I/NAV	E5b-I and E1 OS
F/NAV	E5a-I
C/NAV	E6-B

The navigation message carried by Galileo E1 OS is called the I/NAV message, consisting of one frame, divided into 24 subframes. Each subframe is divided into 15 pages, as it is illustrated in Figure 16.

E1-B Content						E1-B Page	E1B Sub frame ID
Spare Word (2/2)	Res	SAR	Spare	CRC	Res	Odd	N-1
Word 2 (1/2)						Even	N
Word 2 (2/2)	Res	SAR	Spare	CRC	Res	Odd	N
Word 4 (1/2)						Even	N
Word 4 (2/2)	Res	SAR	Spare	CRC	Res	Odd	N
Word 6 (1/2)						Even	N
Word 6 (2/2)	Res	SAR	Spare	CRC	Res	Odd	N
Word 7 or 9 (1/2)						Even	N
Word 7 or 9 (2/2)	Res	SAR	Spare	CRC	Res	Odd	N
Word 8 or 10 (1/2)						Even	N
Word 8 or 10 (2/2)	Res	SAR	Spare	CRC	Res	Odd	N
Reserved (1/2)						Even	N
Reserved (2/2)	SAR	Spare	CRC	Res		Odd	N
Reserved (1/2)						Even	N
Reserved (2/2)	SAR	Spare	CRC	Res		Odd	N
Reserved (1/2)						Even	N
Reserved (2/2)	SAR	Spare	CRC	Res		Odd	N
Reserved (1/2)						Even	N
Reserved (2/2)	SAR	Spare	CRC	Res		Odd	N
Reserved (1/2)						Even	N
Reserved (2/2)	SAR	Spare	CRC	Res		Odd	N
Word 1 (1/2)						Even	N
Word 1 (2/2)	Res	SAR	Spare	CRC	Res	Odd	N
Word 3 (1/2)						Even	N
Word 3 (2/2)	Res	SAR	Spare	CRC	Res	Odd	N
Word 5 (1/2)						Even	N
Word 5 (2/2)	Res	SAR	Spare	CRC	Res	Odd	N
Spare Word (1/2)						Even	N
Spare Word (2/2)	Res	SAR	Spare	CRC	Res	Odd	N
Spare Word (1/2)						Even	N
Spare Word (2/2)	Res	SAR	Spare	CRC	Res	Odd	N

1 Page

Figure 16: Galileo E1 OS nominal subframes structure [17]

A nominal page is the basic structure of the I/NAV message. Nominal pages are transmitted sequentially in time in two parts. The first part of a page is denoted ‘even’ and the second one is

denoted 'odd', as it is described in Figure 17. Each page part is finished by tail bits, used for the channel decoding process.

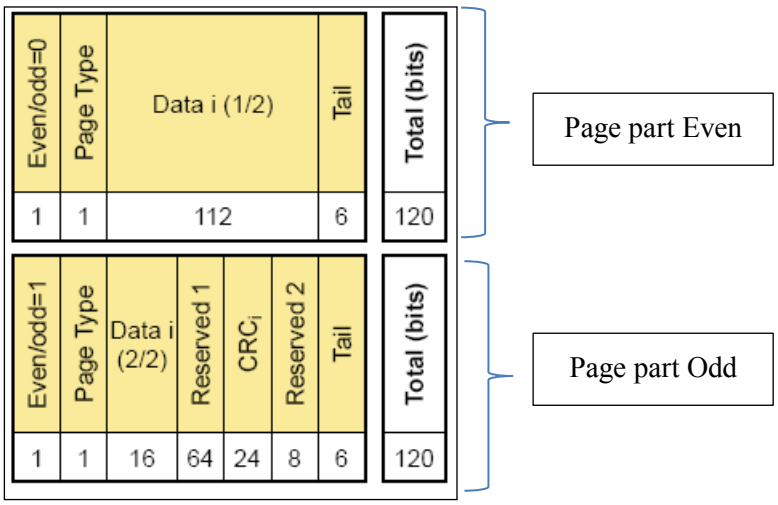

Figure 17: I/NAV nominal page structure [17]

The data field is always composed of a nominal word of 128 bits (112 bits + 16 bits). The word type depends on the contained data type, as it is described in Table 3. CED are contained in words 1, 2, 3 and 4.

Table 3: I/NAV word types according to the contained data

Word type	Data type
1	Ephemeris (1/4)
2	Ephemeris (2/4)
3	Ephemeris (3/4), SISA
4	Ephemeris (4/4), SVID, Clock correction parameters
5	Ionospheric correction, BGD, signal health, data validity status, GST
6	GST-UTC conversion parameters
7	Almanac, Almanac reference time, almanac reference week number
8	Almanac
9	Almanac
10	Almanac, GST-GPS conversion parameters
0	I/NAV spare word

2.1.4.4 Channel Coding

All the Galileo signals are encoded in the same way.

The Galileo navigation messages are encoded by two encoders in serial, exactly just like for SBAS, GPS L2C and GPS L5, detailed in section 2.1.2.3: the outer channel code is a cyclic code called CRC-24Q and the inner channel code is a convolutional code (171, 133, R = ½). Nevertheless, tail bits are

added at the end of each page part, indicating the coded word end, which simplifies the decoding process [4].

Another major improvement in terms of channel coding for Galileo signals is the addition of an interleaver (see Annex B). Each page is interleaved after being encoded. The interleaver characteristics are presented in Figure 18.

Parameters	Message Type	
	F/NAV	I/NAV
Block interleaver size (Symbols)	488	240
Block interleaver dimensions (n columns x k rows)	61 x 8	30 x 8

Figure 18: Galileo interleaver description [17]

2.1.4.5 Conclusion

The Galileo E1 OS signal is quite different from the signals described before. Nevertheless, the implemented channel code is the same than for GPS L2C and GPS L5. However, two major innovations have been implemented on Galileo E1 OS:

- Tail bits:

  This is the only GNSS signal to use tail bits, in order to improve the decoding performance. Figure 19 provided in [10] shows the gain induced by the tail bits added in Galileo E1 OS (blue line), compared with convolutional encoded GPS signals (green line). These both curves have been obtained with the ½ code rate convolutional code of GPS L2C (without tail bits) and Galileo E1 OS (with tail bits), considering a 600 bits length message. Moreover, they are compared with a 600 bits length message encoded by the ½ code rate LDPC code of GPS L1C subframe 2 (solid black line), a 6 bits length message encoded by the 9/52 code rate BCH code of GPS L1C subframe 1 (dotted black line) and a 26 bits length message encoded by the Hamming code (32,26) of GPS L1 C/A (red line), which demodulation performance is really close to an uncoded BPSK modulation [10] (see section 2.1.5.4 for more details about the GPS L1C channel encoding). The demodulation performance is presented through the Frame Error Rate, which is the ratio, between the number of erroneous messages and the total number of messages.

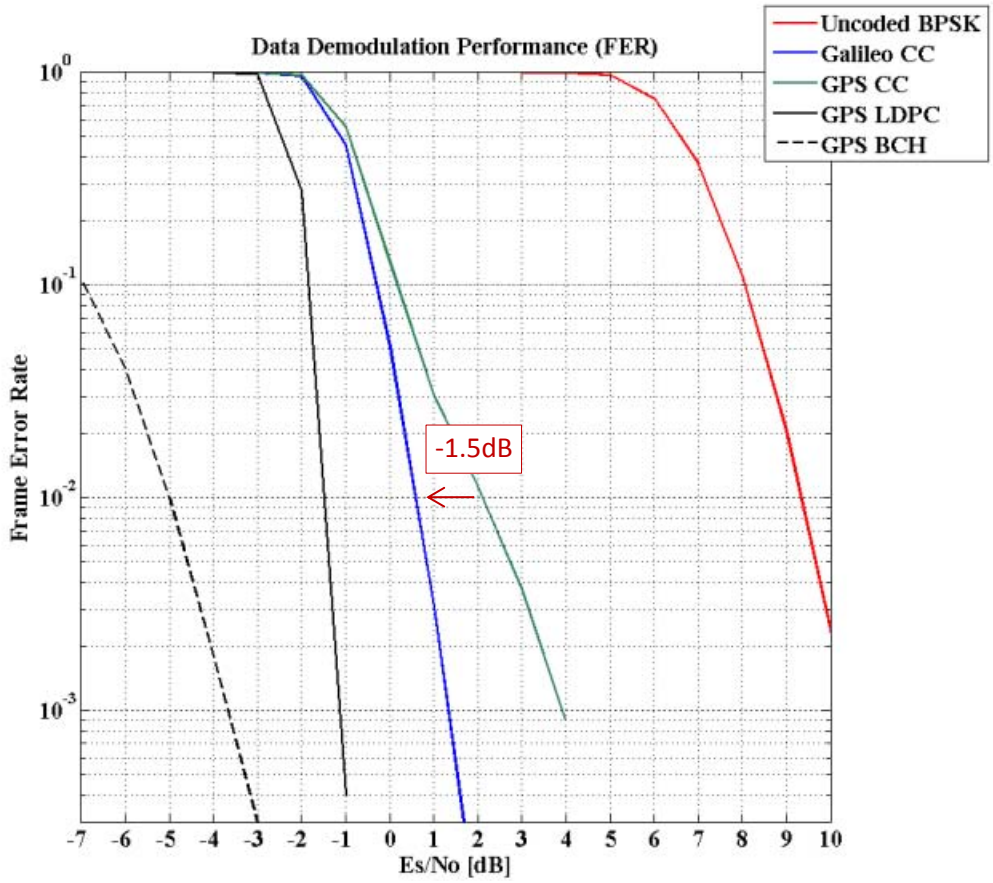

Figure 19: Performance of FEC techniques used in GPS and Galileo data messages [10]

The comparison between the green lines (GPS signals encoded with the (171, 133, R = ½) convolutional channel code) and the blue lines (Galileo signals encoded with the same convolutional channel code but with tail bits insertion) demonstrates that tail bits induce better demodulation performance. For a frame error rate equal to 10^{-2}, the gain obtained with tail bits is equal to 1.5 dB.

- Block interleaving:

  It is the first time that interleaving is implemented. It permits to counteract the burst errors provided by urban propagation channels. Figure 20 and Figure 21 [10] allow showing the impact of the interleaver, comparing GNSS signals demodulation performance in an AWGN propagation channel model (Figure 20) and in an urban propagation channel model (Figure 21).

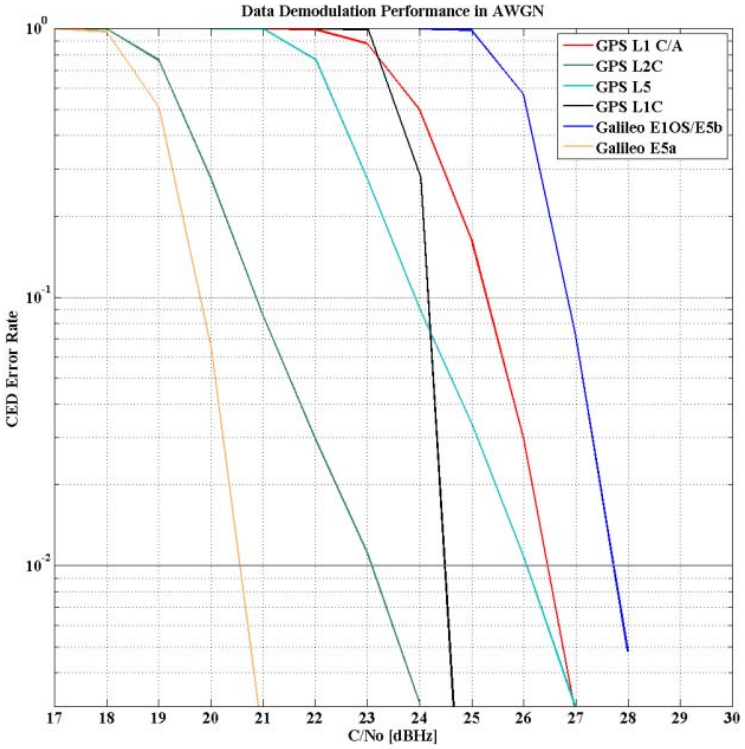

Figure 20: CED error rate as function of the total signal C/N0 in the AWGN channel [10]

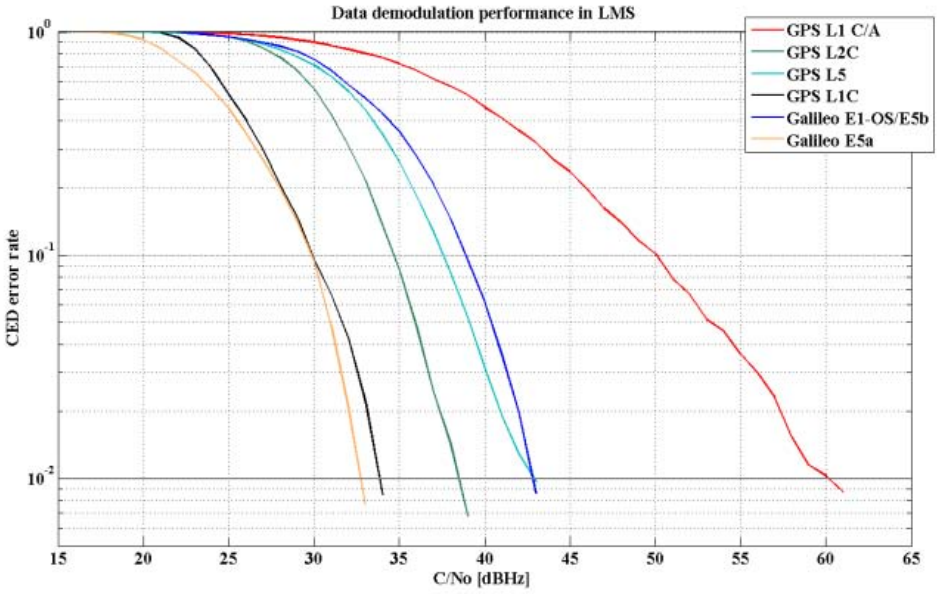

Figure 21: CED error rate as function of the total signal C/N0 in the urban channel [10]

If we compare plots corresponding to convolutional encoded GPS signals without interleaving (GPS L5 in light blue and GPS L2C in green) and Galileo E1 OS encoded with the same convolutional code but interleaved, the gap between them is narrower in the urban channel case.

It can be noticed that Figure 21 provides the GNSS signals demodulation performance in urban environments, which is one of the objectives of this PhD thesis. Nevertheless, another way of

representing GNSS signals demodulation performance adapted to urban environments will be provided in this work in Chapter 4.

2.1.5 GPS L1C

GPS L1C is not yet broadcast. This is a modernized signal for which the design was completed in 2005 [18]. GPS L1C will be emitted by the new generation of GPS III satellites, for which the launch is expected to begin in 2016 [1]. It represents the opportunity to improve the L1 civilian signal. It was designed in order to improve performance and to enable greater interoperability with other international GNSS signals. A major innovative part of this future GNSS signal is the advanced channel code which protects the navigation message.

2.1.5.1 Modulation: BOC

As for Galileo E1 OS (see section 2.1.4.1), a MBOC(6,1,1/11) modulation is implemented on the GPS L1C signal. But it is a different implementation, the Time-Multiplexed BOC (TMBOC) version which is used, in the pilot component. It means that the power between BOC(1,1) and BOC(6,1) is temporally divided: over 33 symbols, 29 symbols are BOC(1,1) modulated whereas 4 symbols are BOC(6,1) modulated. The data component is modulated by a simple BOC(1,1).

2.1.5.2 Signal Structure

GPS L1C signal is divided into two parts, a data channel and a pilot channel with a power unequally distributed. The pilot channel power represents 75% whereas the data channel power represents 25% of the total power. The signal is the combination of these components [19]:

- A carrier:

The carrier frequency L_1 (see Figure 22) is used to transmit the signal with a TMBOC(1,1,6,1) modulation on the pilot component and a BOC(1,1) modulation on the data component.

- PRN codes $L1C_D(t)$ and $L1C_P(t)$:

  They are made by a sequence of 10 230 chips lasting 10 ms. The PRN code chipping rate is thus 1.023 Mchips/s.

- The CNAV-2 navigation message $D_{L1C}(t)$:

  The encoded data stream rate is 100 sps. Each symbol lasts thus 10 ms.

- Subcarriers $sc_D(t)$ and $sc_P(t)$:

  The bit stream of the data channel is modulated by a BOC(1,1) technique whereas the bit stream of the pilot channel modulation is a TMBOC technique which uses a combination of BOC(1,1) and BOC(6,1), explained before. The data subcarrier frequency is thus 1*1.023 = 1.023 MHz and the pilot subcarrier frequencies are 1*1.023 = 1.023 MHz and 6*1.023 = 6.138 MHz.

- An overlay code $L1C_o(t)$:

  It is made by a sequence of 1800 bits which lasts 18 seconds. The rate is thus 100 bps and the bit duration is 10 ms. Each overlay code bit is multiplied by the $L1C_P(t)$ ranging sequence.

Firstly the data ranging code is multiplied by the data which provides the data bit stream, and the pilot ranging code is multiplied by the overlay code which provides the pilot bit stream.

In order to respect the power proportion imposed by the MBOC modulation, coefficients are applied on each signal component. The process is illustrated by the block diagram of Figure 22.

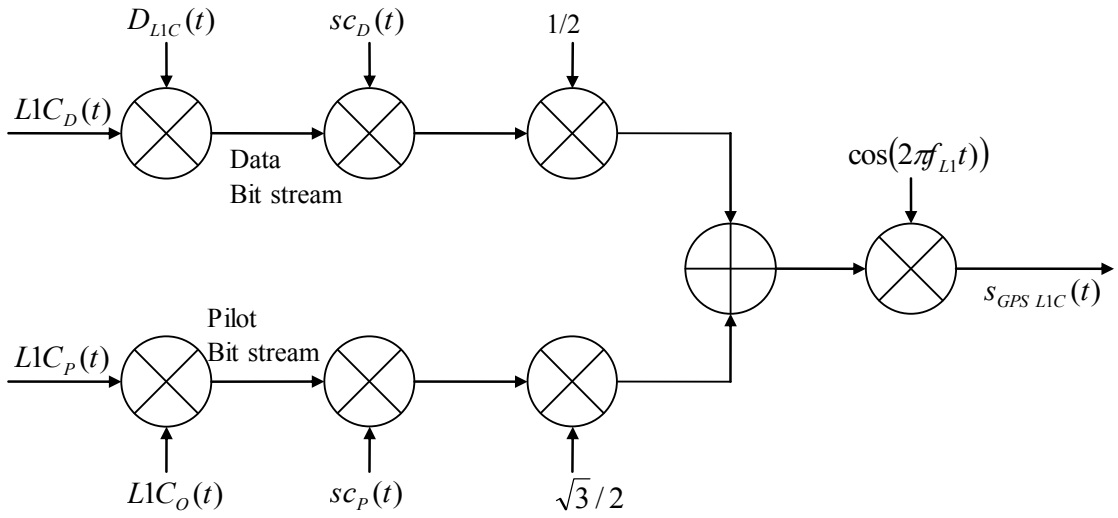

Figure 22: GPS L1C signal modulation block diagram

The fraction of total power finally devoted to BOC(6,1) symbols is thus written in equation (2.6). Only 4 bits on 33 are modulated by a BOC(6,1) and always on the pilot channel.

$$P_{fraction\ BOC(6,1)} = \frac{4}{33} * \frac{3}{4} = \frac{1}{11} \tag{2.6}$$

Whereas the modulation BOC(1,1) is present on 29 bits on 33 on the pilot channel and on all the bits on the data channel:

$$P_{fraction\ BOC(1,1)} = \frac{29}{33} * \frac{3}{4} + \frac{33}{33} * \frac{1}{4} = \frac{10}{11} \tag{2.7}$$

We find the MBOC coefficients described before.

Finally, the mathematical expression corresponding to Figure 22 is developed in equation (2.8).

$$s(t) = \left[\frac{1}{2}D(t)\ sc_D(t) + \frac{\sqrt{3}}{2}L1C_o(t)\ sc_P(t)\right] cos\left(2\pi f_{L_1} t\right) \tag{2.8}$$

where:

- $D(t)$ is the CNAV-2 navigation message, protected by a channel code,

- $f_{L_1} = 1575.42\ MHz$ is the carrier frequency.

2.1.5.3 Navigation Message Structure

The GPS L1C navigation message is called CNAV-2. It consists of frames, each frame being divided into 3 subframes [19].

The subframe 1 is formed by 9 bits. It provides the Time Of Interval (TOI) information which is related to the emission time. The subframe 2 is composed of 600 bits: 576 bits of non-variable data and 24 CRC bits. The data are non-variant over a period of multiple frames and provide the CED information. The subframe 3 is formed by 274 bits: 250 bits of variable data and 24 CRC bits. Figure 23 illustrates the CNAV-2 message structure.

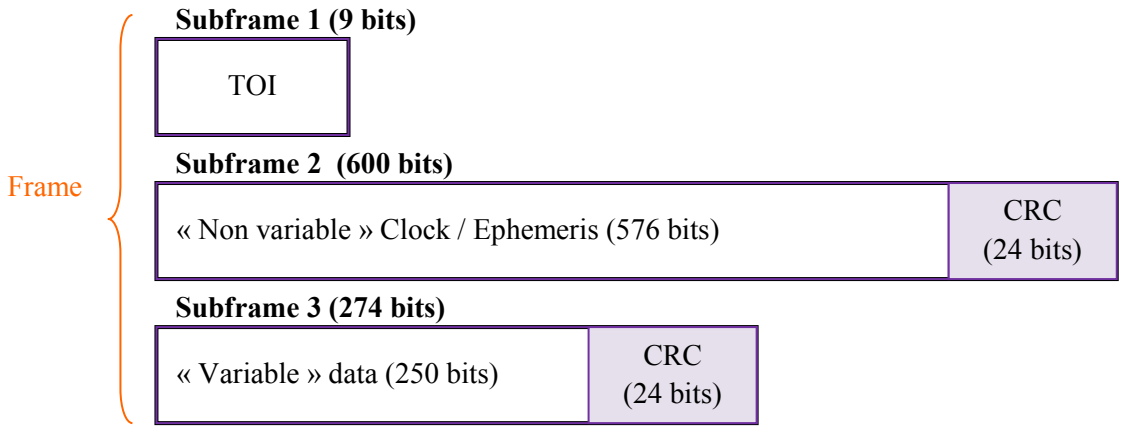

Figure 23: GPS L1C navigation message structure

CED are contained by the subframe 2. This CED set is applicable during three hours, but only transmitted during two hours [19].

2.1.5.4 Channel Coding

2.1.5.4.1 Subframe 1

The subframe 1 is encoded by a BCH (51, 8) code. The 8 Least Significant Bits (LSB) are encoded using the polynomial generator $763_{\ octal} = 111\ 110\ 011_{\ binary}$ via a Linear Shift Register (LSR) generator (see Figure 24). The first bit to pass through the LSR generator is the Most Significant Bit (MSB) of the 8 bits. Then the LSR process occurs 51 times. The 9^{th} bit is modulo-2 added to each 51 coded symbols. And finally, the encoded word is the 9^{th} bit as MSB and the 51 coded symbols. The result consists of 52 symbols [19].

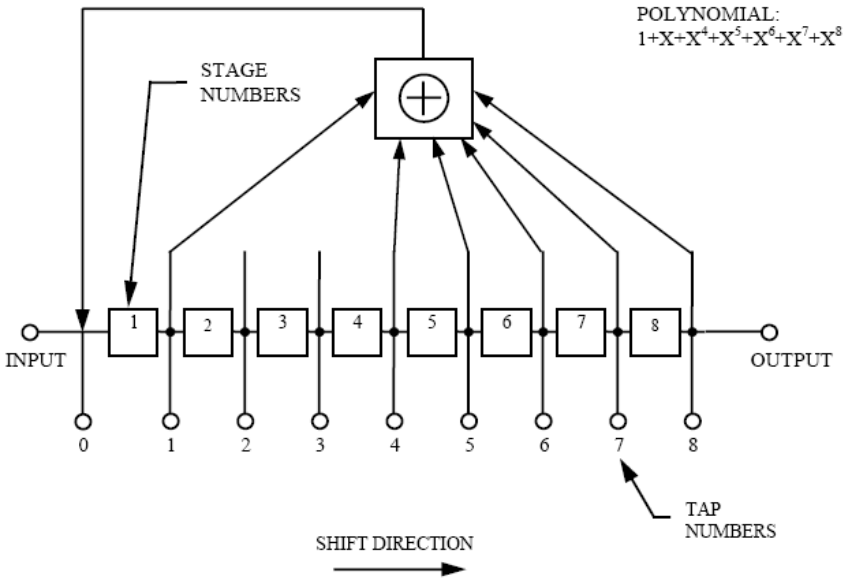

NOTE: INITIAL CONDITIONS ARE 8 LSBs of TOI DATA (MSB IS SHIFTED IN FIRST)

Figure 24: BCH encoder for the subframe 1 of the GPS L1C message [19]

2.1.5.4.2 Subframes 2 and 3

The GPS L1C subframes 2 and 3 are each of them encoded by two encoders in a serial form. For each subframe see Figure 25 and Figure 26, the outer channel code is a cyclic code called CRC-24Q (described in section 2.1.2.3.1) and the inner channel code is a LDPC code (refer to the next section 2.2 for more details) with a rate equal to ½, but with a different size for each subframe.

Subframe 2:

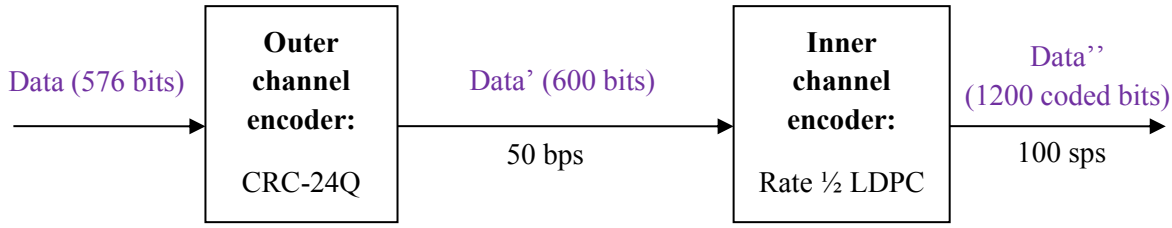

Figure 25: GPS L1C subframe 2 channel encoding description

Subframe 3:

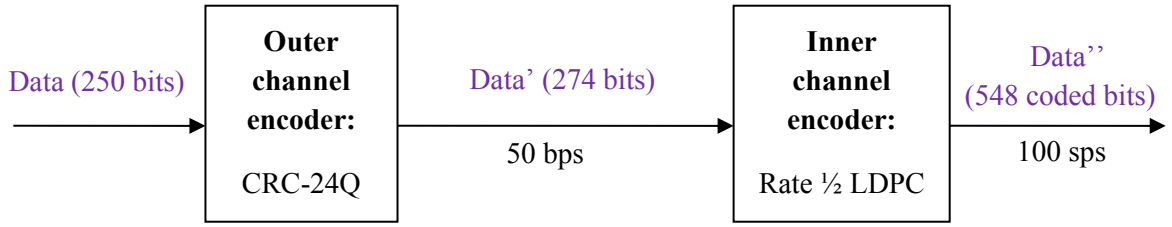

Figure 26: GPS L1C subframe 3 channel encoding description

Each subframe thus has its own parity-check matrix (see section 2.2) $H(m,n)$, with $\begin{cases} m = 600 \\ n = 1200 \end{cases}$ for the subframe 2 and $\begin{cases} m = 274 \\ n = 548 \end{cases}$ for the subframe 3 [19]. But both have the same shape, decomposed into 6 sub-matrices A, B, C, D, E and T, as it is described in Figure 27 and Figure 28.

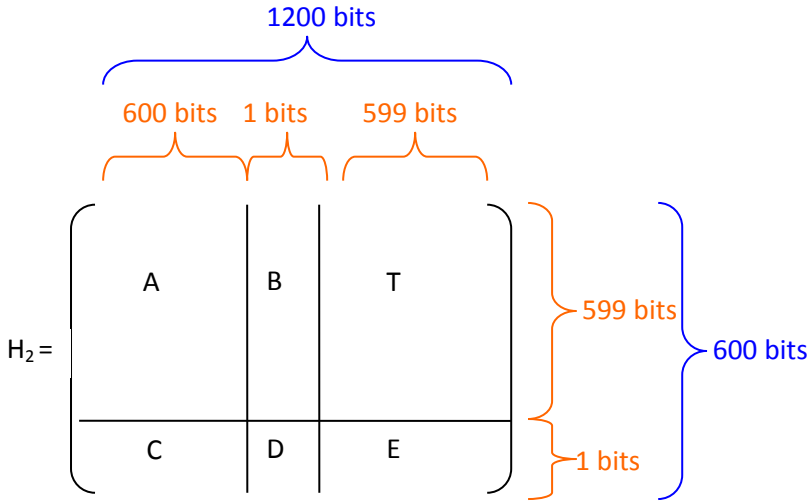

Figure 27: Parity-check matrix of the GPS L1C message subframe 2

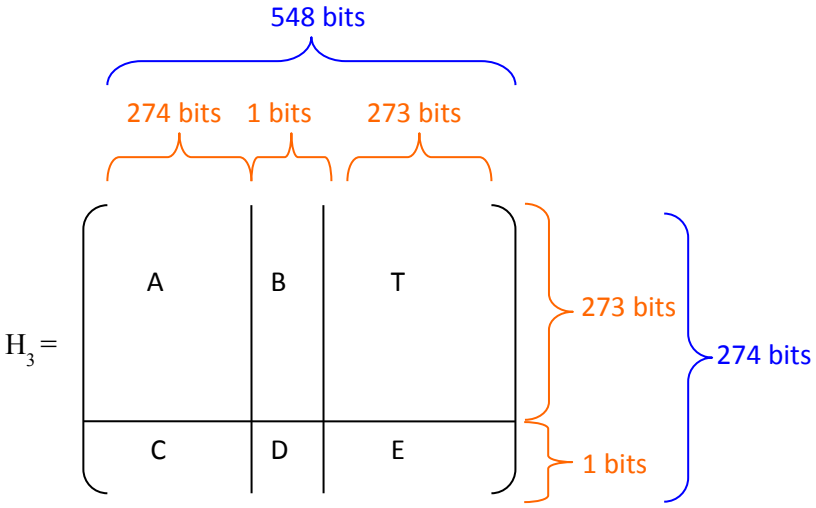

Figure 28: Parity-check matrix of the GPS L1C message subframe 3

The parity bits are encoded according to:

$$\begin{cases} p_1^t = -\phi^{-1}(-E\,T^{-1}\,A + C)s^t \\ p_2^t = -T^{-1}(A\,s^t + B\,p_1^t)s^t \end{cases} \tag{2.9}$$

where:

- p_1: the first part of parity bits,
- p_2: the second part of parity bits,

- s: the subframe 2 or 3,
- $\phi = -E\,T^{-1}\,B + D$.

The final encoded word is (s, p_1, p_2), as depicted in Figure 29.

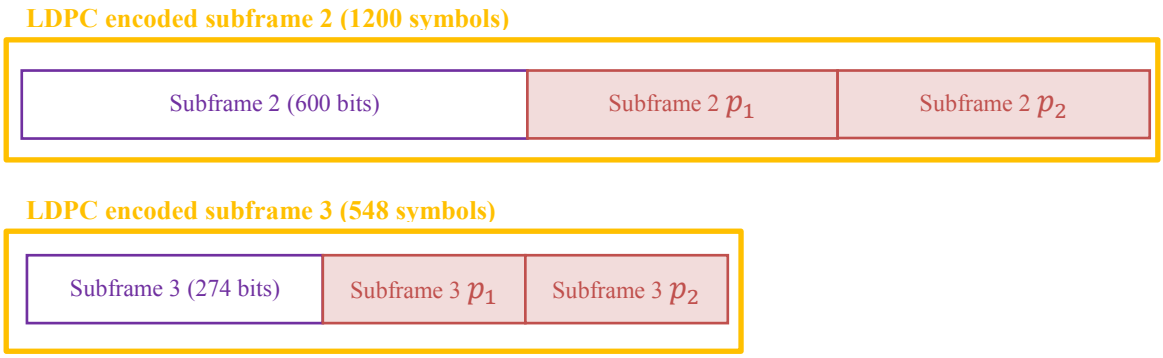

Figure 29: Resulting LDPC encoded subframes

Then the 1748 encoded symbols are interleaved (as for Galileo E1 OS) by a block interleaver of 38 arrows and 46 columns.

2.1.5.5 Conclusion

The GPS L1C signal is finally the one which has the best demodulation performance, thanks to:

- A modern channel code: LDPC

  Contrary to the channel codes mentioned before, LDPC codes (and turbo codes) are able to approach the best achievable performance possible for a channel model, called the channel-capacity, determined by Shannon in 1948 [20].

- A more powerful interleaver:

  The interleaver matrix being more extended for GPS L1C than for Galileo E1 OS, the burst errors induced by urban propagation channels are more attenuated (see Annex B). For GPS L1C, consecutive navigation message data bits become more far after interleaving than for Galileo E1 OS thanks to the interleaving matrix size. The propagation channel effect is thus more temporally uncorrelated for GPS L1C, and consequently the channel coding is more able to correct the errors due to the propagation channel.

- An advanced navigation message structure:

  The navigation message is favourable to the accumulation process, due to the use of non-variant data on subframe 2, which can be a good way to improve the demodulation performance. Data remaining unchanged from one emitted message to the next emitted messages can be accumulated, which corresponds to the addition of correlator outputs, the final result being finally divided by the total number of accumulated messages. The advantage of GPS L1C compared with Galileo E1 OS is that subframe 2 is entirely repeated over 2 hours [19], subframes 1, 2 and 3 being emitted consecutively and continuously.

Figure 30 provided by [4] demonstrates the enhanced capacities of GPS L1C in urban environments. The demodulation performance is provided through the CED error rate (see Annex A for more details

about CED error rate), denoted in this figure by EER, according to the C/N_0 for different configurations. We are interested by the black curves, corresponding to the demodulation performance obtained in an urban environment with the received signal phase estimation made by PLL tracking (as it is done in GNSS receivers).

If the demodulation performance in urban environments of GPS L1C (solid black line) is compared with Galileo E1 OS (dotted black line), a minimum gain of -2.5 dB is achieved with GPS L1C.

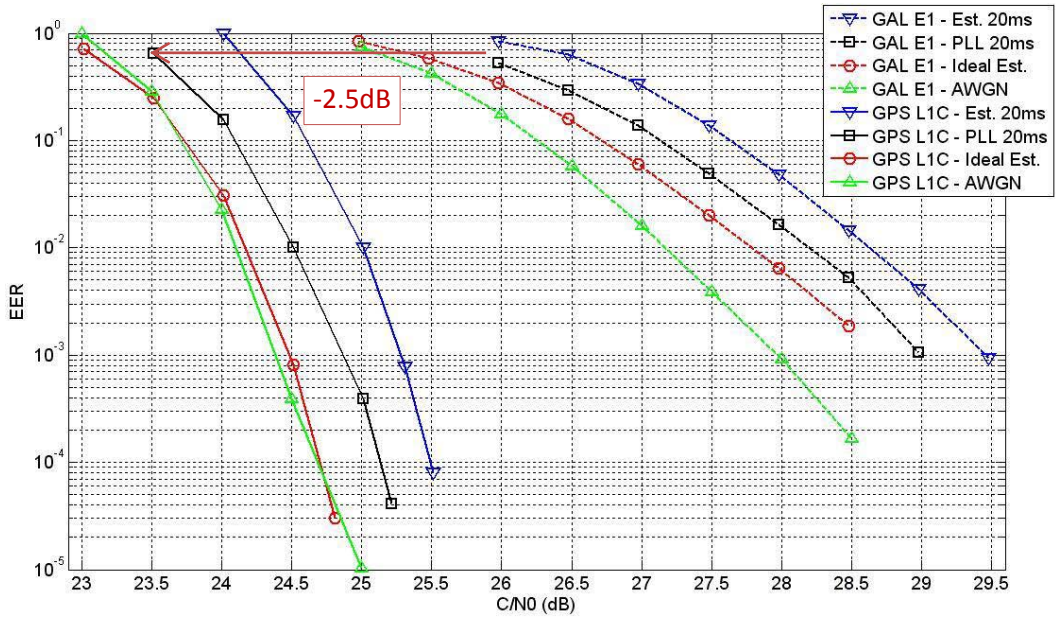

Figure 30: EER comparison between GPS L1C and GALILEO E1 OS signals for a mobile channel transmission with a receiver travelling at 30 km/h [4]

The GPS L1C signal is finally the GNSS civil signal for mass-market needs that appears to be the most powerful, with the expected best performance in urban environments, as it has been shown in Figure 21. It will thus be our GNSS signal reference throughout this PhD rapport, the aim being to design a new GNSS signal with better performance in urban environments.

2.2 LDPC Channel Coding and Decoding

Low-Density Parity-Check (LDPC) codes belong to the linear block codes family, with the specificity that they are able to provide performance which approaches the best possible performance [20]: the channel capacity or Shannon limit (see Annex B). This kind of codes which provide near-capacity performance are named modern channel codes (LDPC and turbo-codes), in comparison with classical codes (such as convolutional codes).

LDPC codes were invented in the early 1960s by Gallager [20], but they had been forgotten because they were impossible to implement at that time. However they were rediscovered (see Table 4) with the appearance of turbo-codes [21], firstly by Tanner in 1981 and more recently by MacKay in 1995 [22].

Table 4: LDPC channel coding background

1963: Gallager (regular LDPC codes, first decoders)
1981: Tanner (codes build from graphs)
1995: MacKay (Belief-Propagation algorithm decoding)
2001: Richardson and **Urbanke** (irregular LDPC codes)

Linear block codes are introduced in section 2.2.1. Then, generalities about LDPC codes are presented in section 2.2.2. And finally, iterative decoding methods used to decode LDPC encoded messages are detailed in section 2.2.3.

2.2.1 Linear Block Codes

A channel encoder transforms an information sequence u composed of k bits into an encoded sequence c composed of n bits (see Figure 31), adding redundancy in order to counteract the impact of errors created by the propagation channel. The code which allows transforming u into c will be designated by the (n, k) code C.

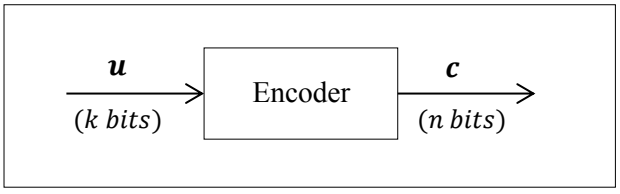

Figure 31 : Classical encoder representation

$$u = (u_0, u_1, \dots, u_{k-1})$$
$$c = (c_0, c_1, \dots, c_{n-1}) \quad (2.10)$$

Linear block codes are error-correcting codes that encode data in blocks. They are described in terms of generator and parity-check matrices [23].

The coded word is the result of a generator matrix applied to the information word, as it is described in equation (2.11). The generator matrix *G* row space gives the code *C* [23].

$$c = uG \tag{2.11}$$

where:

- G is the generator matrix with $(k \times n)$ dimensions.

For any $(k \times n)$ matrix G with k linearly independent rows, it exists a $\left((n-k) \times n\right)$ matrix H with $(n-k)$ linearly independent rows such that any vector in the row space of G is orthogonal to the rows of H, and any vector that is orthogonal to the rows of H is in the row space of G. The linear code C can thus be generated by another way, thanks to the parity-check matrix H, as described before [23].

A vector *c* is a codeword in the code *C* generated by *G* if and only if [23]:

$$cH^T = 0 \tag{2.12}$$

The resulting equations are called the parity check equations and completely specifies the code *C* [23].

The parity check matrix is obtained from the generator matrix by:

$$GH^T = 0 \tag{2.13}$$

The parity check matrix elements will be noted as h_{ij} for the ith row and the jth column, resulting in this notation:

$$H = \begin{pmatrix} h_{11} & \dots & h_{1n} \\ \dots & h_{ij} & \dots \\ h_{(n-k)1} & \dots & h_{(n-k)n} \end{pmatrix} \tag{2.14}$$

2.2.2 LDPC Codes Generalities

Only binary LDPC codes will be treated in this PhD thesis rapport, although LDPC codes can be generalized to nonbinary alphabets [20].

2.2.2.1 LDPC Codes Definition

A LDPC code is a linear block code defined by the **null space** of an $\left((n-k) \times n\right)$ parity-check matrix *H* that has a **low density of 1s** [20].

This LDPC code definition is detailed below:

- The **null space** of an $\left((n-k) \times n\right)$ parity-check matrix *H* is defined by [20]:

$$C = \{c \in GF(2)^{\times n} / cH^T = 0\} \tag{2.15}$$

where:

- C: the null space of H,
- c: the coded word vector,
- $GF(2)$: the Galois field of two elements.

➢ A $((n-k) \times n)$ parity-check matrix H that has a **low density of 1s** is defined by [22]:

$$\frac{number\ of\ non\ null\ elements\ of\ H}{(n-k) * n} \underset{n \to 0}{\longrightarrow} 0 \tag{2.16}$$

2.2.2.2 Graphical Representation : Tanner Graph

A LDPC encoder can be completely represented by a Tanner graph [20], which is based on the parity-check matrix H. A Tanner graph is a bipartite graph, which means a graph whose nodes may be separated into two types:

➢ The Variables Nodes (VN) and

➢ The Check Nodes (CN).

The Check Nodes correspond to the parity check equations resulting from equation (2.12), there are thus as many CN as parity check equations: $(n-k)$. Whereas the Variable Nodes correspond to the coded bits, its number being thus equal to n [20]. Thus, the CNs can be considered as Single Parity Check (SPC) codes and the VNs as repetition (REP) codes [20].

The Tanner graph of a code is drawn as follows: the Check Nodes CN_i are connected to Variable Nodes VN_j whenever element h_{ij} in the parity check matrix H is equal to 1.

For example, if the parity check matrix H is equal to:

$$H = \begin{pmatrix} 10100001 \\ 11010010 \\ 00001101 \\ 11001110 \end{pmatrix} \tag{2.17}$$

The dimension of the parity check matrix being equal to (4×8), the VNs number is equal to 8, representing the coded bits. The parity check equations being equal to the number of parity check matrix transpose columns (see equation (2.11)), there are 4 CNs. Each CN is linked to a VN by the parity check matrix, each column representing a VN and each row a CN.

For this parity check matrix of equation (2.17), the Tanner graph will thus be represented by this way:

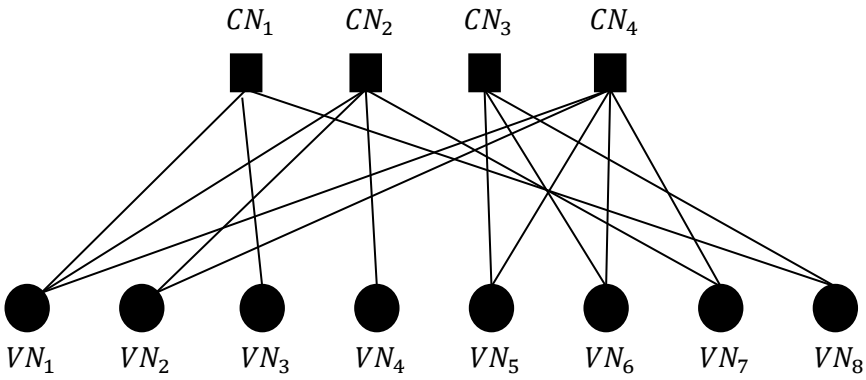

Figure 32: Tanner graph associated to the H matrix example

A Tanner graph allows to completely represent a code and it aids in the description of the decoding algorithm (as it will be used in section 2.2.3) [20]. It can be seen as a trellis for a convolutional code.

2.2.2.3 Definitions

LDPC codes can be divided into two classes: the non-structured codes where the associated parity check matrix is not specific, and the structured codes where the parity check matrix is particular.

Some definitions are given below [20]:

- Cycle:

A cycle is a closed path which comes from and returns to the same node.

- Node degree:

Number of edges connected to a node (equal to 3 for VN_1 in Figure 37 for example),

- Regular code:

A code is said regular when the number of 1s per column and the number of 1s per row in *H*, are constant. It means that each node has the same degree.

- Irregular code:

A code is said irregular when the number of 1s per column or per row in *H*, is not constant. The code represented by the Tanner graph of Figure 37 is for example irregular.

- Degree-distribution polynomials:

For irregular codes, the node degrees being not constant, degree-distribution polynomials are denoted by $\lambda(X)$ for VNs and $\rho(X)$ for CNs, defined by [20]:

$$\begin{cases} \lambda(X) = \sum_{i=1}^{d_{v\,max}} \lambda_i X^{i-1} \\ \rho(X) = \sum_{j=1}^{d_{c\,max}} \rho_j X^{j-1} \end{cases} \tag{2.18}$$

where:

- $d_{v\,max}$ and $d_{c\,max}$ being respectively the maximum VN and CN degrees,

- $\lambda_i = \frac{number\ of\ edges\ connected\ to\ the\ VNs\ of degree\ i}{number\ total\ of\ edges}$ is the fraction of all edges connected to degree-d VNs,
- $\rho_j = \frac{number\ of\ edges\ connected\ to\ the\ CNs\ of degree\ j}{number\ total\ of\ edges}$ is the fraction of all edges connected to degree-d CNs,

Short cycles degrade the performance of the iterative decoding [20].

Irregular LDPC codes allow to closely approaching capacity limits [20]. The GPS L1C channel code is an irregular (1200, 600) LDPC code for the subframe 2 and an (578, 274) irregular LDPC code for the subframe 3 [24].

Degree-distribution polynomials will be used in Chapter 6 for the LDPC code design.

2.2.3 LDPC Iterative Decoding

The maximum likelihood decoding (see Annex B) is too complex in this case, so another algorithm is implemented: the Sum-Product Algorithm (SPA) proposed by Gallager in 1962 [21]. There are two types of such algorithm based on hard or soft decision. The soft decision decoding is more efficient [21] that is why it will be presented in this subsection, by the use of Log Likelihood Ratios (LLRs). Soft-decision decoding of LDPC codes is based on an iterative process: the Belief Propagation (BP) algorithm [21]. It consists on the updating of messages circulating on the branches of the Tanner graph, the information of the received bits (Variable Nodes) being refined after each iteration.

2.2.3.1 Exchanged Messages: LLRs

The SPA decoder follows the Maximum A Posteriori (MAP) optimality criterion [20] (see Annex B). We are thus interested in computing the A Posteriori Probability (APP) that a specific bit in the transmitted codeword c equals 1, given the received word y. The considered messages are Log Likelihood Ratios (LLRs). Indeed, most of existing soft input channel decoding algorithms are using LLRs or related approximated expressions as soft inputs.

For binary random variables as inputs (which is the case in GNSS), the LLR [25] is defined as follows:

$$LLR(c_j/y) = log\left(\frac{p(c_j = 0/y)}{p(c_j = 1/y)}\right) \tag{2.19}$$

where:

- $p(c_j/y)$ is the a posteriori probability that the symbol c_j has been transmitted, knowing the received symbol y.

2.2.3.2 BP Algorithm

The Variable Nodes and Check Nodes can be considered as decoders working cooperatively and iteratively to estimate the final $L_j = LLR(c_j/y)$ for $j = 1, \dots, n$ [20]. The LLRs messages circulating on the branches of the Tanner graph which are updated during the decoding process must only bring

extrinsic information to be efficient. Extrinsic information concept is defined by the fact that a node has not to pass to a neighboring node any information that the neighboring node already has, that is, only extrinsic information is passed [20], the intrinsic information being the complementary concept, corresponding to the information brought by the own considered node. Extrinsic LLRs passing from node *j* to node *i* will be denoted in this work by $L_{j\to i}$.

Thus, all Variable Nodes process their inputs and pass extrinsic information up to their neighboring Check Nodes. The CNs then process their inputs and pass extrinsic information down to their neighboring VNs [20]. And the procedure repeats until it reaches a preset maximum number of iterations or a stopping criterion. Then, the decoder computes the $L_j = LLR(c_j/y)$ from which the decisions on the bits c_j are made. For example if equation (2.20) is verified, thus the coded bit is more likely to be 0 than 1, according to equation (2.21).

$$If\ L_j = LLR(c_j/y) > 0 \tag{2.20}$$

$$Thus\ p(c_j = 0/y) > p(c_j = 1/y) \tag{2.21}$$

The BP algorithm is illustrated in Figure 33 where a Tanner graph portion is represented, explained next and summarized in Table 5.

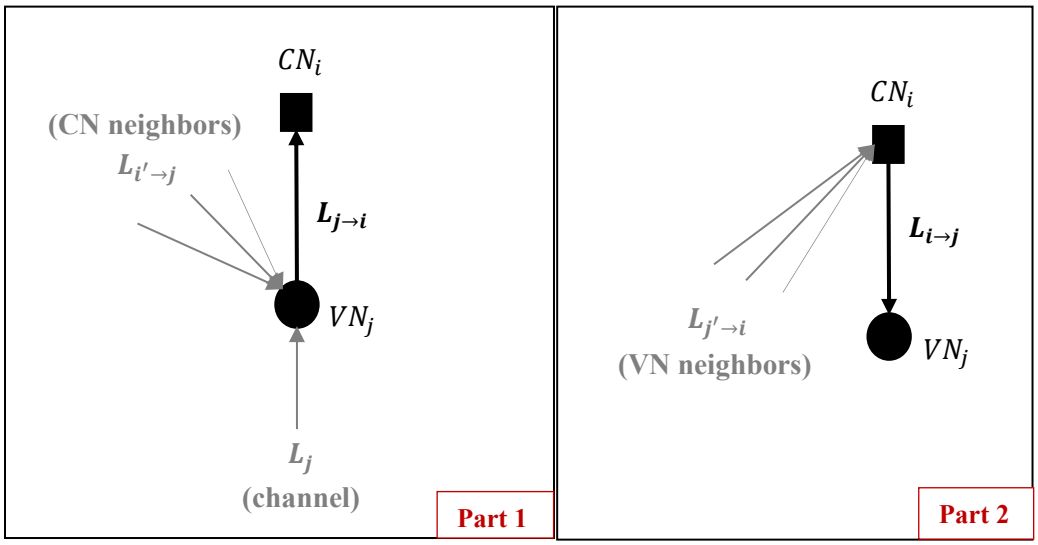

Figure 33: BP algorithm illustration

It should be recalled that VNs correspond to the received coded bits. At the initialization, only the channel contribution is considered in the computation of extrinsic information passing from VN_j to CN_i (see Figure 33 Part 1), since the CNs don't possess enough information to compute their extrinsic information at the first iteration.

Then, in Figure 38 Part 2, extrinsic information coming from CN_i into VN_j is computed considering all the messages which arrive to the CN_i node: extrinsic information brought by all VNs except the node VN_j which will receive the final message, since otherwise VN_j will finally receive information that it

already knows. This extrinsic information computation coming from CN_i into VN_j is called the 'CN update' and derived in Annex C. Its resulting mathematical expression is written in Table 5.

Then, illustrated in Figure 38 Part 1, VN_j is updated (next iteration). The channel contribution, as well as the extrinsic information coming from all the CNs except CN_i which will receive the final message, are taken into account.

The final total LLR which outputs from VN_j and which will be used to make the decision on the bit value $L_j = LLR(c_j/y)$ takes into account all contributions arriving into it, corresponding to each CNs. Its mathematical expression is derived in Annex C and given in Table 5.

Table 5: BP algorithm description

Initialization: (Part 1) For all j, L_j is initialized for the appropriate channel, by: $$L_j = LLR(c_j/y) = log\left(\frac{p(c_j = 0/y}{p(c_j = 1/y}\right)$$ Then $L_{j\to i}$ are initialized by: $$L_{j\to i} = L_j$$
CN update: (Part 2) (derived in Annex C) The CN *i* transmits to the VN *j* the LLR message: $$L_{i\to j} = 2tanh^{-1}\left(\prod_{j' \in CN_i - \{j\}} tanh\left(\frac{1}{2}L_{j'\to i}\right)\right)$$
VN update: (Part 1) The VN computes the sum of all the LLR messages which arrive to it. $$L_{j\to i} = L_j + \sum_{i' \in VN_j - \{i\}} L_{i'\to j}$$
Total LLR: (derived in Annex C) $$L_j^{total} = L_j + \sum_{i \in VN_j} L_{i\to j}$$
Stopping criteria: $$\widehat{c_j} = \begin{cases} 1 \; if \; L_j^{total} < 0 \\ 0 \; else \end{cases}$$

Some simplified BP algorithm exist which reduces the decoder complexity. One of them is the Min-Sum Decoder, detailed in Annex C.

2.3 Urban Propagation Channel Modeling

In the GNSS context, the propagation channel is a Land-Mobile Satellite (LMS) channel. And since the challenging environment concerns urban areas, the propagation channel to be modeled is the urban LMS channel. The urban LMS channel model state-of-the-art analysis shows that two models are mostly used for simulations: the narrowband model designed by F. Perez-Fontan in the early 2000 [26][27] and improved by R. Prieto-Cerdeira in 2010 [28], and the wideband model designed by the DLR (the German Aerospace Center) in 2002 [29].

The narrowband characteristic is used to designate a model which considers that the multipath echoes are received at the same time than the Line-Of-Sight (LOS) signal. On the other hand, the wideband characteristic designates a model which considers the delay between the LOS signal and each of the multipath echoes. To mathematically define the narrowband and wideband characteristics, the Channel Impulse Response (CIR) expression is used. It is defined in section 2.3.1. The narrowband Perez-Fontan/Prieto propagation channel model is then presented in section 2.3.2 and the wideband DLR model in section 2.3.3.

2.3.1 Channel Impulse Response

The impact of the LMS propagation channel on the received signal can be modeled using the equivalent low-pass [25] time-variant channel impulse response h_e, which links the equivalent low-pass emitted signal s_e to the equivalent low-pass received signal r_e by this expression:

$$r_e(t) = \int_{-\infty}^{+\infty} h_e(t;\tau) s_e(t-\tau) d\tau \tag{2.22}$$

where:

- t is the variable determining the instant of time at which the CIR is defined,
- τ is the variable which determines the delay at which the CIR is defined.

Therefore, the CIR mathematical expression depends on the selected channel model; it will be different according to the Perez-Fontan/Prieto or DLR propagation channel model.

2.3.2 The Perez-Fontan/Prieto Propagation Channel Model

The Perez-Fontan/Prieto propagation channel model has been firstly designed by F. Perez-Fontan in the early 2000 [26][27]. This initial model is detailed in section 2.3.2.1. Several evolutions have then been implemented [28]; they are introduced in section 2.3.2.2.

2.3.2.1 The Perez-Fontan Model Base

The Perez-Fontan model is a narrowband statistical 3-state model.

Narrowband Characteristic: The Perez-Fontan model is narrowband, meaning that the delay of the direct signal and the delays of the multipath echoes are assumed to be equal. The CIR is thus modeled as:

$$h_e(t;\tau) = c(t)\delta\big(t - \tau_{direct}(t)\big) \tag{2.23}$$

with:

$$c(t) = a_{channel}(t)e^{j\varphi_{channel}(t)} = a_{direct}(t)e^{j\varphi_{direct}(t)} + a_{multipath}(t)e^{j\varphi_{multipath}(t)} \tag{2.24}$$

where:

- $c(t)$ is the complex envelope of the overall received signal (corresponding to the propagation channel impact),
- $\tau_{direct}(t)$ is the LOS propagation time,
- $a_{channel}(t)$ is the channel attenuation,
- $\varphi_{channel}(t)$ is the channel phase,
- $a_{direct}(t)$ is the direct signal component amplitude and $\varphi_{direct}(t)$ is its phase,
- $a_{multipath}(t)$ is the multipath component amplitude and $\varphi_{multipath}(t)$ is its phase.

The direct signal component corresponds to the LOS signal which can be potentially shadowed or blocked. The multipath component corresponds to the sum of all the reflections/refractions of the transmitted signal found at the RF block output.

Statistical: The Perez-Fontan model is a statistical model based on measurement campaigns carried out in the 90s and conducted by: the University of Bradford (UK) in 1992, the DLR (Germany) in 1994, the Institute for Advanced Studies (Austria) in 1995 and the University of Surrey (UK) in 1996, as it is described in Table 6 [27].

Table 6: Databases for the Perez-Fontan model

Institution	Transmitter platform	Frequency	Bandwidth	Environments	Elevation	Azimuth	Antenna beam width	Application
University of Bradford 1992	Plane	2.618 GHz (S band)	Narrow	Open Suburban Urban Tree shadowed	0° 60° 80°	90°	90°	Car
DLR 1994	Plane	1.820 GHz (L band)	30 MHz	Urban Suburban Rural	10°-80°	0°-360°	180°	Pedestrian Car
IAS 1995	ITALSAT	18.68 GHz (K band)	Narrow	Open Suburban Urban Tree shadowed Mixed	-35°	0° 45° 90°	3°	Car
University of Surrey 1996	Helicopter	1.550 GHz (L band) 2.325 GHz (S band)	20 MHz	Open/Highway Suburban Urban Wooded	15°-80°	90°	42° 71°	Car

The measurement campaigns allowed modeling the received signal complex envelope $c(t)$ behavior with a Loo distribution.

$$c(t) = a_{channel}(t)e^{j\varphi_{channel}(t)} = a_{direct}(t)e^{j\varphi_{direct}(t)} + a_{multipath}(t)e^{j\varphi_{multipath}(t)} \quad (2.25)$$

$\tilde{Loo}$ $\tilde{\text{Log-Normal}}(\propto_{dB}, \Psi_{dB})$ $\tilde{\text{Rayleigh}}(MP_{dB})$ $\tilde{\text{Uniform}}\ (0,2\pi)$

The distribution of the Loo parameters is defined as follows [26]:

- The amplitude of the direct signal component $a_{direct}(t)$ $a_{direct}(t)$ follows a Log-Normal distribution, characterized by its mean α_{dB} and its standard deviation Ψ_{dB},
- The amplitude of the multipath component $a_{multipath}(t)$ follows a Rayleigh distribution, with a standard deviation σ. The value of σ is calculated from the average multipath power with respect to an unblocked LOS signal: MP_{dB} (equation (2.26)). MP_{dB} is the parameter provided in the literature.

$$\sigma = \sqrt{10^{\frac{MP_{dB}}{10}}/2} \quad (2.26)$$

Therefore, the set of parameters (α_{dB}, Ψ_{dB}, MP_{dB}) completely defines the Loo distribution and is referred as the Loo parameters. They are provided in [26] and depend on the environmental conditions:

- The type of environment (semi-urban, urban, deep urban…),
- The satellite elevation angle,
- The signal carrier band,
- The channel states.

From these Loo parameters values, the amplitude of the direct signal component $a_{direct}(t)$ $a_{direct}(t)$ following a Log-Normal distribution can be generated. In fact, to generate a Log-Normal random variable $x_{Log-Normal}$, a Gaussian random variable is firstly drawn with the mean α_{dB} and the standard deviation Ψ_{dB} called A (see Figure 34) and the Log-Normal random variable is obtained via this operation:

$$x_{Log-Normal} = 10^{\frac{A}{20}} \quad (2.27)$$

In parallel, the multipath component Rayleigh random variable $x_{Rayleigh}$ is generated via the addition of two Gaussian random variables $x_{Gauss} \sim Gauss(0,1)$ in quadrature:

$$x_{Rayleigh} = x_{Gauss} + j * x_{Gauss} \quad (2.28)$$

The generation of this Loo distribution is illustrated in Figure 34.

Slow and fast variations: The two signal components constituting the received signal have different variation rates. In other words, the minimum length (or time if converting the length by using the user velocity) between two uncorrelated samples of a component is different for each component. The direct signal component variation rate is slower than the multipath component variation rate.

- For a Log-Normal variable corresponding to the direct signal component, the minimum length separating two uncorrelated samples is referred as the correlation distance l_{corr}. The correlation distance is equal to 1 m for S-band and 2 m for L-band according to [28]. Examples of direct signal component correlation durations t_{corr} corresponding to these correlation distances are showed in Table 7 for different user speed values.

Table 7: Direct signal component correlation time examples

	L-band	S-band
$v_{user} = 5\ km/h$	$t_{corr} = 1.44\ s$	$t_{corr} = 720\ ms$
$v_{user} = 30\ km/h$	$t_{corr} = 240\ ms$	$t_{corr} = 120\ ms$
$v_{user} = 50\ km/h$	$t_{corr} = 144\ ms$	$t_{corr} = 72\ ms$

- For the Rayleigh variables corresponding to the multipath component, the minimum length between two uncorrelated samples when the user is static is usually set in the literature to λ/4 meters [30], where λ is the wavelength of the carrier. But in fact, a minimum length of at least λ/8 meters is usually selected [27] to ensure the uncorrelation property for more strict interpretations. When the user is in motion, the minimum length depends on the user velocity and thus this length is usually expressed in time (see Table 8).

Table 8: Multipath component correlation time examples

	$L_1 = 1575.42\ MHz$	$L_2 = 1227.60\ MHz$
$v_{user} = 5\ km/h$	$\frac{\lambda}{8}_{temporal} = 137\ ms$	$\frac{\lambda}{8}_{temporal} = 176\ ms$
$v_{user} = 30\ km/h$	$\frac{\lambda}{8}_{temporal} = 23\ ms$	$\frac{\lambda}{8}_{temporal} = 29\ ms$
$v_{user} = 50\ km/h$	$\frac{\lambda}{8}_{temporal} = 14\ ms$	$\frac{\lambda}{8}_{temporal} = 18\ ms$

Moreover, although the minimum length definition varies in the literature, the component complex envelope variation in the time domain is well defined and determined by the received signal Doppler spread B_d. The Doppler spread represents the bandwidth occupied by the different Doppler shifts of each multipath component. The Doppler spread of the channel is defined by [25] by this expression:

$$B_D = \frac{v f_c}{c} \tag{2.29}$$

where:

- v is the user speed (m/s),
- f_c is the carrier frequency,

- $c = 3.10^8\ m/s$ is the speed of light.

Table 9: Multipath component Doppler spread examples

	L1	L2
5 km/h	$B_D = 7\ Hz$ $1/B_D = 143\ ms$	$B_D = 6\ Hz$ $1/B_D = 167\ ms$
30 km/h	$B_D = 44\ Hz$ $1/B_D = 23\ ms$	$B_D = 34\ Hz$ $1/B_D = 29\ ms$
50 km/h	$B_D = 73\ Hz$ $1/B_D = 14\ ms$	$B_D = 57\ Hz$ $1/B_D = 18\ ms$

Therefore, in order to guarantee a correct sampling of the multipath component and a correct correlation between consecutive samples, the Rayleigh independent variables are generated at least λ/8 meters and are filtered by a Doppler filter with a cut-off frequency equal to B_d [28]. The Doppler filter suggested by [28] is a Butterworth filter, more realistic than a Jakes filter conventionally used.

$$|H_{Butt}(f)|^2 = \frac{B}{1 + \left(\frac{f}{f_{cut}}\right)^{2k}} \tag{2.30}$$

where:

- k is the filter order,
- $f_{cut} = B_D$ is the cut-off frequency,
- B is a constant used to force the overall filter energy equal to one so that the standard deviation of the complex Gaussian process is not changed after filtering.

Finally, since the direct signal component and the multipath component have to be added in order to generate the received signal, the direct signal component is generated at the same frequency than the multipath component, and its variations are then smooth by a Butterworth filter with a cut-off frequency significantly smaller than the overall channel generation frequency ($f_{cut} = 1/t_{corr}$).

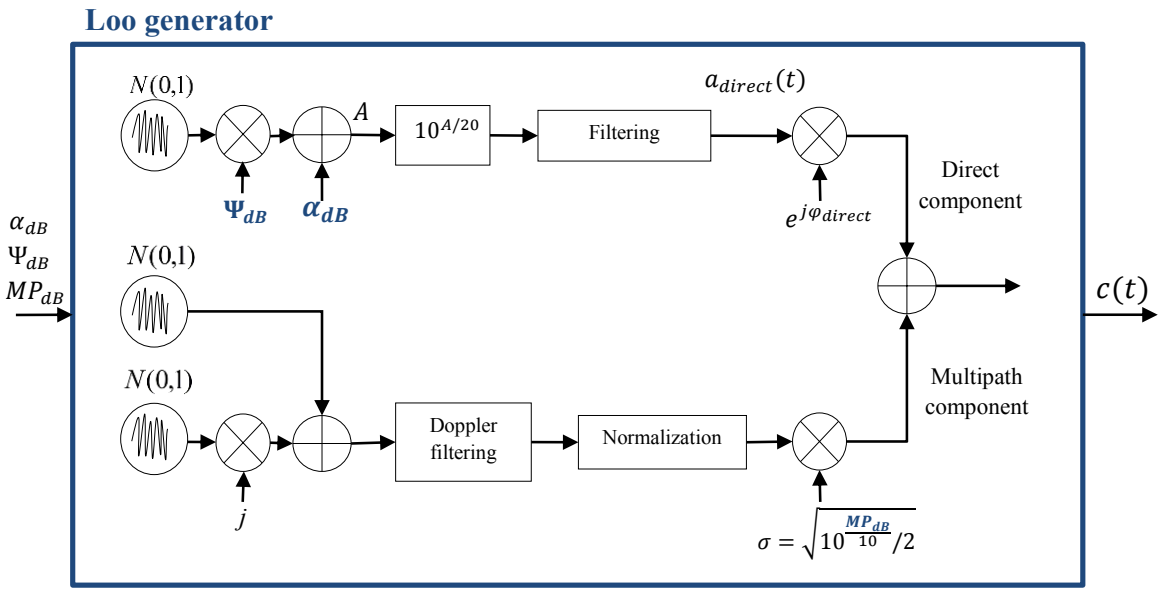

Figure 34: Generation of samples following a Loo distribution

3-state model: The Perez-Fontan model classifies the received signal into three states, according to the impact level of the propagation channel.

More specifically, each state corresponds to a particular environment configuration, representative to the strength of the shadowing/blockage effect on the received direct signal component. The first state corresponds to LOS visibility conditions, the second state to a moderate shadowing and the third state to a deep shadowing. Therefore, each state has associated a different set of Loo parameters for a fixed type of environment, a fixed satellite elevation angle and a fixed signal carrier band.

The state changes are very slow (compared with the direct and multipath signal components amplitude and phase variation) because they represent the transition between two different imposing obstacles [26]. The state frame length l_{frame} corresponds to the average of the state length, in the order of 3-5 meters [27].

The state transitions are dictated by a first-order Markov chain [27], defined by the state transition probability matrix *P* (see Figure 35), provided by [26].

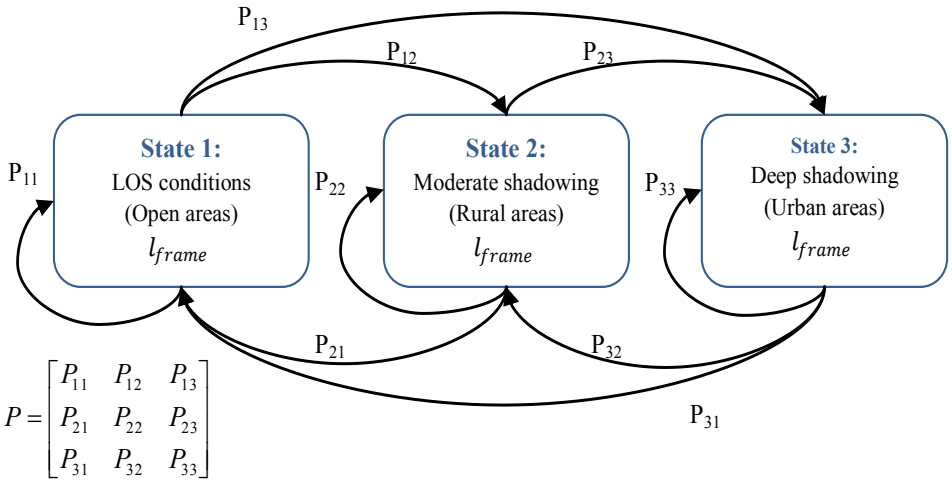

Figure 35: First-order Markov chain state transitions process

This model was referenced in the COST (European Cooperation in the field Of Scientific and Technical Research) in March 2002. Nevertheless, this model presents some limitations.

2.3.2.2 An Evolution of the Perez-Fontan model: the Prieto Model

The Perez-Fontan 3-state model presents some limitations (the states are not enough representative of reality) which involve a mismatch with reality [31]. R. Prieto-Cerdeira proposed an evolution of the Perez-Fontan model, using it as a baseline. The same ensemble of measured data which was used by Perez-Fontan has been re-analysed, considering new assumptions:

- A classification in two states instead of three for the Perez Fontan model, and
- Loo parameters defined by random variables instead of constant values for the Perez-Fontan model.

The mathematical core model is thus similar but two major differences appear.

2-state model: In the Prieto model, environmental conditions are classified in two states instead of the three for the Perez Fontan model:

- "Good" for LOS to moderate shadowing, and
- "Bad" for moderate to deep shadowing.

These two states represent two different macroscopic shadowing/blockage behavior [28].

The state transitions are dictated by a semi-Markov model: the state changes are not anymore ruled by transition probabilities, we directly move from one state to the other (see Figure 36).

The duration of each state τ_{state} is defined by a statistical law. Reference [28] suggests that the duration of each state follows a Log-Normal distribution, whatever the state Good or Bad. The parameters of the Log-Normal distribution depend on the propagation environment. The database used in this thesis to determine the Log-Normal parameters has been extracted from [28]. They depend on the environmental conditions:

- The type of environment (semi-urban, urban, deep urban…),
- The satellite elevation angle,
- The signal carrier band,
- The channel states.

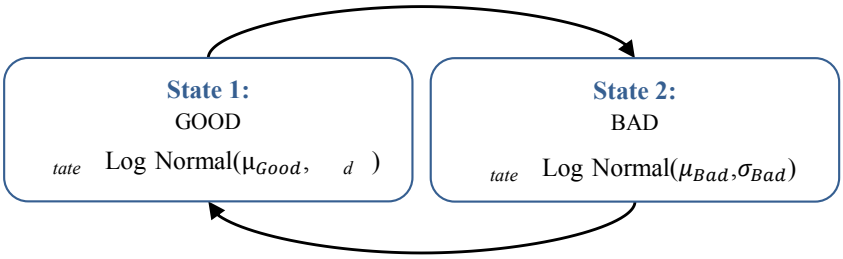

Figure 36: Semi-Markov chain state transitions process

The transitions between states have to be controlled in order to represent the reality as faithfully as possible, avoiding unrealistic jumps of the direct component amplitude. To do so, a maximum slope of 5 dB/m of the direct component is imposed [28].

Loo parameters generation: To compensate the reduction in the number of states (from three to two), both states of the Prieto model are allowed to take up a wide range of possible parameters values, compared to the Perez-Fontan model for which the parameters values were constant. The Loo parameters designated by (α_{db}, Ψ_{db}, MP_{db}) in the Perez Fontan model are noted as (M_A, Σ_A, MP) in the Prieto model [28]. They represent the same physical characteristic in dB but their numerical value is determined in a different way.

The new analysis led by Prieto on the same measurement campaigns as Perez Fontan, shows that the probability distribution which best fits the experimental trend of each one of the Loo parameters value, M_A, Σ_A and MP is Gaussian. Therefore, in order to determine the Loo parameters values associated to each new state, a new random number following a Gaussian distribution should be generated for each Loo parameter instead of determining always the same constant parameters value for a given state. Moreover, the Gaussian distribution for each Loo parameter is different, with its mean noted as μ and its standard deviation as σ. However, analyzed data demonstrates that the standard deviation of the direct signal component Σ_A and its mean M_A are dependent: M_A conditions Σ_A. In order to model this relationship, the Gaussian parameters (μ, σ) associated to Σ_A are determined through second degree polynomials evaluated at M_A. The determination of the Loo parameters are summarized in Table 10.The database used in this paper to determine μ_1, σ_1, a_1, a_2, a_3, μ_3 and σ_3 has been extracted from [28], according to the simulated environmental conditions:

- The type of environment (semi-urban, urban, deep urban…),
- The satellite elevation angle,
- The signal carrier band,
- The channel states.

Table 10: Loo parameters generation

M_A ~ Gaussian(μ_1, σ_1)	μ_1 is fixed, depending on environmental conditions
	σ_1 is fixed, depending on environmental conditions
Σ_A ~ Gaussian(μ_2, σ_2)	❖ $\mu_2 = a_1 * M_A^2 + a_2 * M_A + a_3$ ❖ a_1, a_2, a_3 are fixed, depending on environmental conditions
	❖ $\sigma_2 = b_1 * M_A^2 + b_2 * M_A + b_3$ ❖ b_1, b_2, b_3 are fixed, depending on environmental conditions
MP ~ Gaussian(μ_3, σ_3)	μ_3 is fixed, depending on environmental conditions
	σ_3 is fixed, depending on environmental conditions

The generation of the received signal complex envelope samples following a Loo distribution for the Prieto channel model is exactly the same as for the Perez-Fontan model (Figure 34). The only difference between the channel models is the Loo parameters value determination as it is illustrated in Figure 37.

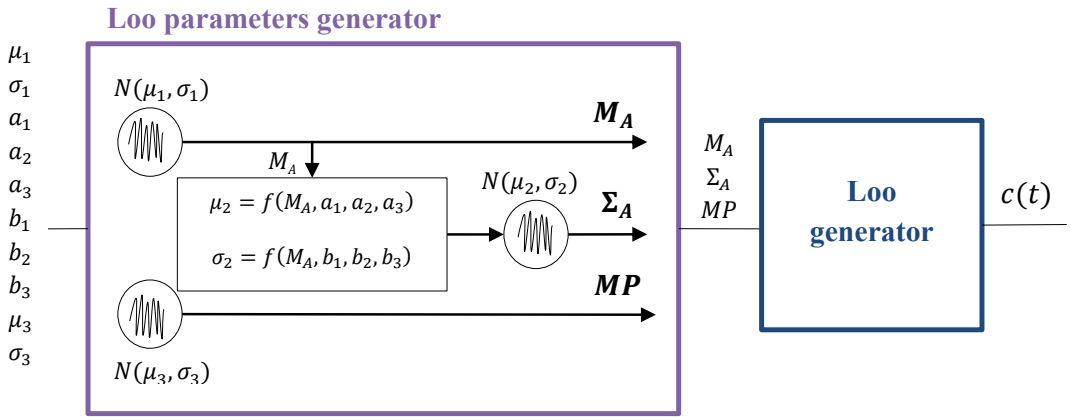

Figure 37: Generation of Loo samples for the Prieto channel model

Figure 38 represents an example of simulated samples with these particular conditions:

Table 11: Simulated conditions for the Prieto channel model

	Prieto
Sampling frequency	20 kHz
Environment type	Urban
User Speed	50 km/h
Band of the measurements	S-band
Satellite Elevation Angle	40°

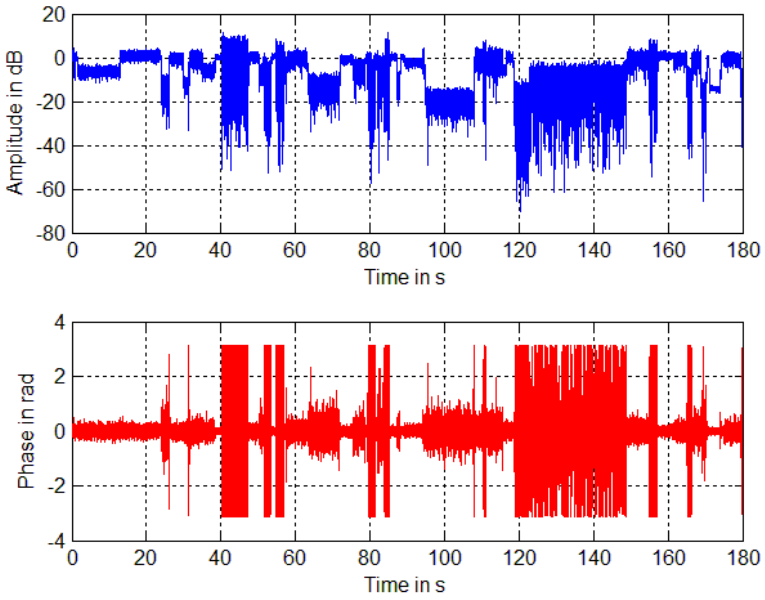

Figure 38: Amplitude and phase of the Prieto channel model simulated samples

However this model presents some limits. Firstly it is a narrowband model, which does not take into account the delay between the LOS signal and the echoes. And in addition, the databases used for the statistic distributions parameters values come from old measurement campaigns (low resolution, satellite azimuth angle missing).

2.3.3 The DLR Propagation Channel Model

The propagation channel model described in this section is wideband, contrary to the previous propagation channel model which is narrowband. The difference lies in the multipath component model. On one hand, in the Prieto channel model, all the components are considered to be received at the same instant of time, the multipath echoes being added among them, resulting into a Rayleigh Distribution, and added to the LOS component as well. In this way, the time delay between the LOS and each multipath echo is not represented and the resulting received component follows a Loo distribution. On the other hand, in the DLR propagation channel model, the time delay between the LOS component and each multipath echo is modeled: each component is considered separately. Indeed, the DLR model targets satellite navigation systems and has been specially designed in order to study the multipath effect in GNSS receivers [32].

Therefore, the propagation channel impulse response provided by the DLR model [33] is represented by the sum of the LOS component and the different multipath echoes (equation (2.31)), each echo being associated with an amplitude, a phase and a time delay (delay between the LOS component and each echo).

$$h_e(t,\tau) = c_{direct}(t)\delta\big(\tau - \tau_{direct}(t)\big) + \sum_{l=1}^{L} c_l(t)\delta(\tau - \tau_l(t)) \tag{2.31}$$

where:

- $c_{direct}(t) = a_{direct}(t)e^{j\varphi_{direct}(t)}$ is the channel impact on the direct signal component,
- $\tau_{direct}(t)$ is the direct propagation time,
- L is the number of echoes,
- $c_l(t) = a_l(t)e^{j\varphi_l(t)}$ is the channel impact on the *l*th echo (or multipath),
- $\tau_l(t)$ is the propagation time of the *l*th echo.

2.3.3.1 Measurement campaign

In 2002, the DLR decided to start by performing a large measurement campaign in Munich and in a small town around Munich. The real innovation of this campaign is in the high delay resolution in the order of a few nanoseconds, which permits to distinguish the different echoes. The DLR then pull out statistical results from this measurement campaign [34] and provided a channel model [35]. The technical breakthrough provided by this model is the wideband characteristic.

Table 12: Characteristics for the DLR measurement campaign

Institution	Transmitter platform	Frequency	Bandwidth	Environments	Elevation	Azimuth	Antenna beam width	Application
DLR 2002	A Zeppelin	1510 MHz (L band)	100 MHz	Large city (Munich) Small town Countryside Motorway Country road	5° to 80°	0° to 180°	180°	Car Pedestrian

2.3.3.2 Modeling

In order to provide the impulse response of the propagation channel, the DLR model generates an artificial scenario representing the characteristics of a given urban environment (see Figure 39) where a user can move, with potential obstacles to the received signal: buildings, trees, lampposts and reflectors.

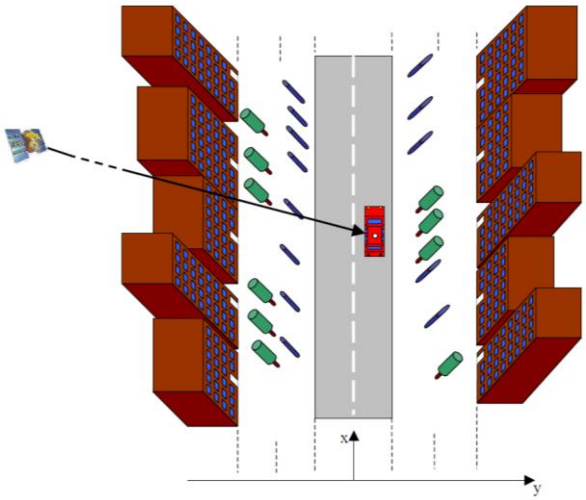

Figure 39: Scene example generated by the DLR propagation channel model [36]

The receiver movement and speed can be parameterized by the user. The hypothesis done by this channel model is that a real user in most cases does move parallel along the road direction. Therefore the user heading in the model is always equal to the direction of the road, as it is showed in Figure 40.

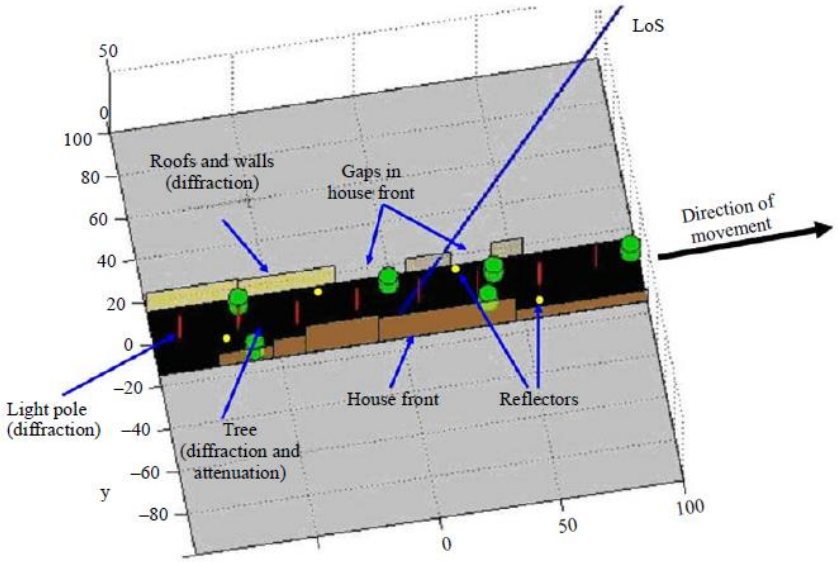

Figure 40: Synthetic environment [35]

These obstacles are statistically generated but the attenuation, the phase and the delay associated to the LOS and multipath components are partly deterministically determined by ray tracing and geometric techniques.

The statistical part of the model comprises [33]:

- The house front, tree and lamp post generation in the artificial scenery,
- The position dependent LOS signal power variations in the shadow of tree tops,
- The position of reflectors dependent on the satellites azimuth and elevation,
- The mean power of echoes depending on their distance to the receiver and on the satellite elevation,
- Rice factor and bandwidth of echo signals depending on the satellite elevation,
- The life span of echoes depending on the satellite elevation,
- The number of coexisting echoes in the channel depending on the satellite elevation,
- And the movement of reflection points, also depending on the satellite elevation.

The deterministic part of the model comprises [33]:

- The diffraction of the LOS signal on houses, tree trunks and lamp posts,
- The delay of diffracted signals received in the shadow of houses,
- The mean attenuation through tree tops,
- And the delay and Doppler shift trends of echo signals due to the receiver and reflector movement.

2.3.3.2.1 LOS behavior modeling

The LOS can be affected by houses, trees and lamp posts. Each of these obstacles are statistically (Gaussian distribution) generated and placed, but their resulting attenuation is deterministic (except for the trees whose treetop behavior is statistically modeled) [36].

The house fronts attenuation is computed thanks to the knife edge model and the associated delays are deduced from the scenery geometry [36]. The lamp posts and tree trunks attenuation is computed thanks to the double knife edge model. The relative delays of the diffracted signals are so small that they are neglected [36]. The attenuation coming from tree tops is computed thanks to the multiplication of a deterministic process (geometrical calculation), and a statistical process (Rice fading) [36].

Sometimes the LOS delay differs from zero and several LOS echoes are considered. This particular representation is considered if the LOS is supposed to be diffracted at a house front [36].

2.3.3.2.2 Multipath component behavior modeling

Then, to model the multipath echoes, reflectors (see Figure 40) are added in the artificial scene, as infinitively small spheres with a given attenuation to the direct path, radiating equally in any direction [36]. A reflector is initialized at a random position. When the receiver moves along the street in the artificial scenery, the path excess delay and the Doppler offset phase of the echo are calculated geometrically [36].

The attenuation associated to each echo is statistically determined. From the results analysis of the measurement campaign, the envelope of each echo signal seems to follow in average a Rician distribution [37]. This process is thus modeled by a Rician distribution. For more details, see [37].

2.3.3.3 Matlab software

The DLR urban propagation channel model has been implemented on Matlab by the DLR and is freely accessible on the DLR website [38]. The model output is a complex time-variant channel impulse response (see equation (2.31)) with up to 80 discrete rays [33].

The outputs of the DLR channel model are thus:

- The channel impact (envelope and phase) of each tap represented by a complex number $c_l(t)$,
- The associated delays between the LOS and each tap $\tau_l(t)$. Normally by definition, the LOS delay is equal to zero. If the LOS is diffracted by a house front, this value will be not null.

A high number of inputs are configurable in the software in addition to the classical parameters, such as the distance from road middle, the Gaussian parameters shaping the buildings and houses (height, width, distance from road middle, gap between two buildings…) and trees and lampposts (height, diameter, distances from the road and buildings…)

2.3.3.4 Generated DLR Channel Model Example

Figure 41, Figure 42, Figure 43 represent an example of simulated samples with these particular conditions:

Table 13: Simulated conditions for the Prieto channel model

	DLR
Sampling frequency	20 kHz
Environment type	Urban
User Speed	50 km/h
Satellite Elevation	40°
Satellite Azimuth Angle	0°, 45°, 90°

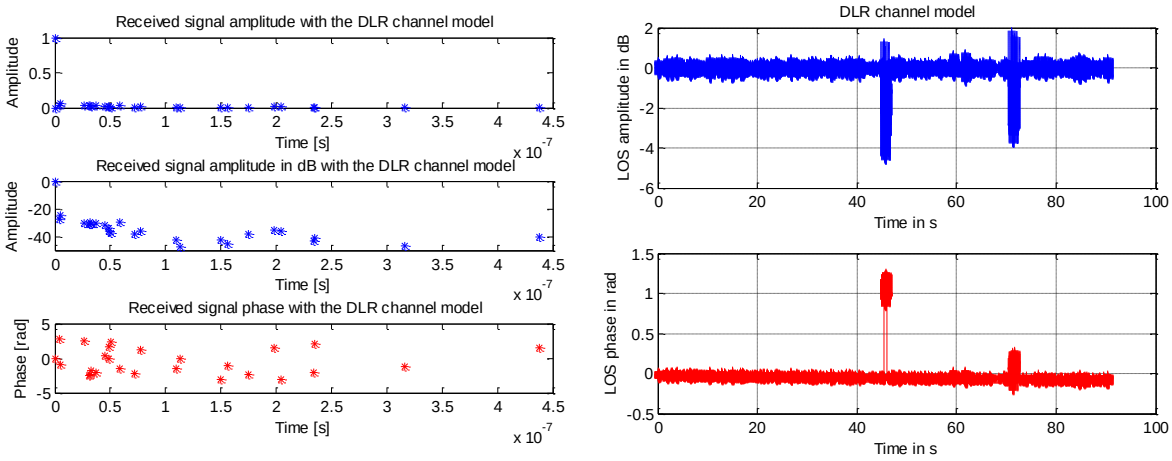

Figure 41: a) DLR channel model CIR example, with 0° of azimuth angle - b) Amplitude and phase of the DLR channel model simulated samples, with 0° of azimuth angle

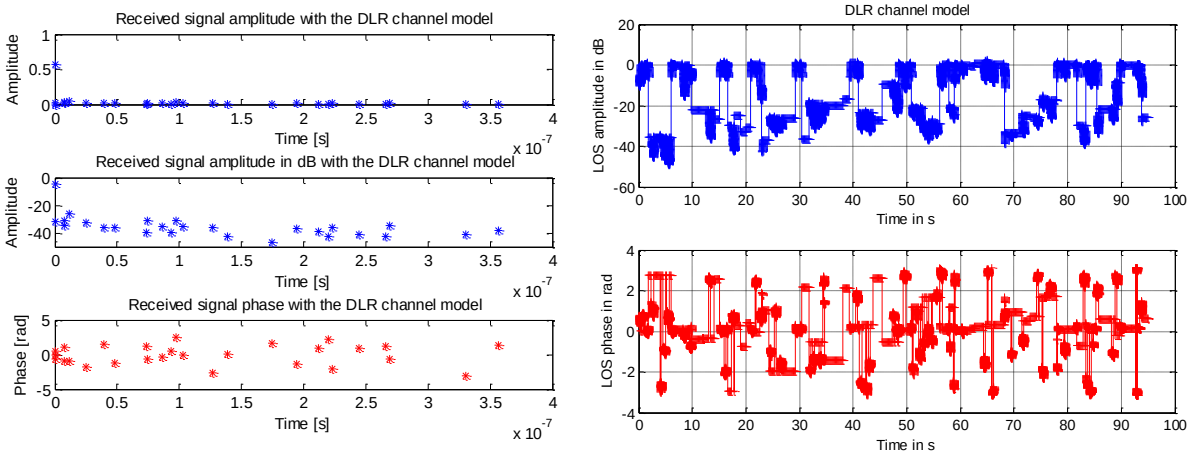

Figure 42: a) DLR channel model CIR example, with 45° of azimuth angle - b) Amplitude and phase of the DLR channel model simulated samples, with 45° of azimuth angle

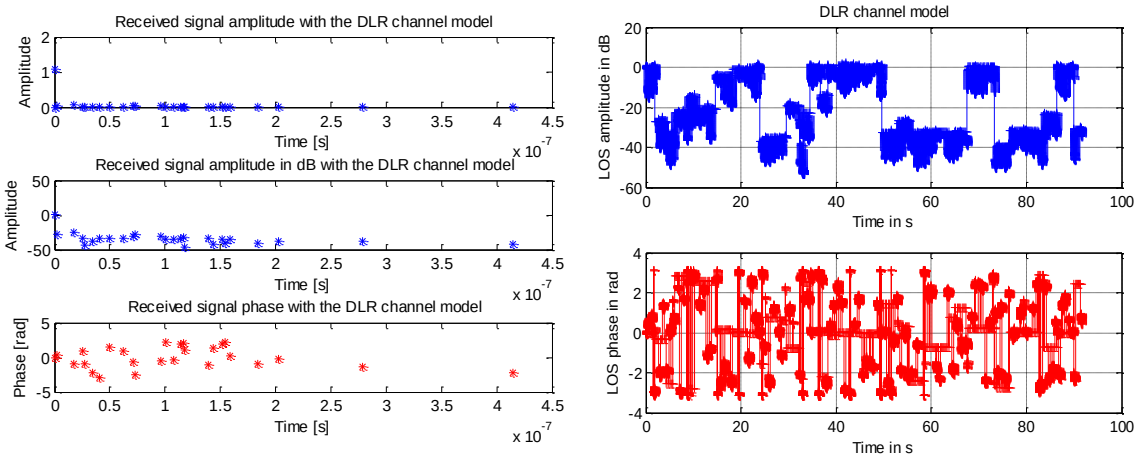

Figure 43: a) DLR channel model CIR example, with 90° of azimuth angle - b) Amplitude and phase of the DLR channel model simulated samples, with 90° of azimuth angle

Finally, this model is the reference wideband model for the ITU (International Telecommunication Union). It is really realistic and seems to be the most appropriate in the navigation application case [39].

Nevertheless, the amount of data necessary to generate enough time series to do statistics with this model is important, as well as the time dedicated to the simulations.

2.3.4 Conclusion

The main characteristics of the both urban LMS propagation channel models Perez-Fontan/Prieto and DLR are summarized in Table 14.

Table 14: Main different characteristics between the Perez-Fontan/Prieto and DLR propagation channel models

	Perez-Fontan/Prieto	DLR
Model Type	Statistical	Hybrid: statistical/deterministic
Multipath Modeling	Narrowband	Wideband
Measurement Campaigns Date	1990	2002
Calculation Burden	Practicable	Heavy and time-consuming

It seems that because its wideband characteristic, the DLR propagation channel model is more realistic than the Perez-Fontan/Prieto model which does not represent the multipath delays. Nevertheless, the DLR propagation channel model is heavy and very time-consuming which represents a real drawback. In comparison, the Prieto propagation channel model seems more practicable.

Another difference concerns the emitted satellite azimuth angle, which is a parameter in the DLR model whereas it is not in the Perez-Fontan/Prieto model. It seems that this model does not take into account the dependence between the generated propagation model and the emitted satellite azimuth angle since the measurement campaigns conducted to develop this model did not allowed it. The azimuth angle can thus be considered as a mean value for the Perez-Fontan/Prieto model.

Because of these differences, both propagation channel models Prieto and DLR will be used for simulations. The Prieto model has been entirely developed in C language to be integrated into the simulator whereas the DLR model is freely accessible in Matlab. The DLR model samples have thus been generated and stored into a file which has been then used in the C language simulator.

The simulations with the Perez-Fontan/Prieto model were conducted assuming a S-band signal since the L-band Prieto channel model parameters [28] seemed to not represent faithfully the real propagation channel.

The parameters used in the DLR model scene representation were determined to match the urban environment in the city center of Munich [31].

Chapitre 3: SiGMeP Simulator Development

The main objective of this PhD thesis is to analyse and to improve current and future GNSS signals demodulation performance in urban environments. GNSS signals demodulation performance can be obtained by using real measurements or by running simulations. Although real measurements should be used for final performance tests, simulations are very important for several reasons:

- Future GNSS signals such as Galileo E1 OS or GPS L1C are not yet available and thus it is not possible to calculate their performance with real measurements. Galileo E1 OS or GPS L1C signals have been especially designed for urban propagation channels [1] and they are expected to have better demodulation performance than current GNSS signals. Therefore, it is particularly interesting to provide their demodulation performance in urban environments and to use it as a benchmark in order to assess the new GNSS signal designs proposed in this PhD research context, which demodulation performance can only be tested by simulations.
- The simulations parameters are totally controlled contrary to the measurements conditions (such as the satellites position with the elevation and azimuth angles, the carrier to noise ratio C/N_0, the user environment, the receiver parameters),
- New configurations can be easily tested with the aim of finely analysing the GNSS signals demodulation performance in urban environments. Thanks to this possibility, new receiver algorithms and new emitted signal structures can be tested and improved.

Therefore, a simulator has been developed during this PhD thesis. The simulator is a C language-software which computes the demodulation performance of any GNSS signal in a realistic urban LMS propagation channel model. For this purpose, the narrowband Perez-Fontan/Prieto and the wideband DLR propagation channel models presented in Chapter 2 have been integrated into the simulator. This simulation tool is called SiGMeP, which stands for Simulator for GNSS Message Performance and is presented in section 3.3.

The following sections present the general GNSS receiver processing, emphasizing on the correlation process in section 3.2. This is an essential function of the GNSS receiver since the correlation is the fundamental operation of the receiver signal processing block and of the receiver demodulation process. The classical correlator output mathematical model is provided. However, this PhD thesis focusing on urban environments, it will be showed that the classical correlator output model is not adapted in our context when considering classical correlation duration. Thus, the use of partial correlation is proposed. This concept is explained in section 3.2.2.

Finally, for a practical use of the simulator, simulations are desired to be as short as possible but without degrading the simulated results. Thus, investigations have been made with the simulator in order to determine the optimized duration of the partial correlations. This is the aim of section 3.4.

3.1 GNSS Receiver Processing Presentation

The aim of this section is to present the GNSS receiver general structure. To do that, the GNSS emitted signal mathematical expression is firstly given. Then, the urban propagation channel model impact on this emitted signal is reminded, through the channel impulse response. And finally, the mathematical expression of the received signal considered after the conversion into a digital signal is provided.

3.1.1 Emitted Signal

As it has been presented in Chapter 2, the mathematical expression of future GNSS signals written in equations (2.5) and (2.8) is separated into two components: the data component which carries the information data symbols, and the pilot or dataless component, which has been designed to allow the implementation of data sensitive discriminators for the PLL and to allow the extension of the coherent integration time for the PLL, DLL and FLL [2]. Each component is spread by a spreading code: $C_{data}(t)$ and $C_{pilot}(t)$ and emitted on a carrier frequency, as it has been described in Chapter 2.

In this chapter, the signal will be represented through its equivalent low-pass expression [25]. The equivalent low-pass emitted signal can thus be mathematically expressed by:

$$s_e(t) = A_{data}\, C_{data}(t)\, D(t) + A_{pilot}\, C_{pilot}(t) \tag{3.1}$$

where:

- $s_e(t)$ is the emitted modern GNSS signal complex envelope (see Annex D),
- A_{data} and A_{pilot} are respectively the data and pilot emitted amplitudes,
- $C_{data}(t)$ and $C_{pilot}(t)$ correspond to the spreading codes,
- $D(t)$ is the data stream, protected by a channel code.

3.1.2 Propagation Channel

The propagation channel can be modeled by the AWGN, the narrowband Perez-Fontan/Prieto or the wideband DLR channel models (presented in Chapter 2). As it has been detailed in Chapter 2, the equivalent low-pass received signal r_e after its passage through the propagation channel can be linked to the equivalent low-pass emitted signal s_e by the equivalent low-pass channel impulse response h_e:

$$r_e(t) = \int_{-\infty}^{+\infty} h_e(t;\tau) s_e(t-\tau) d\tau + n(t) \tag{3.2}$$

with $n(t)$ the equivalent low-pass AWGN, and with h_e having a different mathematical expression for each propagation channel model type:

- Narrowband channel model: Perez-Fontan/Prieto

$$h_e(t;\tau) = c(t)\delta\big(t - \tau_{direct}(t)\big) \tag{3.3}$$

with:

$$c(t) = a_{channel}(t)e^{j\varphi_{channel}(t)} = a_{direct}(t)e^{j\varphi_{direct}(t)} + a_{multipath}(t)e^{j\varphi_{multipath}(t)} \quad (3.4)$$

where:

- $c(t)$ is the complex envelope of the overall received signal (corresponding to the propagation channel impact),
- $\tau_{direct}(t)$ is the LOS propagation time,
- $a_{channel}(t)$ is the channel attenuation,
- $\varphi_{channel}(t)$ is the channel phase,
- $a_{direct}(t)$ is the direct signal component amplitude and $\varphi_{direct}(t)$ is its Doppler phase,
- $a_{multipath}(t)$ is the multipath component amplitude and $\varphi_{multipath}(t)$ is its phase.

➢ Wideband channel model: DLR

$$h_e(t,\tau) = c_{direct}(t)\delta\big(\tau - \tau_{direct}(t)\big) + \sum_{l=1}^{L} c_l(t)\delta(\tau - \tau_l(t)) \quad (3.5)$$

where:

- $c_{direct}(t) = a_{direct}(t)e^{j\varphi_{direct}(t)}$ is the channel impact on the direct signal component,
- $\tau_{direct}(t)$ is the direct propagation time,
- L is the number of echoes,
- $c_l(t) = a_l(t)e^{j\varphi_l(t)}$ is the channel impact on the *l*th echo (or multipath),
- $\tau_l(t)$ is the propagation time of the *l*th echo.

For the sake of simplicity, the narrowband propagation channel model will be firstly considered, and the wideband case will be then derivate from the narrowband case.

The data component is separated from the pilot component. According to equation (3.1), each component can thus be written as:

$$s_{e\,comp}(t) = A\,C_{comp}(t)\,d_{comp}(t) \quad (3.6)$$

where:

- $comp$ refers to the data or pilot component, associated with A_{data} and $C_{data}(t)$ for the data component and with A_{pilot} and $C_{pilot}(t)$ for the pilot component,
- $d_{comp}(t) = \begin{cases} D(t) for\ the\ data\ component \\ 1\ for\ the\ pilot\ component \end{cases}$, with $D(t)$ the data stream.

The received signal after its passage through a narrowband propagation channel can thus be written as (without specifying which signal component is being inspected for simplification purposes):

$$r_{e_{nb}}(t) = c(t)A\,C(t-\tau)\,d(t-\tau) \tag{3.7}$$

where:

- $r_{e_{nb}}(t)$ is the equivalent low-pass received signal after its passage through the narrowband propagation channel.

3.1.3 Receiver Processing

After its passage through the propagation channel, the signal is received by the GNSS receiver antenna. The received signal undergoes then several processings, as it is illustrated in Figure 44: the front-end components, the signal acquisition and tracking, and finally the data processing consisting in demodulating the navigation message.

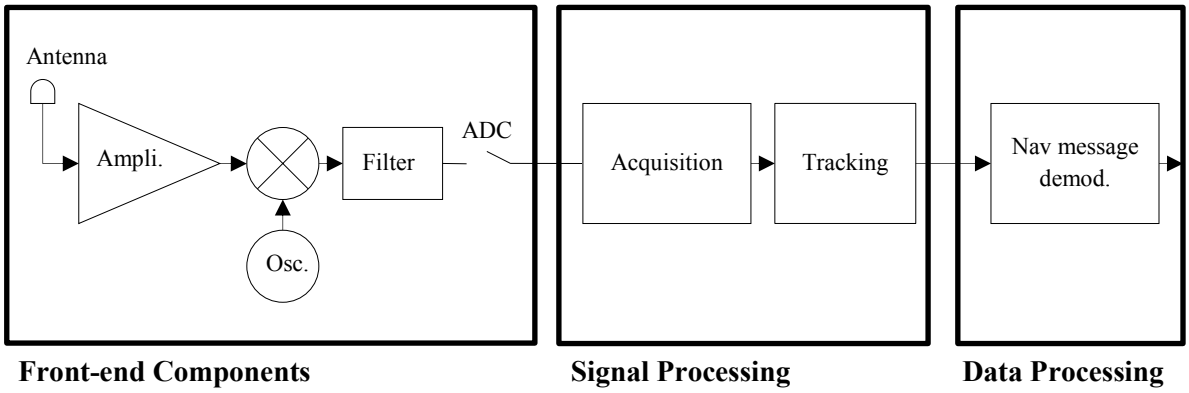

Figure 44: Real GNSS receiver block diagram

Assuming that the filter let pass all the useful signal and that the Analog to Digital Converter (ADC) block directly provides the sampled received signal [40], the noiseless sampled received signal when transmitted through a narrowband mobile channel at the ADC output can be modelled as [41]:

$$r_{nb}[k] = r_{nb}(kT_s) = \frac{A}{2}\,a_{channel}[k]\,C(k-\tau[k])\,d(k-\tau[k])cos(2\pi f_{IF}k + \varphi_{channel}[k]) \tag{3.8}$$

where:

- f_{IF} is the intermediate frequency, normalized by the sampling frequency. Indeed, the RF received signal has been translated around an intermediate frequency to help the signal processing.

For a wideband mobile channel, the noiseless sampled received signal at the ADC output can be modelled as:

$$r_{wb}[k] = \frac{A}{2}\sum_{l=1}^{L} a_{channel}[k;l]\, C(k-\tau[k;l])\, d(k-\tau[k;l])cos(2\pi f_{IF}k + \varphi_{channel}[k;l]) \quad (3.9)$$

Then, the signal passes through the signal processing block, starting by the acquisition. The acquisition purpose is to identify all satellites visible by the user and to provide a first approximation of the code delay $\tau[k]$, the Doppler frequency generated by the motion of the emitting satellite relative to the receiver, and the oscillators' drift. Then, the purpose of the tracking is to refine these values and to track them, in order to be able to demodulate the navigation message [41] and in order to provide the code/phase pseudo-range measurements. In fact, the fundamental and common processing of each of these stages (acquisition, tracking and demodulation) is the correlation. Thus, the next section will focus on the correlation description.

3.2 Correlation Process Description

The correlation operation is illustrated by Figure 45 and then mathematically derived considering the narrowband propagation channel model first, and then the wideband model.

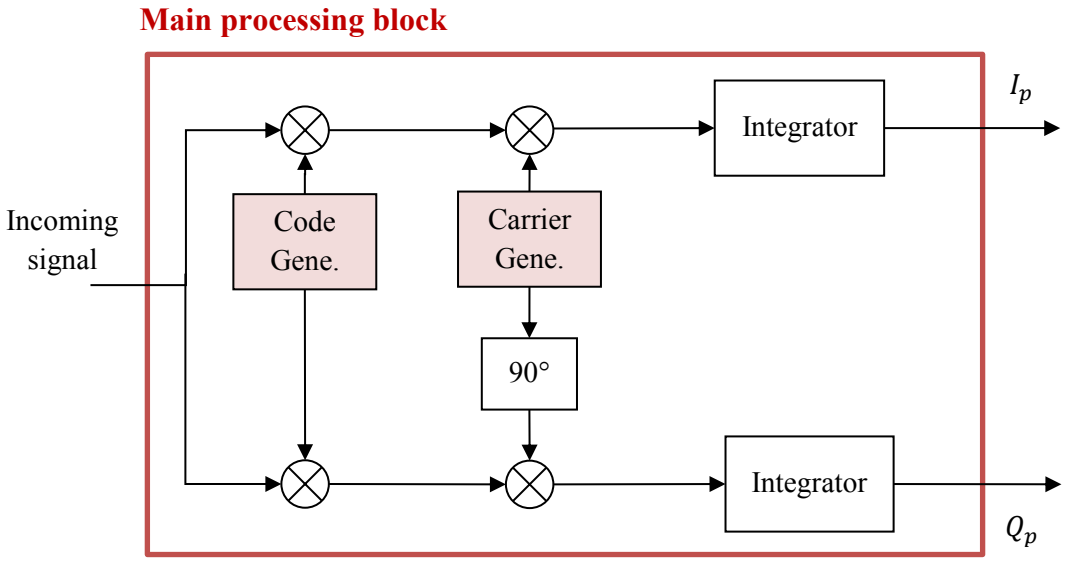

Figure 45: Main processing block for acquisition and tracking processes

The received sampled signal $r_{nb}[k]$ of equation (3.8) is multiplied by a local code replica C_{rep} delayed by the same code delay $\hat{\tau}[k]$ than the received signal, determined during the acquisition process:

$$r_{2_{nb}}[k] = r_{nb}[k]\, C_{rep}(k-\hat{\tau}[k]) \quad (3.10)$$

$$r_{2_{nb}}[k] = \frac{A}{2} a_{channel}[k] C(k-\tau[k]) C_{rep}(k-\hat{\tau}[k]) d(k-\tau[k]) cos(2\pi f_{IF}k + \varphi_{channel}[k]) \quad (3.11)$$

Then the received signal is multiplied by a local cosine and sine carrier replica with the same phase than the received signal (see Figure 45) in order to create the in-phase and quadrature components:

$$I_{nb}[k] = r_{2_{nb}}[k]\, cos\big(2\pi f_{IF} k + \varphi_{rep}[k]\big) \tag{3.12}$$

Taking into account the fact that the integrator will act as a low pass filter, the expression can be simplified into:

$$I_{nb}[k] = \frac{A}{2} a_{channel}[k] C(k - \tau[k]) C_{rep}(k - \hat{\tau}[k]) d(k - \tau[k])\, cos\big(\varphi_{channel}[k] - \varphi_{rep}[k]\big) \tag{3.13}$$

Then the correlated samples corresponding to $I_{nb}[k]$ and $Q_{nb}[k]$ are accumulated over T_I seconds, the Integration Time [41].

$$I_{2_{nb}}(i) = \frac{1}{M_E} \sum_{k=1}^{M_E} I_{nb}[k] \tag{3.14}$$

where:

- M_E is the number of samples per Integration Time T_I.

The correlation duration is classically chosen as a multiple of the spreading code sequence duration. Indeed the minimum value of T_I is currently equal to the spreading code sequence duration (see Table 15 for some examples [9][19][17]).

Table 15: Spreading code sequence duration for several GNSS signals

GNSS signal	Data component spreading code sequence duration	Data symbol duration
GPS L1 C/A	1 ms	20 ms
GPS L2C	20 ms	20 ms
GPS L1C	10 ms	10 ms
Galileo E1 OS	4 ms	4 ms

According to [41], since the accumulation process serves as a time average and since the spreading codes C and C_{rep} can be considered as random variables, the result (3.14) needs to be evaluated as a mean. The prompt in-phase and quadrature correlator outputs $I_{p_{nb}}$ and $Q_{p_{nb}}$ are thus equal to:

$$I_{p_{nb}}(i) = E\big[I_{2_{nb}}(i)\big] \tag{3.15}$$

$$I_{p_{nb}}(i) = \frac{1}{M_E} \sum_{k=1}^{M_E} \frac{A}{2} a_{channel}[k] E\big[C(k - \tau[k]) C_{rep}(k - \hat{\tau}[k])\big] d(k - \tau[k])\, cos\big(\varphi_{channel}[k] - \varphi_{rep}[k]\big) \tag{3.16}$$

The $E\left[C(k-\tau[k])C_{rep}(k-\hat{\tau}[k])\right]$ term of equation (3.16) is in fact the autocorrelation function of the spreading code:

$$I_{p_{nb}}(i) = \frac{1}{M_E}\frac{A}{2}R\left[\varepsilon_{\tau_i}\right]\sum_{k=1}^{M_E} a_{channel}[k]d(k-\tau[k])\,cos\left(\varphi_{channel}[k]-\varphi_{rep}[k]\right) \tag{3.17}$$

where:

- $\varepsilon_\tau[k] = \tau[k] - \hat{\tau}[k]$ is the code delay estimation error,
- $R\left[\varepsilon_{\tau_i}\right]$ is the autocorrelation function of the spreading code, in ε_{τ_i}.

The spreading code autocorrelation function is different according to the signal modulation; it does not have the same shape whether it is a BOC or a BPSK modulation. Spreading code autocorrelation functions corresponding to several modulations are illustrated in Figure 46 [42].

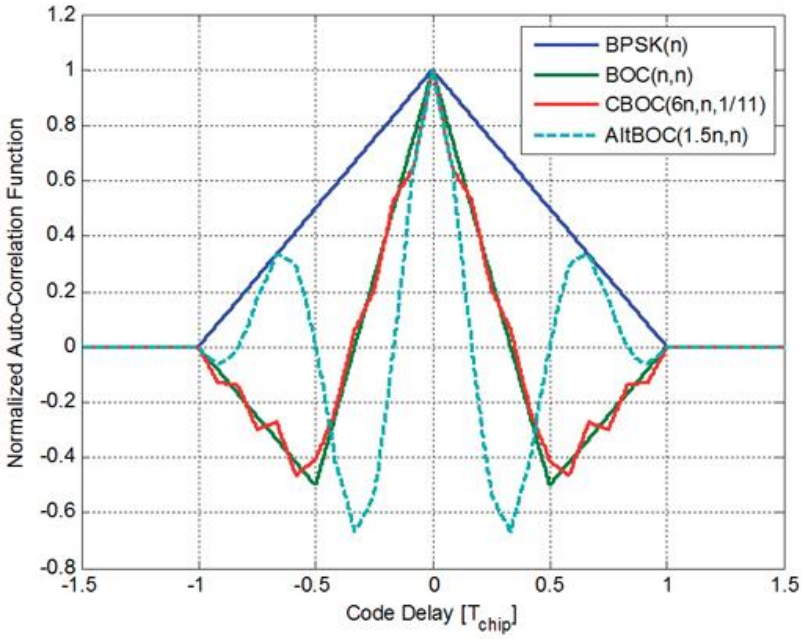

Figure 46: Spreading code autocorrelation functions for different modulations

Since the data symbol duration is equal to or longer than the selected integration time, the $d(k-\tau[k])$ value can be considered as constant and noted d_i for the i-th integration time.

$$I_{p_{nb}}(i) = \frac{1}{M_E}\frac{A}{2}R\left[\varepsilon_{\tau_i}\right]d_i\sum_{k=1}^{M_E} a_{channel}[k]\,cos\left(\varphi_{channel}[k]-\varphi_{rep}[k]\right) \tag{3.18}$$

3.2.1 Classical Correlation Modeling

As it has been derived in the last subsection, the prompt in-phase correlator output $I_{p_{nb}}$ for a narrowband propagation channel model is equal to the mathematical expression (3.18). From this equation, the classical correlator output model will be derived in this section [41].

We consider the following approximation:

$$\sum_{k=1}^{M_E} s[k].T_s \approx \int_0^{T_I} s(t)\,dt \tag{3.19}$$

where:

- T_s is the sampling period and thus $M_E \cdot T_s = T_I$

It gives:

$$I_{p_{nb}}(i) = \frac{A}{2}\, d_i\, R[\varepsilon_{\tau_i}] \frac{1}{T_s M_E} \int_0^{T_I} \left(a_{channel}(t)\, cos\left(\varphi_{channel}(t) - \varphi_{rep}(t)\right)\right) dt \tag{3.20}$$

Then two main assumptions are made to derivate the classical correlator output model:

- The total phase error between the received signal and the local replica is assumed to vary linearly over T_I.

  Thus the Doppler error is considered constant over T_I, as well as the phase error. This assumption can be written as:

  $$\varphi_{channel}(t) - \varphi_{rep}(t) \approx 2\pi\left(f_{Dop} - \hat{f}_{Dop}\right)t + \varepsilon_\varphi \tag{3.21}$$

  where:
  - $\varepsilon_f = \left(f_{Dop} - \hat{f}_{Dop}\right)$ and ε_φ are constant over the integration time.
- The propagation channel amplitude $a_{channel}(t)$ is assumed to be constant over T_I.

Finally, after integration and addition of a white Gaussian noise, we obtain the classical correlator output model for a narrowband propagation channel model [41]:

$$I_{p_{nb}}(i) = \frac{A}{2}\, d_i\, R[\varepsilon_{\tau_i}] a_{channel}(i) \frac{sin\left(\pi\, \varepsilon_{f_i}\, T_I\right)}{\pi\, \varepsilon_{f_i} T_I} cos\left(\pi\, \varepsilon_{f_i} T_I + \varepsilon_{\varphi_i}\right) + n_I(i) \tag{3.22}$$

where:

- n_I and n_Q are the AWGN at the correlator outputs. They follow thus a centered Gaussian distribution $N(0, \sigma_n^2)$ with σ_n^2 equal to [43]:

$$\sigma_n^2 = \frac{N_0}{4\,T_I} \tag{3.23}$$

and N_0 the noise spectral density.

3.2.2 Simulator Correlation Modeling with Partial Correlations

However, as it has been seen in the last section, the standard correlator output model for a signal transmitted through a narrowband mobile channel is only valid when the variation of the incoming signal's parameters is limited. In particular, it is imposed to have constant incoming amplitude and linear Doppler phase error during the integration time T_I.

As a consequence, such assumption might not be valid over long periods for a received signal that went through an urban LMS channel. In these kind of environments, the received signal phase and amplitude change very quickly. It is thus necessary to review this classical model, to adapt it to urban environments constraints and to implement it in the simulator. This section thus proposes to model the correlator outputs according to partial correlations, as it is described below.

This proposed correlator output model from partial correlations can be adapted for narrowband or wideband propagation channel models. Thus, the correlator output model will be firstly derived for the narrowband case and then it will be extended to the wideband case.

The classical correlator output model presented in equation (3.22) will be divided into several terms, corresponding to shorter integration duration referred as $T_{I_{part}}$. Moreover, the Doppler frequency is assumed to be perfectly estimated. The propagation channel amplitude and phase will be integrated over shorter durations, which allows the validation of these both assumptions:

- Assumption 1:

  The total phase error between the received signal and the local replica is assumed to be constant over $T_{I_{part}}$,

  This assumption can be written as:

$$\varphi_{channel}(t) - \varphi_{rep}(t) \approx \varepsilon_\varphi \tag{3.24}$$

  where:
  - ε_φ is constant during the partial integration time.

- Assumption 2:

  The propagation channel amplitude $a_{channel}(t)$ is assumed to be constant over $T_{I_{part}}$.

From equations (3.18), the T_I interval is divided into N portions, each portion lasting $T_{I_{part}}$ seconds, leading to:

$$I_{p_{nb}}(i) = \frac{1}{M_E}\frac{A}{2}R\left[\varepsilon_{\tau_i}\right] d_i . \sum_{n=1}^{N}\left[\sum_{k=1}^{K} a_{channel}[k+(n-1)K]\, cos\left(\varphi_{channel}[k+(n-1)K] - \varphi_{rep}[k+(n-1)K]\right)\right] \quad (3.25)$$

where:

- K is the number of samples per $T_{I_{part}}$,
- N is the number of $T_{I_{part}}$ per T_I,
- Thus, $N.K = M_E$.

$$I_{p_{nb}}(i) = \frac{1}{NK}\frac{A}{2}R\left[\varepsilon_{\tau_i}\right] d_i . \sum_{n=1}^{N}\left[\sum_{k=1}^{K} a_{channel}[k+(n-1)K]\, cos\left(\varphi_{channel}[k+(n-1)K] - \varphi_{rep}[k+(n-1)K]\right)\right] \quad (3.26)$$

Approximation (3.19) is then used, leading to:

$$I_{p_{nb}}(i) = \frac{1}{NK}\frac{A}{2}R\left[\varepsilon_{\tau_i}\right] d_i \sum_{n=1}^{N}\left[\frac{1}{T_s}\int_0^{T_{I_{part}}}\left(a_{channel}(t)\, cos\left(\varphi_{channel}(t) - \varphi_{rep}(t)\right)\right)dt\right] \quad (3.27)$$

$$I_{p_{nb}}(i) = \frac{R\left[\varepsilon_{\tau_i}\right]}{N}\frac{A}{2} d_i \sum_{n=1}^{N}\left[\frac{1}{KT_s}\int_0^{T_{I_{part}}}\left(a_{channel}(t)\, cos\left(\varphi_{channel}(t) - \varphi_{rep}(t)\right)\right)dt\right] \quad (3.28)$$

Then, in order to be able to integrate on the $T_{I_{part}}$ interval we consider that Assumptions 1 and 2 are validated.

$$I_{p_{nb}}(i) = \frac{R\left[\varepsilon_{\tau_i}\right]}{N}\frac{A}{2} d_i \sum_{n=1}^{N}\left[\, a_{channel}[n+(i-1)N]\, cos\left(\varphi_{channel}[n+(i-1)N] - \varphi_{rep}[n+(i-1)N]\right)\right] \quad (3.29)$$

We thus finally obtain the new correlator output model from partial correlations:

$$I_p(i) = \sum_{n=1}^{N} I_{p\,part}(n+(i-1)N) + n_I(i) \quad (3.30)$$

With the expression of $I_{p\,part}(n)$ for the narrowband propagation channel model equal to:

$$I_{p\,part_{nb}}(n) = \frac{R\left[\varepsilon_{\tau_i}\right]}{N}\frac{A}{2}d_i\,a_{channel}(n)\,cos\left(\varphi_{channel}(n) - \varphi_{rep}(n)\right) \tag{3.31}$$

Extending this expression to the wideband propagation channel model when taking into account that the mathematical model of the wideband received sampled signal is the linear addition of delayed and attenuated versions of the emitted signal, and that the correlation process is a linear operation, we obtain:

$$I_{p\,part_{wb}}(n) = \frac{A}{2}d_i\sum_{l=1}^{L}\frac{R\left[\varepsilon_{\tau_i}(l)\right]}{N}a_{channel}(n;l)\,cos\left(\varphi_{channel}(n;l) - \varphi_{rep}(n)\right) \tag{3.32}$$

where:

- L is the number of echoes.

In both cases, the spreading code autocorrelation function can thus be decomposed of several partial correlations lasting $T_{I_{part}}$. It will be assumed that these partial correlations are equal over each portion. For a T_I duration divided into N portions, each portion lasting $T_{I_{part}}$, the partial correlation $R\left[\varepsilon_{\tau_i}\right]_{Partial}$ will be thus written as:

$$R\left[\varepsilon_{\tau_i}\right]_{Partial} = \frac{R\left[\varepsilon_{\tau_i}\right]}{N} \tag{3.33}$$

The received signal will directly modeled at the correlator output in the simulator, with this model using partial correlations to ensure that Assumptions 1 and 2 written before are valid over $T_{I_{part}}$ in an urban environment.

3.3 Simulator Structure Description

The SiGMeP simulator developed in this PhD thesis context is a C language-software which simulates a GNSS signal transmission-reception chain (see Figure 47).

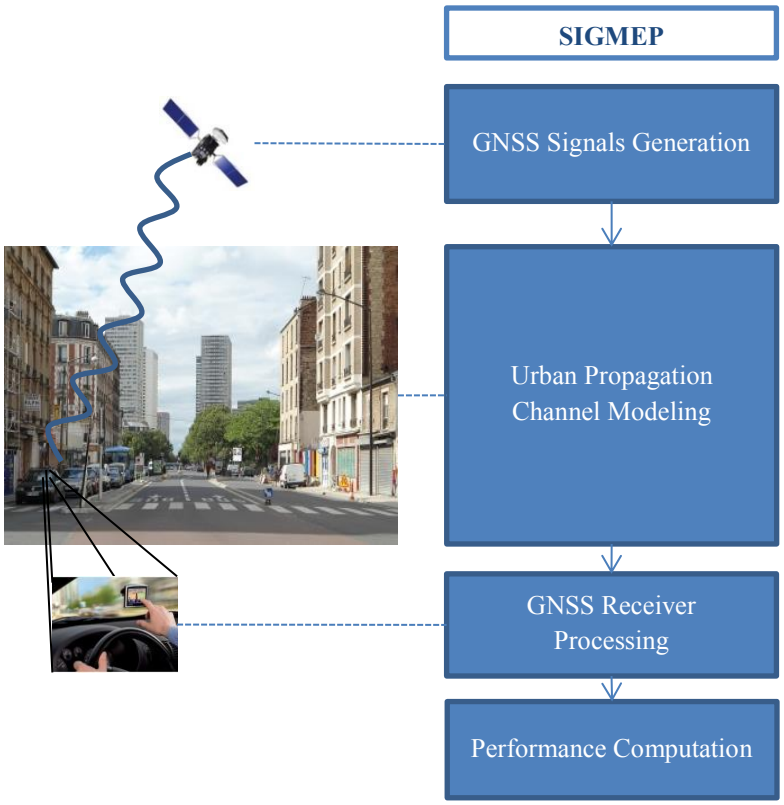

Figure 47: Simulation of a GNSS signal transmission/reception chain by SiGMeP

The SiGMeP overall structure is presented in Figure 48 and then developed. The received signal is directly modeled at the correlator output level, through partial correlations as it has been explained in section 3.2.2.

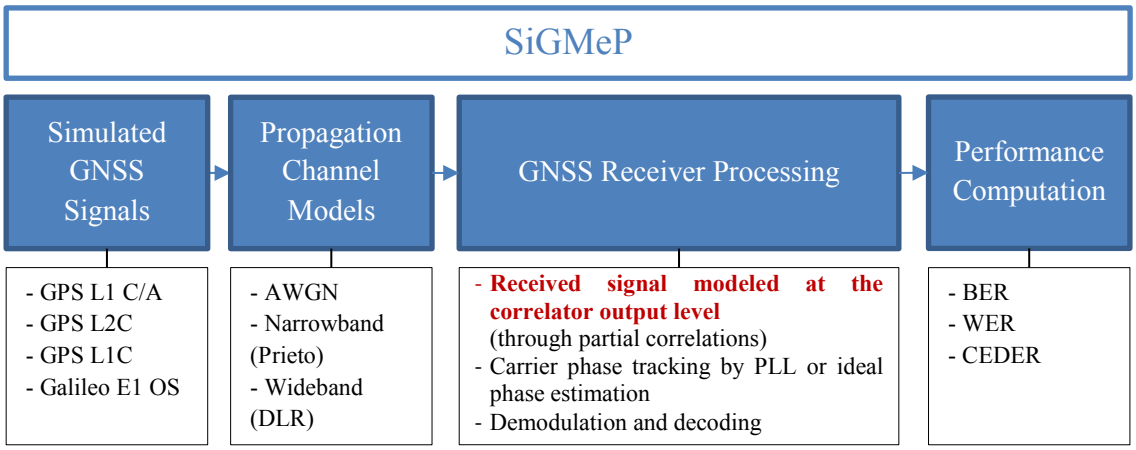

Figure 48: Simulation tool SiGMeP structure presentation

3.3.1 Simulated GNSS Signals

Existing signals (GPS L1 C/A and GPS L2C) or future signals (GPS L1C and Galileo E1 OS) can be simulated. They have been described in Chapter 2.

3.3.2 Propagation Channel Models

The choice is proposed between the AWGN, the narrowband Perez-Fontan/Prieto and the wideband DLR channel models (refer to section 3.1.2).

3.3.3 GNSS Receiver Processing

The following signal processings are assumed to be already done:

- The acquisition process: a rough estimation of the received signal phase and code delay is supposed to be made,
- The bit synchronization: the beginning of one bit is supposed to be known,
- The frame synchronization: the beginning of the received message is supposed to be known.

Moreover in the simulator, this assumption will be made:

- The code delay, between the received LOS signal component and the receiver spreading code locally generated, is assumed perfectly estimated, $\varepsilon_{\tau_{direct}} = 0$. Thus, $R\left[\varepsilon_{\tau_{direct}}\right]$ is equal to 1 (see Figure 46).

3.3.3.1 Modeling at the Correlator Output Level from Partial Correlations

The received signal is modeled at the correlator output level, according to the partial correlations. One of the advantages of modeling the received signal at the correlator output level is that it allows avoiding the spreading codes generation. In fact, since this model involves directly the spreading code autocorrelation function *R* and since this function is perfectly known, the spreading code does not need to be generated.

As explained before, since the urban propagation channel is really different from the AWGN channel, the classical correlator output model usually used in GNSS has been replaced by the proposed correlator output model computed through partial correlations (equation (3.30)), in order to better simulate the impact of the fast variations of the received signal.

3.3.3.2 Received Signal Phase Estimation

In SiGMeP, the received signal phase changes very quickly because of the urban propagation channel impact (see Chapter 2). In this context, it is not representative to reality if the phase is assumed perfectly estimated, as it is often considered in the literature. Thus, a realistic phase estimation process is considered through a PLL. Nevertheless, in order to investigate the PLL impact on the demodulation performance, ideal phase estimation can be selected in SiGMeP to be compared with the PLL tracking. Moreover, the ideal phase estimation allows providing the best achievable demodulation performance.

3.3.3.2.1 Ideal Phase Estimation

For the narrowband Perez-Fontan/Prieto channel model, if ideal phase estimation is considered, each sample is compensated by the channel model phase exact value:

$$\varphi_{rep}(n) = \hat{\varphi}_{ideal}(n) = phase\{c(n)\} = \varphi_{channel}(n) \tag{3.34}$$

Whereas for the wideband DLR channel model, each sample is compensated by a channel model phase resulting value defined by the following expression:

$$\varphi_{rep}(n) = \hat{\varphi}_{ideal\ resulting}(n) = phase\left\{\sum_{l=1}^{L} \frac{R[\varepsilon_\tau(l)]}{N} a_{channel}(n;l)\, e^{j\varphi_{channel}(n;l)}\right\} \tag{3.35}$$

3.3.3.2.2 PLL Phase Estimation

In a GNSS receiver, the received signal phase is estimated by using a PLL. In SiGMeP, a PLL has thus been implemented to faithfully represent the real GNSS receiver process.

A PLL consists of [44]:

- A multiplier,
- A phase detector (the discriminator),
- A loop filter,
- A Voltage-Controlled Oscillator (VCO).

To allow the use of a discriminator which does not need to be insensitive to bit transitions, and thus to make the PLL more robust [45], the PLL in SiGMeP is controlled by the correlator outputs computed on the pilot component ($I_{p_{pilot}}$ and $Q_{p_{pilot}}$) . The PLL output is then used for the computation of the correlator outputs on the data channel, as it is illustrated in Figure 49.

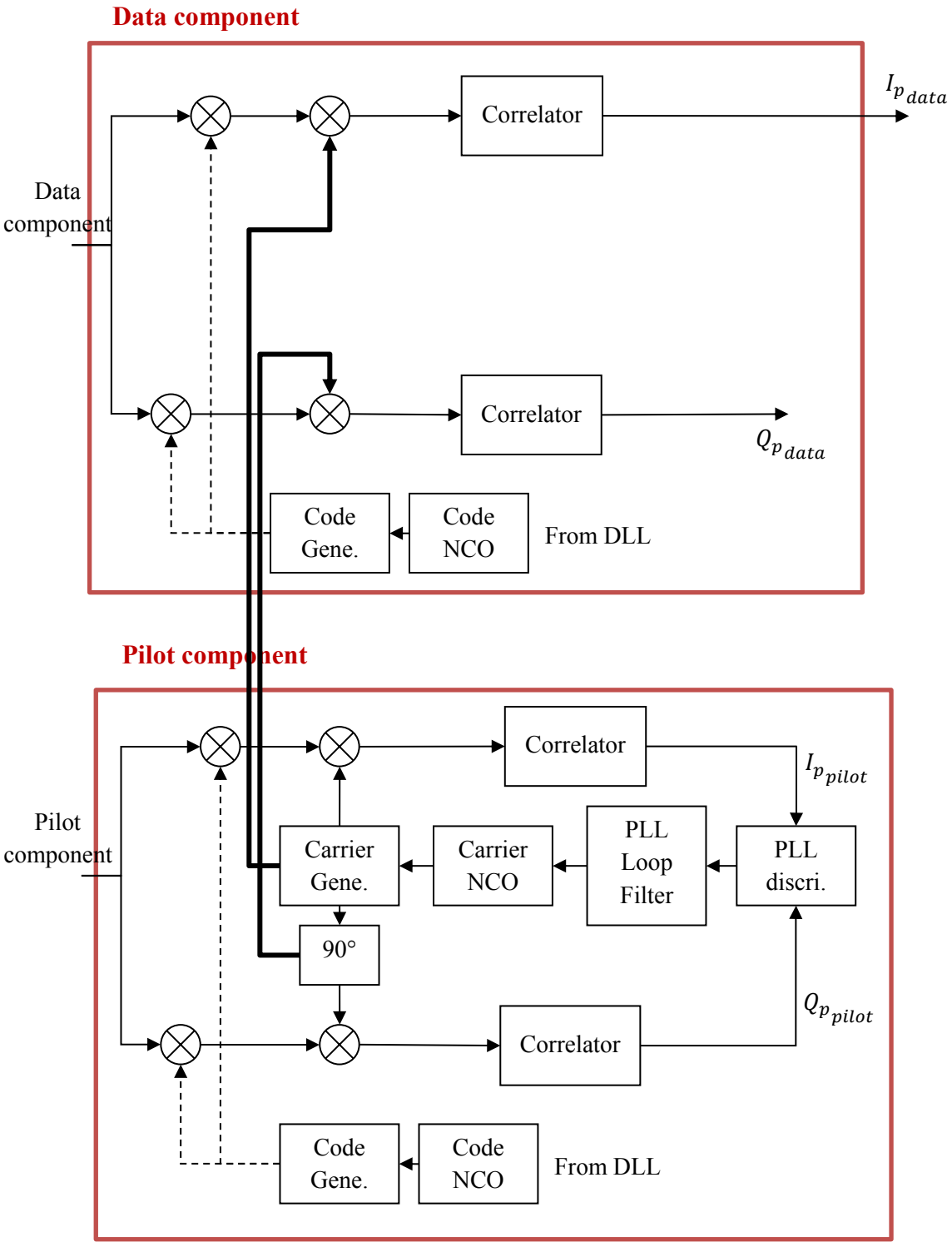

Figure 49: PLL operation between the data and pilot components in SiGMeP

The parameters of the PLL implemented in SiGMeP are presented in Table 16. The loop bandwidth and the loop order correspond to the loop filter parameters.

Table 16: SiGMeP PLL parameters

PLL parameters	
Loop bandwidth	10 Hz
Discriminator	Atan2 [8]
Loop order	3

The Atan2 discriminator is used by the PLL:

$$tan2 = \left[tan^{-1}\left(\frac{Q_{p_{pilot}}}{I_{p_{pilot}}} \right) \right]^2 \tag{3.36}$$

3.3.3.3 C/N_0 Estimation

The received C/N_0 needs to be estimated for many reasons in a GNSS receiver (quality indicator, weighting of the measurements, etc…) In the specific case of data demodulation, this value is used to compute the detection function LLR_{AWGN} at the decoder input (see Chapter 5 for more details about the detection function) for the decoding process. The corresponding average received C/N_0 is estimated in this case for each message.

The received carrier to noise ratio C/N_0 is estimated on the data component by the Van Dierendonck estimator [41] via the following equations:

$$\frac{\widehat{C}}{N_0}_{data} = 10log\left(\frac{1}{T_I} \frac{\mu_{NP} - 1}{1 - \mu_{NP}} \right) \quad [dB\ Hz] \tag{3.37}$$

and:

$$\begin{cases} \mu_{NP} = \dfrac{1}{J}\displaystyle\sum_{i=1}^{J} NP(i) \\ NP(i) = \dfrac{NBP(i)}{WBP(i)} \\ NBP(i) = I_p\,(i)^2 + Q_p\,(i)^2 = \left(\displaystyle\sum_{n=1}^{N} I_{p\,part}(n + (i-1)N) \right)^2 + \left(\displaystyle\sum_{n=1}^{N} Q_{p\,part}(n + (i-1)N) \right)^2 \\ WBP(i) = \left(I_p\,(i) + Q_p\,(i) \right)^2 = \displaystyle\sum_{n=1}^{N} \left(I_{p\,part}(n + (i-1)N)^2 + Q_{p\,part}(n + (i-1)N)^2 \right) \end{cases} \tag{3.38}$$

where:

- J is the number of correlation intervals by the duration used to make the estimation. Here $J = 1800$ for the LLR_{AWGN} computation.

3.3.3.3.1 Navigation Message Demodulation

The navigation message can then be demodulated. The main process of this part is the channel decoding (see Annex B), specific to each channel code (different according to the emitted GNSS signal) and each receiver. Then, the demodulation performance can be computed, as it is explained in section 3.3.3.3.1.ii.

3.3.3.3.1.i *Channel Decoding*

The decoding process of GPS L1C has been detailed in Chapter 2.

As LLR detector function at the decoder input (see Chapter 2), the classical mathematical expression which assumes an AWGN propagation channel model is usually used in the simulations, but more advanced detection functions adapted to urban propagation channels will be implemented in order to improve the GNSS signals demodulation performance in urban environments. All of these LLR mathematical expressions are derived in Chapter 5.

3.3.3.3.1.ii *Performance Computation*

Once the signal processing stage is over, it is interesting to compute the number of errors among the demodulated data, called the error rate.

Since the essential demodulated data to compute a position are the Clock error and Ephemeris Data (CED), the most relevant error rate to compute is the CED Error Rate (CEDER) (more details in Annex A). For GPS L1C, the CED are contained in subframe 2 (more details in Chapter 2). Nevertheless SiGMeP allows computing the subframe 3 error rate as well. The error rate is determined by computing the ratio between the number of wrong estimated data sets (corresponding to the data type of interest, subframe 2 or subframe 3) and the total number of estimated data sets.

Finally, the GNSS signals demodulation performance is presented thanks to a particular plot: the error rate as a function of the carrier to noise ratio C/N_0. It allows determining the minimum C/N_0 which permits to achieve a given error rate.

3.4 Partial Correlation Duration Analysis

This section investigates the optimal choice of the partial correlation duration $T_{I_{part}}$ to ensure that the simulation results will be as close as possible to reality, while maintaining the simulations durations as short as possible (the more partial correlations have to be generated, the longer the simulation will be). For this purpose, the partial correlation duration $T_{I_{part}}$ used for the simulator correlator output model presented in section 3.2.2 is determined. To do that, several values of $T_{I_{part}}$ have been tested with the simulator SiGMeP. The simulations are described in section 3.4.1 and the results are presented and analyzed in section 0.

3.4.1 Simulations Description

To determine the minimum necessary partial correlation duration $T_{I_{part}}$, two principles are followed:

- The $T_{I_{part}}$ value has to be as long as possible in order to reduces the number of partial correlations to be generated, *N* (see Figure 50),
- The error rates computed at the receiver output must be as faithful as possible to reality (assuming that the real results can be obtained by using the proposed LMS propagation channel models).

It has been seen in Chapter 2 that the coherent channel duration is recommended by [30] to be equal to λ/4 meters, where λ is the wavelength of the carrier, and to at least λ/8 meters by [27]. For a user speed example equal to 50 km/h, the corresponding λ/8 temporal value is equal to 14 ms. These considerations will be taken into account to determine the tested $T_{I_{part}}$ values.

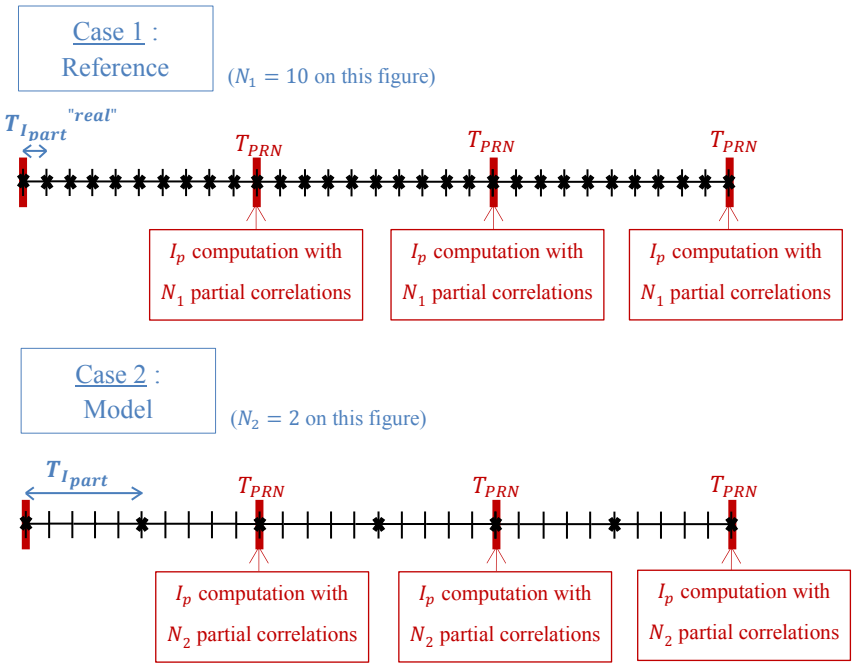

Figure 50: SiGMeP correlator output modeling

A first case (represented by the case 1 in Figure 50) is supposed to represent the real GNSS receiver processing behavior, considering a short value of the $T_{I_{part}}$ duration, in order to ensure the Assumptions 1 and 2. For simulation burden and time purposes, this shortest $T_{I_{part}}^{"real"}$ has firstly been chosen equal to 0.01 ms (but this value can be reduced if the simulation results impose it). The propagation channel model is generated at this frequency equal to 0.01 ms, and the simulations are made with SiGMeP to compute the associated BER and CED Error Rate (CEDER) (see Annex A for BER and CEDER definitions) with the GPS L1C signal and PLL tracking.

A second case is considered (represented by the case 2 in Figure 50), in order to test the impact of longer values of $T_{I_{part}}$ on the GPS L1C demodulation performance (BER and CEDER). The aim consists in increasing the $T_{I_{part}}$ while keeping the same BER and CEDER that those obtained in the first case, supposed to be representative to reality. If the degradation between both BERs and CEDERs (between cases 1 and 2 in Figure 50) is judged too important, the tested $T_{I_{part}}$ value is considered to be too long.

Moreover, the AWGN is forced to zero in order to only investigate the urban propagation channel impact on the correlator output modeling.

To simulate the PLL tracking, two different receiver oscillators have been considered: a quartz and a TCXO. The impact of the PLL phase noise n_{clock} due to these more or less stable oscillators (see parameters in Table 17) has been compared with the one obtained without PLL phase noise.

Table 17: Receiver oscillators parameters for the PLL phase noise modeling

	Quartz	TCXO
h_0	2.10^{-19}	1.10^{-21}
h_1	7.10^{-21}	1.10^{-20}
h_2	2.10^{-20}	2.10^{-20}

In order to compare similar conditions, the different $T_{I_{part}}$ values have been tested in the same simulation conditions. The generated propagation channel is the same for each test (Figure 50), leading to firstly generate the propagation channel model samples $a_{channel,n}$ and $\varphi_{channel,n}$ at the frequency equal to 0.01 ms, and then, to use these same samples, but under-sampled at the frequency which corresponds to the tested $T_{I_{part}}$ value. Similarly, the same PLL phase noise $n_{clock,n}$ samples have been used for each simulation.

For illustration purposes, according to equation (3.29), the correlator output model mathematical expression corresponding to the "real case or case 1" of Figure 50 in a narrowband propagation channel model can thus be written as:

$$I_{p_{nb}}(i) = \frac{A}{2} d_i \sum_{n=1}^{10} \frac{R[\varepsilon_{\tau_i}]}{10} a_{channel}[n + (i-1)N_1]. \cos\left(\varphi_{channel}[n + (i-1)N_1] - \varphi_{rep\ case\ 1}[n + (i-1)N_1] + n_{clock}[n + (i-1)N_1]\right) \tag{3.39}$$

And the correlator output model mathematical expression corresponding to the "case 2" of Figure 50 in a narrowband propagation channel model can thus be written as:

$$I_{p_{nb}}(i) = \frac{A}{2} d_i \frac{R[\varepsilon_{\tau_i}]}{2} a_{channel}[5n + (i-1)N_2]. \cos\left(\varphi_{channel}[5n + (i-1)N_2] - \varphi_{rep\ case\ 2}[5n + (i-1)N_2] + n_{clock}[5n + (i-1)N_2]\right) + \frac{A}{2} d_i \frac{R[\varepsilon_{\tau_i}]}{2} a_{channel}[10n + (i-1)N_2]. \cos\left(\varphi_{channel}[10n + (i-1)N_2] - \varphi_{rep\ case\ 2}[10n + (i-1)N_2] + n_{clock}[10n + (i-1)N_2]\right) \tag{3.40}$$

The parameters used for the simulations have been selected in order to be representative of difficult signal reception conditions. In fact, for better signal reception conditions, the $T_{I_{part}}$ should be longer whereas we are interested in determining the minimum necessary $T_{I_{part}}$ value to faithfully represent reality. The signal reception conditions are listed in Table 18.

Table 18: Simulated conditions for the propagation channel model

	Prieto	DLR
GNSS signal	GPS L1C	GPS L1C
Environment type	Urban	Urban
User Speed	50 km/h	50 km/h
Band of the measurements	S-band	-
Satellite Elevation Angle	40°	40°
Satellite Azimuth Angle	-	45°
Receiver clock	Quartz/TCXO	Quartz/TCXO

3.4.2 Simulations Results

To determine the maximum acceptable $T_{I_{part}}$ duration for each of the propagation channel models, two demodulation performance have been computed and compared: the final BER at the receiver output and the CEDER (see Annex A for definitions of BER and CEDER).

3.4.2.1 Perez-Fontan/Prieto Propagation Channel Model

The Perez-Fontan/Prieto propagation channel model samples $a_{channel,n}$ and $\varphi_{channel,n}$ have been generated with a frequency equal to 0.01 ms to represent the "real case". The SiGMeP simulator has then been used to compute the BER and the CEDER associated with 500 GPS L1C messages, with these channel model samples. Secondly, to test $T_{I_{part}} = 0.05\ ms$, the same channel model samples have been used, but just one sample over 5 samples is considered, to finally obtain a frequency equal to 0.05 ms using the same generated propagation channel model. The associated BER and CEDER have then been computed with SiGMeP. The same process has been applied for testing $T_{I_{part}} = 0.1\ ms$ and $T_{I_{part}} = 1\ ms$.

Table 19: BER and CEDER values as a function of $T_{I_{part}}$ for the Prieto propagation channel model

		Prieto BER					
		Without Phase Noise		TCXO Clock		Quartz Clock	
		BER	CEDER	BER	CEDER	BER	CEDER
$T_{I_{part}}^{"real"} = 0.01\ ms$	$N = 1000$	0.1020	0.6	0.1035	0.6	0.1106	0.7
$T_{I_{part}} = 0.05\ ms$	$N = 200$	0.1076	0.6	0.1072	0.6	0.1048	0.6
$T_{I_{part}} = 0.1\ ms$	$N = 100$	0.1104	0.6	0.1081	0.6	0.1084	0.6
$T_{I_{part}} = 1\ ms$	$N = 10$	0.075	0.4	0.074	0.4	0.1615	0.7

For the 'without phase noise' case, the BER degradation between the simulations made with $T_{I_{part}}^{"real"}$ and $T_{I_{part}}$ has been computed in Table 20. It clearly shows that $T_{I_{part}} = 1\ ms$ is a too high value.

Table 20: BER degradation for the Prieto propagation channel model

	Prieto BER
	Without Phase Noise
	BER degradation
$\frac{BER_{0.01ms}}{BER_{0.05ms}}$ in dB	0.5
$\frac{BER_{0.01ms}}{BER_{0.1ms}}$ in dB	0.7
$\frac{BER_{0.01ms}}{BER_{1ms}}$ in dB	2.7

This conclusion can be supported by the $T_{I_{part}}$ impact on the CEDER too. Indeed, for $T_{I_{part}}^{"real"} = 0.01\ ms$, $T_{I_{part}} = 0.05\ ms$ and $T_{I_{part}} = 0.1\ ms$, CEDER is equal to 0.6 whereas for $T_{I_{part}} = 1\ ms$, CEDER equal to 0.4. The longer $T_{I_{part}}$ value which ensures results close to reality seems to be $T_{I_{part}} = 0.1\ ms$. The same conclusions can be made for the quart clock and the TCXO clock cases.

The recommended $T_{I_{part}}$ duration value at least equal to λ/8 meters or equivalently to 14 ms for a user speed equal to 50 km/h thus seems to be a too high value.

3.4.2.2 DLR Propagation Channel Model

The DLR propagation channel model samples $a_{channel,n}(l)$ and $\varphi_{channel,n}(l)$ have been generated with a frequency equal to 0.01 ms to represent the "real case". The SiGMeP simulator has then been used to compute the BER and the CEDER associated with 8 GPS L1C messages (due to the very high time-consuming simulations) with these channel model samples. Secondly, to test $T_{I_{part}} = 0.05\ ms$, the same channel model samples have been used, but just one sample over 5 samples is considered, to finally obtain a frequency equal to 0.05 ms using the same generated propagation channel model. The associated BER and CEDER have then been computed with SiGMeP. The same process has been applied for testing $T_{I_{part}} = 1\ ms$.

Table 21: BER and CEDER values as a function of $T_{I_{part}}$ for the DLR propagation channel model

		DLR BER					
		Without Phase Noise		TCXO Clock		Quartz Clock	
		BER	CEDER	BER	CEDER	BER	CEDER
$T_{I_{part}}^{"real"} = 0.01\ ms$	$N = 1000$	0.2242	0.9	0.2234	0.9	0.2214	0.9
$T_{I_{part}} = 0.05\ ms$	$N = 200$	0.2187	0.9	0.2157	0.9	0.2143	0.9
$T_{I_{part}} = 1\ ms$	$N = 10$	0.1687	0.8	0.1643	0.8	0.1670	0.8

For the 'without phase noise' case, the BER degradation between the simulations made with $T_{I_{part}}^{"real"}$ and $T_{I_{part}}$ has been computed in Table 22. It clearly shows that $T_{I_{part}} = 1\ ms$ is a too high value.

Table 22: BER degradation for the Prieto propagation channel model

	DLR BER
	Without Phase Noise
	BER degradation
$\frac{BER_{0.01ms}}{BER_{0.05ms}}$ in dB	0.2
$\frac{BER_{0.01ms}}{BER_{1ms}}$ in dB	2.5

This conclusion can be supported by the $T_{I_{part}}$ impact on the CEDER too. Indeed, for $T_{I_{part}}^{"real"} = 0.01\ ms$ and $T_{I_{part}} = 0.05\ ms$, CEDER is equal to 0.9 whereas for $T_{I_{part}} = 1\ ms$, CEDER equal to 0.8. The longer $T_{I_{part}}$ value which ensures results close to reality seems to be between 0.05 ms and 1 ms. Same conclusions can be made for the quart clock and the TCXO clock cases.

According to the results obtained with the Perez-Fontan/Prieto propagation channel model, and since the results obtained with the DLR model show that $T_{I_{part}} = 1\ ms$ is a too high value and that $T_{I_{part}} = 0.05\ ms$ is acceptable, the intermediate $T_{I_{part}}$ value equal to 0.1 ms seems to be the longer possible value.

3.4.2.3 $T_{I_{part}}$ Duration Impact on the Demodulation Performance Investigation

In order to complement results obtained in section 3.4.2.1 and section 3.4.2.2, the GPS L1C signal demodulation performance has been computed with the classical way of using SiGMeP in the Prieto propagation channel model, without phase receiver clock phase noise, but with AWGN (see Figure 51). It means that the propagation channel model samples are newly generated for each simulation. Several $T_{I_{part}}$ values have been tested: 0.01 ms, 0.1 ms and 1ms, with parameters of Table 18.

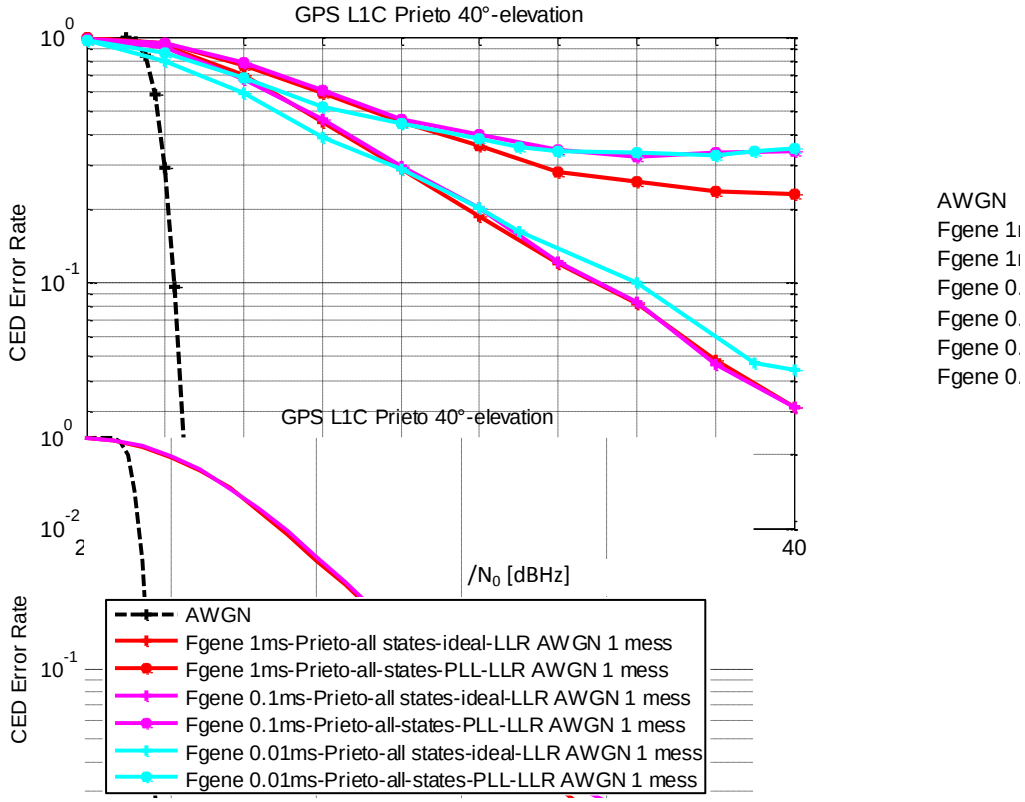

Figure 51: GPS L1C demodulation performance in the Prieto model for different propagation channel generation frequencies

The demodulation performance represented in Figure 51 confirms the conclusions of the preceding sections. For the PLL tracking case, the curves corresponding to $T_{I_{part}}^{"real"} = 0.01\ ms$ (assumed to be representative of real demodulation performance) and $T_{I_{part}} = 0.1\ ms$ are really similar, whereas the demodulation performance obtained with $T_{I_{part}} = 1\ ms$ is very far from them. It is thus showed that the recommended value of $T_{I_{part}}$ duration least equal to λ/8 meters or equivalently to 14 ms for a user speed equal to 50 km/h, is not satisfactory, since $T_{I_{part}} = 1\ ms$ is already not satisfactory. However, $T_{I_{part}} = 0.1\ ms$ seems to be a sufficient value for a PLL tracking.

3.4.2.4 Receiver Clock Phase Noise Impact on the BER Investigation

The receiver clock phase noise impact has been more investigated in this section. To do that, BER and CEDER provided by different receiver clock have been compared. In order to only study the clock phase noise, the AWGN propagation channel model has been used, for a high C/N_0 value.

The propagation channel model is generated for each simulation, but 10 000 messages are simulated every time. Table 23 summarizes the corresponding results.

Table 23: BER values as a function of receiver clock for the AWGN propagation channel model

	AWGN BER		
	Without phase noise	**TCXO clock**	**Quartz clock**
C/N0 = 25 dB-Hz	0.00071 (CEDER=0.01)	0.00056 (CEDER=0.01)	0.00360 (CEDER=0.04)

It can be concluded that the receiver clock phase noise influences the BER and CEDER values. The TCXO clock phase noise error is negligible whereas the quartz clock has real impact on the GNSS signals demodulation performance.

3.4.2.5 Conclusion

Since the GNSS user environment of interest is urban in this PhD thesis, it is not possible to model the received signal with the classical correlator output model. Indeed, this model assumes that the Doppler frequency error and the phase error are constant during the integration time. However in urban environments, the received signal phase and amplitude change really fast. As a consequence, the integration time is too long to consider the Doppler frequency and the phase errors as constant. Thus, a new model has been proposed based on shorter integration duration values: $T_{I_{part}}$, associated with a partial correlation model.

Moreover, it can be deduced from this chapter, that a $T_{I_{part}}$ duration equal to 0.1 ms is a good compromise between the samples generation time and the demodulation performance degradation. Thus, all the simulations of this PhD thesis have been done based on the use of partial correlations generated every 0.1 ms.

Chapitre 4: GNSS Signals Demodulation Performance Assessment in Urban Environments

The majority of new GNSS applications takes place in urban environments. In these obstructed environments, the received signal is severely impacted by obstacles which induce fading of the resulting received signal that is detrimental to both the ranging and demodulation capability of the receiver. The GNSS signals demodulation performance is thus degraded in urban environments compared against the one obtained in the Additive White Gaussian Noise (AWGN) propagation channel model. Since the first GNSS signals were developed in an open environment context, the AWGN propagation channel model was adapted to provide their demodulation performance. However nowadays satellite navigation is more and more used in cities and constrained environments. Indeed the recently developed modernized GNSS signals have taken into account this new constraint in their design. The current and future GNSS signals demodulation performance thus need to be assessed in an urban propagation channel.

As it has been explained in Chapter 3, the GNSS signals demodulation performance is provided in this work thanks to the simulator SiGMeP. In fact, the use of a simulator allows getting away from dependence of real signals availability, controlling the simulation parameters and testing new configurations. This simulator allows calculating the current and future GNSS signals demodulation performance as faithful to the reality as possible due to the implementation of realistic urban propagation channel models (described in Chapter 2) and receiver models (described in Chapter 3).

Moreover, since the urban propagation channel is very different from the AWGN propagation channel, it is necessary to adapt the methodology of representing the GNSS signals demodulation performance in these environments. In this sense, [10] proposes to represent the usual BER/WER curve as a function of the signal C/N_0, but since the received signal power is fluctuating in urban environments (this will be more detailed in section 4.1.2.1), [10] proposed to normalize it for each received message, translating the average received signal power level after its passage through the propagation channel around 1, in order to keep a constant C/N_0 value. However, we propose in this Chapter another methodology, consisting in two main parts:

- The introduction of a new figure of merit better representing the GNSS specific characteristics with respect to a classic communication system than the usual BER/WER curve as a function of the signal C/N_0,
- The choice of the direct C/N_0 without channel propagation attenuation instead of the instantaneous received C/N_0.

The first part of this chapter describes in detail the new methodology developed to provide a demodulation performance figure of merit adapted to the GNSS specific characteristics in an urban environment. The second part provides the results obtained with this new methodology when using SiGMeP.

4.1 Methodology Presentation to Assess the GNSS Signals Demodulation Performance in Urban Environments

At the beginning, GNSS signals were designed for open environments. It is thus natural that GNSS signals demodulation performance has been studied in the AWGN propagation channel model. However since an important need in GNSS applications is emerging in urban environments, it is necessary to assess the GNSS signals demodulation performance in an adapted propagation channel model. It is the case of the simulator SiGMeP, which provide the GNSS signals demodulation performance in the urban narrowband Perez-Fontan/Prieto model and in the urban wideband DLR model. In addition, since these urban propagation channels are very different from the AWGN channel, the way of computing and representing the GNSS signals demodulation performance in urban environments cannot be the same as for open environments. It is thus necessary to adapt. In this sense, a new methodology has been developed to provide a different view of the current and future GNSS signals demodulation performance in urban environments.

This section firstly presents the classical way of representing GNSS signals demodulation performance, adapted to AWGN propagation channels. Then, the limitations of this classical method are underlined for the case of urban propagation channels. According to these limitations, a new methodology is proposed, adapted to provide and represent GNSS signals demodulation performance in urban environments.

4.1.1 Classical Figure of Merit Used for AWGN channels

In the classic method of representing the GNSS signals demodulation performance, inspired by the telecommunications field, the error rate (BER, WER or CEDER, defined in Annex A) is represented as a function of the received carrier to noise density ratio C/N_0 at the correlator output level.

For example, the main objective of a GNSS receiver which targets mass-market users is the user position computation. The most relevant error rate to compute is thus the CED Error Rate (CEDER) since the essential data used in the user position calculation is the Clock error and Ephemeris Data (CED).

Figure 52 represents the GNSS signals CEDER with the classical method in the AWGN propagation channel model, obtained with SiGMeP.

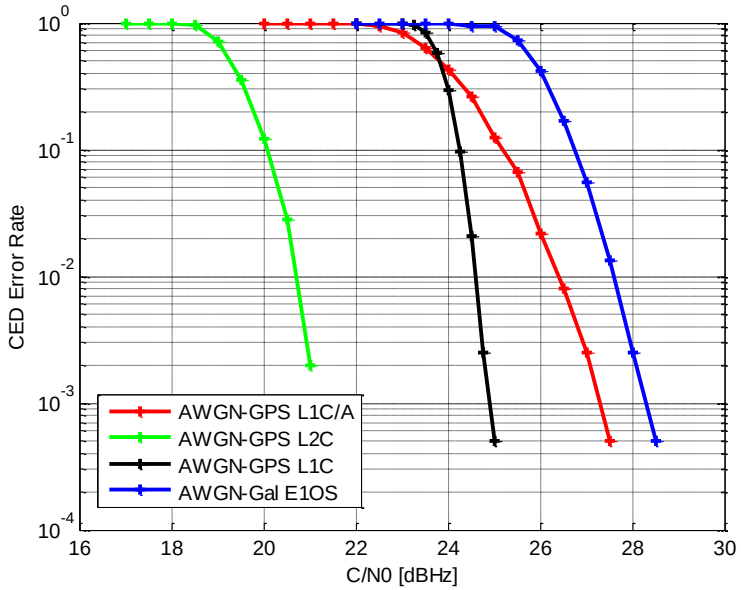

Figure 52: GNSS signals demodulation performance in the AWGN channel model with the classical methodology

However, this way of representing the GNSS signals demodulation performance presents two main limitations for the PhD thesis objective:

- The received carrier to noise density ratio C/N_0 is not constant in urban environments,
- Only punctual instead of continuous message demodulations are required because the same CED information set is repeated for a given time interval. Therefore, in general, the information transmitted inside a GNSS message does not have to be continuously demodulated.

To overcome these limitations, a new methodology to compute and to represent the GNSS signals demodulation performance, adapted to urban environments has been developed; it is detailed in the next sections.

4.1.2 New Methodology

After the problematic issues presentation of applying the classical method to represent GNSS signals demodulation performance in urban environments, the new method is introduced.

4.1.2.1 Limitation n°1: Fluctuating Received C/N_0

4.1.2.1.1 Problematic

Contrary to an open environment modelled by an AWGN propagation channel, the urban environment, modelled by a mobile propagation channel, is dynamic. In a dynamic environment, the reception conditions change over time (as can be observed on the time variant property of the channel impulse response h_e, equation (2.22) because of the user motion and the environmental fluctuations around the user. Therefore, the received signal can be attenuated and directly impacted by multipath generated by this obstructed environment; and the attenuation and the multipath impact change over time. As a consequence, the useful received signal power C can fluctuate significantly over time, even over the duration of a message.

It is thus impossible to represent an Error Rate (ER) value as a function of a fixed received C/N_0 value in an urban environment as it does not represent a realistic situation.

In order to solve this first limitation, the new methodology must:

- Determine a C/N_0 which is constant a long time for any urban user,
- Determine a C/N_0 which is representative from an operational point of view.

4.1.2.1.2 Proposition

The new methodology thus proposes to use the theoretical C/N_0 value representing the ratio between the received direct signal power without channel attenuation noted as $C_{pre\text{-}urban}$ and illustrated in Figure 53, and the noise power spectral density N_0 considered at the correlator output level. This ratio can thus be considered as constant over periods of time much longer than the message duration (1st condition fulfilled). Moreover, from an operational point of view, a user moving inside an urban environment receives a signal with a constant $C_{pre\text{-}urban}/N_0$ from a satellite with a fixed elevation (2nd condition fulfilled). Therefore, to represent the demodulation performance as a function of the $C_{pre\text{-}urban}/N_0$ seems adapted since it fulfills the two required conditions. Nevertheless, the reader must note that this value is not available at the receiver; it is thus just a theoretical value used to evaluate the message demodulation performance.

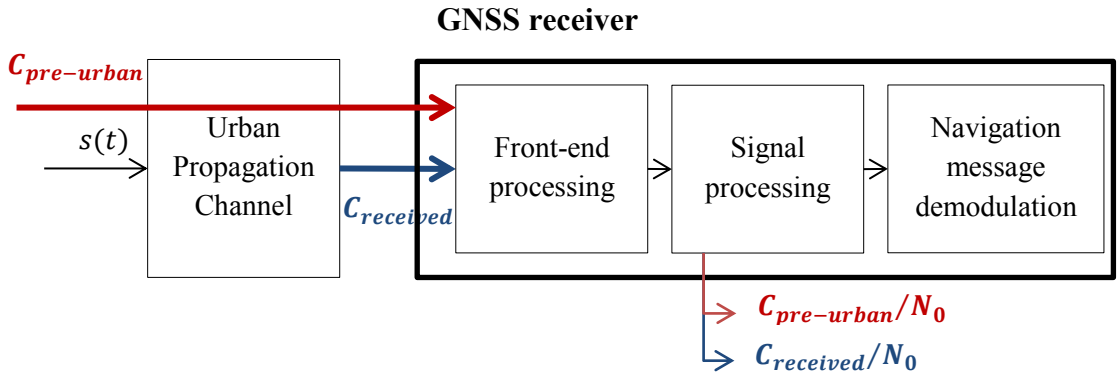

Figure 53: Comparison between the useful received signal power C and the received direct signal power without channel attenuation $C_{pre\text{-}urban}$

Additionally, knowing the receiver architecture and interference environment, the demodulation performance could be expressed as a function of the satellite elevation as a more operational alternative to a representation as a function of $C_{pre\text{-}urban}/N_0$. Indeed, $C_{pre\text{-}urban}$ directly depends on the power emitted by the satellite and on its antenna gain pattern. Because the satellite emitting antenna gain pattern has been designed to take the shape of the Earth surface, the received direct signal power without channel attenuation $C_{pre\text{-}urban}$ directly depends on the emitting satellite elevation angle. Then, N_0 can be established through a refined link budget, depending on the user platform. Representing the GNSS signals demodulation performance as a function of the emitted satellite elevation angle can thus be a very useful tool. However, since it highly depends on the user platform, the analysis in in this PhD thesis has not delved that far.

The GNSS signal demodulation performance in urban environments will thus be represented by the CEDER as a function of the theoretical value $C_{pre\text{-}urban}/N_0$.

4.1.2.2 Limitation n°2: Messages Don't Need to Be Demodulated Continuously

4.1.2.2.1 Problematic

Since only punctual instead of continuous message demodulations are required in GNSS, the classical figure of merit originating from the telecommunications field which considers each received message in the error rate computation is not adapted. In fact, the classical way of representing GNSS signals demodulation performance hides relevant information since it considers that all the received messages, in bad or good reception conditions, must be demodulated for the correct functioning of the GNSS instead of just a few ones, received in good conditions for example. Therefore, the classical demodulation performance representation fails to cope with the specific GNSS user needs with respect to a classical communication system and with the specific characteristics of a received signal in an urban environment.

4.1.2.2.1.i *Specific GNSS System Characteristic*

For a classical communication system, the receiver must continuously demodulate the received signal. It is not the case for GNSS. For example, inspecting again the fundamental objective of a GNSS receiver, to compute a position, the receiver only needs to demodulate once the CED during the CED validity period. More specifically, for GPS L1C signal, an entire CED data set is contained inside the subframe 2. This CED data set is applicable during three hours, but only transmitted during two hours [19]. The emitted CED data is thus invariant during two hours, but applicable one more hour. It means that over two hours, the GNSS receiver needs just to demodulate one subframe 2 content per visible satellite for at least 4 satellites, to be able to compute a position during at least one hour.

Following the example, in this work, we consider a continuous use of the receiver, meaning that for a first approach we do not take into account the time required for the first position computation, called as the Time-To-First-Fix (TTFF).

4.1.2.2.1.ii *Specific Characteristic of the Received GNSS Signal in Urban Environments*

When a GNSS signal is received into an urban environment, its received amplitude and phase are very distorted and change over time (see equations (2.22), (2.23) and (2.31)). We can thus observe (see Figure 54 and Figure 55 obtained using the Perez-Fontan/Prieto model) a series of consecutives states, more or less favorable from a demodulation point of view (see Figure 56). For example, the received signal into the intervals [31s, 36s], [37s, 52s] and [59s, 65s] corresponds to unfavorable reception conditions, since the correlator output Ip cannot clearly determine the emitted bits value, and the interval [17s, 23s] corresponds to favorable reception conditions since the emitted bit value can be clearly determined. Therefore, the instantaneous signal demodulation performance depends on the current signal received conditions.

Table 24: Simulation conditions for the Perez-Fontan/Prieto propagation channel model

Simulation Conditions	
Signals	GPS L1C
Channel Model	Perez-Fontan/Prieto
Channel Generation Fs	0.1 ms
Environment	Urban
Database Band	S
Satellite Elevation Angle	40°
Phase Estimation	PLL
C/N_0	40 dB-Hz

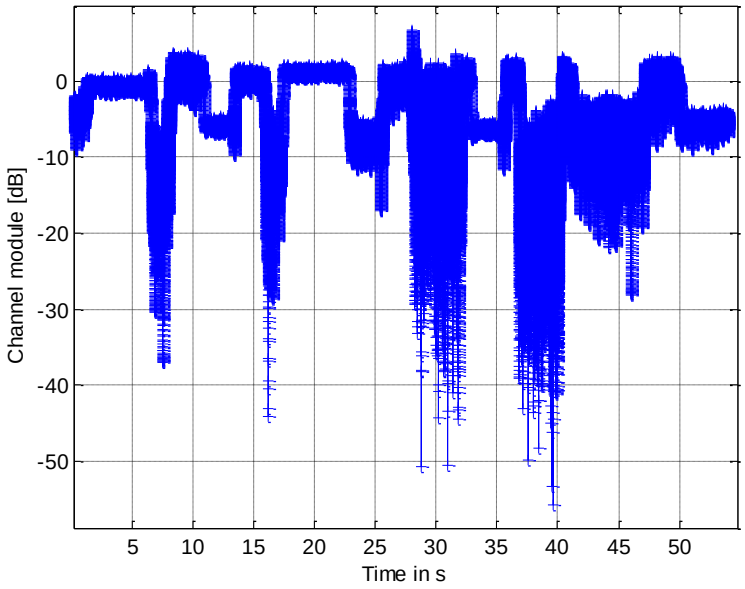

Figure 54: The received signal amplitude with the Prieto channel model

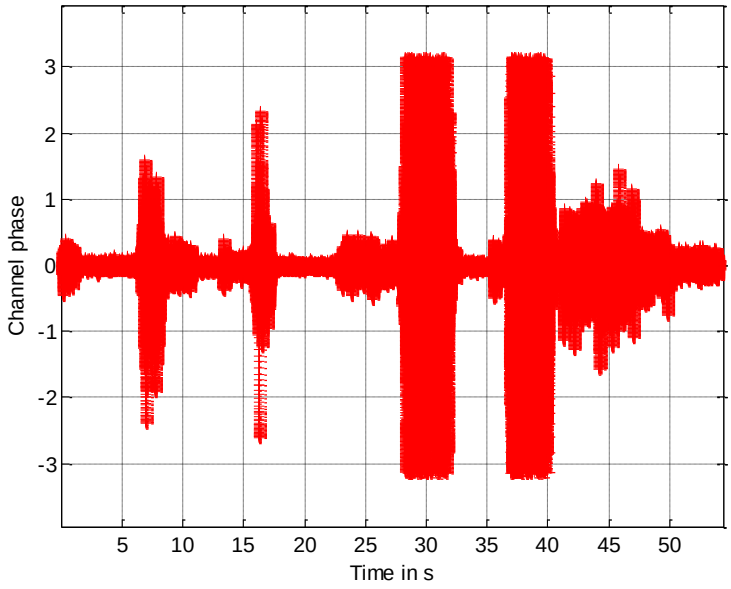

Figure 55: The received signal phase with the Prieto channel model

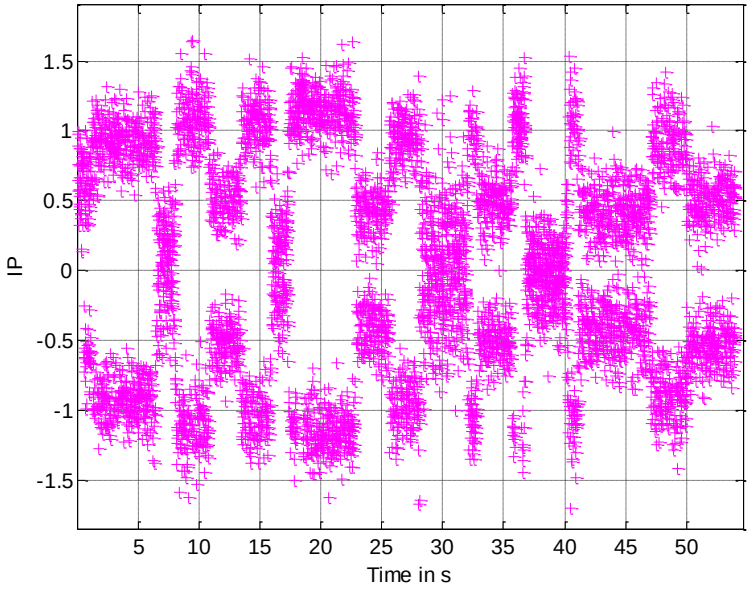

Figure 56: The correlator outputs Ip with the Prieto channel model

These two GNSS specific characteristics will thus be together exploited in order to adapt the GNSS signals demodulation performance representation to urban environments.

4.1.2.2.2 Proposition

The new methodology thus proposes to provide the demodulation performance for favorable reception conditions together with statistical information about the occurrence of these favorable reception conditions.

Indeed, during unfavorable reception conditions, the demodulation performance can be so bad that a very low probability of successful demodulations is expected compared with the probability during favorable reception conditions. Therefore, the continuous ER shows the average of these low and high ER values, and the result hides the possibility of punctually getting the information with a low ER in these favorable states. Moreover, taking into account that it is not necessary to demodulate each received message, it thus seems adapted to specifically look at the performance in favorable reception conditions.

This method can be summarized as follows:

Table 25: New methodology

New methodology
1) The received signal conditions could be classified into 2 states: ➢ Favorable reception conditions to demodulate the message ➢ Unfavorable reception conditions to demodulate the message
2) The performance is provided through these results: ➢ The data error rate is computed only for the messages entirely received during favorable reception conditions ➢ Statistical results of occurrence of these messages entirely received during favorable reception conditions are also computed

4.1.2.2.3 No Modifications on the Receiver Demodulation Architecture/Strategy

It must be noted that this new methodology DOES NOT involve any change in the receiver demodulation architecture/strategy. The receiver still demodulates each received message, but the way of representing the demodulation performance takes into account only messages received during favorable reception conditions and their associated occurrence.

4.1.2.2.4 Favorable/Unfavorable States Separation

The fundamental part of the new proposed methodology consists in defining an adapted criterion to separate the messages received in favorable reception conditions from the messages received in unfavorable reception conditions, for each operational need.

Two criteria have been inspected:

1) The messages considered as received in favorable reception conditions are the messages for which the Prieto channel model is in 'GOOD states' (see Chapter 2) during the entire message duration. Obviously, this assumes that the Prieto model perfectly represents the operational scenario.
2) The messages considered as received in favorable reception conditions are the messages for which its estimated received C/N_0 is above a threshold.

   First, the received C/N_0 is estimated for intervals of one second. Second, the minimum estimated received C/N_0 value among all the estimated received C/N_0 of one message is compared with a threshold (e.g. for GPS L1C, 18 C/N_0 estimations are made for one message). If the minimum value is above this threshold, the message is considered to be received in favorable reception conditions. The threshold value depends on the conducted strategy, described in section 4.2.1.3.2.

The messages entirely received in favorable reception conditions will be referred as 'favorable state messages'.

4.1.2.2.5 Occurrence Rate

Once the criterion to determine a 'favorable state message' is defined, the 'favorable state message' can be characterized by their occurrence rate, representing the proportion of 'favorable state message' during a given duration T_{occ}. This occurrence rate is represented through the 'favorable state message' histogram (see Figure 57 as example with the given duration $T_{occ} = 1h$).

In order to calculate the occurrence rate, the GNSS signal reception during the duration of interest T_{occ} is simulated and the number of observed 'favorable state message' is computed. This process is repeated several times N. Finally, the column X of the occurrence rate is calculated by dividing the number of times that X "favorable state messages" are received during T_{occ} by the number of simulated T_{occ} durations, N. Two key statistical values (illustrated in Figure 57) are then needed to assess the operational performance:

- The probability that there is no 'favorable state message' during the interval of interest T_{occ}, noted as P_{0fav} (leading to the minimum required availability),
- The 'favorable state message' average occurrence corresponding to the occurrence rate mean.

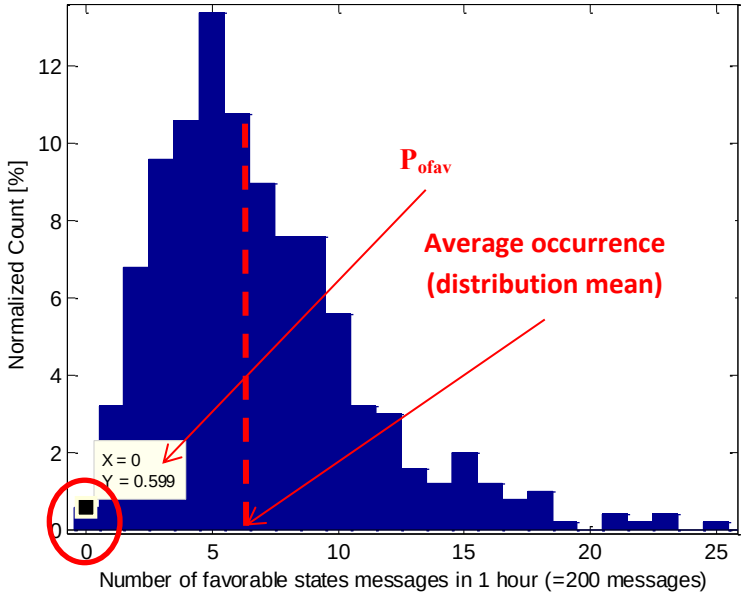

Figure 57: 'Favorable state messages' histogram and associated statistical values, for GPS L1C in the Prieto channel model with 40° of elevation considering the Prieto channel GOOD states as favorable reception conditions

4.1.2.2.6 Operational Requirements

The new methodology has been developed to meet operational requirements. These operational requirements can be firstly enounced at a 'high level' but they will be then translated at a lower level in order to easily link the 'high level' requirements to the new methodology and to finally be re-written with the statistical parameters defined above (P_{0fav} and average occurrence).

4.1.2.2.6.i *'High Level' Operational Requirements*

Some 'high level' operational requirements could be:

- To guarantee that the receiver is able to access a given data set in a given time,

  Example: be able to compute a position continuously
- To guarantee that the information error rate is below a given value,

  Example: CED error rate = 10^{-2}
- To guarantee a given information average availability.

In order to be able to link these 'high level' operational requirements to the proposed methodology, a preliminary step will consist in adapting these 'high level' operational requirements to 'low level' requirements.

4.1.2.2.6.ii *'Low level' Operational Requirements*

The 'low level' requirements specify the 'high level' requirements, in providing the necessary requirements associated with 1 satellite for a continuous duration, needed to achieve the 'high level' requirements. In this sense, the 'low level' requirements are the results of the translation of the final operational need ('high level' requirement) into the corresponding induced requirement on 1 satellite for a continuous duration.

'Low level' requirements are based on the following definitions: MRA, AMRA, AA and GA. Two 'high level' requirement types are defined, according to the involving 'low level' requirements, MRA/AMRA or AA/GA.

A first type of 'high level' requirement will be considered, for which the associated 'low level' requirements are the MRA and the AMRA. These 'low level' requirements can be linked to P_{0fav}. They are defined by this way:

- Minimum Required Availability (MRA):

  The couple GNSS signal/receiver meets the MRA requirement if with probability P_{mra}, the receiver receives at least ONE data set in a given time T_{mra}, associated to a data set error rate ER_{mra}.

- Absolute Minimum Required Availability (AMRA):

  The couple GNSS signal/receiver meets the AMRA requirement if with probability P_{amra}, the receiver is able to successfully demodulate at least ONE data set in a given time T_{amra}, for a given $C_{pre\text{-}urban}/N_0$ value $C_{pre-urban}/N_{0_{amra}}$.

In plain words:

- AMRA represents the percentage of blocks of length T_{amra} for which at least one data set is successfully demodulated inside a block of T_{amra} seconds. An AMRA requirement is always associated to a $C_{pre-urban}/N_{0_{amra}}$ value.
- MRA represents the percentage of blocks of length T_{mra} for which it is possible to achieve a given demodulation performance ER_{mra}, for at least one data set inside a block of T_{mra} seconds.

The first type of 'high level' requirement which has to be finally achieved is better translated in 'low level' requirements through the AMRA requirement. However with the new proposed methodology, it is necessary to firstly determine the MRA in order to be able to finally determine the AMRA.

A second type of 'high level' requirement will be considered, for which the associated 'low level' requirements are the AA and the GA. These 'low level' requirements can be linked to the occurrence histogram. They are defined by this way:

- Average Availability (AA):

  The couple GNSS signal/receiver meets the AA requirement if the receiver can demodulate an average percentage of data sets Per_{aa}, in a given time T_{aa}, with a given data set error rate ER_{aa}.

- Guaranteed Availability (GA):

  The couple GNSS signal/receiver meets the GA requirement if with a probability P_{ga}, the receiver can demodulate a percentage of data sets Per_{ga}, in a given time T_{ga}, with a given data set error rate ER_{ga}.

In plain words:

- AA represents the average percentage of data sets inside a block of T_{aa} seconds for which it is possible to achieve a given demodulation performance ER_{aa},
- GA represents the percentage of data sets inside a block of T_{ga} seconds for which the AA is guaranteed (with $T_{ga} = T_{aa}$).

The second type of 'high level' requirement which has to be finally achieved is better traduced in 'low level' requirements through the AA requirement. However the GA is provided in addition, as a complementary result.

The preliminary step of this new methodology thus consists in translating the 'high level' operational requirements in 'low level' operational requirements defined above.

Depending on the 'high level' operational requirement type, and how this requirement is translated into 'low level' requirements (in terms of MRA/AMRA or in terms of AA/GA), two strategies can be conducted to apply the new methodology.

4.1.2.2.6.iii *Transcribed in the New Methodology*

Once the "low level" operational requirements are determined, they have to be translated into statistical values provided by the new methodology, related to the 'favorable states messages' occurrence rate ($P_{0\text{-}fav}$ and average occurrence).

The main step of the new methodology thus consists in defining the separation between 'favorable and unfavorable states messages' which fulfill these statistical values.

4.1.2.2.7 Two Strategies According to the Operational Requirements

Two strategies can be used to apply this new methodology depending on the desired operational requirements:

- Strategy n°1 is applied for the desired Minimum Required Availability (MRA) and the corresponding Absolute Minimum Required Availability (AMRA) is derived,
- Strategy n°2 is applied for a desired Average Availability (AA) and the corresponding Guaranteed Availability (GA) is given as additional information.

4.1.2.2.7.i *Strategy n°1*

Strategy n°2 is applied for an operational requirement which implies a Guaranteed Availability (GA) and/or an Average Availability (AA), and the corresponding Guaranteed Availability (GA) is given as additional information. The strategy steps are:

Table 26: Strategy n°1

Strategy n°1	
Step 0	Determining MRA (P_{mra}, T_{mra} and ER_{mra}) from the high level operational needs.
Step 1	Determining P_{0fav} (the probability that no 'favorable state message' has been received during the duration of interest T_{mra}) according to the probability associated to the minimum required availability P_{mra}.
Step 2	Searching for the favorable reception condition which induces this P_{0fav} probability value.
Step 3	Calculating the data error rate only for the data sets of interest contained in these 'favorable state messages'.
Step 4	Determining AMRA: the probability P_{amra} that the receiver is able to successfully demodulate a given data set in the given time T_{amra} for a given $C_{pre-urban}/N_{0_{amra}}$.

4.1.2.2.7.ii *Strategy n°2*

Strategy n°2 is applied for an operational requirement which implies an Average Availability (AA), and the corresponding Guaranteed Availability (GA) is given as additional information.

The strategy steps are different from strategy n°1:

Table 27: Strategy n°2

Strategy n°2	
Step 0	Determining AA: (Per_{aa} and T_{aa}) from the high level operational needs.
Step 1	Searching for the favorable reception condition which induces the desired Per_{aa} for the desired interval of time T_{aa}.
Step 2	Calculating the data error rate only for the data sets of interest contained in these 'favorable state messages' and determining at which $C_{pre\text{-}urban}/N_0$ the ER_{aa} is obtained.
Step 3	Providing GA: the average percentage of data sets Per_{ga}, that the receiver can demodulate in a given time T_{ga}, with a given data set error rate ER_{ga} and a guaranteed probability P_{ga}.

4.2 Results

In this section, the new methodology proposed to assess the GNSS signals demodulation performance in urban environments has been applied to two different operational requirements examples. Each operational requirements example has been chosen to use one of the two strategies defined earlier and to represent a real need. For each conducted strategy, both propagation channel models (described in Chapter 2) have been used.

In main considerations, an important assumption has been made for a first approach: four emitted satellites are considered as visible, with the same elevation angle, and for the DLR model with the same azimuth angle. This assumption has been made for time constraints in terms of simulations, but the results can be expanded.

4.2.1 Strategy n°1 Application

The operational requirement example chosen to develop the strategy n°1 of the new methodology is:

Table 28: Strategy n°1 operational requirement example

Strategy n°1 Operational Requirement Example
To determine if a GPS L1C receiver can calculate a continuous valid position during 4 consecutive hours, with a probability greater than 95%, and with a CED error rate equal to 10^{-2}. Note: a valid position means a position computed based on an applicable CED information.

4.2.1.1 Preliminary Step or Step 0

The preliminary step consists in interpreting this 'high level' operational requirement need through a 'low level'.

To compute a valid position continuously, it is necessary to ensure that the receiver can demodulate at least one CED set from at least four satellites during the same CED set validity period.

For GPS L1C, the emission period of a CED set is equal to two hours, and its validity period is equal to three hours [19]. We define t_0 as the beginning of the CED set emission period (see Figure 58). We assume that at time t_0 the receiver is able to compute a position: the receiver knows the CED sets of at least 4 satellites. To be sure that the receiver can compute a position continuously, since it remains one hour of validity for the CED sets demodulated before t_0, the receiver needs to demodulate at least one message from 4 different satellites during the next hour.

A valid position computation during:

- Interval $(t_0, t_0 + 1h)$ is guaranteed by previous demodulated CED sets.
- Interval $(t_0 + 1h, t_0 + 2h)$ is guaranteed by CED sets demodulated in interval $(t_0, t_0 + 1h)$.
- Interval $(t_0 + 2h, t_0 + 3h)$ is guaranteed by CED sets demodulated in interval $(t_0, t_0 + 2h)$.
- Etc.

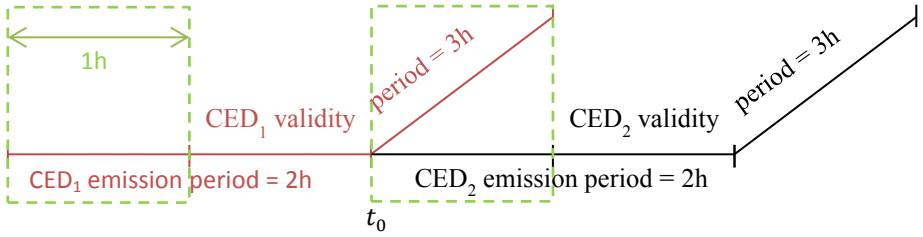

Figure 58: CED emission and validity periods diagram for GPS L1C

Considering these notations:

- $\mathbf{P_{final\text{-}4h}}$: the probability of receiving the necessary number of CED sets to allow the valid user position calculation during 4h from 4 different satellites,
- $\mathbf{P_{1sat\text{-}4h}}$: the probability of receiving at least 1 CED set from 1 satellite during the 1st hour and at least another message during the 3rd hour in a block of 4h,
- $\mathbf{P_{1sat\text{-}1h}}$: the probability of receiving at least 1 CED set from 1 satellite during 1h.

Assuming independent emitting satellite propagation channels, the probability $P_{final\text{-}4h}$ is equal to:

$$P_{final-4h} = {P_{1sat-4h}}^4 \tag{4.1}$$

And assuming independence between emitting satellite propagation channels intervals spaced by 1 hour:

$$P_{final-4h} = \left({P_{1sat-1h}}^2\right)^4 \tag{4.2}$$

And since $P_{final\text{-}4h}$ is required to be greater than 95% in the 'high level' requirements, it gives a lower bound of $P_{1sat\text{-}1h}$ equal to:

$$P_{1sat-1h} = \left(P_{final-4h}\right)^{1/8} = 0.9936 \tag{4.3}$$

Although AMRA requirement is more intuitive from the operational point of view and easily determined, its fulfilment cannot be directly assessed since the CEDER values of the received CED set with respect to the $C_{pre\text{-}urban}/N_0$ are not known in advance (this is one of the objectives of the methodology). Therefore, we must determine first the MRA requirement, derive the statistical occurrence values for the MRA parameters, and from these parameters and from a given ${C_{pre-urban}/N_0}_{amra}$ a bound on the AMRA requirement probability P_{amra} can be provided.

Therefore, recalling that a CEDER equal to 10^{-2} is required ($ER_{mra} = 10^{-2}$), we redefine:

- $\mathbf{P_{1sat\text{-}1h}}$: the probability of receiving at least 1 CED set from 1 satellite during 1h which can be demodulated with a CEDER=10^{-2}, which is the P_{mra}.

Finally, from the previous development, the 'low level' requirements MRA parameters are defined as:

Table 29: Operational requirement example 'low level' interpretation through the strategy n°1

Strategy n°1	
Step 0	MRA: $T_{mra} = 1h$, $P_{mra} = 0{,}9936$, $ER_{mra} = 10^{-2}$.

4.2.1.2 With the Perez-Fontan/Prieto Channel Model

4.2.1.2.1 Step 1: Determining $P_{0fav\ max}$

From the MRA 'low level' requirements, the $P_{0fav\text{-}1h}$ is derived. Since just at least one CED set has to be received with the required CEDER demodulation performance 10^{-2}, we can look for the most advantageous receiver conditions for the reception of these CED sets. Remember that the most advantageous receiver conditions represent the messages (which contains the data set of interest) entirely received in favorable reception conditions (determining by the criterion 1 or 2 introduced in section 4.1.2.2.4), referred as 'favorable state messages'. Note that in this case (Strategy n°1 Operational Requirement Example given in Table 28), the data set of interest is the CED set, and the message represents the subframe 1, 2 and 3 altogether. We thus consider the most advantageous receiver conditions for the reception of these CED sets: the entire message (subframes 1, 2 and 3) is received during favorable reception conditions.

Therefore, the probability that none message is received in favorable reception conditions $P_{0fav\text{-}1h}$ has to be smaller than or equal to the required probability $(1 - P_{mra})$:

$$P_{0fav-1h} \leq 1 - P_{mra} \tag{4.4}$$

Leading to:

$$P_{0fav-1h\ max} = 0.0064 \tag{4.5}$$

4.2.1.2.2 Step 2: Searching for the Favorable States that Meet $P_{0fav} < P_{0fav\ max}$

It is difficult to find the criterion to separate the 'unfavorable state messages' from the 'favorable state messages' which provides the best demodulation performance and which suits the operational requirements as well. Therefore, a first solution (introduced in section 4.1.2.2.4) is proposed which exploits the fact that the Perez-Fontan/Prieto propagation channel model is built on two states (see Chapter 2):

- 'Good' for LOS to moderate shadowing, and
- 'Bad' for moderate to deep shadowing.

The messages received entirely in 'Good' state conditions will be considered as the 'favorable state messages'.

In order to ensure that the desired $P_{0fav\text{-}1h\ max}$ value is respected, the occurrence rate of the 'favorable state messages', approximated by the 'favorable state messages' histogram, has been computed with SiGMeP. To do that, the number of messages which are received in favorable reception conditions has been calculated during $T_{occ} = T_{mra} = 1h$ (see Figure 57), for the simulation parameters of Table 30.

For a first approach, we consider that the four emitted satellites have the same elevation angle. Thus, the same favorable reception conditions are considered for all satellites.

Table 30: Simulation conditions for the Perez-Fontan/Prieto propagation channel model

Simulation Conditions	
Signals	GPS L1C
Channel Model	Perez-Fontan/Prieto
Channel Generation Fs	0.1 ms
Environment	Urban
Database Band	S
Satellite Elevation Angle	40°

The P_{0fav} value can then be extracted from Figure 57: it is the probability that no message has been received in favorable reception conditions over one hour.

$$P_{0fav-1h} = 0.6\% < P_{0fav-1h\,max} = 0.64\% \tag{4.6}$$

Thus, the criterion which has been chosen to determine the 'favorable state messages' and which induces $P_{0fav\text{-}1h} = 0.6\%$ allows fulfilling the required $P_{0fav\text{-}1h\ max} = 0.64\%$, involving the validation of P_{mra} and thus of $P_{final\text{-}4h}$, required to be higher than 95%.

4.2.1.2.3 Step 3: Calculating the CED Error Rate during 'Favorable States'

The GPS L1C 'favorable states CED' error rate is then computed with SiGMeP with the Perez-Fontan/Prieto propagation channel model, with ideal phase estimation and PLL tracking (simulation conditions are detailed in Table 29) and shown in Figure 59. Remember that the 'favorable states' correspond to an entire message (subframes 1, 2 and 3) but the data set of interest being the CED set, the demodulation performance (ER) is only computed on the CED sets.

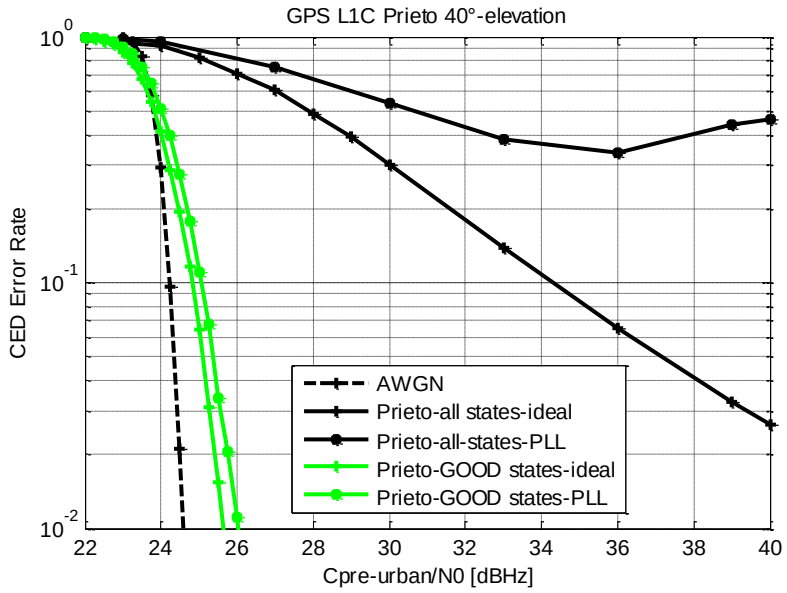

Figure 59: GPS L1C GOOD state CED demodulation performance and total CED demodulation performance with the Prieto model and emitting satellite elevation angle equal to 40°

Figure 59 represents in black solid lines the GPS L1C demodulation performance considering every received message whatever their reception conditions: favorable or unfavorable reception conditions, as it is made in the classical method. The classical methodology shows that it seems never possible to demodulate with an error rate equal to 10^{-2}. In fact, the classical methodology is not adapted to a GNSS since each received message does not need to be successfully demodulated. The most interesting information is hidden, which is the possibility of punctually obtaining much better demodulation performance for the 'favorable states messages'. Therefore, the CED can be demodulated with a CEDER much lower than the CEDER provided by the classical methodology for a given $C_{pre\text{-}urban}/N_0$ value for these messages. Moreover, from the setting of $P_{0fav\text{-}1h\ max}$, the demodulation performance of at least one CED set will have, with a probability P_{mra}, the demodulation performance of the 'state favorable CED'.

The floor observed for the GPS L1C signal demodulation performance with the Prieto propagation channel model considering all states (solid black lines) and PLL tracking seems due to the PLL losses of lock.

It thus seems that it is never possible to demodulate with the required error rate equal to 10^{-2} with the classical methodology and PLL tracking. In fact this representation (in black) is not adapted to a GNSS, since with the new way of representing the demodulation performance (in green), it can be seen that the GPS L1C CED can be demodulated with an error rate of 10^{-2} for a minimum $C_{pre\text{-}urban}/N_0$ value equal to 26 dB-Hz in the PLL tracking configuration in favorable reception conditions cases. In addition, these 'favorable states CED' are available enough to ensure that at least for 95% of the time the receiver can demodulate, with the "favorable state CED" demodulation performance, enough CED sets from 4 different satellites to continuously calculate its position during 4 consecutive hours.

4.2.1.2.4 Step 4: Providing P_{amra}

The new proposed methodology also allows providing P_{amra} which is the most intuitive requirement from the operational point of view. P_{amra} depends on the $C_{pre\text{-}urban}/N_0$ and can be calculated as follows, considering:

- $\mathbf{P_{1sat\text{-}1h,\ abs}}$: the probability of successfully demodulating at least 1 CED set from 1 satellite during $T_{amra} = T_{mra} = 1h$, which is the P_{amra},
- $\boldsymbol{P_{nfav}}$: the probability of receiving in favorable reception conditions *n* messages from 1 satellite during $T_{amra} = 1h$,
- $\boldsymbol{P_n}$: the probability that at least one message received in favorable reception conditions among n messages received in favorable reception conditions is successfully demodulated.

According to equation (4.2):

$$P_{final-4h} = {P_{1sat-1h,abs}}^{8} = {P_{amra}}^{8} \tag{4.7}$$

with:

$$P_{amra} = P_{1fav}.P_1 + P_{2fav}.P_2 + \cdots + P_{200fav}.P_{200} \tag{4.8}$$

$$P_{amra} = P_{1fav} * \left(1 - CEDER_{\frac{C}{N_0}}\right) + P_{2fav} * \left(1 - {CEDER_{\frac{C}{N_0}}}^{2}\right) + \cdots + P_{200fav} * \left(1 - {CEDER_{\frac{C}{N_0}}}^{200}\right) \tag{4.9}$$

Recalling that a CEDER equal to 10^{-2} is required ($ER_{mra} = 10^{-2}$), the corresponding $C_{pre-urban}/{N_0}_{amra} = 26.25\ dB\ Hz$ value is taken from Figure 59 for PLL tracking. Thus, from equation (2.9) and Figure 57, the final P_{amra} can be computed, it is equal to:

$$P_{amra} \approx 0.994 \tag{4.10}$$

According to equation (4.7), this approximate P_{amra} value finally leads to $P_{final\text{-}4h}$ = 95.3%, the required $P_{final\text{-}4h}$ equal to 95% being thus validated.

It can be concluded that a GPS L1C receiver can calculate a continuous valid position during 4 consecutive hours, with a probability approximately equal to 95.3%, for a $C_{pre\text{-}urban}/N_0$ higher than 26.25 dB-Hz, considering the Perez-Fontan/Prieto propagation channel model and parameters of Table 30 for each of the 4 emitting satellites.

4.2.1.2.5 Additional Results Obtained with Different Satellites Elevation Angles

These preceding results have been obtained in computing the GPS L1C signal demodulation performance in the Perez-Fontan/Prieto propagation channel with the simulation parameters of Table

30. In order to observe the emitting satellite elevation angle impact of the results provided by the classical and the new methodology, additional simulations have been made with 80° of elevation.

Figure 60 represents the 'favorable state messages' occurrence rate considering GPS L1C and an emitting satellite with 80° of elevation. This figure has to be compared with Figure 57, obtained with GPS L1C and 40° of elevation. The average number of 'favorable state messages' received in 1 hour from 1 emitting satellite is clearly higher for the elevation case equal to 80°. Indeed, in urban environments, a higher elevation allows avoiding some impacts between the satellite and the user, inducing less attenuation on the received signal. Thus, the favorable reception conditions occur more often.

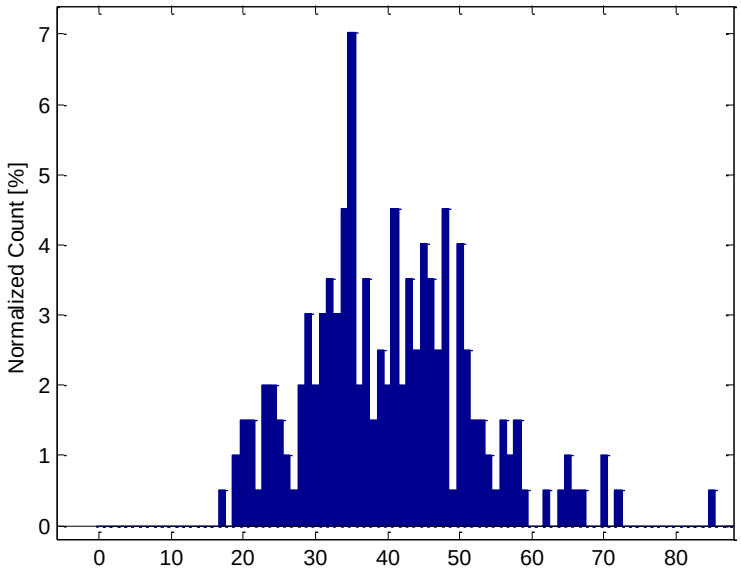

Figure 60: 'Favorable state messages' histogram, for GPS L1C in the Prieto channel model with 80° of elevation considering the Prieto channel GOOD states as favorable reception conditions

The demodulation performance has then been computed with the classical methodology (solid lines) and with the new methodology (dotted lines), considering a PLL tracking. The results obtained with the emitting satellite elevation equal to 80° are compared with those obtained before with 40°.

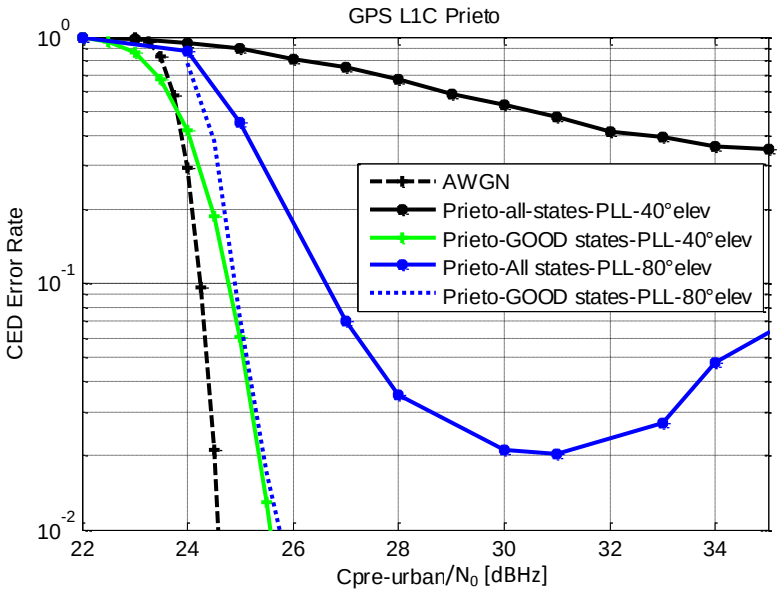

Figure 61: GPS L1C GOOD state CED demodulation performance and total CED demodulation performance with the Prieto model and emitting satellite elevation angle equal to 40° and 80°, considering a PLL tracking

Moreover, according to equation (4.9) and results of Figure 60 and Figure 61, the P_{amra} probability has been computed for the 80° elevation case. For a $C_{pre-urban}/N_{0_{amra}} = 25.8$ dB Hz leading to CEDER equal to 10^{-2}, and PLL tracking, it is approximately equal to:

$$P_{amra} \approx 1 \tag{4.11}$$

According to equation (4.7), this approximate P_{amra} value finally leads to $P_{final\text{-}4h} = 100\%$, the required $P_{final\text{-}4h}$ equal to 95% being thus validated.

It can be concluded that a GPS L1C receiver can calculate a continuous valid position during 4 consecutive hours, with a probability approximately equal to 100%, for a $C_{pre\text{-}urban}/N_0$ higher than 25.8 dB-Hz, considering the Perez-Fontan/Prieto propagation channel model and 80° of elevation for each of the 4 emitting satellites.

If we consider 4 different satellites: two with elevation angles equal to 80° (satellite 1 and 2) and the others with 40° (satellites 3 and 4), the $P_{final\text{-}4h}$ is equal to:

$$P_{final-4h} = P_{sat1-4h} . P_{sat2-4h} . P_{sat3-4h} . P_{sat4-4h} \tag{4.12}$$

Leading to:

$$P_{final-4h} = P^2_{amra-sat1} . P^2_{amra-sat2} . P^2_{amra-sat3} . P^2_{amra-sat4} \tag{4.13}$$

According to equation (4.13), the approximate P_{amra} values associated with a 80° of elevation satellite (equation (4.11)) and 40° (equation (4.10)), finally lead to $P_{final\text{-}4h} = 97.6\%$, the required $P_{final\text{-}4h}$

equal to 95% being thus validated. This $P_{final\text{-}4h}$ = 97.6% value can be compared with the value obtained with 4 emitting satellites elevation angles equal to 40°. In this case, $P_{final\text{-}4h}$ was equal to 95.3%, which is coherent since 40° of elevation is less advantageous in terms of favorable reception conditions compared with 80°.

4.2.1.2.6 Additional Results Obtained with Galileo E1 OS

In order to compare the demodulation performance obtained with the GPS L1C and Galileo E1 OS signals, additional simulations have been made. The Galileo E1 OS signal has been tested, with the same parameters than Table 30 and with a PLL tracking.

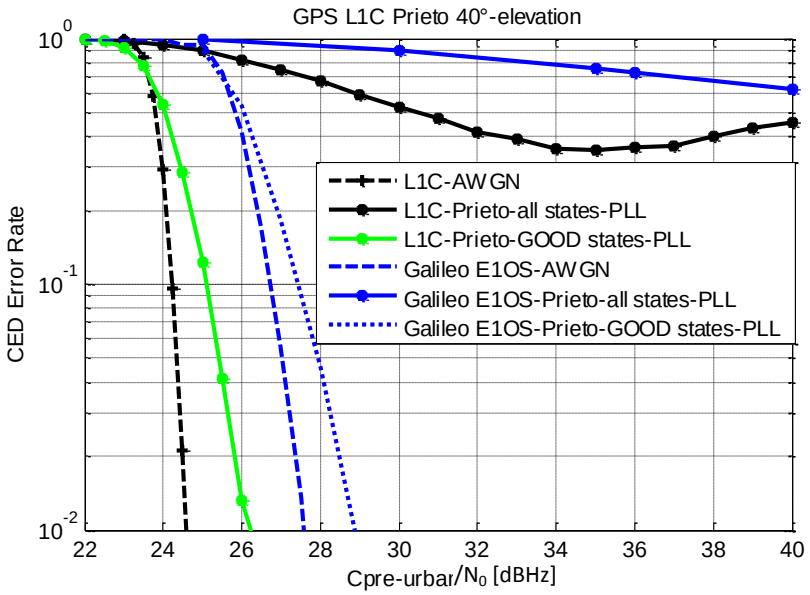

Figure 62: GPS L1C and Galileo E1 OS GOOD state CED demodulation performance and total CED demodulation performance with the Prieto model and emitting satellite elevation angle equal to 40°, considering a PLL tracking

The classical methodology (solid lines) provides really degraded demodulation performance whereas the new methodology (dotted lines) approaches the near optimum performance provided with the AWGN propagation channel model. In fact, the Galileo E1 OS CED can be demodulated with an error rate of 10^{-2} for a minimum $C_{pre\text{-}urban}/N_0$ value equal to 29 dB-Hz in the PLL tracking configuration in favorable reception conditions cases.

The 'favorable state messages' occurrence rate has thus been computed for Galileo E1 OS, considering that one message (the subframe of 15 pages lasting 30 s, refer to Chapter 2) is in favorable reception conditions if each page of the considered subframe containing the CED (word type 1, 2, 3 and 4, refer to Chapter 2) is entirely received during the same Prieto channel GOOD state (refer to section 4.2.1.2.2).

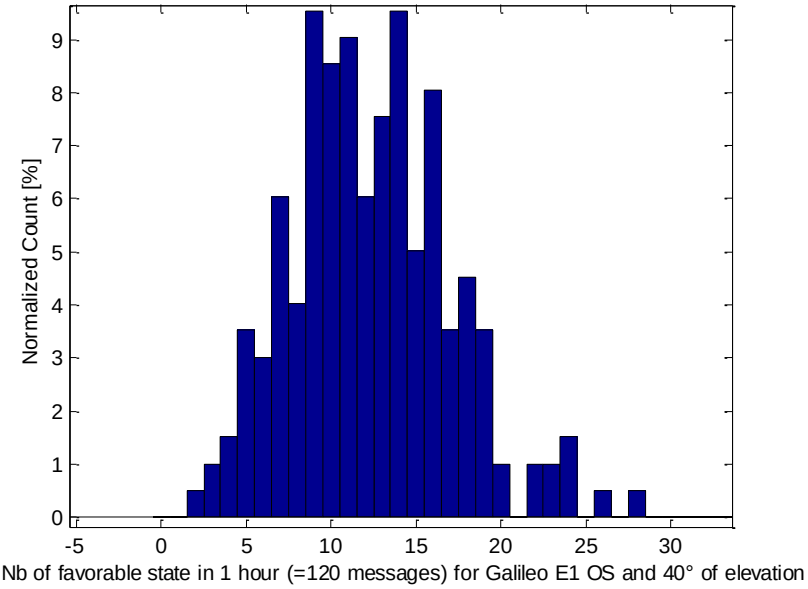

Figure 63: 'Favorable state messages' histogram, for Galileo E1 OS in the Prieto channel model with 40° of elevation considering the Prieto channel GOOD states as favorable reception conditions

If we consider the same validity period than for GPS L1C, the same process of Figure 58 is applied in the Galileo E1 OS case: to be sure that the receiver can compute a position continuously, since it remains one hour of validity for the CED sets (word types 1, 2, 3 and 4, refer to Chapter 2)) demodulated before t_0, the receiver needs to demodulate at least one message from 4 different satellites during the next hour.

According to equation (4.9) and results of Figure 63 and Figure 62, the P_{amra} probability has been computed for the Galileo E1 OS signal case. For a $C_{pre-urban}/N_{0_{amra}} = 29$ dB Hz leading to CEDER equal to 10^{-2}, and PLL tracking, it is approximately equal to:

$$P_{amra} \approx 1 \tag{4.14}$$

This P_{amra} value finally leads to the $P_{final\text{-}4h}$ equal to 100%.

It can be concluded that a Galileo E1 OS receiver can calculate a continuous valid position during 4 consecutive hours, with a probability approximately equal to 100%, for a $C_{pre\text{-}urban}/N_0$ higher than 29 dB-Hz, considering the Perez-Fontan/Prieto propagation channel model and parameters of

Table **30** (40° of elevation) for each of the 4 emitting satellites. This result can be compared with the result obtained with GPS L1C in section 4.2.1.2.4: probability approximately equal to 95.3%, for a $C_{pre\text{-}urban}/N_0$ higher than 26.25 dB-Hz. The lower probability value for GPS L1C can be explained by the fact that in this case, the 'favorable state messages' occurrence rate has been computed through the entire message (since subframes 2 and 3 are interleaved and since the subframe 1 duration is negligible) lasting 18 s, whereas for Galileo E1 OS, just two message parts each lasting approximately 4 s, over the message duration equal to 30 s have been considered. It is thus easier to have twice 4 s in favorable reception conditions for the Galileo E1 OS case than 18 s for GPS L1C. However, the demodulation performance obtained with GPS L1C is better than Galileo E1 OS.

4.2.1.3 With the DLR Channel Model

The same strategy is then applied with the DLR propagation channel model for GPS L1C.

4.2.1.3.1 Step 1: Determining $P_{0fav\ max}$

Since this $P_{0fav\ max}$ value only depends on the emission and validity interval of the transmitted GNSS signal CED set, the propagation channel model has no impact on it. Therefore, the same reflections than made in section 4.2.1.2.1 for the Perez-Fontan/Prieto propagation channel model case lead to:

$$P_{0fav-1h\ max} = 0.0064 \tag{4.15}$$

4.2.1.3.2 Step 2: Searching for the Favorable States that Meet $P_{0fav} < P_{0fav\ max}$

The aim of this step consists in determining a separation between 'favorable state messages' and 'unfavorable state messages' which ensures that the probability that no messages are received in favorable reception conditions during the interest interval $T_{mra} = 1h$, $P_{0fav\text{-}1h}$, is lower than $P_{0fav\text{-}1h\ max}$.

It is difficult to find the best criterion to separate the 'favorable state messages' from the 'unfavorable state messages' and the first solution used for the Perez-Fontan/Prieto propagation channel model cannot be used with the DLR model, since 'good' and 'bad' states do not longer exist in the DLR model generation. The separation between 'favorable state messages' and 'unfavorable state messages' has thus been made by applying the second criterion of section 4.1.2.2.4: through the estimation of the received C/N_0.

Figure 64 illustrates the separation process between 'favorable state messages' and 'unfavorable state messages'. The first stage consists in computing the degradation distribution between the received C/N_0 and the $C_{pre\text{-}urban}/N_0$ over one message. Then, this C/N_0 degradation distribution associated with one message is used to determine a threshold value. A given proportion X of 'favorable state messages' is wanted, determined thanks to the C/N_0 message degradation distribution and leading to the associated threshold determination. If the C/N_0 message degradation is below the threshold, the message is considered as 'favorable state message'. The process thus needs to be conducted for each $C_{pre\text{-}urban}/N_0$, since the degradation distribution depends on this value. A more detailed explanation is given next.

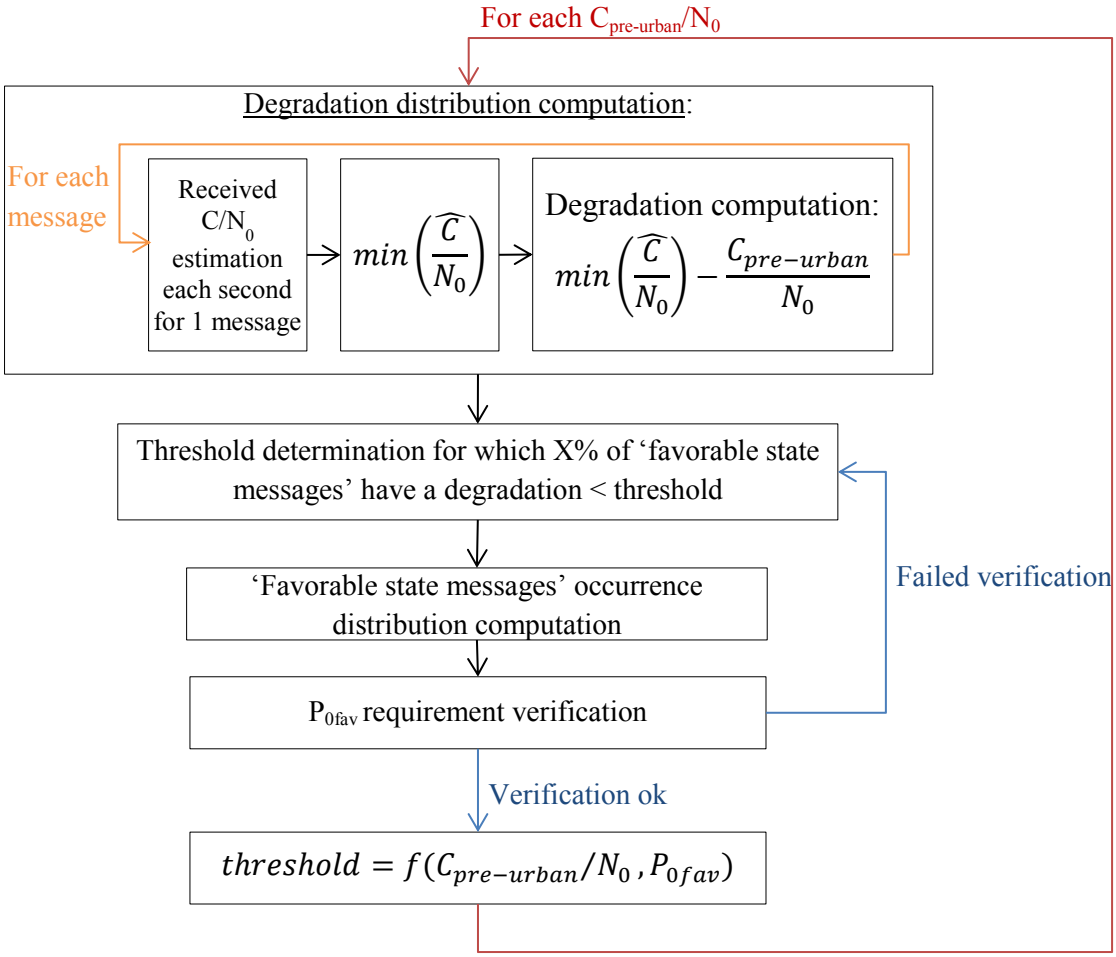

Figure 64: 'Favorable state messages' determination through the received C/N_0 estimation

Degradation distribution computation block:

First, the received C/N_0 is estimated for intervals of 1 second. Second, the minimum estimated received C/N_0 value among all the estimated received C/N_0 of one message is selected. Third, the distribution of the degradation between $C_{pre\text{-}urban}/N_0$ and the selected C/N_0 value is computed (see Figure 65 as example with the simulation parameters given in Table 31).

Table 31: Simulation conditions for the DLR propagation channel model

Simulation Conditions	
Signals	GPS L1C
Channel Model	DLR
Channel Generation Fs	0.1 ms
Environment	Urban
Satellite Elevation Angle	40°
Satellite Azimuth Angle	30°

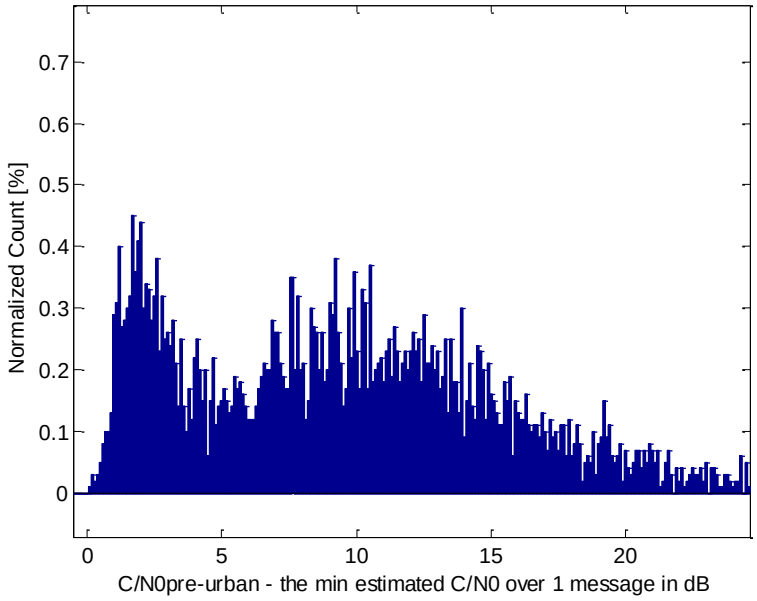

Figure 65: Distribution of the degradation between the $C_{pre\text{-}urban}/N_0$ value and the minimum estimated received C/N_0 over 1 message, for $C_{pre\text{-}urban}/N_0$ = 25 dB-Hz and PLL tracking with the DLR model

Threshold selection:

From this figure, a threshold is determined. The messages for which the degradation is below this threshold will be considered as 'favorable states messages'.

Since the separation between 'favorable state messages' and 'unfavorable state messages' made for the Perez-Fontan/Prieto propagation channel model has implied an average occurrence equal to 3.4%, this is this value which will be first used for the DLR model 'favorable state messages' definition (X = 3,4% as been chosen in this case). It means that the threshold value is chosen to ensure that 'favorable states messages' are available at least 3.4% of the time in average (refer to Figure 66 as example).

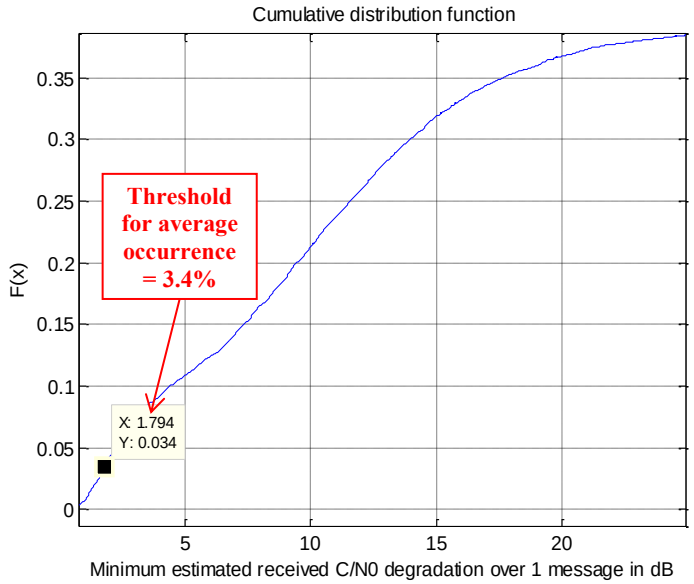

Figure 66: Cumulative distribution function of the degradation between the $C_{pre\text{-}urban}/N_0$ value and the minimum estimated received C/N_0 over 1 message, for $C_{pre\text{-}urban}/N_0$ = 25 dB-Hz and PLL tracking with the DLR model

In Figure 66 for example, the degradation threshold value corresponding to an average occurrence of 3.4% is equal to 1.79 dB. It induces that a received message for which the minimum estimated received $C/N_{0\ min}$ fulfills this following condition (equation (4.16)) is considered as a 'favorable state message'.

$$C/N_{0_{min}} > C_{pre-urban}/N_0 + threshold \tag{4.16}$$

Finally, remember that since this degradation depends on the $C_{pre\text{-}urban}/N_0$ input value, this process is made for each $C_{pre\text{-}urban}/N_0$.

$$threshold = f(C_{pre-urban}/N_0\,, P_{0fav}) \tag{4.17}$$

'Favorable state message' distribution:

Then, it remains to ensure that $P_{0fav\text{-}1h} < P_{0fav\text{-}1h\ max}$. The occurrence rate of the 'favorable states messages' has been computed with SiGMeP (refer to section 4.1.2.2.5) during $T_{mra} = 1h$ (see Figure 67).

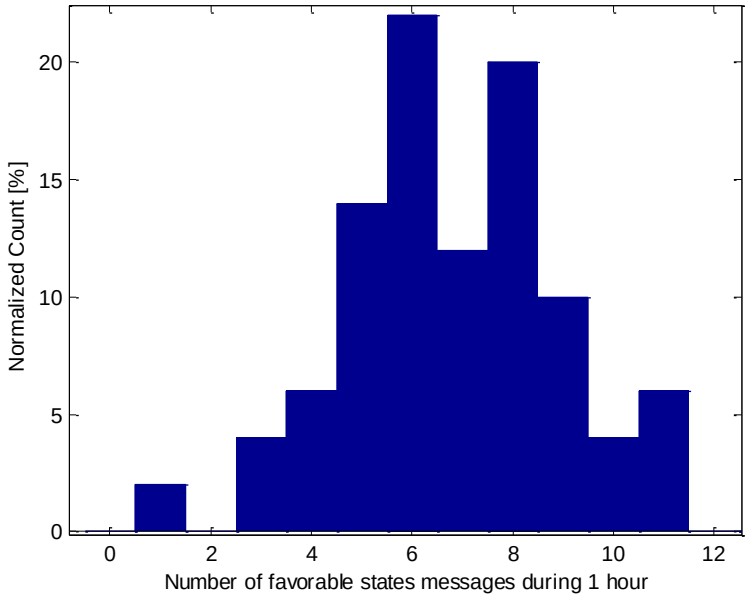

Figure 67: Favorable states message over 1 hour distribution with 3.4% of average availability, for $C_{pre\text{-}urban}/N_0$ = 25 dB-Hz and PLL tracking, with the DLR model

It may be recalled that this method of 'favorable state messages' and 'unfavorable state messages' separation depends on the $C_{pre\text{-}urban}/N_0$ value. Thus, all the preceding figures depends on the $C_{pre\text{-}urban}/N_0$ value.

$P_{0fav\text{-}1h}$ requirement verification:

The $P_{0fav\text{-}1h}$ value can then be extracted from this figure: it is the probability that no message has been received in favorable reception conditions over one hour. Thus:

$$P_{0fav-1h} = 0\% < P_{0fav-1h\,max} = 0.64\% \tag{4.18}$$

Thus, the criterion which has been chosen to determine the 'favorable state messages' and which induces $P_{0fav\text{-}1h} = 0\%$ allows fulfilling the required $P_{0fav\text{-}1h\ max} = 0.64\%$, involving the validation of P_{mra} and thus of $P_{final\text{-}4h}$, required to be higher than 95%.

4.2.1.3.3 Step 3: Calculating the CED Error Rate during Favorable Reception Conditions

The 'favorable states CED' (corresponding to CED contained by messages entirely received during favorable reception conditions) error rate is then computed with SiGMeP with the DLR propagation channel model, with ideal phase estimation and PLL tracking (considering the simulation parameters of Table 31) and showed in Figure 68:

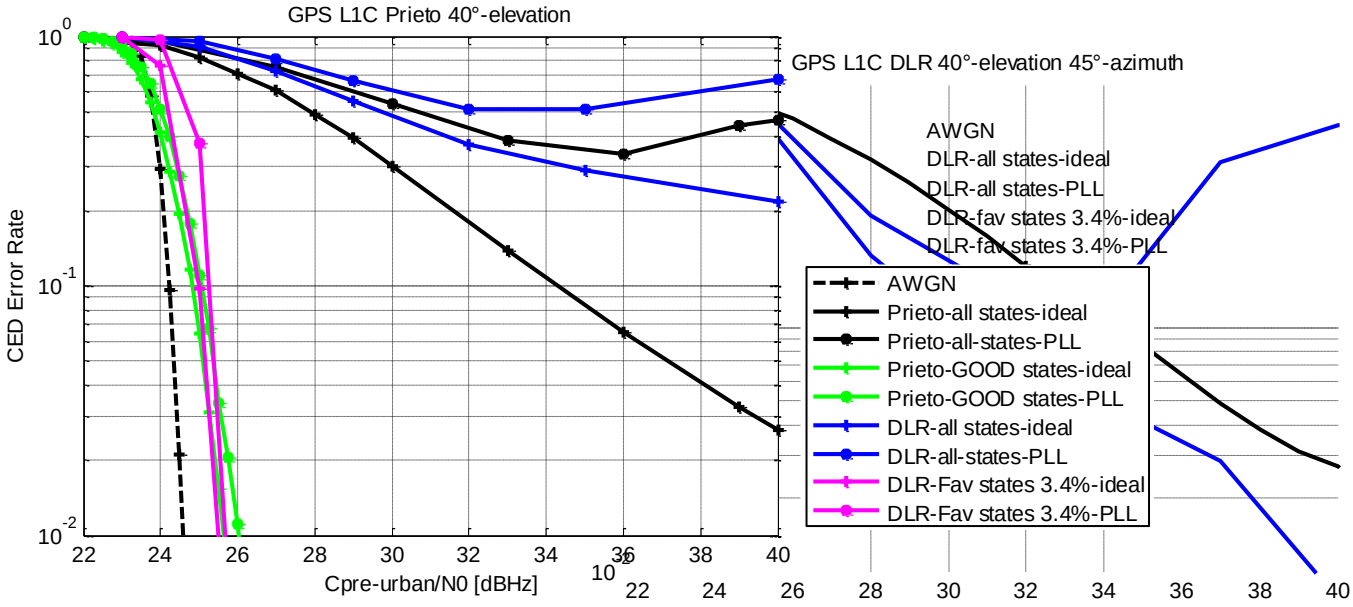

Figure 68: GPS L1C favorable states CED demodulation performance and total demodulation performance with the DLR model

As for the Perez-Fontan/Prieto propagation channel model case, the demodulation performance with the classical methodology (dark blue lines) are really bad in comparison with the one obtained with the new methodology (magenta lines) considering only the 'favorable states CED'. The classical methodology shows that it seems never possible to demodulate with an error rate equal to 10^{-2}. With the new way of representing the demodulation performance, it can be seen that the GPS L1C CED can be demodulated with an error rate of 10^{-2} for a minimum $C_{pre\text{-}urban}/N_0$ value greater than 25.5 dB-Hz in the PLL tracking configuration in favorable reception conditions. . In addition, these 'favorable states CED' are available enough to ensure that at least for 95% of the time the receiver can demodulate, with the 'favorable state CED' demodulation performance, enough CED messages from 4 different satellites to continuously calculate its position during 4 consecutive hours.

The PLL floor observed in section 4.2.1.2.3 for the Prieto channel model is still present for the DLR channel model, also due to the PLL losses of lock.

4.2.1.3.4 Step 4: Providing P_{amra}

Recalling that a CEDER equal to 10^{-2} is required ($ER_{mra} = 10^{-2}$), the corresponding $C_{pre-urban}/N_{0}{}_{amra} = 25.5\ dB\ Hz$ value is taken from Figure 68 for PLL tracking. According to equation (4.9) and Figure 67, the final P_{amra} is thus equal to:

$$P_{amra} \approx 0.9997 \tag{4.19}$$

According to equation (4.7), this approximate P_{amra} value finally leads to $P_{final\text{-}4h}$ = 99.8%, the required $P_{final\text{-}4h}$ equal to 95% being thus validated.

It can be concluded that a GPS L1C receiver can calculate a continuous valid position during 4 consecutive hours, with a probability approximately equal to 99.8%, for a $C_{pre\text{-}urban}/N_0$ higher than 25.5 dB-Hz, considering the Perez-Fontan/Prieto propagation channel model and parameters of Table 31 for each of the 4 emitting satellites.

4.2.2 Strategy n°2 Application

The operational requirement example chosen to develop the strategy n°2 of the new methodology is:

Table 32: Strategy n°2 operational requirement example

Strategy n°2 Operational Requirement Example
To determine if a receiver is able to demodulate 10% of time the GPS L1C **subframe 3** with an error rate equal to 10^{-2}, during 1h.

4.2.2.1 Preliminary Step or Step 0

The preliminary step consists in interpreting the 'high level' operational requirement need through a 'low level'. In this case, the conversion is immediate:

Table 33: Operational requirement example interpretation through the strategy n°2

Strategy n°2	
Step 0	AA: $Per_{aa} = 10\%, T_{aa} = 1h, ER_{aa} = 10^{-2}$.

This example has been chosen to remind that this new methodology is not exclusively focused to the CED. Whatever the employed strategy (n°1 or n°2), the goal consists in developing a methodology able to provide the GNSS signals demodulation performance adapted to urban environments, whatever the data of interest. Both strategies can be used for any data type in the navigation message.

4.2.2.2 With the Perez-Fontan/Prieto Channel Model

4.2.2.2.1 Step 1: Searching for the Favorable States that Meet $Per_{aa} = 10\%$,

The aim of this step consists in determining a division between 'favorable state messages' and 'unfavorable state messages' which obtains a 'favorable state messages' average occurrence equal to Per_{aa} (=10%). Obviously, the determination of the 'favorable state messages' will determine the demodulation performance of the 'favorable state messages'. Therefore, the 'favorable state messages' which provide the best demodulation performance must be searched. This means that if the 'favorable state messages' are optimally chosen, the demodulation performance achieved by an average of Per_{aa} 'favorable state messages' will be the best possible one. And, if for these 'favorable state messages', the ER_{aa} required by the AA requirement is not obtained, we can concluded that the AA requirement cannot be met.

However, since there is no developed method to obtain the optimal 'favorable states messages' (future work) in this PhD thesis, we will test a 'favorable state message' determination criterion and we will inspect the demodulation performance of the resulting 'favorable state messages'. If the demodulation performance provides the ER_{aa} required by the AA requirement, we will conclude that the AA requirement is met. If not, since the tested method is not the optimal one, we will not able to conclude about the AA requirement. In any case, a first criterion to know if the chosen 'favorable state messages' determination criterion is near the optimal one will be to compare the 'favorable state messages' demodulation performance with the AWGN channel demodulation performance: in the best case scenario, the 'favorable state messages' with an average occurrence equal to Per_{aa} will have the optimal demodulation performance of the AWGN channel.

The division between 'favorable state messages' and 'unfavorable state messages' has been made through the estimation of the received C/N_0 as detailed in section 4.2.1.3.2, as it is illustrated in Figure 69.

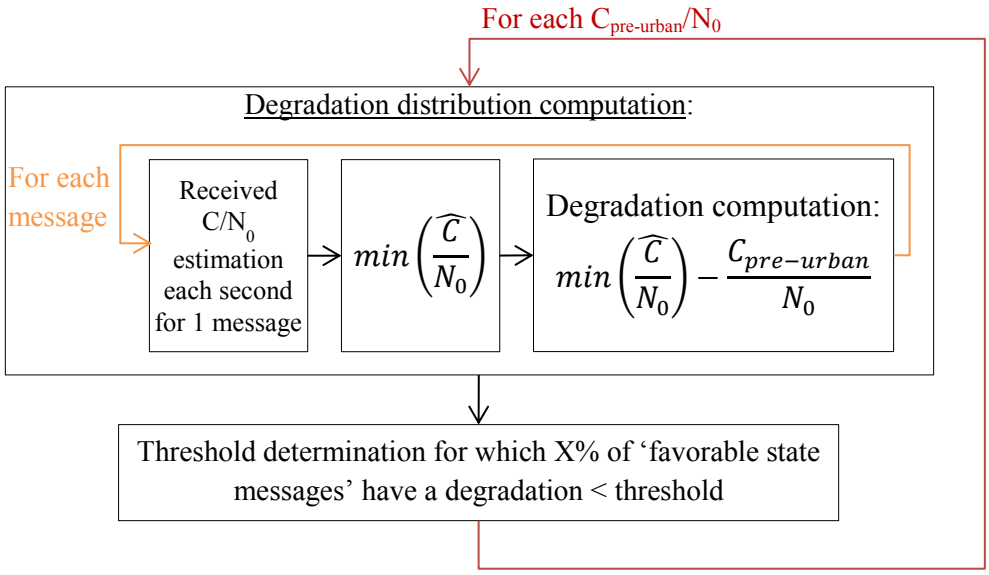

Figure 69: 'Favorable state messages' determination through the received C/N_0 estimation

In Figure 70 for example, the degradation threshold value corresponding to an average occurrence of 10% ($Per_{aa} = 10\%$) is equal to 3.5 dB for a $C_{pre\text{-}urban}/N_0$ = 37 dB-Hz and PLL tracking. It induces that a received message for which the minimum estimated received $C/N_{0\,min}$ fulfills the condition (4.16) is considered as a 'favorable state message', the threshold depending on the $C_{pre\text{-}urban}/N_0$ value.

Table 34: Simulation conditions for the Perez-Fontan/Prieto propagation channel model

Simulation Conditions	
Signals	GPS L1C
Channel Model	Perez-Fontan/Prieto
Channel Generation Fs	0.1 ms
Environment	Urban
Database Band	S
Satellite Elevation Angle	40°

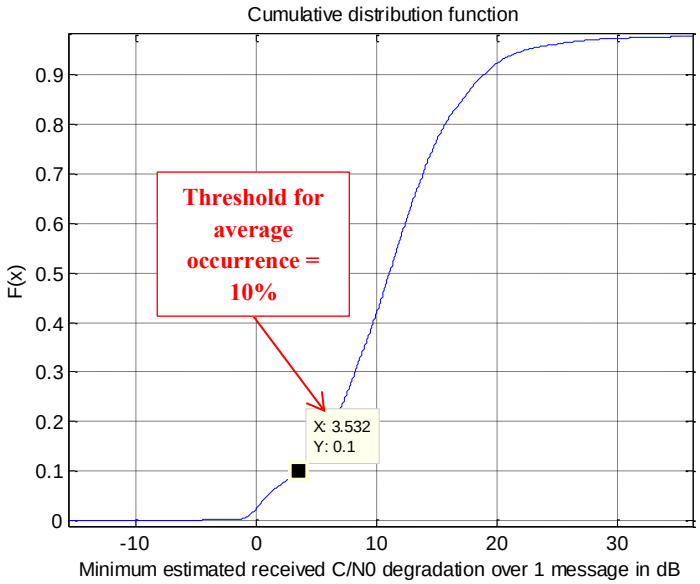

Figure 70: Cumulative distribution function of the degradation between the $C_{pre\text{-}urban}/N_0$ value and the minimum estimated received C/N0 over 1 message, for $C_{pre\text{-}urban}/N_0$ = 37 dB-Hz and PLL tracking, with the Prieto model

4.2.2.2.2 Step 2: Calculating the Subframe 3 Error Rate during Favorable Reception Condition

The 'favorable states subframe 3' error rate is then computed with SiGMeP with the Perez-Fontan/Prieto propagation channel model, with ideal phase estimation and PLL tracking:

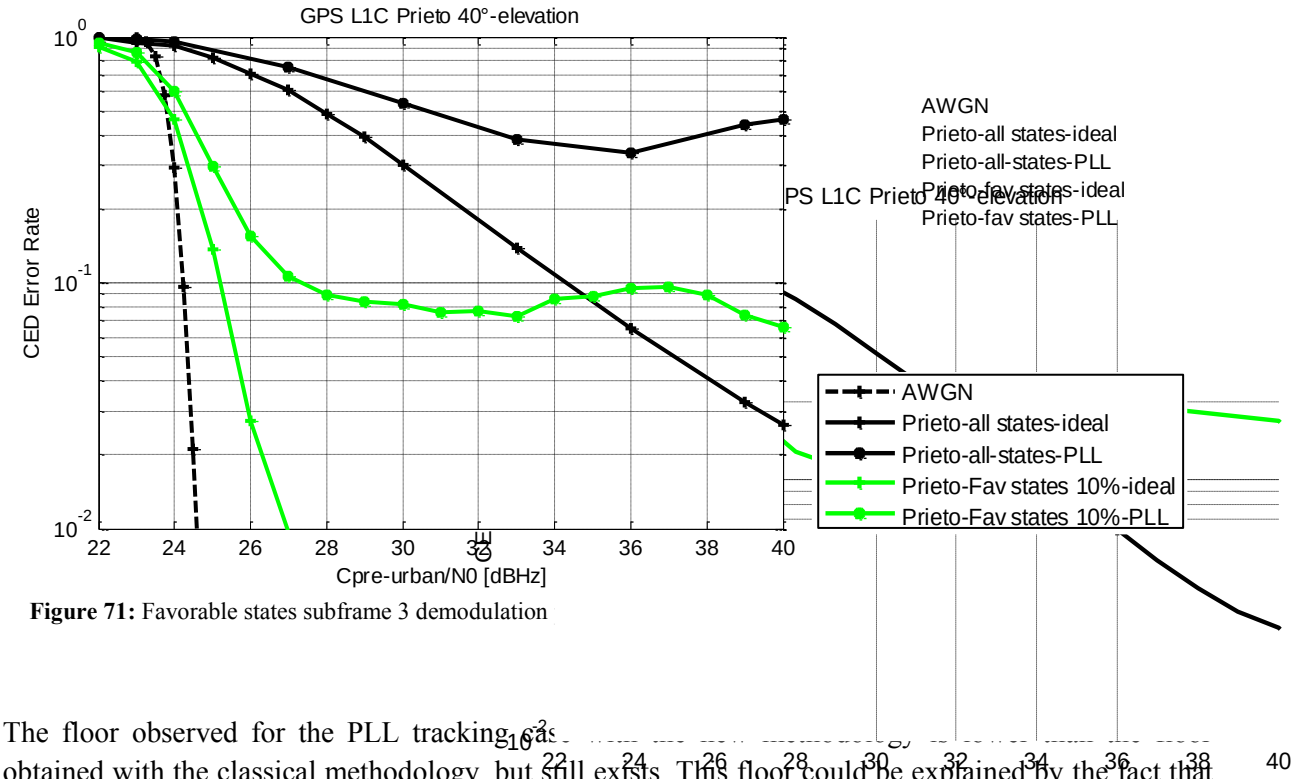

Figure 71: Favorable states subframe 3 demodulation

The floor observed for the PLL tracking was [illegible] obtained with the classical methodology, but still exists. This floor could be explained by the fact that this criterion of separating 'favorable state messages' from 'unfavorable state messages' does not specifically tackle the PLL losses of lock, which is an essential parameter of successful demodulation. Therefore, it can be concluded that for the 'favorable state messages' division criterion defined in this part according to the estimated received C/N_0 value, the AA requirement is not fulfilled. And, as explained before, a different criterion for separating both states should be tested. Unfortunately, at the moment of the manuscript writing, it was not possible to determine the optimal 'favorable state messages' division criterion, and thus it was not possible to determine if the AA requirement with the desired parameters could be fulfilled when using the Prieto propagation channel mathematical model.

4.2.2.2.3 Optional Step 3: Determining GA

An additional objective consists in determining the percentage of data sets inside a block of $T_{ga} = T_{aa} = 1h$ seconds for which the AA (the receiver can demodulate with a given data set error rate ER_{aa}) is guaranteed with a high probability P_{ga}.

To do that, the 'favorable state messages' occurrence rate has to be computed. Since it has been showed in Figure 71 that the 'favorable state subframe 3' demodulation performance never achieves $ER_{aa} = 10^{-2}$, and that the 'favorable state messages' occurrence rate depends on the $C_{pre\text{-}urban}/N_0$ value, an arbitrary value of $C_{pre\text{-}urban}/N_0$ has been chosen, equal to 37 dB-Hz (this choice has been motivated by the real $C_{pre\text{-}urban}/N_0$ value which is expected in GNSS, around 35 dB-Hz). The corresponding 'favorable state messages' occurrence rate is showed in Figure 72.

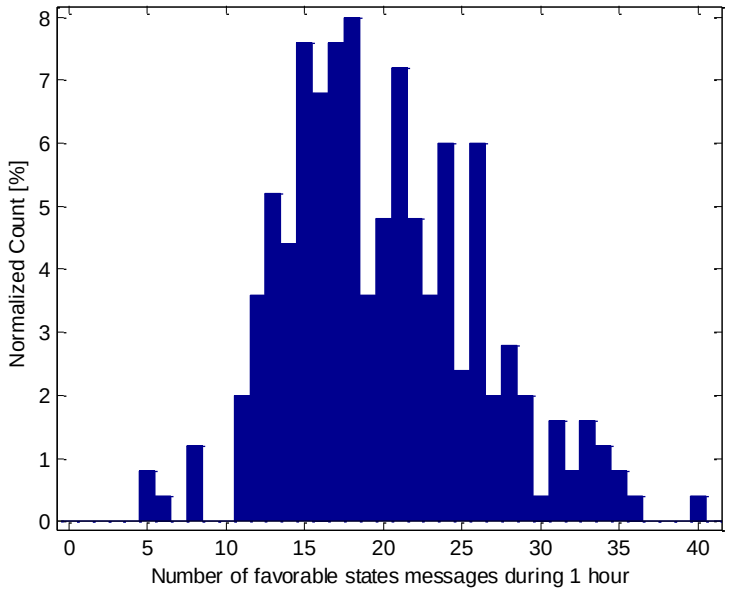

Figure 72: Favorable state messages over 1 hour distribution, for $C_{pre\text{-}urban}/N_0$ = 37 dB-Hz and PLL tracking with the Prieto model

According to this figure, the percentage of 'favorable state messages' Per_{ga} inside a block of $T_{ga} = 1h$ for which the receiver can demodulate the subframe 3 with a given ER, can be computed associated with a probability P_{ga}:

Table 35: GA for the Perez-Fontan/Prieto model, for $C_{pre\text{-}urban}/N_0$ = 37 dB-Hz

	Statistical results			
GA	T_{ga}	ER	Per_{ga}	P_{ga}
	1h	0.18	6%	96%

It can be concluded that, the receiver can demodulate 6% of the total number of subframes 3 received in 1h, with an error rate of 0.18, for 96% of the blocks of 1h length.

This bad demodulation performance result can be due to the 'favorable state messages' division criterion defined in this part according to the estimated received C/N_0 value, which is not optimal. As explained before, further works remain to be done on this issue.

4.2.2.3 With the DLR Channel Model

4.2.2.3.1 Step 1: Searching for the Favorable States that Meet $Per_{aa} = 10\%$,

The division between 'favorable state messages' and 'unfavorable state messages' has been made through the estimation of the received C/N_0 as detailed in section 4.2.1.3.2 and illustrated in Figure 69.

4.2.2.3.2 Step 2: Step 2: Calculating the Subframe 3 Error Rate during Favorable Reception Conditions

The 'favorable states subframe 3' error rate is then computed with SiGMeP with the DLR propagation channel model, with ideal phase estimation and PLL tracking. The simulations have been made with the parameters given in Table 36.

Table 36: Simulation conditions for the DLR propagation channel model

Simulation Conditions	
Signals	GPS L1C
Channel Model	DLR
Channel Generation Fs	0.1 ms
Environment	Urban
Satellite Elevation Angle	40°
Satellite Azimuth Angle	30°

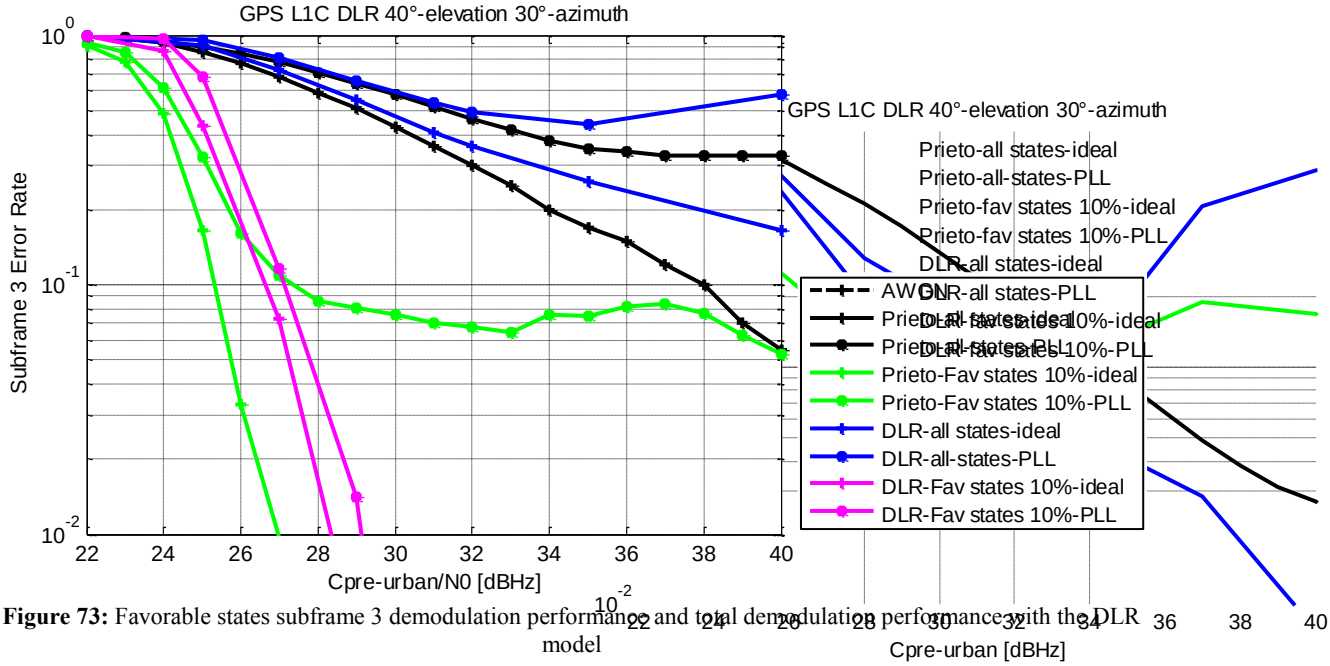

Figure 73: Favorable states subframe 3 demodulation performance and total demodulation performance with the DLR model

The demodulation performance represented by the classical methodology (blue lines) seems really bad in comparison with the one represented by the new methodology (magenta lines) considering only the 'favorable states messages'. It seems never possible to demodulate with an error rate equal to 10^{-2} with the classical methodology. With the new way of representing the demodulation performance, it can be seen that the GPS L1C subframe 3 can be demodulated with an error rate of 10^{-2} for a minimum $C_{pre\text{-}urban}/N_0$ value greater than 29 dB-Hz in the PLL tracking configuration in 'favorable state messages' cases. In addition, these 'favorable states subframes 3' are in average available 10% of time.

The floor observed for the PLL tracking case with the classical methodology and with the new methodology for the Perez-Fontan/Prieto propagation channel model does not exist with the new methodology and the DLR model. It can be supposed that the PLL losses of lock are less present when the DLR propagation channel model is generated instead of the Perez-Fontan/Prieto propagation channel model. Finally, the Perez-Fontan/Prieto and the DLR propagation channel models seem to provide different demodulation performance.

Therefore, it can be concluded that for the 'favorable state messages' division criterion defined in this part according to the estimated received C/N_0 value, the AA requirement is fulfilled if we consider the DLR propagation channel model, for a $C_{pre\text{-}urban}/N_0$ higher than 29 dB-Hz.

4.2.2.3.3 Optional Step 3: Determining GA

An additional objective consists in determining the percentage of data sets inside a block of $T_{ga} = T_{aa} = 1h$ seconds for which the AA (the receiver can demodulate with a given data set error rate ER_{aa}) is guaranteed with a high probability P_{ga}.

To do that, the 'favorable state messages' occurrence rate has to be computed. Since it has been showed in Figure 73 that the 'favorable state subframe 3' demodulation performance achieves $ER_{aa} = 10^{-2}$ for $C_{pre\text{-}urban}/N_0$ equal to 29 dB-Hz, the 'favorable state messages' occurrence rate has been computed for this $C_{pre\text{-}urban}/N_0$ value:

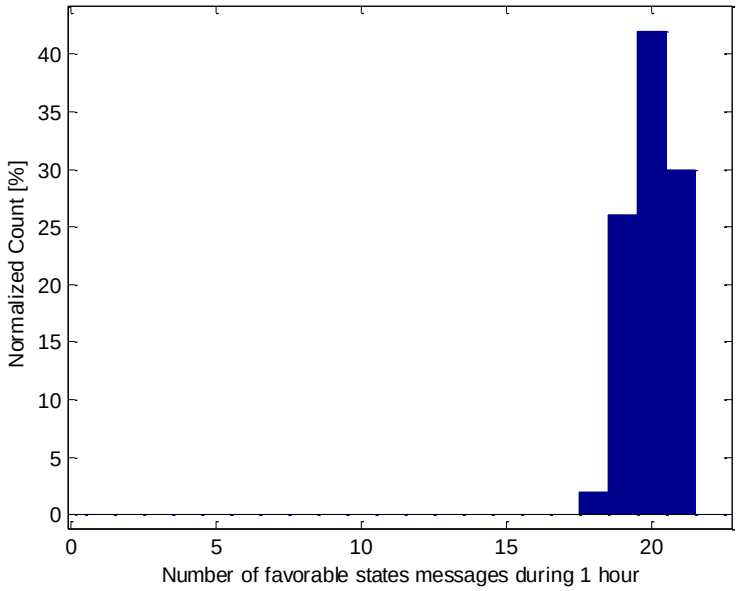

Figure 74: Favorable state messages over 1 hour distribution, for $C_{pre\text{-}urban}/N_0$ = 29 dB-Hz and PLL tracking with the DLR model

According to this figure, the percentage of 'favorable state messages' Per_{ga} inside a block of $T_{ga} = 1h$ for which the receiver can demodulate the subframe 3 with $ER_{aa} = 10^{-2}$, can be computed associated with a probability P_{ga}:

Table 37: GA for the DLR model, for $C_{pre\text{-}urban}/N_0$ = 29 dB-Hz

	Statistical results			
GA	T_{ga}	ER_{aa}	Per_{ga}	P_{ga}
	1h	10^{-2}	9.5%	98%

It can be concluded that, the receiver can demodulate 9.5% of the total number of subframes 3 received in 1h, with an error rate of 10^{-2}, for 98% of the blocks of 1h length.

The bad demodulation performance results obtained with the Perez-Fontan/Prieto propagation channel model in the previous section can be compared with these results. It seems that the 'favorable state messages' division criterion defined in this part according to the estimated received C/N_0 value is well defined for the DLR propagation channel model.

4.3 Conclusion

The classical methodology used to provide the GNSS signals demodulation performance is not adapted to urban environments. The first limitation concerns the C/N_0 parameter used to represent the data error rate. In urban environment, the received C/N_0 is not constant, thus, it is not anymore possible to use it as it was the case for AWGN channels. Moreover, providing the data error rate for each received message is not representative of reality since just punctual messages need to be demodulated in GNSS.

It has thus been proposed in this chapter a new methodology adapted to urban propagation channels to represent the GNSS signals demodulation performance in urban environments. This new methodology is based on a fundamental characteristic of the GNSS: only punctual messages need to be demodulated with success. For example, since the CED is emitted each 2 hours and valid during 3 hours, it is enough to demodulate with success one CED set in 1 hour per each satellite to be able to compute the user position. Thus, only favorable reception conditions have been take into account to compute the GNSS signals demodulation performance, associated with results about the 'favorable state messages' occurrence, in order to determine if the considered favorable reception conditions are enough to meet operational requirements. Two strategies have been conducted to apply the new methodology, depending on the operational requirement.

It has been showed that the demodulation performance obtained with the classical methodology are really degraded in comparison with the one obtained with the new methodology considering only the 'favorable state messages', nevertheless, the reader must note that it is the same demodulation performance which is considered, but represented by different ways. In fact, the most interesting information is hidden with the classical methodology, which is the demodulation performance corresponding to the minimum number of messages which are needed to be successfully demodulated, taken here as 'favorable state messages'.

However the 'favorable state messages' determination is not easy and still needs to be more investigated. In particular, it seems more representative of reality if the parameter used to make the separation between 'favorable state messages' and 'unfavorable state messages' takes into account the detected PLL losses of lock.

Moreover, the new methodology has only been developed for a continued usage in this paper, without constraints concerning the TTFF, whereas it is relevant information. Thus, this aspect remains to be investigated.

In addition, the emitting satellites have been considered with the same elevation angle equal to 40°, and with the same azimuth angle for the DLR model equal to 30°. This is a worst case. To provide more realistic results, different elevation and azimuth angles need to be considered.

Chapitre 5: Decoding Optimization in Urban Environment

To be able to ensure the principal GNSS function consisting in providing positioning capabilities, the receiver needs to access the useful information transmitted by the GNSS signal, called the navigation message (see Chapter 2). The navigation message is structured in different basic units of information, called codewords. Each codeword, in addition to containing useful information, carries redundant bits which are the result of applying a channel code to the useful information bits. The reason of introducing a channel code is to protect these information bits against errors introduced by the propagation channel. Consequently, at the receiver, the GNSS navigation message, or more especially the associated codewords, needs to be decoded by the receiver to reliably recover the transmitted useful bits.

Therefore, channel coding is essential to allow a better rate of data demodulation success in difficult environments. This process is very sensitive to the correct computation of the detection function which will feed the decoder input. Significant improvements are obtained by considering soft detection enabling the use of soft input channel decoders. In this context, the channel decoders need to be fed by soft inputs that are sufficient statistics from a detection point of view. This is usually achieved by computing Log-Likelihood Ratios (LLRs) based on both observation samples and channel parameters (see Chapter 2).

Usually, without any a priori information on the encountered channel, the expression of the detection function in GNSS receivers is obtained assuming an Additive White Gaussian Noise (AWGN) propagation channel. However since we are interested by urban applications, the detection function expression should be adapted to the urban propagation channel in order to improve the GNSS signals decoding performance and to avoid mismatched decoding errors (providing by the use of a detection function not computed for the considered propagation channel).

The aim of this chapter is thus to propose an advanced processing algorithm in order to improve the receiver sensibility in urban channels. More specifically we have tried to determine whether the decoder used in classical GNSS receivers with a detection function computed for an AWGN channel model is satisfactory in urban environments, or whether it is better to integrate an advanced detection function adapted to an urban channel model, in order to improve the GNSS signals decoding performance in urban environments.

The soft detection function at the GNSS decoder input has been derived according to different levels of knowledge of the propagation channel fading behavior, hereafter referred to as Channel State Information (CSI), in urban environments. Three configurations have been considered in this work for the detection function derivation based on analytical or approximated LLR derivations,

- Perfect CSI,
- Statistical CSI,
- No CSI.

In order to numerically determine the GNSS signal decoding gain obtained by the adaptation of the detection function to an urban environment, the detection function expressions derived from the three use cases listed above have been integrated in the SiGMeP simulator described in Chapter 3. The results obtained with the refined detection function expressions will be compared with those obtained with a classical decoder using the detection function corresponding to the AWGN channel model.

The chapter is organized as follows. Section 5.1 introduces the soft input channel decoding concept and describes the modeling of the received GNSS data symbol signals in urban environments. Section 5.2 details the derivation of the soft detection function expressions for perfect CSI, statistical partial CSI and no CSI. Section 5.3 presents the simulation conditions and the results obtained with SiGMeP. Finally, conclusions are given in section 5.4.

5.1 System Model

5.1.1 Soft Input Channel Decoding

The navigation message, protected against errors by channel coding, is carried by the propagation channel. At the receiver end, the decoder uses a decoding algorithm (see Figure 75) in order to recover the transmitted useful bits.

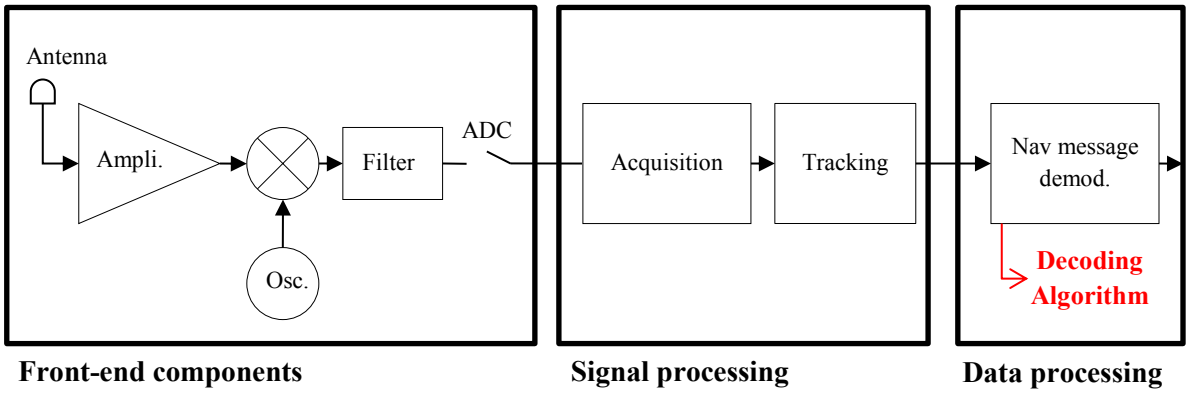

Figure 75: GNSS receiver block diagram

The channel decoding algorithms we are considering are using soft inputs generally such as Log-Likelihood Ratios (LLRs) based on A Posteriori Probability (APP) [5][46] (presented in Chapter 2 and detailed in Annex B). Indeed, most of existing soft input channel decoding algorithms such as Viterbi decoding of trellis based codes, or message passing algorithms based on sub-optimal decoding algorithms like the Belief Propagation for the LDPC codes (see chapter 2), or BCJR for turbo-codes, are using LLRs or related approximated expressions as soft inputs.

For binary random variables as inputs (which is the case in GNSS), the LLR [25] is defined as follows:

$$LLR = log\left(\frac{p(x = +1/y)}{p(x = -1/y)}\right) \tag{5.1}$$

where:

- $p(x/y)$ is the a posteriori probability that the symbol x has been transmitted, knowing the received symbol y (see Figure 76).

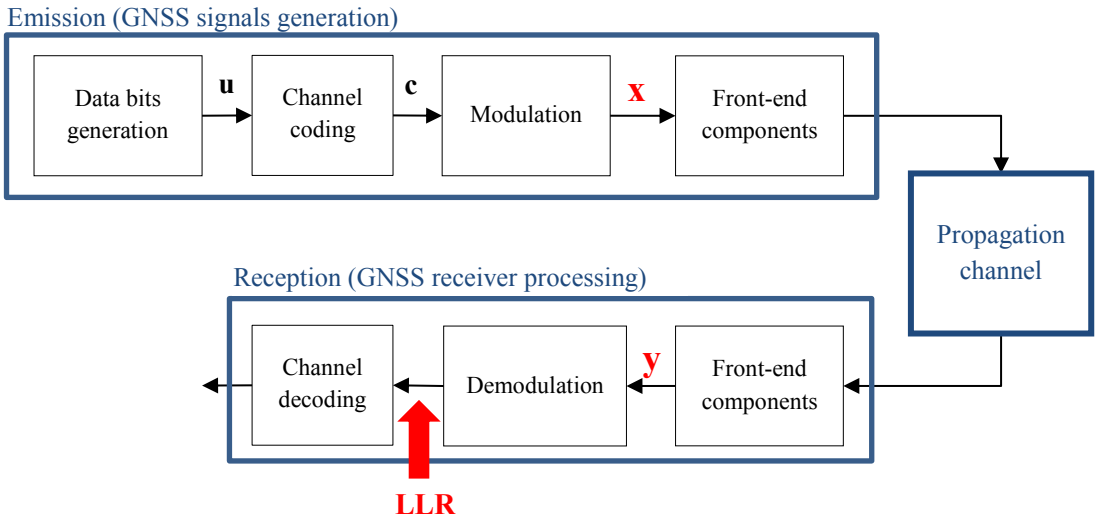

Figure 76: GNSS emission/reception chain block diagram

This LLR is thus the detection function at the decoder input which will be derived in the urban environment case for this work. Using the Bayes rule and in our context, the LLR expression can finally be re-written as:

$$LLR = log\left(\frac{p(y/x = +1)}{p(y/x = -1)}\right) \tag{5.2}$$

where:

- $p(y/x)$ is the transition probability density function associated with the channel.

This is the soft detection function expression that will be derived in section 5.2 according to the CSI knowledge level.

5.1.2 Received Symbol Modeling

In a GNSS receiver, the received symbol y to be decoded corresponds to the correlator output of the I channel of the data component I_p, modeled through partial correlations by the expression (3.29) given in Chapter 3 for a narrowband propagation channel model.

Following assumptions are considered:

- The code delay is perfectly estimated, thus $R[\tau_i] = 1$,
- The received signal Doppler frequency is perfectly compensated, thus $\varepsilon_{f_i} = 0$,
- The integration time T_I is considered equal to the symbol duration.

The received symbol y, which corresponds in GNSS to I_p, can thus be modeled by the following mathematical expression:

$$y(i) = \sqrt{P}x(i)\frac{1}{N}\sum_{n=1}^{N}\left[a_{channel}[n + (i-1)N]\, cos\left(\varepsilon_{\varphi}(n + (i-1)N)\right)\right] + n_I(i) \tag{5.3}$$

where:

- P is the useful signal power,
- $x(i)$ is the emitted symbol.

In order to simplify the notation, the correlator output I_p can be normalized by $\sqrt{P}$ before feeding the decoder. The decoder input model can be finally written as:

$$y(i) = x(i)\frac{1}{N}\sum_{n=1}^{N}\left[a_{channel}[n + (i-1)N]\, cos\left(\varepsilon_{\varphi}(n + (i-1)N)\right)\right] + n_I{}'(i) \tag{5.4}$$

where:

- $n_I{}'(i)$ is the normalized AWGN at the correlator output, with:

$$\sigma^2_{n_I'} = \frac{N_0}{T_I} \tag{5.5}$$

In our context, we assume perfect interleaving before transmission. As a result, the fading process associated with $a_{channel}[n + (i-1)N]$ will be considered as an uncorrelated fading process.

5.2 Derivation of the Soft Detection Function

By default, if no a priori knowledge on the channel is available at the receiver end, the detection function which is implemented in GNSS receivers is generally computed assuming an AWGN propagation channel as the default channel. In this work urban environments are targeted, thus it seems more adapted to compute the detection function considering an urban propagation channel. This derivation highly depends on the CSI available at the receiver and on the channel parameters which can be estimated.

It is really important to notice that this chapter targets to improve GNSS signals demodulation performance in optimizing the decoding process in the receiver. It implies that this performance improvement in urban environments just involves the receiver.

The detection function will be firstly reviewed for the AWGN propagation channel case (section 5.2.1), as it is used in the current GNSS receivers. Then, according to the knowledge of the propagation channel fading parameters, the detection function will be derived for mainly three different cases. The first case assumes a perfect CSI knowledge (section 5.2.2), the second considers a partial knowledge of statistical CSI (section 5.2.3), and the third case corresponds to no a priori CSI (section 5.2.4).

5.2.1 LLR Expression in the AWGN Case

The detection function used classically in the GNSS context corresponds to the AWGN propagation channel model. In this channel model, if we consider a perfect phase estimation and a normalized version of equation (5.4), the received symbol is written as:

$$y(i) = x(i) + n_I'(i) \tag{5.6}$$

with channel transition probability given by:

$$p(y(i)/x(i)) = \frac{1}{\sqrt{2\pi\sigma^2{}_{n_I'}}} e^{\frac{-(y(i)-x(i))^2}{2\sigma^2{}_{n_I'}}} \tag{5.7}$$

And thus from equation (5.2) we can deduce that:

$$LLR_{AWGN}(i) = log\left(\frac{\frac{1}{\sqrt{2\pi\sigma^2{}_{n_I'}}} e^{-(y(i)-1)^2/2\sigma^2{}_{n_I'}}}{\frac{1}{\sqrt{2\pi\sigma^2{}_{n_I'}}} e^{-(y(i)+1)^2/2\sigma^2{}_{n_I'}}}\right) \tag{5.8}$$

And thus, as classically known, we have:

$$LLR_{AWGN}(\mathrm{i}) = \frac{2y(\mathrm{i})}{\sigma^2{}_{n_I'}} \tag{5.9}$$

Note that it is implicitly assumed that the signal to noise ratio can be estimated, since the corresponding *LLR* is a scaled version of the observation by a constant proportional to the signal to noise ratio. Considering this model at the receiver is equivalent to consider that we only have access to the average signal-to-noise ratio for the received signal model of equation (5.4) assuming perfect phase compensation, if a BP algorithm is assumed (see Chapter 2 for more details about the BP algorithm). Note that for some low-complexity decoding algorithms such as the Min-Sum, the signal-to-noise ratio estimation can be avoided.

5.2.2 LLR Expression in an Urban Channel with Perfect CSI

We then consider an urban propagation channel model and we firstly assume in this part that we have a perfect CSI. In this context, the symbol attenuation $a_{channel}[n+(i-1)N]$, the phase error $\varepsilon_{\varphi}(n+(i-1)N)$ and the noise power ${\sigma^2}_{n_I'}$ are perfectly known at the receiver. These hypotheses are not always realistic for practical scenarios but allow us to derive the optimized detection function providing a lower bound on the best achievable decoding performance.

From equation (5.4) the received symbol is thus modeled as:

$$y(i) = x(i)\frac{1}{N}\sum_{n=1}^{N}\left[\, a_{channel}[n+(i-1)N]\, cos\left(\varepsilon_{\varphi}(n+(i-1)N)\right)\right] + {n_I}'(i) \tag{5.10}$$

Thus we can write:

$$p(y(i)/x(i)) = \frac{1}{\sqrt{2\pi{\sigma^2}_{n_I'}}}\, e^{\frac{-\left(y(i)-\frac{1}{N}\sum_{n=1}^{N}\left[\, a_{channel}[n+(i-1)N]\, cos\left(\varepsilon_{\varphi}(n+(i-1)N)\right)\right]x(i)\right)^2}{2{\sigma^2}_{n_I'}}} \tag{5.11}$$

And thus from equation (5.2) we can deduce that:

$$LLR_{Perfect\ CSI}(i) = log\left(\frac{\frac{1}{\sqrt{2\pi{\sigma^2}_{n_I'}}}\, e^{-\left(y(i)-\frac{1}{N}\sum_{n=1}^{N}\left[\, a_{channel}[n+(i-1)N]\, cos\left(\varepsilon_{\varphi}(n+(i-1)N)\right)\right]\right)^2 \Big/ 2{\sigma^2}_{n_I'}}}{\frac{1}{\sqrt{2\pi{\sigma^2}_{n_I'}}}\, e^{-\left(y(i)+\frac{1}{N}\sum_{n=1}^{N}\left[\, a_{channel}[n+(i-1)N]\, cos\left(\varepsilon_{\varphi}(n+(i-1)N)\right)\right]\right)^2 \Big/ 2{\sigma^2}_{n_I'}}}\right) \tag{5.12}$$

The final expression is given by:

$$LLR_{Perfect\ CSI}(i) = \frac{2\frac{1}{N}\sum_{n=1}^{N}\left[\, a_{channel}[n+(i-1)N]\, cos\left(\varepsilon_{\varphi}(n+(i-1)N)\right)\right]y(i)}{{\sigma^2}_{n_I'}} \tag{5.13}$$

5.2.3 LLR Expression in an Urban Channel with Partial CSI

We then consider an urban propagation channel model assuming partial statistical CSI. The symbol attenuation $\frac{1}{N}\sum_{n=1}^{N}\left[\, a_{channel}[n+(i-1)N]\, cos\left(\varepsilon_{\varphi}(n+(i-1)N)\right)\right]$ value is not known anymore but the statistical behavior of $a_{channel}$ is, assuming that the Probability Density Function (pdf) of $a_{channel}$ is known as well as its related parameters (it implicitly assumes that the estimation of these parameters is possible in a practical scenario). In addition, the phase is assumed perfectly estimated thus $\varepsilon_{\varphi}(n+(i-1)N) = 0$.

The *LLR* is derived from equation (5.2) according to the received symbol expression (5.4), and considering statistical partial CSI as follows:

$$p(y(i)/x(i)) = \int_0^{+\infty} p(y(i), a_{channel}/x(i))da_{channel} \tag{5.14}$$

with:

$$p(y(i), a_{channel}/x(i)) = \frac{1}{\sqrt{2\pi\sigma^2{}_{n_I}{}'}} e^{\frac{-\left(y(i)-\frac{1}{N}\sum_{n=1}^{N}\left[a_{channel}[n+(i-1)N]\,cos\left(\varepsilon_\varphi(n+(i-1)N)\right)\right]x(i)\right)^2}{2\sigma^2{}_{n_I}{}'}} p(a_{channel}) \tag{5.15}$$

Thus:

$$\begin{aligned} LLR_{Statistical\ CSI}(i) &= log\left(\frac{\int_0^{+\infty} p(y, a_{channel}/x=1)da_{channel}}{\int_0^{+\infty} p(y, a_{channel}/x=-1)da_{channel}}\right) \\ &= log\left(\frac{\int_0^{+\infty} p(y/a_{channel}, x=1)p(a_{channel})da_{channel}}{\int_0^{+\infty} p(y/a_{channel}, x=-1)p(a_{channel})da_{channel}}\right) \end{aligned} \tag{5.16}$$

We finally have:

$$\begin{aligned} &LLR_{Statistical\ CSI}(i) \\ &= log\left(\frac{\int_0^{+\infty}\left(e^{\frac{-\left(y(i)-\frac{1}{N}\sum_{n=1}^{N}\left[a_{channel}[n+(i-1)N]\,cos\left(\varepsilon_\varphi(n+(i-1)N)\right)\right]\right)^2}{2\sigma^2{}_{n_I}{}'}} p(a_{channel})\right)da_{channel}}{\int_0^{+\infty}\left(e^{\frac{-\left(y(i)+\frac{1}{N}\sum_{n=1}^{N}\left[a_{channel}[n+(i-1)N]\,cos\left(\varepsilon_\varphi(n+(i-1)N)\right)\right]\right)^2}{2\sigma^2{}_{n_I}{}'}} p(a_{channel})\right)da_{channel}}\right) \end{aligned} \tag{5.17}$$

For the Perez-Fontan/Prieto propagation channel model, it can be assumed that the symbol duration being longer than the correlation duration of the direct signal component samples, the pdf of $a_{channel}$ is equal to the pdf of $a_{channel}$ knowing the direct signal component. In this way $a_{channel} \sim Rice(z, b_0)$ [28] and the complete expression of the *LLR* is given by:

$$LLR_{Statistical\ CSI}(i) = log\left(\frac{\int_0^{+\infty} e^{\frac{-\left(y(i)-\frac{1}{N}\sum_{n=1}^{N}\left[a_{channel}[n+(i-1)N]\,cos\left(\varepsilon_{\varphi}(n+(i-1)N)\right)\right]\right)^2}{2\sigma^2 n_I'}} \frac{a_{channel}}{b_0} e^{-\frac{(a_{channel}^2+z^2)}{2b_0}} I_0\left[\frac{z\,a_{channel}}{b_0}\right] da_{channel}}{\int_0^{+\infty} e^{\frac{-\left(y(i)+\frac{1}{N}\sum_{n=1}^{N}\left[a_{channel}[n+(i-1)N]\,cos\left(\varepsilon_{\varphi}(n+(i-1)N)\right)\right]\right)^2}{2\sigma^2 n_I'}} \frac{a_{channel}}{b_0} e^{-\frac{(a_{channel}^2+z^2)}{2b_0}} I_0\left[\frac{z\,a_{channel}}{b_0}\right] da_{channel}}\right) \quad (5.18)$$

where:

- z is the direct signal component amplitude,
- b_0 is the average multipath power with respect to an unblocked direct signal,
- $I_0\left[\frac{za_{channel}}{b_0}\right] = \int_0^{\pi} e^{\frac{za_{channel}}{b_0}cos\theta}\, d\theta$ is the modified Bessel function of first kind and zero order.

The above expression has no closed form expression and it can be computationally prohibitive to evaluate for every soft inputs. If valuable, this approach is from far too complex for a practical application. Note also that in a real scenario, the different parameters have to be estimated.

5.2.4 LLR Expression in an Urban Channel with No CSI

We finally consider the case where no CSI is available at the receiver. The fading gain $\frac{1}{N}\sum_{n=1}^{N}\left[a_{channel}[n+(i-1)N]\,cos\left(\varepsilon_{\varphi}(n+(i-1)N)\right)\right]$ is assumed unknown as well as the $a_{channel}$ statistical behavior, and the noise power is assumed unknown too. The phase can be considered as perfectly estimated or PLL estimated. The results will be analysed in these two settings.

Motivated by the *LLR* mathematical expression (5.13) assuming an urban propagation channel and perfect CSI, and inspired by [47], we are looking for a linear expression of the *LLR* expression considering an urban propagation channel without CSI. The idea is to find a method that can help to find the best linear approximation for an *LLR* soft input avoiding the complexity burden induced by some statistical knowledge at the receiver end. The linear approximation can be written as a linear function of the observation sample y(i) as:

$$LLR(i) = \alpha y(i) \quad (5.19)$$

The method proposed in [47] consists in determining the scaling coefficient α that maximizes the mutual information between the transmitted symbol x(i) and the detector input LLR(i) which is a sufficient statistics:

$$I(LLR;X) = H(X) - H(X/LLR) \quad (5.20)$$

where:

- $H(X)$ and $H(X/LLR)$ denote the entropy of a random variable X and the conditional entropy of X given LLR respectively.

When considering binary input memoryless channels as in our case, this expression can be easily expressed as a function of the pdf of the *LLR* at the input of the receiver [5], considering $X = +1$:

$$I(LLR;X) = 1 - \int_{-\infty}^{+\infty} log_2(1 + e^{-LLR}) p(LLR/X = +1) dLLR \tag{5.21}$$

Using this expression a good choice for α is given by:

$$\alpha_{MCLA} = arg\ \max_{\alpha}\ I(LLR;X) \tag{5.22}$$

A simple line search algorithm can be used to evaluate the optimum value.

Originally in [47], the proposed optimization method to find the optimal α assumes the knowledge of the LLR's pdf. Unfortunately, this knowledge is not always available in practical situations. We aim to go a step further to find an efficient method for computing a good approximation of this quantity without any statistical knowledge.

If we first assume that the emitted symbol $x(\mathrm{i})$ is known, the mutual information between X and LLR can be approximated using a time average estimation by the following expression [48]:

$$I(LLR;X) \approx 1 - \frac{1}{N}\sum_{i=1}^{N} log_2\left(1 + e^{-x(i)\alpha y(i)}\right) \tag{5.23}$$

where:

- N is the number of symbols used to estimate $I(LLR;X)$.

Although computationally efficient, this method assumes the use of a learning sequence to evaluate the mutual information at the channel decoder input. Fortunately, this assumption can be relaxed to enable approximated blind estimation. Indeed, if the emitted symbol $x(\mathrm{i})$ is unknown, the mutual information between X and LLR can be well approximated using the following expression [48]:

$$I(LLR;X) \approx 1 - \frac{1}{N}\sum_{i=1}^{N}\left[-P_{en}(i) log_2\left(P_{en}(i)\right) - (1 - P_{en}(i)) log_2(1 - P_{en}(i))\right] \tag{5.24}$$

where:

- $P_{en}(\mathrm{i}) = \dfrac{e^{\frac{|\alpha y(\mathrm{i})|}{2}}}{e^{\frac{|\alpha y(\mathrm{i})|}{2}} + e^{-\frac{|\alpha y(\mathrm{i})|}{2}}}$

Thus, the obtained blind estimation is only dependent of the *LLR* magnitude and independent of the emitted sequence.

Finally, once the coefficient α maximizing $I(LLR; X)$ has been determined, the LLR can be deduced by:

$$LLR_{No\ CSI}(i) = \alpha y(i) \tag{5.25}$$

This can be efficiently done by one dimensional line search algorithms.

We finally have an efficient method to compute a low complexity linear *LLR* expression that enables to have near maximum mutual information between the emitted symbols and the linear approximated *LLRs*. The AWGN case appears as a special case when α is equal to the average signal to noise ratio. So we expect to have better performance using our method than using the default AWGN expression.

5.3 Simulation Results

The detection function expressions adapted to an urban propagation channel have been derived for different levels of CSI in the last section and have been tested in this section with the software SiGMeP described in Chapter 3. The GPS L1C navigation message demodulation performance through the Perez-Fontan/Prieto propagation channel model (see Table 38), with these different detection function expressions, are provided and compared with the results obtained with the LLR_{AWGN} used currently in GNSS receivers.

Table 38: Simulation conditions

Simulation Conditions	
Signals	GPS L1C
Channel Model	Perez-Fontan/Prieto
Channel Generation Fs	0.1 ms
Environment	Urban
Database Band	S
Satellite Elevation Angle	40°
Phase Estimation	Ideal/PLL

The advanced detection function expressions adapted for an urban propagation channel and derived according to the CSI knowledge have been implemented in the simulator SiGMeP. The $LLR_{statistical\ CSI}$ function has not been integrated because of its complexity for a practical application. The Clock and Ephemeris Data (CED) Error Rate (CEDER), contained by subframe 2 for GPS L1C (being the only necessary data to compute a first position) has been computed with each of the detection function expressions and compared.

5.3.1 LLR_{AWGN}

The results obtained with the LLR_{AWGN} function represent the performance provided by a current GNSS receiver for GPS L1C with an urban channel model, firstly with perfect phase estimation and then with PLL phase estimation.

To compute the LLR_{AWGN} function given in equation (5.9), the noise power value $\sigma^2{}_{n_I'}$ is needed. Since this value is not directly accessible in the GNSS receiver, the estimated received C/N_0 ratio is

used (see Chapter 3 for more details about the received C/N_0 estimation in SiGMeP). Several time durations used to estimate the received C/N_0 have been compared, as it is summarized in Table 39.

Table 39: Time durations used to compute the estimated received C/N_0

Time durations (in GPS L1C symbols)
10 symbols = 0.1s
50 symbols = 0.5s
100 symbols = 1s
500 symbols = 5s
1800 symbols = 1 message = 18s

GPS L1C demodulation performance obtained with the LLR_{AWGN} function in the Perez-Fontan/Prieto propagation channel model with SiGMeP is thus presented in Figure 77, LLR_{AWGN} being computed each symbol, but the estimated received C/N_0 used as the $\sigma^2{}_{n_I'}$ value being updated each 10 symbols (red lines), 50 symbols (green lines), 100 symbols (dark blue lines), 500 symbols (light blue lines) and 1800 symbols (magenta lines).

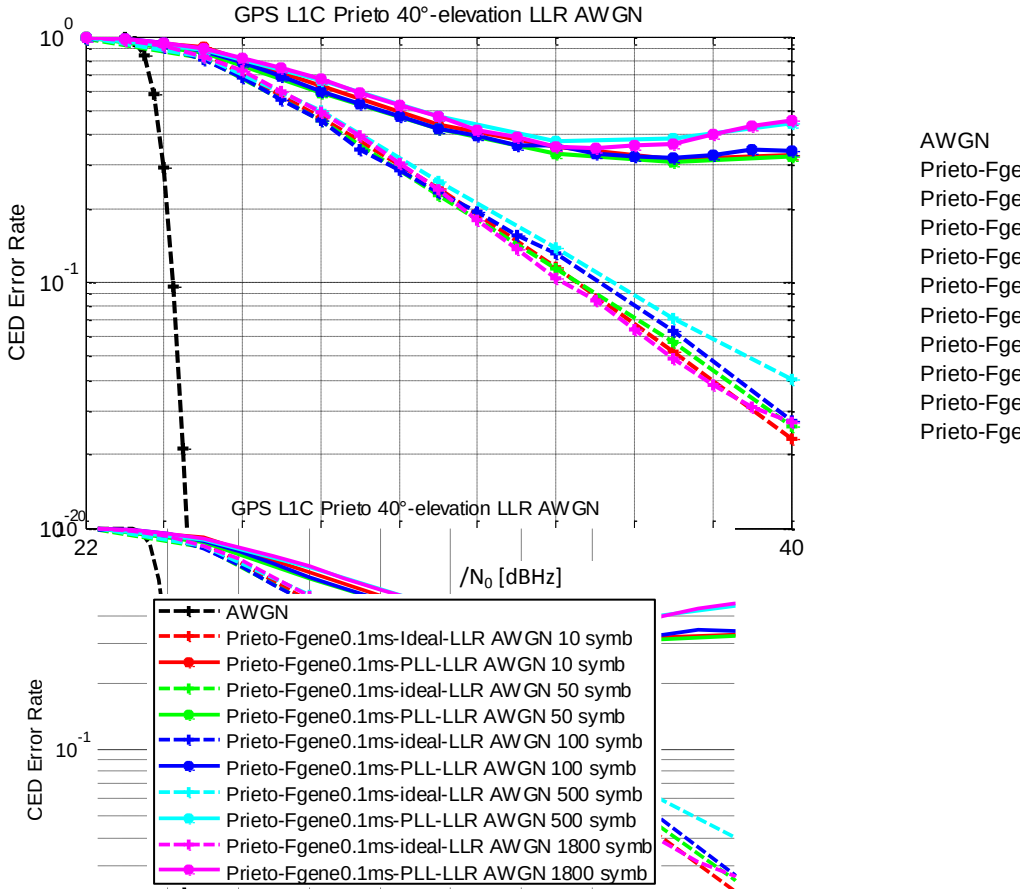

Figure 77: GPS L1C demodulation performance obtained with LLR_{AWGN} in the Prieto channel model

Figure 77 shows that for the PLL tracking case, a received C/N_0 estimation made more often provides better performance. This can be explained by the urban propagation channel variations divided into two states. Each state is generated with its particular and associated parameters (see Chapter 2),

involving different received C/N_0 values for different channel states. The received C/N_0 thus needs to be computed at the channel states duration scale.

Good and bad states duration statistical means have thus been searched through Figure 78 and Figure 79. To do that, each channel state duration has been stored every channel state transition, and the resulting histogram has been plotted.

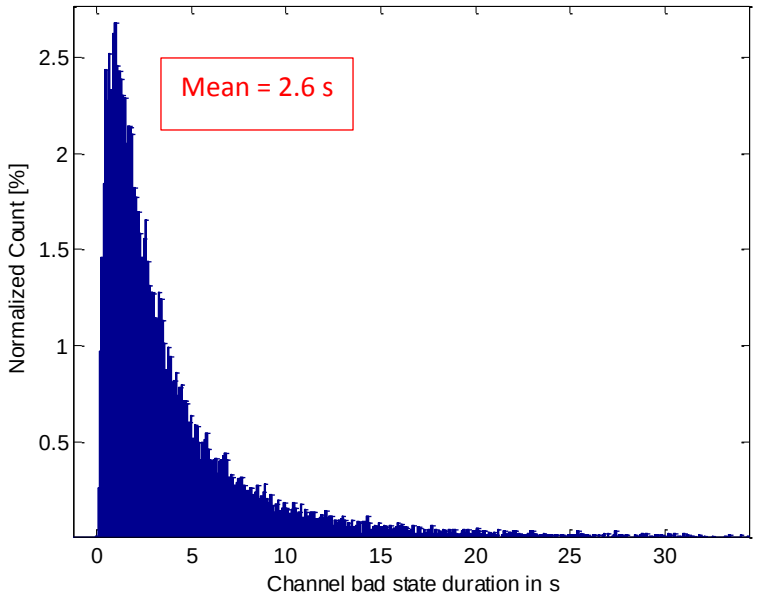

Figure 78: Channel bad state duration distribution

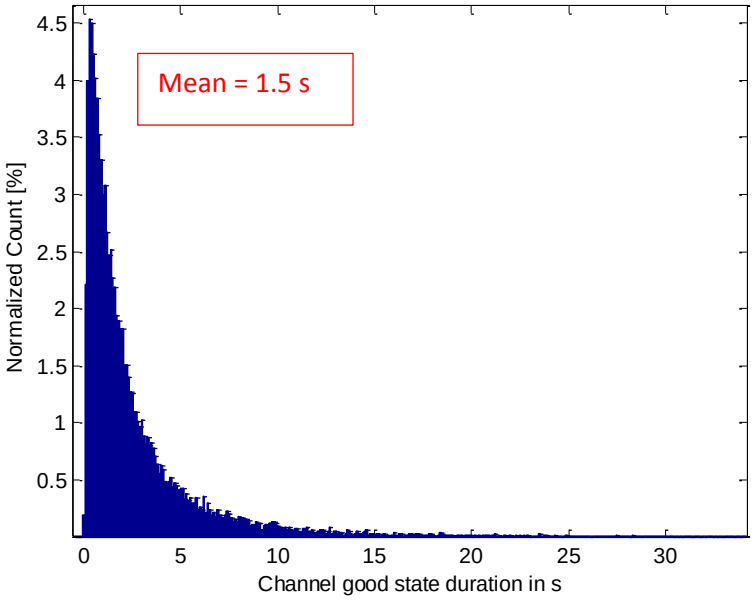

Figure 79: Channel good state duration transition

Since the mean duration of bad states is equal to 2.6 seconds and the mean duration of good states is 1.5 second, it seems that the received C/N_0 can be well estimated on 1 second or less. In GPS L1C symbols, it corresponds to 100 symbols or less.

5.3.2 $LLR_{perfect\ CSI}$

The results obtained with the $LLR_{perfect\ CSI}$ function are not really representative of the reality because it is not possible to perfectly estimate the fading gains of the urban channel. This case has to be seen as a lower bound on the achievable performance.

To compute the $LLR_{perfect\ CSI}$ function given in equation (5.13), the attenuating factor $\frac{1}{N}\sum_{n=1}^{N}\left[a_{channel}[n+(i-1)N]\,cos\left(\varepsilon_{\varphi}(n+(i-1)N)\right)\right]$ and the noise power $\sigma^2{}_{n_I'}$ are needed. These values are computed in SiGMeP, along with the normal process. The attenuating factor is taken at the correlator output $I_{p\ without\ noise}$ computed without taking into account the noise. In addition, the noise power is computed for each symbol.

GPS L1C demodulation performance obtained with the $LLR_{perfect\ CSI}$ function (blue lines) in the Perez-Fontan/Prieto propagation channel model with SiGMeP is thus presented in Figure 80, and compared with results obtained with classical GNSS receivers, computed with the LLR_{AWGN} function (magenta lines).

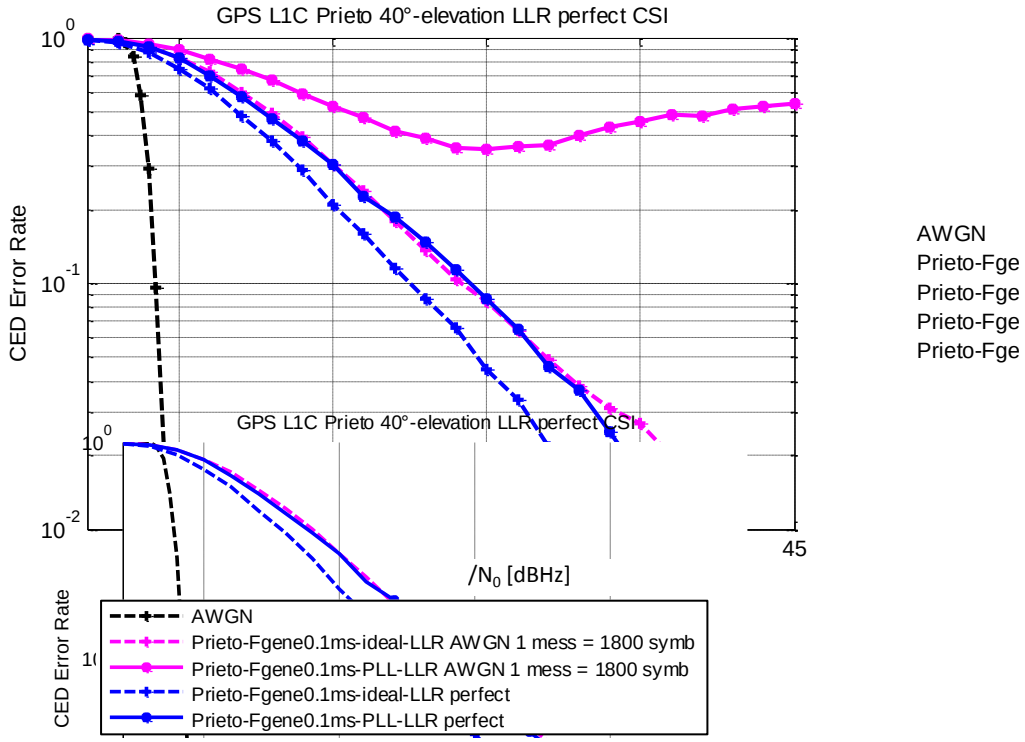

Figure 80: GPS L1C demodulation performance obtained with $LLR_{perfect\ CSI}$ in the Prieto channel model

The floor observed with the LLR_{AWGN} function and PLL tracking is completely eliminated with the $LLR_{perfect\ CSI}$ function use. It is a very encouraging result, which shows that it is possible to remove this floor, and to spectacularly improve demodulation performance in urban areas. However, to be able to remove this floor, the estimation of the attenuating factor $\frac{1}{N}\sum_{n=1}^{N}\left[a_{channel}[n+(i-1)N]\,cos\left(\varepsilon_{\varphi}(n+(i-1)N)\right)\right]$ and the noise power $\sigma^2{}_{n_I'}$ has been necessary. But it is not so easy in practice.

5.3.3 $LLR_{No\ CSI}$

Since a perfect estimation of the attenuation factor $\frac{1}{N}\sum_{n=1}^{N}\left[a_{channel}[n+(i-1)N]\,cos\left(\varepsilon_{\varphi}(n+(i-1)N)\right)\right]$ and of the noise power ${\sigma^2}_{n_I'}$ is not feasible in practice, another method adapted to urban environments to compute the detection function without any CSI knowledge has been developed in this work (see section 5.2.4). GPS L1C demodulation performance has thus been computed with the $LLR_{no\ CSI\ x\ unknown}$ detection function expression (5.25) corresponding to no CSI and assuming that the emitted symbol $x(i)$ is unknown. The α coefficient optimization is made on a sliding window. Several sliding window lengths have been tested, as showed in Figure 81: 1800 symbols, 100 symbols, 50 symbols and 10 symbols.

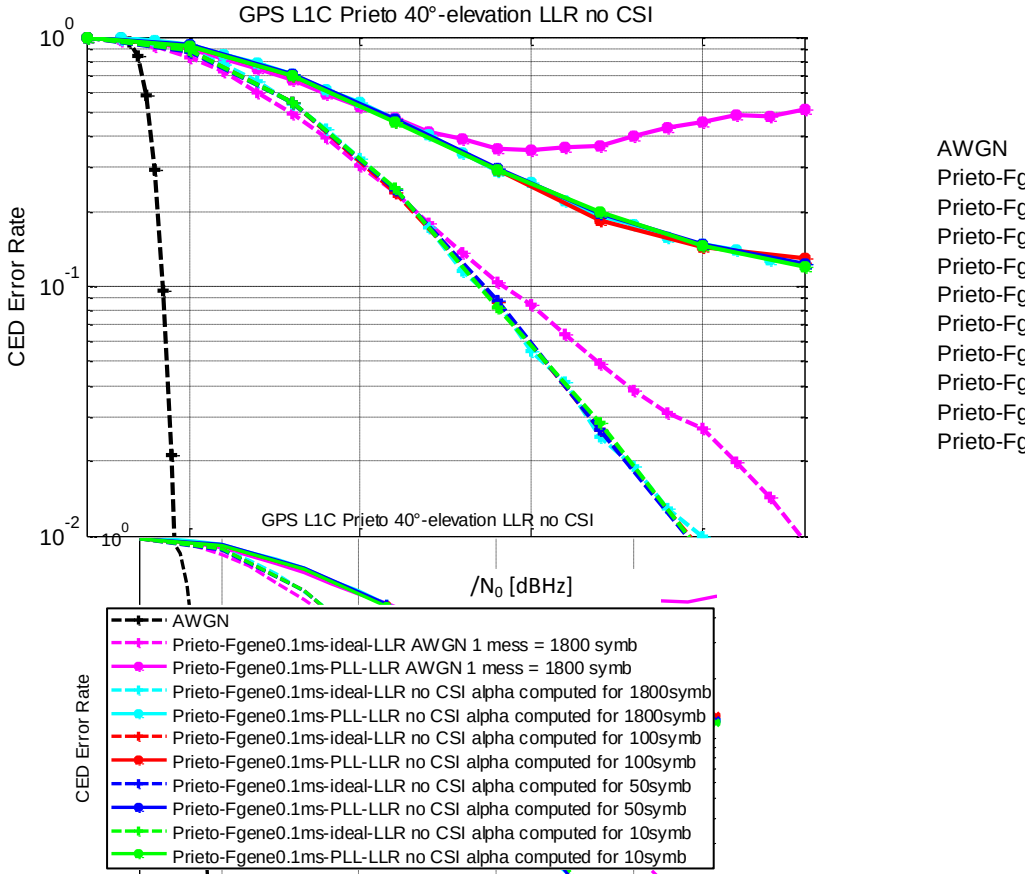

Figure 81: GPS L1C demodulation performance obtained with $LLR_{no\ CSI}$ in the Prieto channel model

First of all, it seems that the sliding window length can be as well as 1800 symbols and 10 symbols.

Then, it can be noticed that to achieve an error rate of 10^{-2} with GPS L1C in an urban propagation channel with perfect phase estimation, a classical receiver (with the LLR_{AWGN} function) needs a minimal $C_{pre\text{-}urban}/N_0$ value equal to 43 dB-Hz, whereas if the advanced detection function $LLR_{no\ CSI\ x\ unknown}$ is used, this minimal $C_{pre\text{-}urban}/N_0$ value decreases until 40 dB-Hz. It means that if $LLR_{no\ CSI\ x\ unknown}$ is used instead of LLR_{AWGN} the demodulation performance is improved by approximately 3 dB in this case, needing absolutely no additive knowledge of CSI compared to the LLR_{AWGN} case.

If a PLL phase tracking is considered, the use of the advanced detection function $LLR_{no\ CSI\ x\ unknown}$ adapted to an urban propagation channel and assuming no CSI instead of the detection function LLR_{AWGN} assuming an AWGN propagation channel, brings GPS L1C demodulation performance improvement. However, the floor existing in the LLR_{AWGN} case is always present in the $LLR_{no\ CSI\ x\ unknown}$ case.

Technically, this new method should take into account the attenuation factor due to the PLL phase error and resolve it. But it can be observed in Figure 82 that even the results obtained with $LLR_{no\ CSI\ x\ unknown}$ are really better than those obtained with LLR_{AWGN} (with the estimated received C/N_0 computed each 1800 symbols and each 100 symbols), they are far from the results obtained with a perfect CSI knowledge for the PLL case (solid blue line), representing the lower bound of the demodulation performance achievable in computing the detection function adapted to the propagation channel.

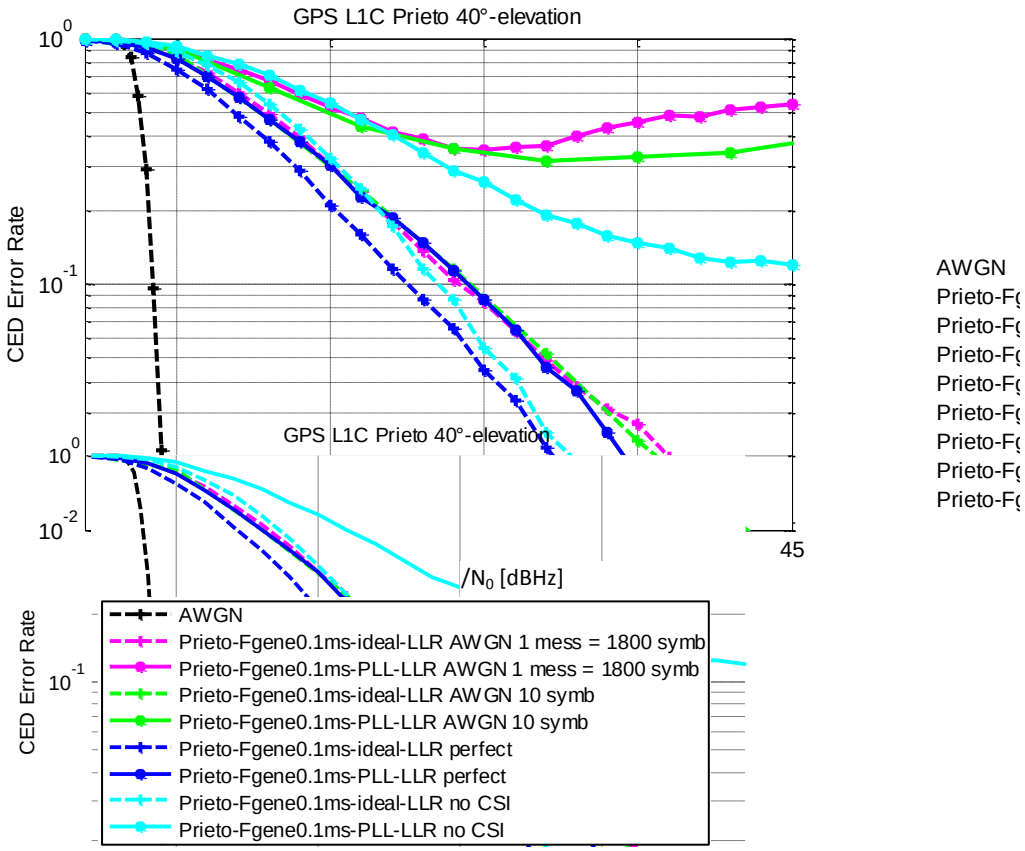

Figure 82 : GPS L1C demodulation performance obtained with advanced detection functions in the Prieto channel model

It seems that the gap between the results obtained with $LLR_{no\ CSI\ x\ unknown}$ (solid cyan line) and $LLR_{perfect\ CSI}$ (solid blue line) in the PLL tracking case is due to the PLL losses of lock. One way to reduce this gap would thus consist in estimating the PLL phase error. The propagation channel estimation, or a PLL phase error model, or the PLL losses of lock detector output could be used in this sense.

5.4 Conclusion

This chapter proposes a computationally efficient advanced processing algorithm that significantly improves the receiver sensibility in urban propagation channels. We have demonstrated that the use of a refined detection function adapted to the urban environment considerably increases the demodulation performance of GNSS signals. For a CEDER of 10^{-2} a decoding gain of approximately 3 dB is obtained between the detection function corresponding to the AWGN propagation channel and the advanced detection function corresponding to an urban propagation channel and considering no CSI at all, with ideal phase estimation.

The simulations of this chapter have been done with LDPC channel codes (computation of GPS L1C demodulation performance), but it is important to notice that the advanced detection functions derived in this work can be applied to all soft input decoders such as Viterbi decoder for trellis based codes, the MAP/BCJR decoding for turbo-codes and the Belief Propagation decoding for LDPC codes.

It is really important to notice that this chapter targets to improve GNSS signals demodulation performance in optimizing the decoding process in the receiver. It implies that this performance improvement in urban environments just involves the receiver.

Nevertheless, the demodulation performance obtained with a PLL phase tracking in urban environments (which is the realistic case) is not satisfactory, even if an improvement has been brought by the advanced detection function. It seems that the optimization process could be improved thanks to additional information about the PLL phase error, which can be obtained by the propagation channel estimation, or by the PLL phase error modeling, or using the PLL losses of lock detector output.

Chapitre 6: LDPC Channel Code Design and Optimization for GNSS CSK-Modulated Signals

GNSS signals demodulation performance in urban environments has been analysed in Chapter 4 and improved in Chapter 5 at the receiver level by the optimization of the detection function. This chapter is dedicated to the design of a new GNSS signal with the aim of improving the demodulation performance in urban environments. The well-known convolutional code with rate ½ and constraint length 7 used in SBAS, GPS L2C, GPS L5 and Galileo signals (see Chapter 2) shows some limitations at low C/N_0 values, especially in urban environments. Modern channel codes (turbo-codes, LDPC) are thus investigated in order to approach the channel capacity. In this work, only LDPC channel codes will be studied.

As said before, GNSS are becoming more and more present in our everyday life and new needs are emerging. A large part of these new needs takes place in urban environment, which is a new challenge in terms of demodulation performance. In addition, another challenge is appearing: the increase of the current useful data rate as explained next. First, the implementation of new services implies a new larger navigation message since more information must be transmitted. Second, new services such as precise positioning or safety-of-life, require a significantly higher data rate than the current available one to be efficiently deployed. Third, a significant amount of the new applications targets users in environments with difficult reception conditions such as urban or indoor areas. In these obstructed environments, the received signal is severely impacted by obstacles that are detrimental to both the ranging and demodulation capability of the receiver. One possible option to improve the receiver's demodulation capability is to enhance the transmitted information temporal diversity (repetition of key information), which implies again a larger quantity of bits to be transmitted. Therefore, the demand for a data rate increase is largely justified and vital for the future expansion of the GNSS market.

However, the increase of the current data rate also presents a great challenge due to the GNSS signals Direct-Sequence Spread Spectrum (DS-SS) characteristic and the implemented BPSK modulation. In fact, the symbol period of the BPSK modulation is limited by the PRN code; consequently, the increase of the symbol rate (directly related to the increase of the data rate) is directed into two undesired solutions: either to increase the PRN code chip rate, resulting in a wider spectrum, or to decrease the PRN code length, resulting in a loss of PRN code isolation and orthogonality properties.

One possible solution to deal with the BPSK modulation limitation consists in implementing the Code Shift Keying (CSK) modulation instead (QZSS LEX signals are the only ones being modulated by a CSK). Note that the GNSS signal modulation can be modified thanks to the introduction of a pilot component which allows the calculation of pseudo-range measurements by itself. A CSK modulation is specially designed to increase the transmission rate of a spread spectrum signal. The CSK modulation consists in circularly shifting each transmitted PRN code in order to represent with each

PRN code shifted version a different CSK symbol mapping a set of bits. Therefore, if each data channel PRN code period is equal to the data symbol duration, the bit transmission rate is increased proportionally to the number of bits mapped by a CSK symbol.

Previous analysis of the CSK technique introduction in a GNSS signal has already been addressed in [49][50] presenting a methodology for designing a CSK modulated signal. Finally, CSK-based signals for GNSS were proposed in [49][50] using the subframe 2 GPS L1C LDPC channel code. However, the subframe 2 GPS L1C LDPC channel code was originally designed to be implemented in a BPSK modulation and thus better demodulation performances should be attained for channel code specifically optimized for a CSK modulation. Moreover, the association between non binary LDPC codes and the CSK modulation has been investigated in [51][52]. Nevertheless, we will focus on binary LDPC codes in this work.

The aim of this chapter consists in investigating the asymptotic design of binary irregular LDPC codes optimized for a GNSS CSK-based signal in an AWGN channel. The analysis will be done using the EXtrinsic Information Transfer (EXIT) charts analysis and an asymptotic optimization method will be proposed. From the obtained LDPC code profiles, finite length codes will be designed. Finally, the simulation results will be compared to the demodulation performance of the most powerful GNSS signal in terms of channel coding: GPS L1C (modulated with a BPSK).

The chapter will be organized as follows. The first section provides the context of this study: the CSK modulation is presented and its associated detection function is derived: the LLRs (see Chapters 2 and 5) in the AWGN propagation channel for a GNSS CSK-modulated signal, used for the EXIT chart analysis; as well as the iterative decoding. Section 6.2 describes the EXIT chart generation and some examples are provided for different CSK modulations in an AWGN propagation channel. Finally in section 6.3, LDPC code profiles are optimized for the AWGN channel adapted to a CSK-modulated signal according to the EXIT charts determined in section 6.2. Simulation results for finite length performance assessment are also provided.

6.1 Context of the Study

The purpose of this chapter is to optimize LDPC code profiles for a GNSS CSK-modulated signal (see Figure 83), the final goal being to design a new GNSS signal with powerful channel coding and increased data rate. For this purpose, the optimization will be lead for an AWGN propagation channel.

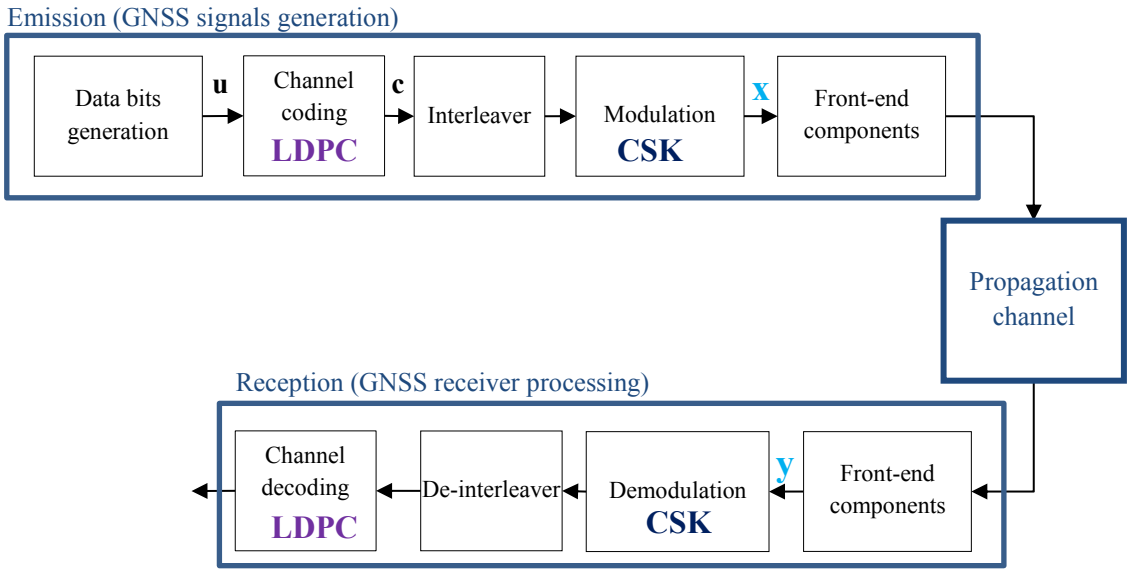

Figure 83: GNSS emission/reception chain block diagram

6.1.1 CSK Modulation

The Code Shift Keying (CSK) modulation is a M-ary orthogonal modulation, since M waveforms are used. Each waveform corresponds to the same PRN sequence (see Chapter 2), but circularly shifted [53]. Figure 84 shows CSK waveforms for the particular example of N equal to 10230 chips, the PRN sequence length, and M equal to 4 different symbols with Q equal to 2 bits per symbol. In this case the mapping (the way to associate a waveform to a CSK symbol) is made considering consecutive shifts, but this can be different.

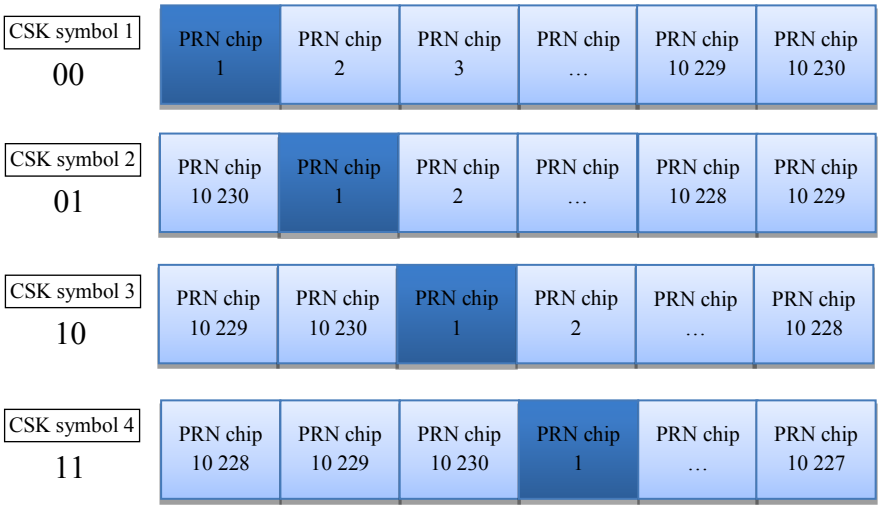

Figure 84: CSK waveforms example

A shifted version $c_x(t)$ of the fundamental PRN sequence $c_{fond}(t)$ can thus been written as the mathematical expression of equation (6.1), for $x = 0, \ldots, M-1$ [50]:

$$c_x(t) = c_{fond}(mod[t - m_x T_C, NT_C]) \tag{6.1}$$

where:

- $mod(x, y)$ is the modulus operation of y over x,
- m_x is the integer number corresponding to the shift of the *x*-th symbol,
- T_C is the PRN sequence chip period,
- N is the number of chips in the PRN sequence (*M* is not necessarily equal to *N*).

According to equation (6.1) and Chapter 2 and 3 considerations, the equivalent low-pass received waveform complex envelope can thus be written as:

$$r(t) = A\, a_{channel}(t) e^{j\varphi_{channel}(t)}\, c_x(t) + n(t) \tag{6.2}$$

where:

- A is the emitted signal amplitude,
- $a_{channel}(t)e^{j\varphi_{channel}(t)}$ is the propagation channel complex envelope,
- $c_x(t)$ is the emitted shifted version of the fondamental PRN sequence (the CSK waveform),
- $n(t)$ is the AWGN.

In order to determine which shifted version has been emitted, a matched filter is used for each symbol of the signal space basis [25]. Each matched filter output is the result of the correlation between the received waveform and one of the shifted versions of the fundamental PRN sequence [50]. This process results in a matched filters bank, which can be implemented using Fast Fourier Transform and Inverse Fourier Transform blocks, since it completes efficiently the correlation process in the frequency domain [50]. The resulting operation is thus written as:

$$y[k] = IFFT\left(FFT(r[k]) \times FFT\left(c_{shifted\ fond}[k]\right)\right) \tag{6.3}$$

where:

- FFT is the Fast Fourier Transform,
- $IFFT$ is the Inverse Fast Fourier Transform.

Finally, the CSK demodulator can be represented by Figure 85 [50]:

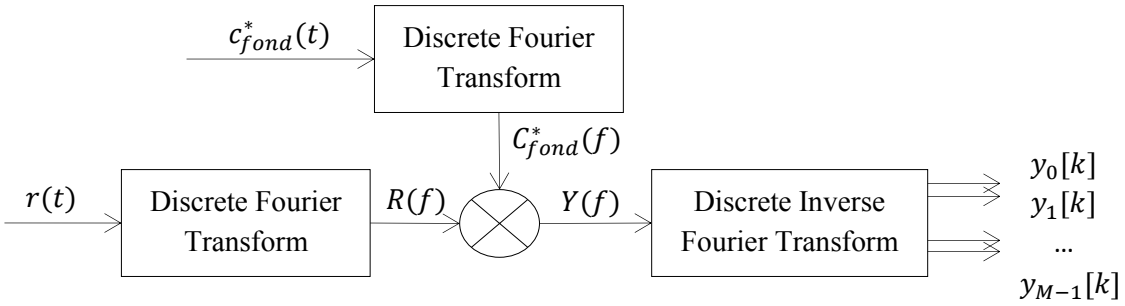

Figure 85: CSK FFT-based demodulator representation

The CSK modulation allows transmitting several bits using one waveform, which implies very high possible data rates, contrary to the BPSK modulation which imposes a same single data bit value during an entire PRN sequence duration.

6.1.2 CSK-Modulated Signal Detection Function: LLR Expression Derivation

During the decoding process, messages are exchanged between the CSK demodulator and the LDPC decoder which can be seen as a Bit Interleaved Coded Modulation (BICM) [54] (see Figure 86). These exchanged messages are typically LLRs based on A Posteriori Probability (APP) [5][46], as it is explained in Chapter 5.

The APP LLR mathematical expression is based on both observation samples and channel parameters. Since the observation samples depend on the modulation under review, the LLR_{APP} mathematical expression for a CSK-modulated signal will be different from a BPSK-modulated signal. It is thus necessary to derive the LLR_{APP} function for a CSK-modulated signal.

In this chapter, the following assumptions have been made:

- The APP LLR mathematical expression is derived considering an AWGN propagation channel model,
- The carrier phase tracking error is equal to 0,
- The knowledge of the beginning of the transmitted sequence is assumed.

The LLR_{APP} expression corresponding to a GNSS CSK-modulated signal in an AWGN propagation channel is derived as follows. It is computed for each bit q of the emitted CSK symbol (see Figure 86):

$$LLR_{APP_q} = log\left(\frac{p\left(b_{x_q} = 1/y\right)}{p\left(b_{x_q} = 0/y\right)}\right) \tag{6.4}$$

where:

- b_{x_q} is the q-th bit of the emitted CSK symbol x,
- y is the received CSK symbol,

- $p\left(b_{x_q} = 1/y\right)$ is the APP that the q-th bit of the emitted CSK symbol x equal to 1 has been transmitted, knowing the received symbol y.

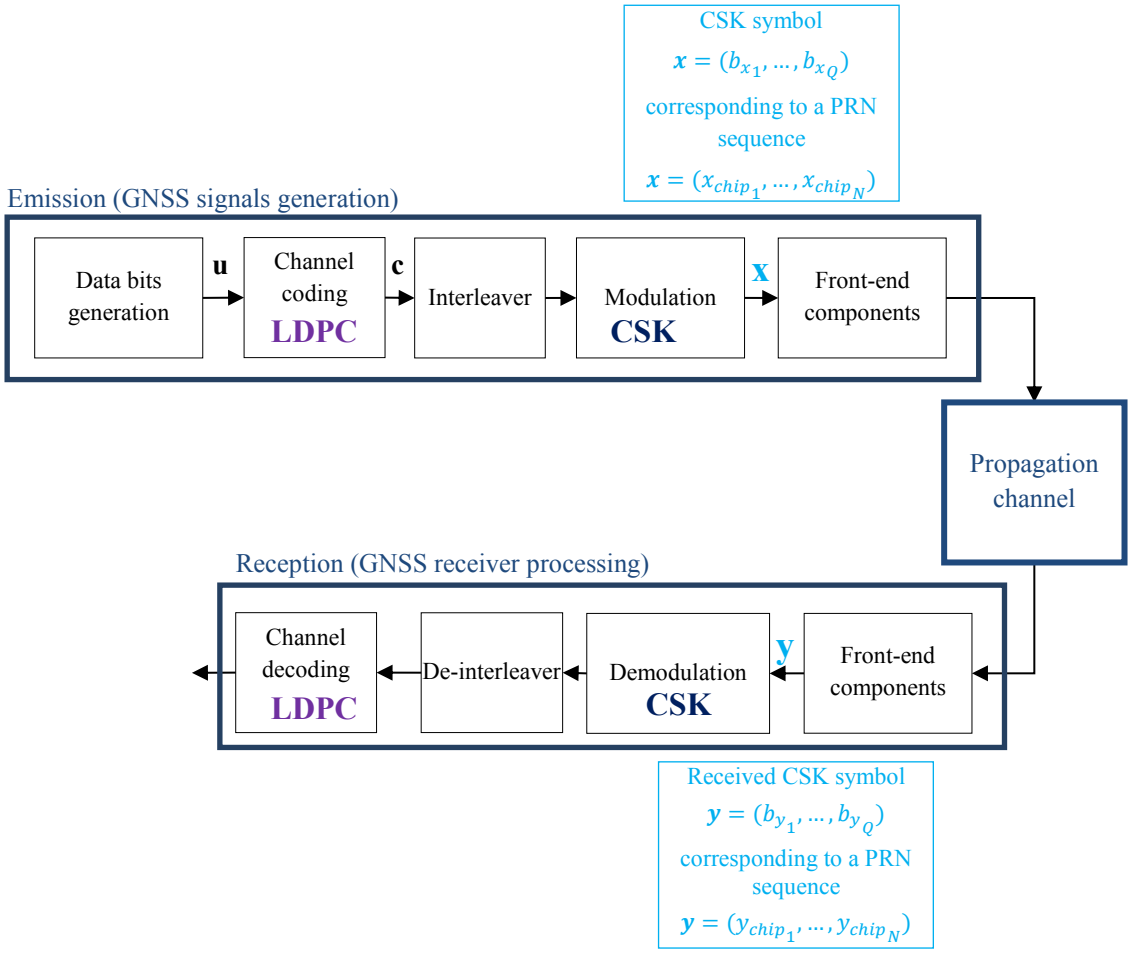

Figure 86: GNSS emission/reception chain block diagram

From Bayes' rules, it follows:

$$LLR_{APP_q} = log\left(\frac{p\left(y, b_{x_q} = 1\right)p(y)}{p(y)p\left(y, b_{x_q} = 0\right)}\right) \tag{6.5}$$

with:

$$p\left(y, b_{x_q} = 1\right) = \sum_{\substack{All\ CSK\ symbols \\ which\ b_{x_q}=1}} p\left(y, b_{x_1}, b_{x_2}, \dots, b_{x_q}, \dots, b_{x_Q}\right) \tag{6.6}$$

$$p\left(y, b_{x_q} = 1\right) = \sum_{\substack{All\ CSK\ symbols \\ which\ b_{x_q}=1}} p\left(y/b_{x_1}, b_{x_2}, \dots, b_{x_q}, \dots, b_{x_Q}\right) p\left(b_{x_1}, b_{x_2}, \dots, b_{x_q}, \dots, b_{x_Q}\right) \tag{6.7}$$

and:

$$p\left(y/b_{x_1}, b_{x_2}, \dots, b_{x_q}, \dots, b_{x_Q}\right) = p\left(y_{chip_1}, \dots, y_{chip_N}/x_{chip_1}, \dots, x_{chip_N}\right) \tag{6.8}$$

$$p\left(y/b_{x_1}, b_{x_2}, \dots, b_{x_q}, \dots, b_{x_Q}\right) = \prod_{i=1}^{N} p\left(y_{chip_i}/x_{chip_i}\right) \tag{6.9}$$

because y_{chip_i} is completely defined by x_{chip_i}.

Since the propagation channel is modeled by an AWGN channel:

$$p\left(y/b_{x_1}, b_{x_2}, \dots, b_{x_q}, \dots, b_{x_Q}\right) = \prod_{i=1}^{N} \frac{1}{\sqrt{2\pi\sigma_n^2}} e^{-\frac{\left(y_{chip_i} - x_{chip_i}\right)^2}{2\sigma_n^2}} \tag{6.10}$$

$$p\left(y/b_{x_1}, b_{x_2}, \dots, b_{x_q}, \dots, b_{x_Q}\right) = \frac{1}{(2\pi\sigma_n^2)^{\frac{N}{2}}} e^{-\frac{1}{2\sigma_n^2}\sum_{i=1}^{N}\left({y_{chip_i}}^2 - {x_{chip_i}}^2\right) + \frac{1}{\sigma_n^2}\sum_{i=1}^{N}\left(y_{chip_i} x_{chip_i}\right)} \tag{6.11}$$

Finally:

$$LLR_{APP_q} = log\left(\frac{\sum_{\substack{All\ CSK\ symbols \\ which\ b_{x_q}=1}} e^{\frac{1}{\sigma_n^2}\sum_{i=1}^{N}\left(y_{chip_i} x_{chip_i}\right)} p\left(b_{x_1}, b_{x_2}, \dots, b_{x_q}, \dots, b_{x_Q}\right)}{\sum_{\substack{All\ CSK\ symbols \\ which\ b_{x_q}=0}} e^{\frac{1}{\sigma_n^2}\sum_{i=1}^{N}\left(y_{chip_i} x_{chip_i}\right)} p\left(b_{x_1}, b_{x_2}, \dots, b_{x_q}, \dots, b_{x_Q}\right)}\right) \tag{6.12}$$

$$LLR_{APP_q} =$$

$$log\left(\frac{\sum_{\substack{All\ CSK\ symbols \\ which\ b_{x_q}=1}} \left[e^{\frac{1}{\sigma_b^2}\sum_{i=1}^{N}\left(y_{chip_i} x_{chip_i}\right)} p\left(b_{x_1}, b_{x_2}, \dots, b_{x_{q-1}}, b_{x_{q+1}}, \dots, b_{x_Q}\right) p\left(b_{x_q} = 1\right)\right]}{\sum_{\substack{All\ CSK\ symbols \\ which\ b_{x_q}=0}} \left[e^{\frac{1}{\sigma_b^2}\sum_{i=1}^{N}\left(y_{chip_i} x_{chip_i}\right)} p\left(b_{x_1}, b_{x_2}, \dots, b_{x_{q-1}}, b_{x_{q+1}}, \dots, b_{x_Q}\right) p\left(b_{x_q} = 0\right)\right]}\right) \tag{6.13}$$

$$LLR_{APP_q} = log\left(\frac{\sum_{\substack{All\ CSK\ symbols \\ which\ b_{x_q}=1}} \left[e^{\frac{1}{\sigma_b^2}\sum_{i=1}^{N}\left(y_{chip_i}x_{chip_i}\right)} p\left(b_{x_1}, b_{x_2}, \dots, b_{x_{q-1}}, b_{x_{q+1}}, \dots, b_{x_Q}\right)\right]}{\sum_{\substack{All\ CSK\ symbols \\ which\ b_{x_q}=0}} \left[e^{\frac{1}{\sigma_b^2}\sum_{i=1}^{N}\left(y_{chip_i}x_{chip_i}\right)} p\left(b_{x_1}, b_{x_2}, \dots, b_{x_{q-1}}, b_{x_{q+1}}, \dots, b_{x_Q}\right)\right]}\right) + log\left(\frac{p\left(b_{x_q}=1\right)}{p\left(b_{x_q}=0\right)}\right) \quad (6.14)$$

$$LLR_{APP_q} = log\left(\frac{\sum_{\substack{All\ CSK\ symbols \\ which\ b_{x_q}=1}} \left[e^{\frac{1}{\sigma_b^2}\sum_{i=1}^{N}\left(y_{chip_i}x_{chip_i}\right)} \prod_{j\neq q} p\left(b_{x_j}\right)\right]}{\sum_{\substack{All\ CSK\ symbols \\ which\ b_{x_q}=0}} \left[e^{\frac{1}{\sigma_b^2}\sum_{i=1}^{N}\left(y_{chip_i}x_{chip_i}\right)} \prod_{j\neq q} p\left(b_{x_j}\right)\right]}\right) + log\left(\frac{p\left(b_{x_q}=1\right)}{p\left(b_{x_q}=0\right)}\right) \quad (6.15)$$

with:

- $\sum_{i=1}^{N}\left(y_{chip_i}x_{chip_i}\right)$ the correlation operation between the emitted and the received PRN sequences. Since the code delay is assumed to be perfectly estimated, this value is equal to 1 if the received PRN sequence y_{PRN} (corresponding to a CSK symbol) is the same than the emitted PRN sequence x_{PRN} (corresponding in this case to the same CSK symbol), and this value is equal to 0 otherwise (see Chapter 3). In fact, a correlator filter bank is used at the GNSS reception level: one correlator for one CSK symbol, to determine which CSK symbol has been received.

From equation (6.15), the LLR_{APP_q} can be divided into two components, as it is done into the equation (6.16):

- The extrinsic part LLR_E which represents the information exclusively brought by the demodulator process, only considering its structure [55]. This is the information that will be fed to the SISO (Soft-Input Soft-Output) BP LDPC decoder.
- The a priori part LLR_{A_q} which represents the a priori information that is fed back by the BP LDPC decoder [56].

$$LLR_{APP_q} = LLR_{E_q} + LLR_{A_q} \quad (6.16)$$

In fact, the LLR based on a posteriori probability LLR_{APP_q} is computed by the demodulator (as demodulator output) according to the channel observations y and the a priori LLRs: $LLR_{A_q} = log\left(\frac{p\left(b_{x_q}=1\right)}{p\left(b_{x_q}=0\right)}\right)$ for each bit q (see Figure 87). Then, the extrinsic LLR is computed and send to the LDPC decoder.

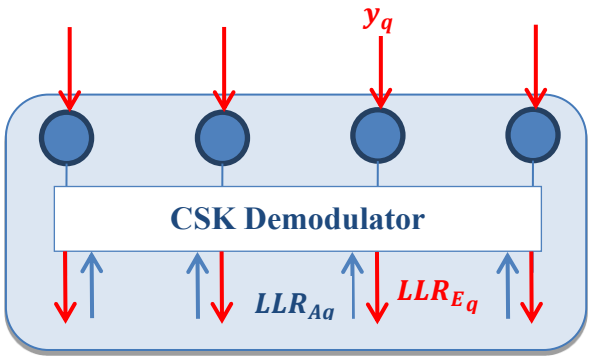

Figure 87: CSK demodulator soft inputs and outputs

The extrinsic LLR noted LLR_{E_q} is then deduced from the LLR_{APP_q} value by the following way:

$$LLR_{E_q} = LLR_{APP_q} - LLR_{A_q} \tag{6.17}$$

Note that the presented soft demodulator as given in equation (6.15) can be efficiently implemented based on LLRs only and using the *max*(.)* operator as given in [20].

6.1.3 Classical and Iterative Decoding

From the detection function $LLR_{APP-CSK}$ derived in section 6.1.2 considering a CSK demodulator in an AWGN propagation channel, the decoding process can be made through two different methods [50]:

- The classical CSK decoding method,
- The iterative decoding method.

The difference between these two decoding methods lies in the exchanges between the CSK demodulator and the LDPC decoder (see the orange frame in Figure 88). In iterative decoding the LDPC decoder provides feedback to the CSK demodulator (see Figure 90), whereas in classical decoding the exchanges are only supported by a downlink stream (see Figure 89).

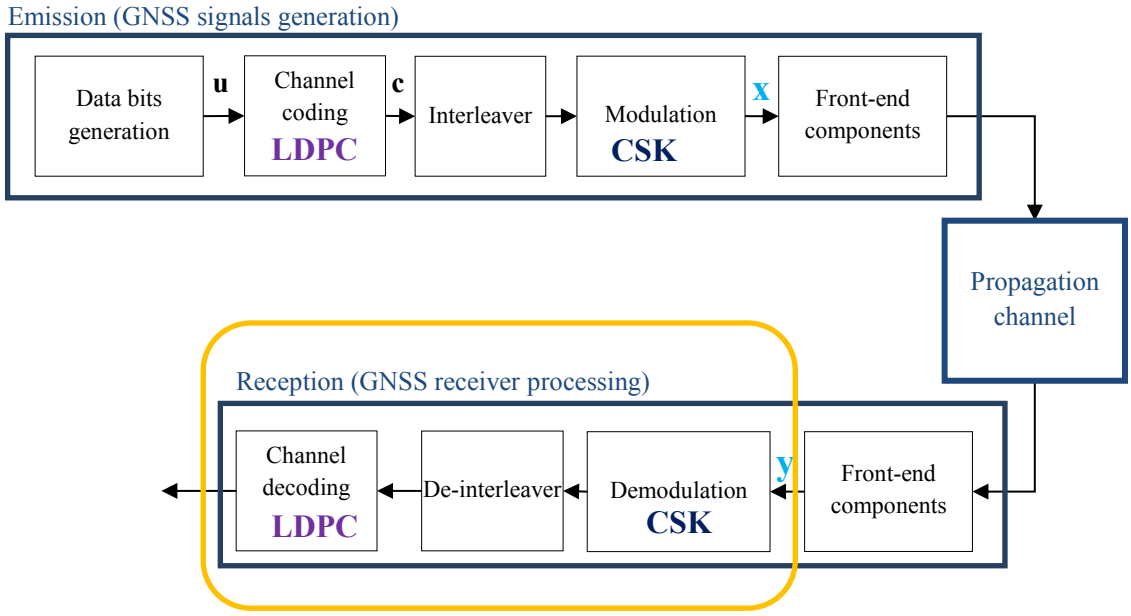

Figure 88: GNSS emission/reception chain block diagram

6.1.3.1 Classical Decoding

In classical decoding, the CSK demodulator is fed by channel observations y and a priori LLRs which are computed considering equiprobable bits. In this context where binary data is used, these a priori LLRs are thus equal to:

$$LLR_{A_q} = log\left(\frac{p\left(b_{x_q}=1\right)}{p\left(b_{x_q}=0\right)}\right) = 0 \tag{6.18}$$

The extrinsic LLRs are then computed by the demodulator according to equations (6.15) and (6.17).

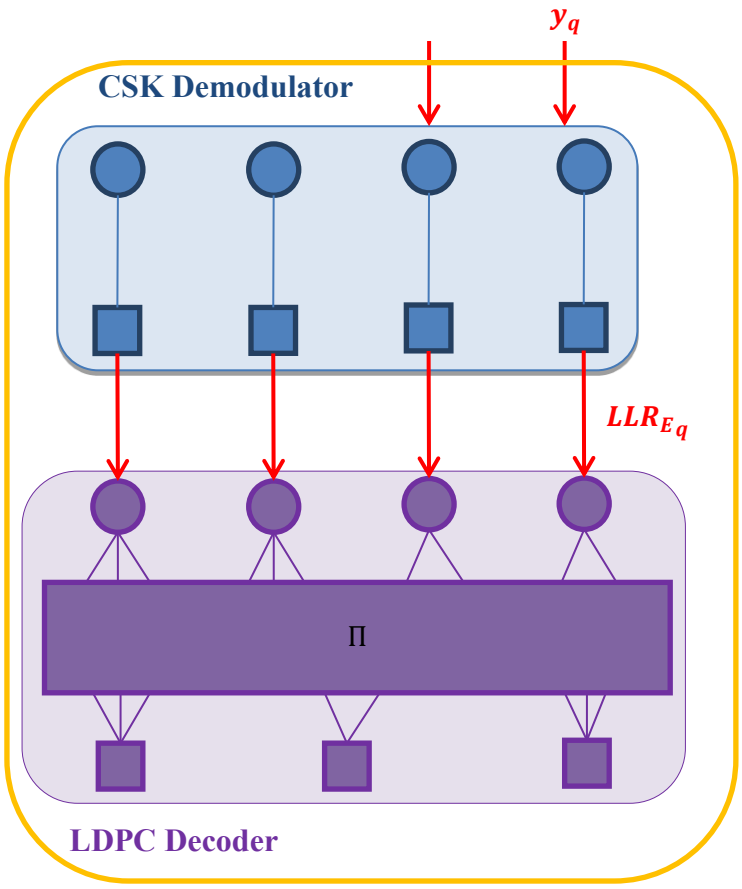

Figure 89: CSK demodulator and LDPC decoder combination, linked by LLR exchanged messages, for the classical decoding method

The LDPC decoder initiates then its Variable Nodes with these CSK extrinsic LLRs (see Chapter 2), and the BP decoding is performed as described in Chapter 2. There is no iterative decoding between the soft demodulator and the LDPC decoder.

6.1.3.2 Iterative Decoding

In iterative decoding, the CSK demodulator is fed by channel observations *y* and a priori LLRs which are computed considering equiprobable bits at the first iteration. Then, the CSK extrinsic LLRs are computed by the CSK demodulator according to equations (6.15) and (6.17). These values are sent to the LDPC decoder and one BP decoding iteration is performed. The LDPC extrinsic LLRs resulting of this LDPC decoding process are then sent back to the CSK demodulator. They are used as CSK a priori LLRs at the CSK demodulator inputs. This is the iterative decoding principle as given in Figure 90. Note that when performing BP decoding, several iterations can be made to lower the latency of the decoding process. However, in that case, it is not easy to perform the asymptotic analysis. Moreover, as reported in several works, the performance is better when considering only one iteration of BP decoding at each global iteration step. In the following, we will consider that only one BP iteration is performed for one global iteration. Note that in the Figure 91, the interleaver is omitted for the ease of presentation. A more detailed discussion about the interleaving will be done in the next sections.

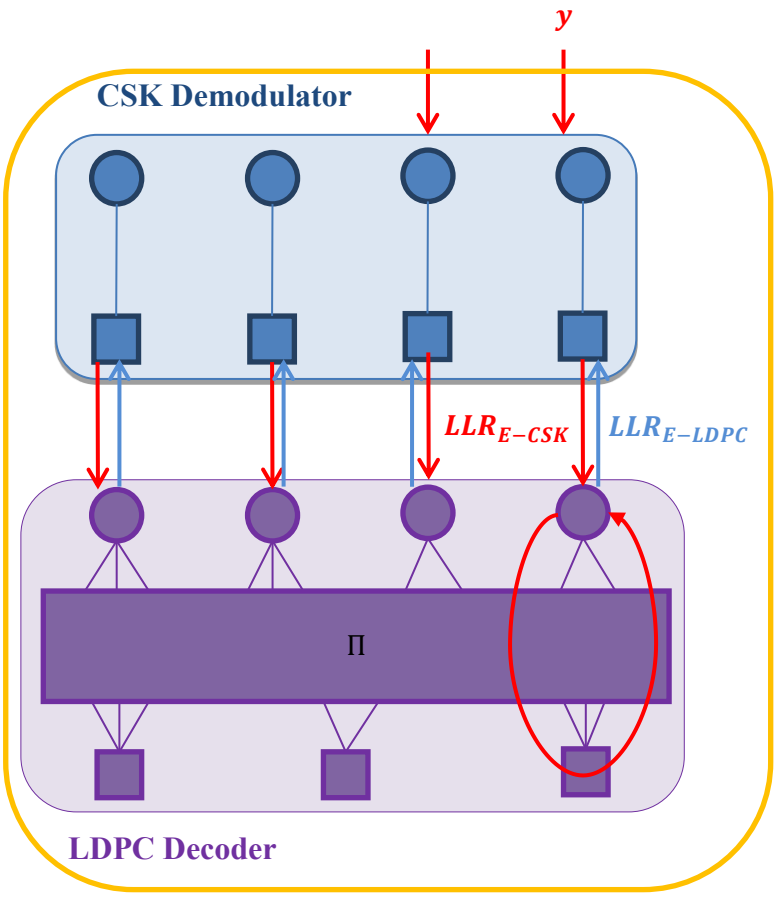

Figure 90: CSK demodulator and LDPC decoder combination, linked by LLR exchanged messages, for the iterative decoding method

In the next section, we will present an asymptotic analysis based on EXIT chart analysis aiming to assess the asymptotic behavior, i.e. in the limit of infinite code word length.

6.2 EXIT Charts for CSK Modulation in AWGN Channel

In this section, the potential benefit of iterative decoding is analyzed for a CSK-modulated GNSS signal in an AWGN propagation channel. In order to determine if iterative decoding provides better performance than non-iterative decoding in the case of a CSK-modulated GNSS signal, the EXtrinsic-Information-Transfer (EXIT) chart is used.

6.2.1 EXIT Chart Generation

The EXIT chart is a graphical tool developed by Ten Brink [57] in the late 1990s which consists in representing the extrinsic mutual information between the send bits and the extrinsic LLRs at the output of a SISO block (demodulator or decoder), as a function of the a priori mutual information between the send bits and the a priori LLRs at the input of a SISO block. If the extrinsic information quantity increases with the a priori information quantity (i.e. the EXIT chart for the given signal to noise ratio in non-flat), it means that an iterative decoding will improve the performance. Indeed, if bringing more a priori information to the demodulator involves a higher extrinsic information quantity (provided exclusively by the demodulator structure) at its output, it means that the demodulator

capacities will be better if the a priori information is increased by the decoder, which is done by iterative decoding.

The aim of this section consists thus in studying the EXIT charts of the CSK demodulator to assess its performance under iterative decoding.

6.2.2 Mutual Information as a Measure for Convergence

6.2.2.1 Definition

In EXIT charts, the extrinsic information which is considered is the mutual information $I(Y;Z)$, defined by the equation (6.19) [46]. It could be another statistic as the LLR mean or the SNR (definition in Annex A) for example [58], but the mutual information is considered as the most accurate and the most robust statistic [55].

An EXIT chart consists thus on plotting the output metric of interest, the extrinsic mutual information I_E, as a function of the input metric of interest, the a priori mutual information I_A.

The a priori information I_A corresponds to the mutual information between the emitted coded bits b_x and the a priori messages LLR_A [46]:

$$I_A = I(LLR_A; b_x) = H(b_x) - H(b_x/LLR_A) \tag{6.19}$$

Whereas the extrinsic information I_E corresponds to the mutual information between the emitted coded bits b_x and the extrinsic messages LLR_E [46]:

$$I_E = I(LLR_E; b_x) = H(b_x) - H(b_x/LLR_E) \tag{6.20}$$

In this context of a binary-input memoryless channel, the mutual information between the emitted coded bit and the LLR is generally defined by [5]:

$$I(LLR; b_x) = \frac{1}{2} \sum_{b_x=\pm 1} \int_{-\infty}^{+\infty} p(LLR/b_x)\, log_2 \left(\frac{2p(LLR/b_x)}{p(LLR/b_x=+1) + p(LLR/b_x=-1)} \right) dLLR \tag{6.21}$$

The above expression can be well evaluated through a Monte-Carlo estimation using histograms, especially when estimating the extrinsic mutual information from Monte-Carlo simulations. For the a priori mutual information, a more direct approach is used to compute it.

6.2.2.2 Consistent Gaussian Approximation

From the above definition, we need to be able to generate the a priori information. For EXIT chart analysis, it is assumed that the a priori LLRs referred as LLR_A can be generated assuming a consistent Gaussian approximation. The consistent Gaussian approximation [5] makes the following assumptions that:

- The a priori LLRs Probability Density Function (pdf) follows Gaussian distribution, with σ its standard deviation and μ its mean.
- This pdf p is assumed exponential consistent [5], implying for a Gaussian pdf that $\sigma^2 = 2\mu$.

In this way, the a priori LLRs pdf is entirely determined by the a priori LLRs mean or standard deviation.

Thus, a priori LLRs can be modeled as:

$$LLR_A = \mu b_x + n \tag{6.22}$$

where:

- μ is the a priori LLR pdf mean and σ^2 its standard deviation,
- b_x is emitted coded bit,
- $n \sim Gauss(0, \sigma^2)$.

And since the a priori LLRs pdf is considered as consistent, $\sigma^2 = 2\mu$ and the pdf of a priori LLRs knowing b_x is characterized by:

$$LLR_A/b_x \sim Gauss\left(\pm\frac{\sigma^2}{2}, \sigma^2\right) \tag{6.23}$$

When considering binary input memoryless channels which are consistent and symmetric, the I_A value can be linked to the LLR_A pdf through this expression [5]:

$$I_A = 1 - \int_{-\infty}^{+\infty} log_2(1 + e^{-LLR_A}) p(LLR_A/b_x = +1) dLLR_A \tag{6.24}$$

This expression can be well approximated based on a functional approximation as discussed latter in this chapter.

6.2.3 EXIT Chart for a CSK-Modulated Signal

In this section we aim at determining if an iterative decoding improves the performance of a CSK-modulated signal. In this way, the EXIT chart of a CSK demodulator has to be provided. To do that, the simulated GNSS signal emission/reception chain only contains the CSK modulator/demodulator, as it is illustrated in Figure 91. The LDPC encoder/decoder has been removed at the moment.

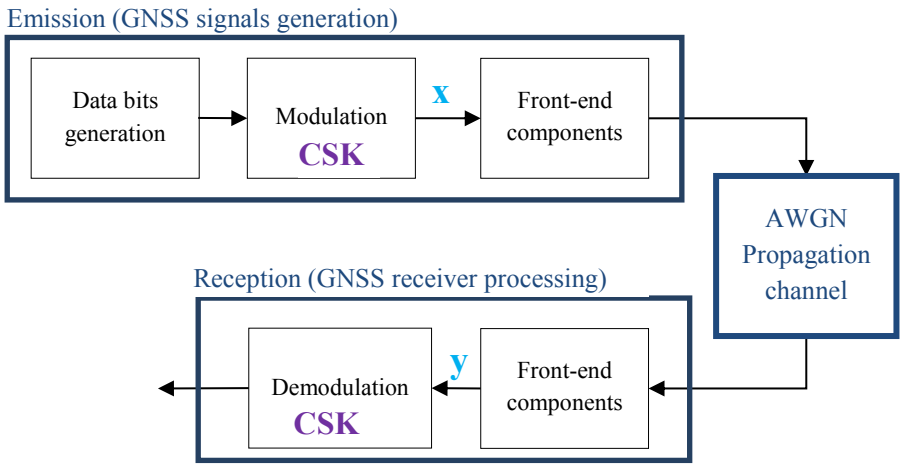

Figure 91: GNSS emission/reception chain block diagram

As explained in the previous subsection, to estimate the CSK EXIT chart, we need to compute the extrinsic mutual information according to the a priori mutual information. If a higher value of a priori information involves a higher value of extrinsic information compared with another point, it means that an iterative decoding will be beneficial to the CSK demodulator, since iterative decoding feeds on a priori information to refine the final demodulator output. If more a priori information does not bring more extrinsic information, it means that an iterative decoding will not improve the performance.

Thus, to plot the EXIT chart of the CSK demodulator to allow determining if an iterative decoding is more beneficial than a non-iterative decoding for a GNSS CSK-modulated signal, the extrinsic mutual information $I_E = I(LLR_E; b_x)$ between the emitted coded bit b_x and the extrinsic LLRs needs to be computed according to a priori mutual information $I_A = I(LLR_A; b_x)$ values ranging from 0 to 1.

Since LLRs are considered as exchanged messages, the mutual information needs to be directly linked to LLRs.

This subsection details this EXIT chart estimation process, summarized by equation (6.25):

- The a priori mutual information I_A value is fixed (following the ranging 0 to 1) which permits to deduce the a priori LLRs (detailed in section 6.2.3.1), assuming the consistent Gaussian approximation (detailed in section 6.2.2.2),
- According to the LLR_A value, the resulting extrinsic LLR is computed through the CSK demodulator output: LLR_E (detailed in section 6.2.3.2),
- And finally, the extrinsic mutual information I_E which corresponds to the a priori mutual information I_A fixed at the process beginning is determined from the LLR_E values (detailed in section 6.2.3.3) based on a Monte-Carlo estimation through histograms. Finally the overall process can be schematically summarized as follows:

$$I_A(consistent - Gaussian) \rightarrow LLR_A \rightarrow LLR_E \rightarrow I_E \quad (6.25)$$

6.2.3.1 From I_A to LLR_A

At the beginning of the EXIT chart estimation process, the a priori mutual information I_A is fixed. It is equal to 0 for the first point, and step by step its value increases to finally approach as close as possible the 1 value, which is the highest possible value for one bit of information [5].

Since LLR_A are assumed being consistent Gaussian (see section 6.2.2.2) and if we assume that the emitted symbol b_x is known and equal to +1, the pdf of LLR_A knowing $b_x = 1$ is characterized by:

$$LLR_A/b_x = 1 \sim Gauss\left(+\frac{\sigma_A^2}{2}, \sigma_A^2\right) \tag{6.26}$$

Finally, according to equations (6.24) and (6.26), the a priori mutual information I_A can be written as a function of σ_A^2, the LLR_A standard deviation, via this expression:

$$I_A = 1 - \int_{-\infty}^{+\infty} log_2(1 + e^{-LLR_A}) \frac{1}{\sqrt{2\pi\sigma_A^2}} e^{-\frac{\left(LLR_A - \frac{\sigma_A^2}{2}\right)^2}{2\sigma_A^2}} dLLR_A \tag{6.27}$$

For more convenience, equation (6.27) is expressed with the $J(.)$ function and reciprocally with the $J^{-1}(.)$ function as it is written below [59]:

$$I_A = J\left(\sqrt{\sigma_A^2}\right) \tag{6.28}$$

$$\sigma_A = J^{-1}(I_A) \tag{6.29}$$

with [59]:

$$J^{-1}(I_A) \approx \begin{cases} 1.09542\ {I_A}^2 + 0.214217\ I_A + 2.33727\sqrt{I_A} & for\ 0 \le I_A \le 0.3646 \\ -0.706692\ ln\big(0.386013 \times (1 - I_A)\big) + 1.75017\ I_A & for\ 0.3646 < I_A < 1 \end{cases} \tag{6.30}$$

Thus, once the a priori mutual information I_A is fixed (which is the plot abscissa), σ_A is directly deduced via equation (6.30). Then, we randomly generate the information bits (mapped into +1 or -1) to be associated with a CSK symbol. Then, since LLR_A are assumed being consistent Gaussian, they are finally drawn as follows: $LLR_{A/b_x=+/-1} \sim Gauss\left(+/-\frac{\sigma_A^2}{2}, \sigma_A^2\right)$.

The preceding function can be easily modified to also link the mean of LLR messages with the associated mutual information. Therefore in the following, for ease of notation, we refer to as the $J(.)$ function as the function that links the LLR mean μ to the mutual information $I = J(\mu)$.

6.2.3.2 From LLR_A to LLR_E

Once the a priori LLRs (LLR_A) are drawn, the CSK-modulated signal transmission in an AWGN propagation channel (see Figure 91) is simulated to compute CSK-demodulator outputs LLR_{APP}, through the equation (6.15).

The extrinsic LLRs are thus deduced from the LLR_{APP} values, as it is written in equation (6.17).

6.2.3.3 From LLR_E to I_E

Finally, to link the extrinsic LLRs (LLR_E) to the extrinsic mutual information I_E, equation (6.21) is used, with the LLR pdfs approximated by LLR_E histograms.

6.2.4 Results

The process described above has been implemented to plot the CSK demodulator EXIT charts in the AWGN propagation channel model.

Figure 91 shows the EXIT charts corresponding to a CSK-modulated signal in an AWGN propagation channel model, with CSK symbols constituted of 10 bits. First of all, a random mapping (which associates the shift applied to the PRN sequence to the CSK symbol) is used, but different mappings have then been tested. Several plots are presented, corresponding to different values of energy per symbol to noise density ratio E_s/N_0.

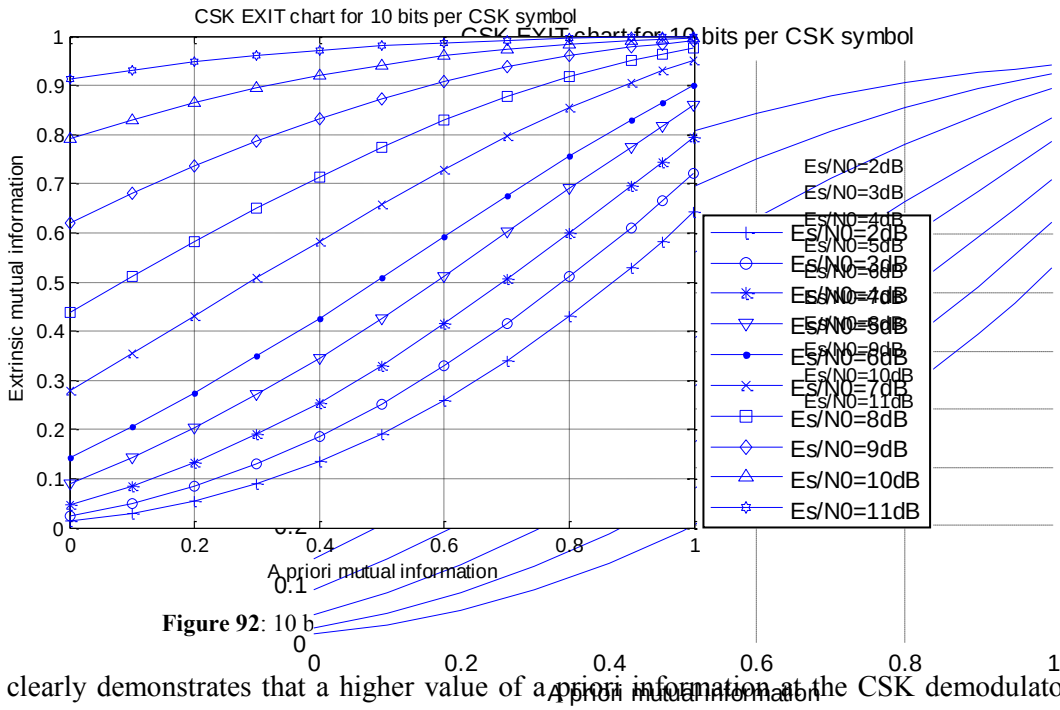

Figure 92: 10 b

This figure clearly demonstrates that a higher value of a priori information at the CSK demodulator input provides a higher value of extrinsic information at the CSK demodulator output. Since iterations after iterations an iterative decoding increases the a priori information at the CSK demodulator input in order to output a more and more refined extrinsic information value, an iterative decoding will significantly improve the CSK demodulator performance.

Nevertheless, the iterative decoding efficiency will depend on the number of bits which are mapped to a CSK symbol, as it is showed in Figure 93.

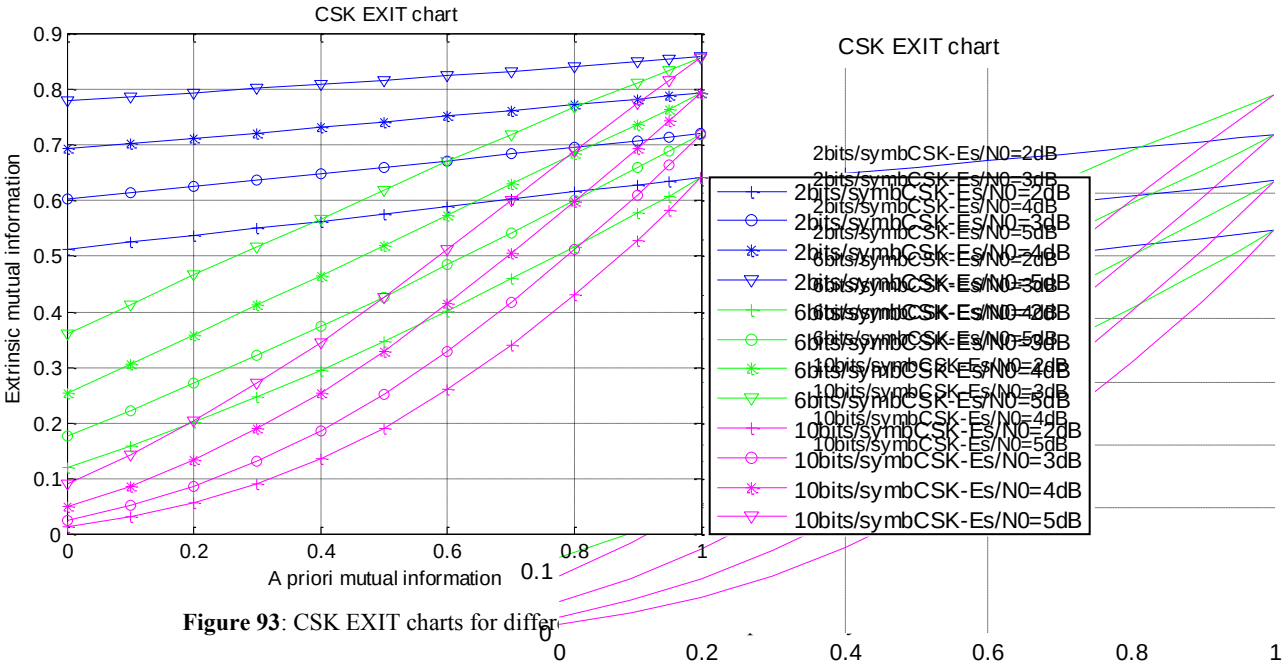

Figure 93: CSK EXIT charts for differ

Indeed, the curves slopes depend on the number of bits per CSK symbol. The more the number of bits per CSK symbol is, the more the EXIT chart curve slope is important, stressing the need for an iterative decoding in this case, compared with a few number of bits per CSK symbol.

In addition, the iterative decoding efficiency depends on the mapping which associates a shifted version of the PRN sequence with a CSK symbol. This aspect has been investigated but it has not been possible to draw significant conclusions. It remains to be further investigated.

Finally, the EXIT chart function T is extracted from these EXIT chart plots (see equation (6.31)), to be used in the LPDC asymptotic and code optimization process, as it is detailed in section 6.3, since analytic expressions of T are not available. In practice, T is approximated using a polynomial curve fitting and is formally written as:

$$I_E = T[I_A] \tag{6.31}$$

6.2.5 Properties about the Area under the EXIT Curve

Properties about the area under the curves have been set out in [55] for the binary erasure channel and generalized in [48], leading to the general acknowledgement that for serial concatenated coders (as it is the case here if we consider the LDPC coder as the outer coder and the CSK modulator as the inner coder), the area under the inner decoder EXIT curve can be linked to the capacity [55][48][60]. In our case, this statement can be written as:

$$A_{CSK} = \int_0^1 T_{CSK}(i)di \approx \frac{C_{csk}}{Q} = R_0 \tag{6.32}$$

where:

- A_{CSK} is the area under the EXIT chart of the CSK demodulator,
- T_{CSK} is the EXIT chart function associated with the inner decoder (here the CSK demodulator, represented in Figure 92 and Figure 93),
- C_{csk} is the capacity considering the inputs uniformly distributed and Q is the number of bits per symbol.

Thus, an upper bound on the maximum achievable code rate R_0 under curve fitting for the LDPC decoder can be efficiently estimated using the area under the CSK demodulator EXIT curve for a given E_s/N_0. This interesting property will be used in the LDPC code optimization process described and implemented in the next section.

For example according to Figure 92, a channel defined by a CSK-modulated signal with 10 bits per CSK symbol in an AWGN propagation channel with E_s/N_0 equal to 2 dB has a maximal code rate approximately equal to 0.2. It means that reliable communication is achievable at code rates R for which $R < \frac{1}{5}$ [5], which implies at least 5 coded bits for 1 information bit.

This bound is increasing with the E_s/N_0 value:

Table 40 Maximum achievable code rate R_0 values deduced from Figure 92 according to E_s/N_0

E_s/N_0	Corresponding C/N_0 for GPS L1C	R_0
2 dB	25 dB	0.2377
3 dB	26 dB	0.2936
4 dB	27 dB	0.3619
5 dB	28 dB	0.4435
6 dB	29 dB	0.5138
7 dB	30 dB	0.6437
8 dB	31 dB	0.7516
9 dB	32 dB	0.8500
10 dB	33 dB	0.9257
11 dB	34 dB	0.9719

These values computed as the area under the CSK demodulator EXIT charts for a CSK symbol composed of 10 bits (Figure 92) and representing the maximum possible LDPC code rate to achieve a reliable communication with iterative decoding, can be compared with the maximum possible code rates obtained with classical decoding (non-iterative), as it is done in Figure 94. To do that, for the iterative decoding case, area values obtained in Table 40 (representing maximum achievable code rates R_0) have been plotted according to E_s/N_0 (red line). For the non-iterative case (blue line), the maximum achievable code rate R_0 have been obtained from Figure 92 for a priori mutual information equal to zero.

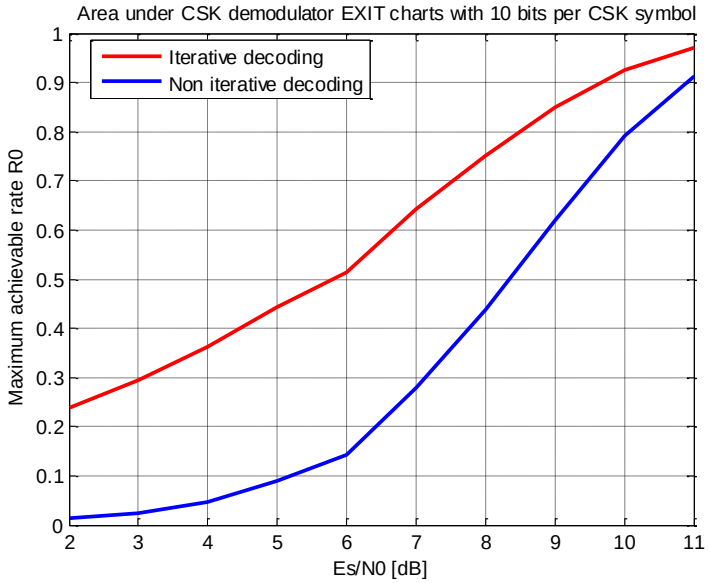

Figure 94: Comparison between the maximum achievable code rate R_0 with iterative and non-iterative decoding, for a CSK symbol composed of 10 bits

Figure 94 shows that for a signal modulated with a CSK with 10 bits per CSK symbol, iterative decoding completely outperforms non-iterative decoding, especially for low E_s/N_0. For example at E_s/N_0 equal to 2 dB, a reliable communication with non-iterative decoding is achievable for a maximum code rate of 0.01, meaning that at least 100 coded bits are necessary to encode 1 information bit. In comparison, with iterative decoding this maximum code rate is equal to 0.25, implying at least 4 coded bits for 1 information bit. The iterative decoding gain with a CSK-modulated signal appears as very impressive compared to the non-iterative case.

6.3 LDPC Code Optimization from EXIT Charts for a CSK-Modulated Signal in an AWGN Channel

In this section we derive the asymptotic analysis [59][61] for the LDPC channel code optimization under iterative decoding. This method is based on the demodulator EXIT chart function (determined in section 6.2 for a CSK modulation) and on the updating equations of the exchanged LLR messages between the demodulator and the decoder (derived in section 6.3.1), considering a priori messages having consistent Gaussian distribution. Under appropriate assumptions, the method consists in solving a linear programming optimization problem under two particular constraints (presented in section 6.3.2), which leads good degree distributions for the LDPC channel code parameters (the edge profiles). The exchanged messages between the CSK demodulator and the LDPC decoder are thus firstly detailed in this part, followed by the optimization problem statement.

In this section a LDPC code is optimized for a CSK-modulated signal, in an AWGN propagation channel model, under iterative decoding, which has to be seen as the first step of a new GNSS signal design.

6.3.1 Mutual Information Evolution

Since this method aims to optimize LDPC codes profiles for iterative decoding, the exchanged messages between the demodulator and the decoder (see Figure 95 and refer to Chapter 2) are studied in this part following an asymptotic analysis. Figure 95 illustrates the scheduling used between the CSK demodulator and the LDPC decoder, each step of the messages evolution being derived in section 6.3.1.1.

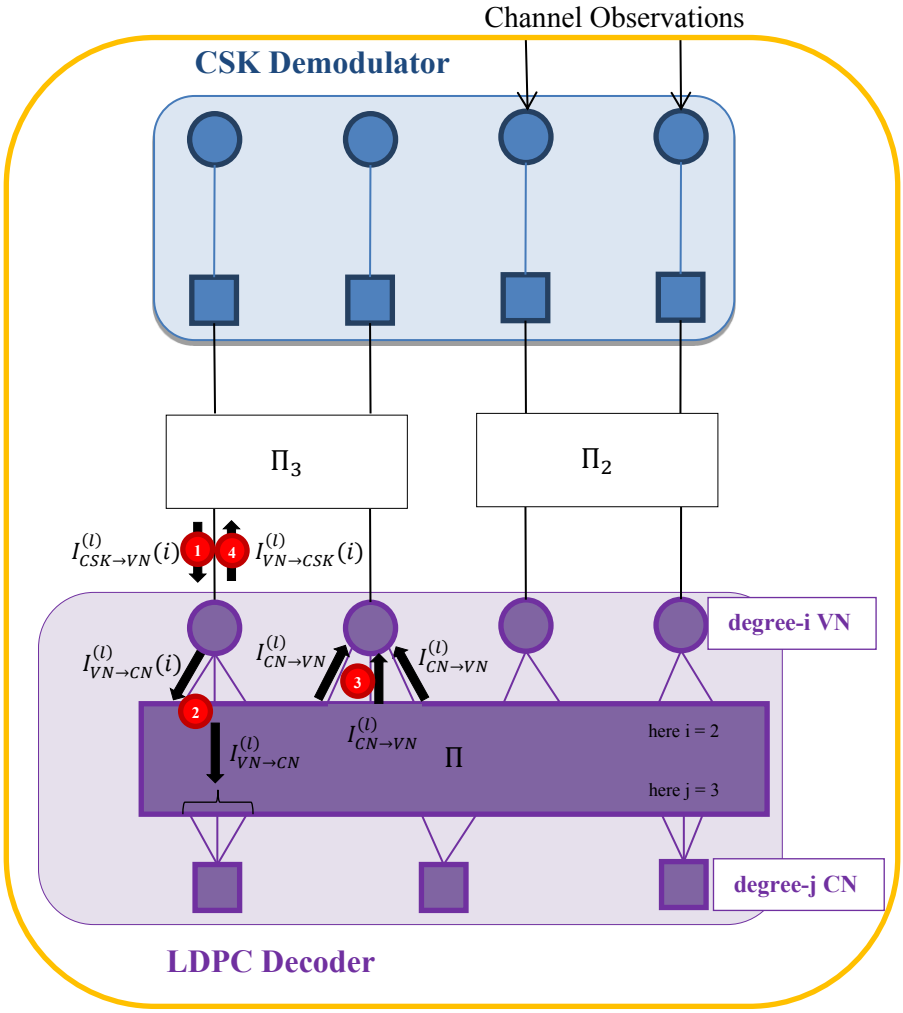

Figure 95: Exchanged messages evolution for one iteration

A large interleaver is assumed to assure statistical independence [48]. However, for the ease of analysis and optimization, we further introduce partial interleavers that are grouping every VNs with the same degree, in order to make the optimization problem linear. Moreover, we also assume that CSK symbols carry coded symbols with the same degree. This scheme can be seen as an extension of [59]. To perform the asymptotic analysis, we assume that interleavers are asymptotically large assuming independence of the extrinsic messages transiting in the combined graph. The asymptotic mutual information evolution aims to track the evolution of the average mutual information associated with the different LLR messages transiting in the graph when considering them as random variables.

6.3.1.1 Updating Equations

For each step (1 to 4 in Figure 95) of exchanged messages evolution, the mutual information expression is derived [61].

6.3.1.1.1 Step 1: Mutual information from the CSK demodulator to *i*-degree VNs

The mutual information which outputs from the CSK demodulator towards the LDPC decoder input, the VNs, corresponds to the CSK demodulator extrinsic mutual information. It has been seen in section 6.2 that this value depends on the a priori mutual information which inputs into the CSK demodulator. The function which links the extrinsic mutual information and the a priori mutual information is the EXIT chart function, noted $T(.)$, determined in section 6.2 for a CSK-modulated signal. Moreover, since the demodulator and the decoder are considered operating within an iterative process, the a priori messages which inputs to the demodulator come directly from the decoder, dating from the last iteration.

Partial interleavers allows that every VNs with the same degree i are grouped together to ease convergence analysis. By doing so, for each VN of degree i, the mutual information from the CSK demodulator to the decoder is thus equal to:

$$I_{CSK\to VN}^{(l)}(i) = I_{E_{CSK}}^{(l)}(i) = T_{CSK}\left[I_{A_{CSK}}^{(l)}(i)\right] = T_{CSK}\left[I_{VN\to CSK}^{(l-1)}(i)\right] \tag{6.33}$$

where:

- l is the iteration number,
- $I_{CSK\to VN}(\mathrm{i})$ is the mutual information coming from the CSK demodulator towards the i-degree VNs,
- $I_{E_{CSK}}$ is the extrinsic mutual information associated with LLR_E messages from the CSK demodulator to the VNs,
- T_{CSK} is the EXIT function associated to the CSK demodulator, computed in section 6.2,
- $I_{A_{CSK}}$ is the a priori mutual information associated with LLR_A messages from the VNs to the CSK demodulator.

In this case, considering partial interleavers enables to not consider a mixture of messages coming from the VNs to the CSK demodulator which leads generally to a non-linear system of equations.

6.3.1.1.2 Step 2: Mutual information from VNs to CNs

The updating equation (6.34) of LLRs coming from VNs towards CNs has been presented in Chapter 2, $L_{n\to m}$ corresponding to the LLR coming from the VN_n to the CN_m (see Figure 96).

$$L_{n\to m} = L_n + \sum L_{m\prime\to n} \tag{6.34}$$

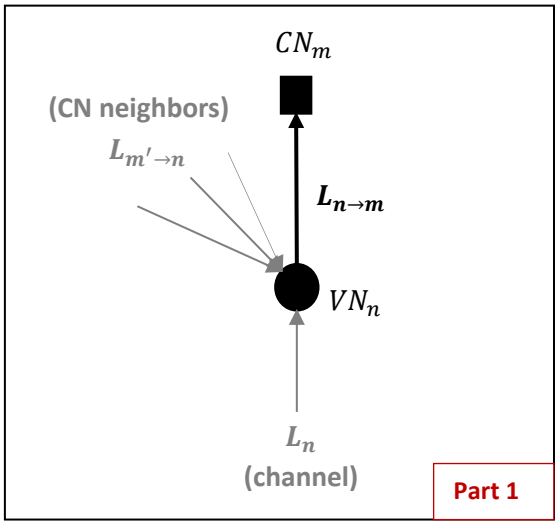

Figure 96 : CN updating (reference to Chapter 2)

where:

- L_n is the LLR coming from the CSK demodulator towards the i-degree VN,
- $L_{m'\to n}$ are the LLRs coming from all the CNs except CN_m towards VN_n. They are assumed to be independent and identically distributed due to the uniform interleaving assumption within the LDPC code.

The means $\mu_{n\to m}$ of the LLR messages $L_{n\to m}$ are then linked to the mutual information thanks to the J function (refer to equation (6.28)) and conversely the J^{-1} function (refer to equation (6.29)). It leads to the following expressions:

$$\mu_{n\to m}(i) = J^{-1}\left(I^{(l)}_{CSK\to VN}(i)\right) + \sum J^{-1}\left(I^{(l-1)}_{CN'\to VN}\right) \tag{6.35}$$

$$I^{(l)}_{VN\to CN}(i) = J\left[J^{-1}\left(I^{(l)}_{CSK\to VN}(i)\right) + (i-1)J^{-1}\left(I^{(l-1)}_{CN\to VN}\right)\right] \tag{6.36}$$

Then according to the mutual information expression between i-degree VNs and CNs (equation (6.35)), the average mutual information at the input of a CN is deduced, adding all the i-degree VNs contribution $I^{(l)}_{VN\to CN}(\mathrm{i})$, weighting each arriving edge by λ_i, the fraction of all edges connected to degree-i VNs (see Chapter 2 for the definition of λ_i).

$$I^{(l)}_{VN\to CN} = \sum_{i=2}^{d_{vmax}} \lambda_i \, I^{(l)}_{VN\to CN}(i) \tag{6.37}$$

6.3.1.1.3 Step 3: Mutual information from CNs to VNs

The updating equation of VNs in terms of mutual information (called the Reciprocal Channel Approximation) is then admitted from [61] (see Chapter 2 for the definition of ρ_j):

$$I_{CN\to VN}^{(l)} = 1 - \sum_{j=2}^{d_{c_{max}}} \rho_j J\left[(j-1)J^{-1}\left(1 - I_{VN\to CN}^{(l)}\right)\right] \tag{6.38}$$

6.3.1.1.4 Step 4: Mutual information from *i*-degree VNs to the CSK demodulator

And finally, the mutual information coming from the LDPC decoder towards the CSK demodulator through a i-degree VN, corresponding to CSK demodulator a priori information, is the sum of all CN's contributions.

$$I_{VN\to CSK}^{(l)}(i) = J\left[iJ^{-1}\left(I_{CN\to VN}^{(l)}\right)\right] \tag{6.39}$$

The total mutual information at each received estimated CSK symbol will then be computed as the average mutual information coming from each of the VN of degree i [59]. Once again, the partial interleaver assumption enables us to not consider a mixture of messages.

6.3.1.2 $I_{VN\to CN}$ Recurrence Relation

The recurrence relation on $I_{VN\to CN}$ is derived in this subsection. Each message is replaced by its updating equation derived in section 6.3.1.1:

$$I_{VN\to CN}^{(l+1)} = \sum_{i=2}^{d_{v_{max}}} \lambda_i I_{VN\to CN}^{(l+1)}(i) \tag{6.40}$$

$$I_{VN\to CN}^{(l+1)} = \sum_{i=2}^{d_{v_{max}}} \lambda_i J\left[J^{-1}\left(I_{CSK\to VN}^{(l+1)}(i)\right) + (i-1)J^{-1}\left(I_{CN\to VN}^{(l)}\right)\right] \tag{6.41}$$

$$I_{VN\to CN}^{(l+1)} = \sum_{i=2}^{d_{v_{max}}} \lambda_i J\left[J^{-1}\left(T_{CSK}\left[I_{VN\to CSK}^{(l)}(i)\right]\right) + (i-1)J^{-1}\left(1 - \sum_{j=2}^{d_{c_{max}}} \rho_j J\left[(j-1)J^{-1}\left(1 - I_{VN\to CN}^{(l)}\right)\right]\right)\right] \tag{6.42}$$

$$\begin{aligned} I_{VN\to CN}^{(l+1)} = \sum_{i=2}^{d_{v_{max}}} \lambda_i J\Bigg[&J^{-1}\left(T_{CSK}\left[J\left[iJ^{-1}\left(I_{CN\to VN}^{(l)}\right)\right]\right]\right) \\ &+ (i-1)J^{-1}\left(1 - \sum_{j=2}^{d_{c_{max}}} \rho_j J\left[(j-1)J^{-1}\left(1 - I_{VN\to CN}^{(l)}\right)\right]\right)\Bigg] \end{aligned} \tag{6.43}$$

$$I_{VN\to CN}^{(l+1)} = \sum_{i=2}^{d_{v\,max}} \lambda_i J\left[J^{-1}\left(T_{CSK}\left[J\left[iJ^{-1}\left(1-\sum_{j=2}^{d_{c\,max}} \rho_j J\left[(j-1)*J^{-1}\left(1-I_{VN\to CN}^{(l)}\right)\right]\right)\right]\right]\right) + (i-1)J^{-1}\left(1-\sum_{j=2}^{d_{c\,max}} \rho_j J\left[(j-1)J^{-1}\left(1-I_{VN\to CN}^{(l)}\right)\right]\right)\right] \quad (6.44)$$

$$I_{VN\to CN}^{(l+1)} = F\left(\lambda(X), \rho(X), T_{CSK}, I_{VN\to CN}^{(l)}\right) \quad (6.45)$$

with:

- $\lambda(X)$ and $\rho(X)$ defined in Chapter 2.

Thanks to the partial interleavers, the obtained recursion is a linear function with respect to parameters λ_i, $i = 1, \dots, d_{v\,max}$ for a given $\rho(X)$ and a given signal to noise ratio (SNR) [61]. Indeed, the transfer function of the CSK demodulator is an implicit function of the SNR. The polynomial $\rho(X)$ is often chosen as a concentrated polynomial, i.e. $\rho(X) = \rho_j X^{j-1} + (1-\rho_j)X^j$, which has been proved to be a good candidate. Doing so, the choice for $\rho(X)$ is reduced to the average degree $\bar{\rho}$ profile.

For a given LDPC code with parameters $(\lambda(x), \rho(x))$, the so-called convergence threshold can be defined as the smallest E_s/N_0 above which an arbitrary small error probabilty can be achieved, i.e. $I_{VN\to CN}^{(l)} \to 1$ as $l \mapsto +\infty$.

6.3.2 Optimization Problem Statement

The method used in this chapter to optimize the LDPC code profile of our new GNSS CSK-modulated signal for an AWGN propagation channel can be seen as a multi-edge generalization of [58]. One strategy to optimize the code profile $\lambda(X)$ for fixed SNR and $\rho(X)$ is to maximize the design code rate given by:

$$R = 1 - \frac{\sum_{j=2}^{d_c} \rho_j / j}{\sum_{i=2}^{d_v} \lambda_i / i} \quad (6.46)$$

For a given $\rho(X)$, this is equivalent to the maximization of the cost function $\sum_{i=2}^{d_v} \lambda_i / i$ which is linear with respect to the coefficients of $\lambda(X)$. Let us denote $\boldsymbol{\lambda} = [\lambda_2, \dots, \lambda_{d_v}]^T$ and $\mathbf{1/d_v} = [1/2, \dots, 1/d_v]^T$. For fixed SNR and $\rho(X)$, the optimization problem can be stated as a linear programming optimization problem as follows:

$$\boldsymbol{\lambda_{opt}} = \underset{\boldsymbol{\lambda}}{argmax}\ \mathbf{1/d_v}^T \boldsymbol{\lambda} \quad (6.47)$$

Under the constraints:

- [C1] *Mixing constraint:*

$$\boldsymbol{\lambda}^T \mathbf{1} = 1 \tag{6.48}$$

- [*C2*] *Proportion constraint:*

$$\lambda_i \epsilon [0,1], \forall i = 2, \dots, d_v \tag{6.49}$$

- [*C3*] *Convergence constraint:*

$$F(\lambda(X), \rho(X), T_{CSK}, x) > x, \forall x \in [0,1] \tag{6.50}$$

- [C4] *Stability condition* [61]:

$$\lambda_2 < \lambda_2^* = \frac{e^{\frac{J^{-1}(T_{csk}(1))}{4}}}{\sum_{j=2}^{d_{cmax}} \rho_j (j-1)} \tag{6.51}$$

As we can see, the cost function and the constraints are all linear functions of the λ_i. Performing the optimization for all SNRs allows to find the code profiles for codes that would achieve the best code rate for these operating points.

6.3.4 Results

This part illustrates the LDPC channel code profile optimization results. In this sense, two cases have been investigated: a CSK modulated signal with 2 bits per CSK symbol and one with 6 bits per CSK symbol.

6.3.4.1 2 Bits per CSK symbols

In Figure 97, we have plotted the achievable code rates for different maximum variable node degrees for the 2 bits per CSK symbol case. These curves are compared to the maximum achievable rate given by the area theorem.

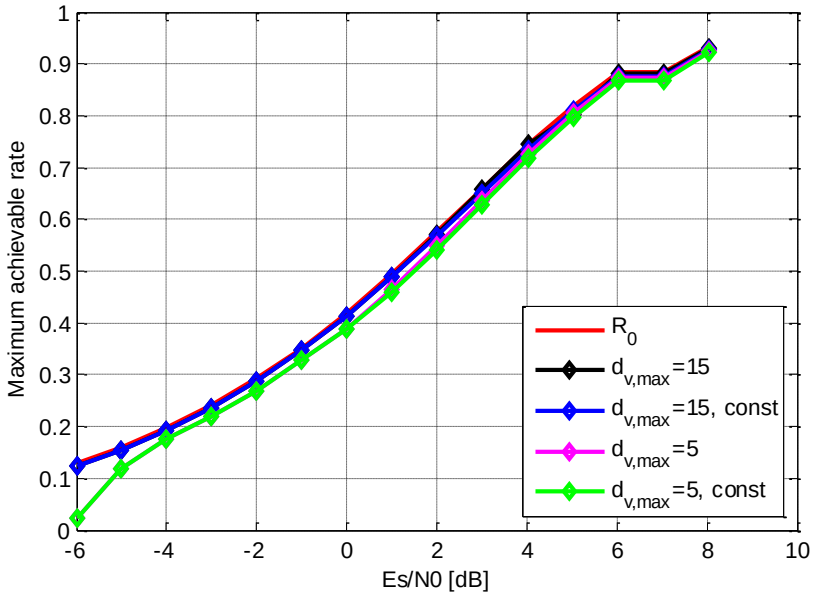

Figure 97: Achievable rate for different maximum variable node degrees for the 2 bits per CSK symbol case

As we can see, the higher the maximum variable node degree, the closer we are from the maximum achievable performance, especially for low coding rates. When looking carefully to the degree profiles we can see that the proportion of degree 2 VNs is higher than (1-R), leading to unavoidable cycles involving degree 2 nodes. This is the price to pay to get closer to the maximum achievable performance under iterative decoding. A similar result can be drawn from the profiles given in [58] even if it has not been pointed out. To avoid this behaviour that can have some impact in the error floor region, one can add a constraint on the variable node of degree two (less than (1-R)) that can be shown to be also linear with respect to λ_i. We have optimized LDPC code profiles with an additional constraint for degree two variable nodes. As shown, in this case there is almost no penalty induced by this constraint on degree 2 nodes.

6.3.4.2 6 Bits per CSK Symbol Case

The same study has been performed for the 6 bits per CSK symbol case.

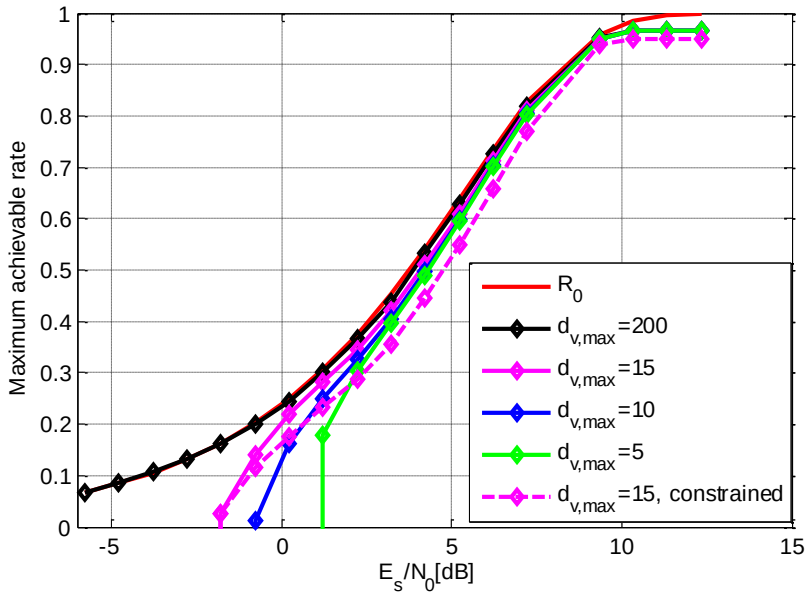

Figure 98: Achievable rate for different maximum variable node degrees for the 6 bits per CSK symbol case

The same observations can be made: the higher the maximum variable degree is, the closer we can get from the maximum achievable rate. This is particularly true for low rates. What can be observed, is that even for a maximum degree 15, we still are far from the best achievable performance. We have a significant degradation when decreasing too much this maximum variable node degree in the low rate regime. Moreover, when constraining the degree 2 nodes to avoid a proportion of degree 2 nodes greater than (1-R), we can see that we have in this case a great penalty on the maximum achievable rate. Thus in this case, approaching the performance limits cannot be done without considering heavy insertion of degree two variable nodes. For example, for a design code rate of around one-half, we have found profiles with almost 95% of degree 2 nodes. The same thing has been observed when 10 bits per CSK symbol has been considered. As a result, it tends to show that for high order CSK modulation, best concatenated codes are almost cycle codes, which are known to be a weak code family (regular (2,dc) LDPC codes). However we will show that under iterative decoding they perform fairly well leading to an efficient class of sparse graph based BICM. It also points out the fact that for high order CSK modulation, maybe non-binary codes could be preferred, since regular non-binary (2,dc) LDPC codes outperforms they binary counterpart especially in the finite length regime.

6.3.4.3 Finite length results

To assess the performance of our code profile optimization, we have designed finite length codes for both 2 bits and 6 bits per CSK symbol modulations. Then, to provide an associated H matrix to entirely define the LDPC channel code, a message length needs to be determined. Since this PhD thesis concerns GNSS signals, and since the GPS L1C signal is used as a benchmark all along this work to test the demodulation performance improvement of our contributions, the same message length that GPS L1C subframe 2 will be used, and equal to 600 information bits with channel code rate ½. So, in both cases, we have designed finite length codes with around 600 information bits and code rate around ½. Several configurations have been tested. First, for the case of the 2 bits per CSK symbol, we have designed two codes with constrained degree 2 nodes for two maximum achievable variable degrees (10 and 15). For these two codes, two parity check matrices have been designed with the PEG algorithm (the minimal girth is 8 and 6 respectively). The performance under iterative

decoding has been then compared to the performance of the GPS L1C LDPC code that has been designed for the AWGN propagation channel.

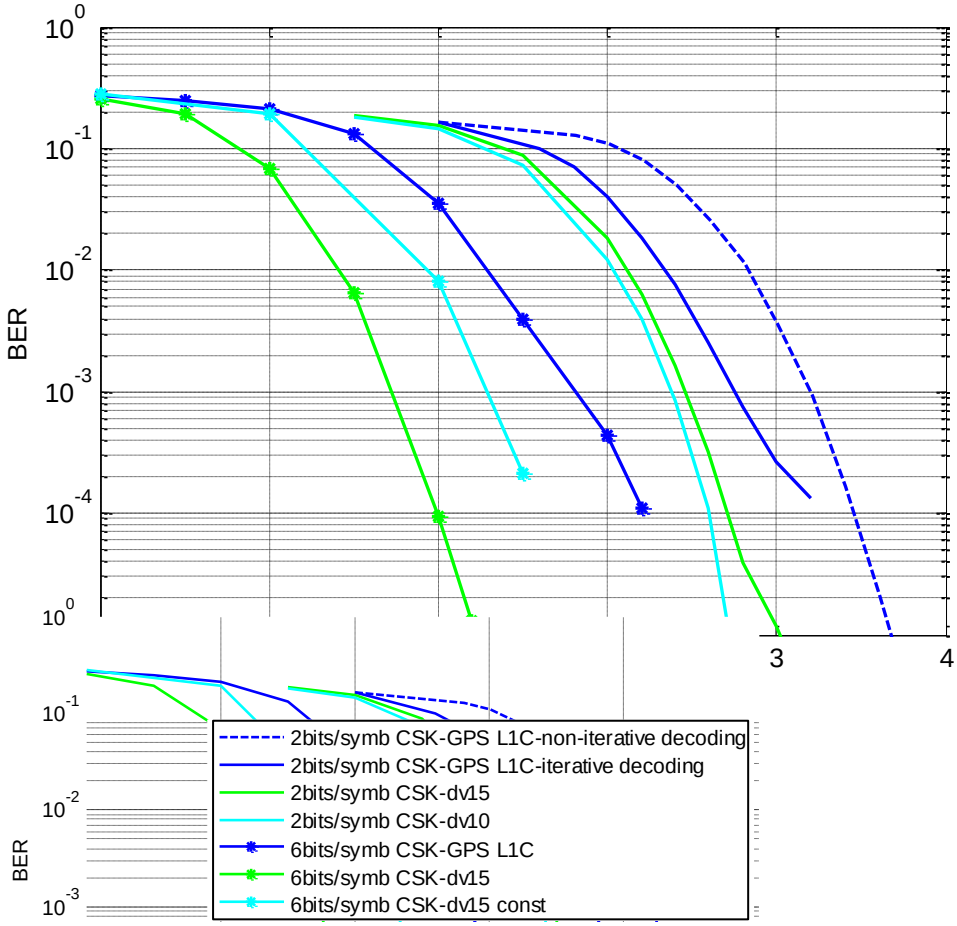

Figure 99: Finite length results: BER according to E_b/N_0 for 2 bits per CSK symbol and 6 bits per CSK symbol

As shown in Figure 101, the proposed codes outperform the GPS L1C LDPC code by about 0.5 dB. We can also show that better performance can be achieved considering lower maximum variable node degrees enabling larger girth without penalizing two much the performance in the waterfall region. For the case of the 6 bits per CSK symbols, we have a maximum variable node degree of 15 and we compare two codes that have been designed with and without the degree 2 node constraint. As we can see there is a non-negligible penalty in the waterfall region when constraining the degree 2 variable nodes. We can also notice that the best performing designed code outperforms significantly the GPS L1C LDPC code under iterative decoding by about 1.2 dB at BER= 10^{-4}.

6.4 Perspectives

The work concerning LDPC code design for CSK modulation is a first step towards joint design of sparse graph based CSK-BICM. Future investigations will consider the design of structured LDPC codes such as Structured IRA (Irregular Repeat Accumulate) or protograph based constructions to enable efficient encoding and decoding. Then, extension to the non-binary case could be considered and compared to existing approaches such as the one proposed in [51].

Chapitre 7: Conclusions and Future Work

7.1 Conclusions

The objective of this PhD thesis was to analyse and to improve GNSS signals demodulation performance in urban environments for mass-market users; the main PhD thesis research axis being the channel coding domain. This objective has to be seen as the first approach for the design of a new GNSS signal, with high demodulation performance in difficult environments.

The first step of this work has thus consisted in studying the current GNSS signals through their temporal evolution in terms of demodulation performance. This preliminary study has showed that GNSS signals are more and more advanced concerning their protection level against errors due to difficult environments. Channel coding gain is increasing signal after signal, starting by no channel code with GPS L1 C/A, to be improved with a convolutional code with SBAS, GPS L2C, GPS L5 and Galileo E1 OS, to finally achieve modern channel codes with GPS L1C and its LDPC code. The latest designed GNSS signal is thus GPS L1C, with the most powerful GNSS signals channel code since it belongs to the LDPC codes family, able to approach the Shannon capacity. It has thus been decided to use the GPS L1C signal as a benchmark in this PhD thesis in terms of demodulation performance currently possible to be provided. It came out from this preliminary study that the final goal to achieve consists in improving the current GPS L1C signal in order to surpass its demodulation performance in urban environments.

To improve GNSS signals demodulation performance in urban environments, it is necessary to be able to make tests. However, it was not possible to make real tests and measurements during this PhD thesis. First of all because the GPS L1C signal is not emitted at this moment, it is expected to be firstly launched in 2016 with GPS III. Then, because the final purpose of this work being to design a new GNSS signal, it is necessary to simulate it to be able to compare its demodulation performance with the one obtained with GPS L1C. Moreover, new algorithms and new configurations should have been tested to analyse and improve demodulation performance. For all these reasons, a software simulation tool able to simulate the entire GNSS signals emission/reception chain in an urban environment should had to be developed during this PhD thesis: SiGMeP, for Simulator for GNSS Message Performance. Since simulations concerning GNSS demodulation performance are really time-consuming, it has appeared necessary to develop this simulator in C language. SiGMeP is based on the work of A. Garcia-Pena who has developed a preliminary version of this simulator for its PhD thesis work in 2010.

The most important part of the software simulator development has been the urban propagation channel model implementation. To do that, a state-of-the-art has been conducted about urban Land-Mobile Satellite (LMS) propagation channel models existing and applicable for this work. Very few realistic models exist, due to the complexity of leading precise measurement campaigns, and to the

difficulty to analyse the data with a sufficient accuracy and representativeness. Several propagation channel models designed for a GNSS context are being in development, but only two are already available (including one which has not been specially designed for GNSS): the Perez-Fontan/Prieto model and the DLR model. These two models have thus been implemented into the simulator. The DLR model being freely accessible on Matlab, the generated channel model samples have been stored and directly used in SiGMeP. Nevertheless for the Prieto model, all the channel model generation has been developed.

Another sensitive part of the simulator development is the GNSS received signal modeling. Generally, the received signal can be easily modeled at the correlator output level. Nevertheless in urban environments, this model might not be valid anymore if care is not taken since it is based on stability assumptions (constant amplitude and Doppler of the incoming signal) that might not be compatible with the phase and amplitude variations of an urban channel. Investigations have thus been conducted during this PhD thesis in order to determine the channel generation rate that was compatible with the correlator output model. To do that, the use partial correlations have been considered and the longest admissible partial correlation duration has been determined. Moreover, it is important to mention that the signal carrier phase estimation in SiGMeP is based on the use of a PLL tracking to ensure a realistic simulator behavior.

One of the aspects of this PhD thesis concerned the analysis of existing GNSS signals demodulation performance in urban environments. Since the current literature is rather poor at this level, it was necessary to provide it. The classical method to represent GNSS signals demodulation performance plots the error rate as a function as the received C/N_0 value. It has been seen in this PhD thesis that this method is not applicable in an urban environment, since the received C/N_0 is fluctuating. Moreover, it has been demonstrated that the classical way to represent GNSS signals demodulation performance is not representative of reality. An innovative methodology has thus been proposed in this work, adapted to urban environments and more adapted to evaluate the fulfillment of operational needs. The GPS L1C demodulation performance has then been provided and analyzed by applying the new methodology to test cases with the narrowband Perez-Fontan/Prieto propagation channel model and then with the wideband DLR model. These results can be viewed as a worst case since a very obstructed configuration was assumed: 4 satellites with the same elevation angle equal to 40° and with an azimuth angle equal to 30° for the DLR model. It has been showed for example that the classical methodology with PLL tracking predicts that the receiver is never able to demodulate CED with an error rate equal or lower than 10^{-2} (whatever the used propagation model), whereas the proposed methodology ensures that with GPS L1C, the receiver is able to calculate a continuous valid position during 4 consecutive hours, with a probability greater than 95%, for a $C_{pre\text{-}urban}/N_0$ higher than 26.25 dB-Hz with the Prieto model (and 'favorable state messages' determination criterion 1) and at least 99.8% of time for a $C_{pre\text{-}urban}/N_0$ value greater than 25.5 dB-Hz for the DLR model (and 'favorable state messages' criterion 2), for 4 satellites with 40° of elevation angle. If 80° is considered, this probability becomes 100% for a $C_{pre\text{-}urban}/N_0$ higher than 25.8 dB-Hz, considering the Prieto model (and 'favorable state messages' determination criterion 1), which is coherent since 80° of elevation is more advantageous in terms of favorable reception conditions compared with 40°. If we try to represent a real case with different satellites elevation angles, two with elevation angles equal to 80° and the others with 40°, the GPS L1C receiver is able to calculate a continuous valid position during 4 consecutive hours, with a probability greater than 97.6%, for a $C_{pre\text{-}urban}/N_0$ higher than 25.8 dB-Hz with the Prieto model. In addition, if the Galileo E1 OS signal is considered, with 4 satellites with 40° of elevation, the receiver can calculate a continuous valid position during 4 consecutive hours, with a probability approximately equal to 100% for a $C_{pre\text{-}urban}/N_0$ higher than 29 dB-Hz, considering the

Prieto model. The higher probability value obtained for Galileo E1 OS can be explained by the fact the 'favorable state messages' occurrence rate has been computed through two message parts each lasting approximately 4 seconds, over the message duration equal to 30 seconds, whereas for GPS L1C, the entire message (since subframes 2 and 3 are interleaved and since the subframe 1 duration is negligible) lasting 18 seconds has been considered. It is thus easier to have twice 4 seconds in favorable reception conditions for the Galileo E1 OS case than 18 seconds for GPS L1C. However, the demodulation performance obtained with GPS L1C is better than Galileo E1 OS.

From this GPS L1C demodulation performance assessment in urban environments, the objective was to find a way to improve it by optimizing the demodulation part. The focus was thus on the receiver. In classical receivers, the detection function at the decoder input has been derived considering an AWGN propagation channel. This function is not adapted to urban propagation channels. The detection function has thus been derived in this dissertation according to different levels of Channel State Information (CSI). If a perfect CSI knowledge is available (thanks to channel estimation for example), the GPS L1C demodulation performance in urban environment is spectacularly improved since the floor due to the PLL observed with the classical detection function totally disappears. Since for this moment it is not possible to perfectly estimate the propagation channel impact on the received signal, an innovative method has been proposed to optimize the detection function to any user environments. With absolutely no channel knowledge, the advanced method allows obtaining a decoding gain of 3 dB for ideal phase estimation and a significant lowering of the floor when considering the more representative use of a PLL. It is important to mention that this innovation solution proposed in this PhD thesis is very easy to implement since it only involves the GNSS receiver.

Finally, the real purpose of this PhD thesis being the design of an innovative signal with high demodulation performance in urban environments, investigations have been made on this point. One of the main challenges in terms of mass-market GNSS applications concerns difficult reception environments such as cities, as it has been already mentioned. But another challenge is appearing: the necessity to increase the current useful data rate, motivated by new services which need lots of information or by a desire of more redundancy to better counteract the impact of difficult environments. Since the spread spectrum characteristic of GNSS signals makes the increase of the data rate impossible with the current GNSS signals modulations because of the PRN code which will be decreased causing a wider spectrum and a loss of orthogonality properties, another modulation was proposed. One possible solution to deal with this limitation consists in implementing the Code Shift Keying (CSK) modulation instead of a BPSK as it is the case at this moment. The new GNSS designed signal proposed in this PhD thesis is thus CSK-modulated.

An important work has been conducted on the design of a new LDPC channel code profile, optimized for a CSK-modulated GNSS signal, in an AWGN propagation channel (with the aim of further testing it in urban environments), for iterative decoding. The optimization process has been conducted using the EXtrinsic Information Transfer (EXIT) charts analysis and asymptotic optimization method. First, the CSK demodulator EXIT charts for 2 bits per CSK symbol, 6 bits and 10 bits, have been provided and analysed, demonstrating that iterative decoding completely outperforms non-iterative decoding, especially for low E_s/N_0. For example for an E_s/N_0 equal to 2 dB (corresponding to a C/N_0 equal to 25.01 dB-Hz for GPS L1C) and considering 10 bits per CSK symbol, it has been showed that 100 coded bits are necessary to encode 1 information bit with non-iterative decoding whereas just 4 coded bits are necessary with iterative decoding. The iterative decoding gain with a CSK-modulated signal is thus really significant. Then, the channel code profile optimization has been made through the

asymptotic method, thanks to EXIT charts analysis. Several finite length codes have then been generated according to the resulting asymptotic optimized profile, for CSK symbols with 2 bits and 6 bits. Finally, they have been tested in an AWGN propagation channel and compared with the channel code of GPS L1C used with a CSK-modulated signal and iteratively decoded. The new proposed codes optimized for CSK-modulated signals clearly outperform the LDPC code of GPS L1C.

7.2 Perspectives for Future Work

The development of a software simulation tool was not the final objective of this PhD thesis, but it was necessary to do it in order to be able to provide GNSS signals demodulation performance. A better simulator could be developed by experts in the Propagation Channel and GNSS fields, with more resources and more time.

In this PhD thesis dissertation, only the GPS L1C signal demodulation performance has been provided because simulations are very time-consuming due the complexity of the channel generation and the need for accurate statistical analysis at the CED level. However it would be interesting to exhibit all the current GNSS signals demodulation performance in urban environments (with the classical method), since the literature is not really furnished in this domain. Moreover, it should be interesting to vary the user speed, the emitting satellites elevation angle and the azimuth angle.

An innovative method has been proposed in this work to provide GNSS signal demodulation performance in urban environments representative to reality, but since the GPS L1C signal has only been studied, the other signals demodulation performance remain to be provided too. In addition, the new methodology has only been developed for a continued usage. Other important figures of merit, such as the TTFF, have not been explored whereas it is relevant information. Thus, this aspect remains to be investigated.

The detection function mathematical expressions, derived in this dissertation in an urban environment and considering different levels of CSI knowledge, and tested with SiGMeP, have allowed opening up some interesting new prospects. The ideal case corresponding to a perfect CSI knowledge has showed that demodulation performance can really be improved by the adaptation of the detection function to the propagation channel. Nevertheless the new method developed during this PhD thesis considering absolutely no CSI knowledge improves the results obtained with the classical detection function, but it remains not satisfactory enough compared with the promising ideal case, due to the remaining PLL phase error. Future work would consist in researching a way to obtain more information about the PLL phase error. In that sense, the propagation channel estimation, or the PLL phase error modeling, or the PLL losses of lock detector output use could be investigated.

The first steps in the design of a new high-performance GNSS signal have been taken with the optimization of a LDPC code profile for a CSK-modulated signal in an AWGN propagation channel, dedicated to iterative decoding. Nevertheless, the work needs to be continued. This new signal must be tested in an urban propagation channel, to be compared with the current GNSS signals. Moreover, the CSK mapping needs to be further investigated.

The work concerning LDPC code design for CSK modulation is a first step towards joint design of sparse graph based CSK-BICM. Future investigations will consider the design of structured LDPC codes such as Structured IRA (Irregular Repeat Accumulate) or protograph based constructions to enable efficient encoding and decoding. Then, extension to the non-binary case could be considered and compared to existing approaches.

Bibliography

[1] U.S. Government, "U.S. Government GPS website", *http://www.gps.gov*.

[2] A. Emmanuele, M. Luise, J.-H. Won, D. Fontanella, M. Paonni, B. Eissfeller, F. Zanier, and G. Lopez-Risueno, "Evaluation of Filtered Multitone (FMT) Technology for Future Satellite Navigation Use", presented at the Proceedings of the 24th International Technical Meeting of The Satellite Division of the Institute of Navigation (ION GNSS 2011), ION GNSS 2011, Portland, OR, 2011.

[3] A. Emmanuele, F. Zanier, G. Boccolini, and M. Luise, "Spread-Spectrum Continuous-Phase-Modulated Signals for Satellite Navigation", *IEEE Trans. Aerosp. Electron. Syst.*, vol. 48, no. 4, pp. 3234–3249, 2012.

[4] A. Garcia-Pena, "Optimization of Demodulation Performance of the GPS and GALILEO Navigation Messages", PhD, Université de Toulouse, 2010.

[5] W. Ryan and S. Lin, *Channel Codes: Classical and Modern*. Cambridge University Press, 2009.

[6] M. Anghileri, M. Paonni, D. Fontanella, and B. Eissfeller, "Assessing GNSS Data Message Performance A New Approach", *GNSS*, pp. 60–70, Apr. 2013.

[7] European Space Agency, "ESA website", *http://www.esa.int/ESA*.

[8] E. D. Kaplan and C. J. Hegarty, *Understanding GPS: Principles and Applications*. Artech House, 2005.

[9] US Government, "INTERFACE SPECIFICATION IS-GPS-200 Navstar GPS Space Segment/Navigation User Interface", 08-Jun-2010.

[10] M. Anghileri, M. Paonni, D. Fontanella, and B. Eissfeller, "GNSS Data Message Performance: A New Methodology for its Understanding and Ideas for its Improvement", presented at the International Technical Meeting (ITM) of The Institute of Navigation, San Diego, CA, 2013.

[11] European Commission, "EGNOS Open Service Service Definition Document v2.0", 18-Mar-2013.

[12] European Commission, "EGNOS Safety of Life Service Definition Document v1.0", 03-Feb-2011.

[13] *Minimum Operational Performance Standards for Global Positioning System/Wide Area Augmentation System Airborne Equipment*, RTCA, 2006.

[14] Richard D. Fontana, Wai Cheung, Paul M. Novak, and Thomas A. Stansell, "The New L2 Civil Signal", presented at the 14th International Technical Meeting of the Satellite Division of The

Institute of Navigation (ION GPS 2001), Salt Palace Convention Center Salt Lake City, UT, 2001.

[15] Emilie Rebeyrol, Christophe Macabiau, Laurent Lestarquit, Lionel Ries, Jean-Luc Issler, Marie-Laure Boucheret, and Michel Bousquet, "BOC Power Spectrum Densities", presented at the Proceedings of the 2005 National Technical Meeting of The Institute of Navigation, The Catamaran Resort Hotel San Diego, CA, 2005.

[16] O. Julien, C. Macabiau, J.-L. Issler, and L. Ries, "Two for One - Tracking Galileo CBOC Signal with TMBOC", *GNSS*, no. Spring 2007, 2007.

[17] European Union 2010, "European GNSS (Galileo) Open Service Signal In Space Interface Control Document", Feb-2010.

[18] J. W. Betz, C. R. Cahn, P. A. Dafesh, C. J. Hegarty, K. W. Hudnut, A. J. Jones, R. Keegan, K. Kovach, L. S. Lenahan, H. H. Ma, J. J. Rushanan, T. A. Stansell, C. C. Wang, and S. K. Yi, "L1C signal design options", United States Geological Survey, 2006.

[19] US Government, "INTERFACE SPECIFICATION IS-GPS-800 Navstar GPS Space Segment/User Segment L1C Interface", Sep-2012.

[20] W. Ryan and S. Lin, *Channel Codes: Classical and Modern*, 1st ed. Cambridge University Press, 2009.

[21] I. Bacic, K. Malaric, and Z. Petrunic, "A LDPC code/decode channel coding model based on sum-product algorithm realization via LabVIEW", in *ICECom, 2010 Conference Proceedings*, 2010, pp. 1–4.

[22] C. Poulliat, "Codes LDPC", Nov-2011.

[23] L. Shu and S. L., Daniel J. Costello, *Error Control Coding*. Pearson Education India.

[24] Dafesh, Vallés, Hsu, Sklar, Zapanta, and Cahn, "Data Message Performance for the Future L1C GPS Signal", presented at the Proceedings of the 20th International Technical Meeting of the Satellite Division of The Institute of Navigation (ION GNSS 2007) September 25 - 28, 2007 Fort Worth Convention Center Fort Worth, TX, pp. 2519 – 2528.

[25] J. G. Proakis and M. Salehi, *Digital communications*. Boston: McGraw-Hill, 2008.

[26] F. Perez-Fontan, M. A. V. zquez-Castro, S. Buonomo, J. P. Poiares-Baptista, and B. Arbesser-Rastburg, "S-band LMS propagation channel behaviour for different environments, degrees of shadowing and elevation angles", *IEEE Trans. Broadcast.*, vol. 44, no. 1, pp. 40–76, 1998.

[27] F. P. Fontan, M. Vazquez-Castro, C. E. Cabado, J. P. Garcia, and E. Kubista, "Statistical modeling of the LMS channel", *IEEE Trans. Veh. Technol.*, vol. 50, no. 6, pp. 1549–1567, 2001.

[28] R. Prieto-Cerdeira, F. Perez-Fontan, P. Burzigotti, A. Bolea-Alamañac, and I. Sanchez-Lago, "Versatile two-state land mobile satellite channel model with first application to DVB-SH analysis", *Int. J. Satell. Commun. Netw.*, vol. 28, no. 5–6, pp. 291–315, 2010.

[29] A. Lehner and E. Steingass, "A novel channel model for land mobile satellite navigation", in *Institute of Navigation Conference ION GNSS 2005*, pp. 13–16.

[30] D. Tse, *Fundamentals of Wireless Communication*. Cambridge University Press, 2005.

[31] A. Lehner, "Multipath Channel Modelling for Satellite Navigation Systems - Mehrwegekanalmodellierung für Satellitennavigationssysteme", PhD, Universität Erlangen-Nürnberg, 2007.

[32] A. L. Alexander Steingass, "Measuring GALILEO's Multipath Channel".

[33] DLR, "Technical Note on the Land Mobile Satellite Channel Model - Interface Control Document", 08-May-2008

[34] A. Steingass and A. Lehner, "Measuring the Navigation Multipath Channel – A Statistical Analysis", in *Proceedings ION GNSS 2004*, Long Beach, California, 2004, vol. Session C3.

[35] A. Lehner and E. Steingass, "A novel channel model for land mobile satellite navigation", *Inst. Navig. Conf. ION GNSS 2005*, pp. 13–16, 2005.

[36] DLR, "Technical Note on the Implementation of the Land Mobile Satellite Channel Model - Software Usage", 06-Jul-2007.

[37] A. Lehner, "Multipath channel modelling for satellite navigation systems", Shaker, Aachen, 2007.

[38] DLR, "DLR Portal", http://www.dlr.de/dlr/desktopdefault.aspx/tabid-10002/.

[39] Report ITU-R P.2145, "Model parameters for an urban environment for the physical-statistical wideband LMSS model in Recommendation ITU-R P.681-6", ITU International Telecommunication Union, 2009.

[40] Heinrich Meyr, Marc Moeneclaey, and Stefan A. Fechtel, *Digital Communication Receivers, Synchronization, Channel Estimation, and Signal Processing*, 1997.

[41] B. W. Parkinson and J. J. Spilker Jr., *Global Positioning System: Theory and Applications Volume I*, vol. 163. Paul Zarchan, 1996.

[42] Ismael Colomina, Christian Miranda, M. Eulàlia Parés, Marcus Andreotti, Chris Hill, Pedro F. da Silva, João S. Silva, Tiago Peres, João F. Galera Monico, Paulo O. Camargo, Antonio Fernández, José Maria Palomo, João Moreira, Gustavo Streiff, Emerson Z. Granemann, and Carmen Aguilera, "Galileo's Surveying Potential: E5 Pseudorange Precision", *GPS World*, Mar-2012.

[43] C. Macabiau, "GPS Signal." 2008.

[44] Rebeyrol E., Macabiau C., Ries L., Bousquet M., and Boucheret M.-L., "Phase Noise in GNSS Transmission/Reception System", presented at the National Technical Meeting of the Institute Of Navigation, Monterey, California, 2006.

[45] J. W. Betz, M. A. Blanco, C. R. Cahn, P. A. Dafesh, C. J. Hegarty, K. W. Hudnut, V. Kasemsri, R. Keegan, K. Kovach, L. S. Lenahan, H. H. Ma, J. J. Rushanan, D. Sklar, T. A. Stansell, C. C. Wang, and S. K. Yi, "Description of the L1C signal", United States Geological Survey, 2006.

[46] S. ten Brink, "Design of concatenated coding schemes based on iterative decoding convergence", Shaker, Aachen, 2002.

[47] R. Yazdani and M. Ardakani, "Linear LLR approximation for iterative decoding on wireless channels", *IEEE Trans. Commun.*, vol. 57, no. 11, pp. 3278–3287, Nov. 2009.

[48] J. Hagenauer, "The EXIT Chart - Introduction to Extrinsic Information Transfer", in *Iterative Processing", In Proc. 12th Europ. Signal Proc. Conf (EUSIPCO*, 2004, pp. 1541–1548.

[49] A. Garcia-Pena, D. Salos, O. Julien, L. Ries, and T. Grelier, "Analysis of the use of CSK for Future GNSS Signals", in *Proceedings of the 26th International Technical Meeting of The Satellite Division of the Institute of Navigation (ION GNSS 2013)*, 2013.

[50] A. Garcia-Pena, P. Paimblanc, D. Salós, O. Julien, M.-L. Boucheret, T. Grelier, L. Ries, A. Garcia-Pena, P. Paimblanc, D. Salós, O. Julien, M.-L. Boucheret, T. Grelier, and L. Ries, "Investigation of CSK as a Candidate for Future GNSS Signals, Investigation of CSK as a Candidate for Future GNSS Signals", presented at the EWGNSS 2013, 6th European Workshop on GNSS Signals and Signal Processing, EWGNSS 2013, 6th European Workshop on GNSS Signals and Signal Processing.

[51] O. Abassi, L. Conde-Canencia, M. Mansour, and E. Boutillon, "Non-Binary Low-Density Parity-Check coded Cyclic Code-Shift Keying", in *2013 IEEE Wireless Communications and Networking Conference (WCNC)*, 2013, pp. 3890–3894.

[52] O. Abassi, L. Conde-Canencia, M. Mansour, and E. Boutillon, "Non-binary coded CCSK and Frequency-Domain Equalization with simplified LLR generation", in *2013 IEEE 24th International Symposium on Personal Indoor and Mobile Radio Communications (PIMRC)*, 2013, pp. 1478–1483.

[53] A. Y.-C. Wong and V. C. M. Leung, "Code-phase-shift keying: a power and bandwidth efficient spread spectrum signaling technique for wireless local area network applications", in *IEEE 1997 Canadian Conference on Electrical and Computer Engineering, 1997, Engineering Innovation: Voyage of Discovery*, 1997, vol. 2, pp. 478–481 vol.2.

[54] G. Caire, G. Taricco, and E. Biglieri, "Bit-interleaved coded modulation", *IEEE Trans. Inf. Theory*, vol. 44, no. 3, pp. 927–946, May 1998.

[55] A. Ashikhmin, G. Kramer, and S. ten Brink, "Extrinsic information transfer functions: model and erasure channel properties", *IEEE Trans. Inf. Theory*, vol. 50, no. 11, pp. 2657–2673, Nov. 2004.

[56] J. R. Barry and E. A. Lee, *Digital Communication*, Édition : 3rd ed. 2003. Boston: Kluwer Academic Publishers, 2003.

[57] S. Ten Brink, "Convergence of iterative decoding", *Electron. Lett.*, vol. 35, no. 10, pp. 806–808, May 1999.

[58] M. Tüchler, S. T. Brink, and J. Hagenauer, "Measures for Tracing Convergence of Iterative Decoding Algorithms", in *in Proc. 4th IEEE/ITG Conf. on Source and Channel Coding*, 2002, pp. 53–60.

[59] S. ten Brink, G. Kramer, and A. Ashikhmin, "Design of low-density parity-check codes for modulation and detection", *IEEE Trans. Commun.*, vol. 52, no. 4, pp. 670–678, Apr. 2004.

[60] A. G. i Fàbregas, A. Martinez, and G. Caire, *Bit-Interleaved Coded Modulation*. Now Publishers Inc, 2008.

[61] C. Poulliat, "Contributions à l'étude et à l'optimisation de systèmes à composantes itératives.", Université de Cergy Pontoise, 2010.

[62] The onsultative Committee for Space Data Systems, “TC Synchronization and Channel Coding - Summary of Concept and Rationale, Report Concerning Space Data System Standards, CCSDS 230.1-G-2, Green Book.” .

[63] D. Forney, “Concatenated codes,” *Scholarpedia*, vol. 4, no. 2, p. 8374, 2009.

Annex A: Demodulation Performance Representation

In order to know if a GNSS signal corresponds to the intended application or to know if it is better than another, it is necessary to study its performance. One way to represent a part of this performance consists in plotting the error rate of interest according to the amount of resources required to achieve that error rate [62]. This classical representation shows the GNSS signal demodulation performance. As illustration, Figure 52 provides demodulation performance of current GNSS signals in the AWGN propagation channel model. The first part of this annex thus presents the error rates of interest in GNSS (ordinate axis), whereas the second is about the parameter representing the amount of required resources (abscissa axis).

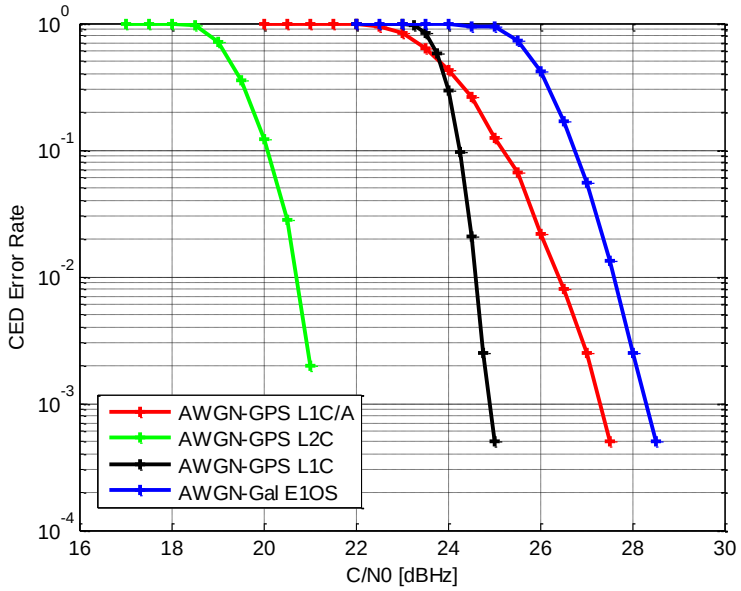

Figure 100: GNSS signals demodulation performance in the AWGN channel model with the classical methodology

A.1 Abscissa Axis: Error Rate

The error rate, as the curve abscissa axis, can be measured by the Bit Error Rate (BER), the Word Error Rate (WER), or especially in GNSS by the Clock error corrections and Ephemeris Data Error Rate (CEDER). Each of these error rates is detailed below.

A.1.1 BER

The Bit Error Rate (BER) is the ratio between the number of erroneous bits which compose the received symbols and the total number of received bits. It can be written as:

$$BER = \frac{number\ of\ erroneous\ bits}{total\ number\ of\ received\ bits} \quad \text{(A.1)}$$

It is often represented as a negative power as 10^{-4} for example, which means that in average 1 bit is false among 1000 received bits.

A.1.2 WER

The Word Error Rate (WER) can be also used which is the ratio between the number of erroneous word and the total number of received words. It can be written as:

$$WER = \frac{number\ of\ erroneous\ words}{total\ number\ of\ received\ words} \quad \text{(A.2)}$$

One word corresponds to one unit of several bits encoded together. For example, the GPS L1C navigation message is divided into 3 words: subframe 1, subframe 2 and subframe 3. Three WERs can thus be computed, each one associated with one subframe (1, 2 or 3).

A.1.3 CEDER

The Clock error corrections and Ephemeris Data Error Rate (CEDER) is the most useful error rate in GNSS, since Clock error corrections and Ephemeris Data (CED) are the essential demodulated data to compute a position. It can be written as:

$$CEDER = \frac{number\ of\ erroneous\ CED}{total\ number\ of\ received\ CED} \quad \text{(A.3)}$$

To continue with the GPS L1C navigation message example, the CED are carried by subframe 2. A CEDER equal to 10^{-2} for example thus means that in average only one subframe 2 contains at least one erroneous bit, among 100 received subframes 2.

A.2 Ordinate Axis: Amount of Required Resources

The amount of required resources to achieve the corresponding error rate, being the curve ordinate axis, can be represented by different parameters such as:

- E_b/N_0, which is the ratio between the energy per bit and the noise power spectral density,
- SNR, which is the ratio between the signal power and the noise power,
- C/N_0, which is the ratio between the signal power and the noise power spectral density.

These different parameters are linked to the others, as it is explained in this part.

A.2.1 Eb/N0

The amount of resources can be measured by E_b/N_0, which is the ratio between the energy per information bit and the noise power spectral density. It can be written as:

$$\frac{E_b}{N_0} = \frac{energy\ per\ bit}{noise\ power\ spectral\ density} \tag{A.4}$$

A.2.2 Es/N0

The amount of resources can be measured by E_s/N_0, which is the ratio between the energy per symbol and the noise power spectral density. It can be written as:

$$\frac{E_s}{N_0} = \frac{energy\ per\ symbol}{noise\ power\ spectral\ density} \tag{A.5}$$

Moreover, the energy per symbol can be linked to the energy per information bit thanks to:

$$E_{symbol\ on\ data\ comp} = Q\ E_{coded\ bit} = Q\ R\ E_{info\ bit} \tag{A.6}$$

where:

- Q is the number of coded bits per symbol,
- R is the code rate (defined in Annex B).

This parameter $E_s/N0$ can thus be linked to E_b/N_0 through this relation:

$$\frac{E_s}{N_0} = QR\ \frac{E_{info\ bit}}{N_0} = QR\ \frac{E_b}{N_0} \tag{A.7}$$

with:

- Q the number of bits per symbol,
- R is the code rate (defined in Annex B).

A.2.3 SNR

The SNR represents directly the ratio between the useful signal power and the noise power [25].

$$SNR = \frac{P_{signal}}{P_{noise}} \tag{A.8}$$

To link it to E_b/N_0, the useful signal power needs firstly to be reduced at the useful bit level. The bits considered here are the data bits. Thus, the useful signal power needs to be linked to the data component power. For GNSS signals which are divided into several components, the useful signal total power is divided among the several components:

$$\begin{cases} P_{data\ comp} = A_{data}^2\ P_{signal} \\ P_{pilot\ comp} = A_{pilot}^2\ P_{signal} \end{cases} \quad \text{(A.9)}$$

For example, for the GPS L1C signal:

$$\begin{cases} A_{data\ GPS\ L1C}^2 = \frac{1}{4} \\ A_{pilot\ GPS\ L1C}^2 = \frac{3}{4} \end{cases} \quad \text{(A.10)}$$

Thus:

$$SNR = \frac{P_{data\ comp}}{A_{data}^2\ P_{noise}} \quad \text{(A.11)}$$

Then, the power can be linked to the energy by this expression:

$$P_{data\ comp}\ T_{symbol\ on\ data\ comp} = E_{symbol\ on\ data\ comp} \quad \text{(A.12)}$$

Moreover, the energy per symbol can be linked to the energy per information bit thanks to:

$$E_{symbol\ on\ data\ comp} = Q\ E_{coded\ bit} = Q\ R\ E_{info\ bit} \quad \text{(A.13)}$$

Thus:

$$SNR = \frac{n\ R\ E_{info\ bit}}{T_{symbol\ on\ data\ comp}\ A_{data}^2\ P_{noise}} \quad \text{(A.14)}$$

Since:

$$P_{noise} = N_0\ B \approx N_0\ \frac{1}{T_s} \quad \text{(A.15)}$$

$$SNR = \frac{Q\ R\ E_{info\ bit}}{A_{data}^2\ N_0} \quad \text{(A.16)}$$

Recalling $E_{info\ bit}$ by E_b and transposing in dB it leads:

$$SNR_{dB} = \frac{E_b}{N_0}_{dB} + 10log_{10}(\frac{Q\ R}{A_{data}^2}) \quad \text{(A.17)}$$

For GPS L1C, the modulation is equivalent to a BPSK and the channel code on subframes 2 and 3 is a LDPC code with a rate equal to ½, thus:

$$SNR_{dB} = \frac{E_b}{N_0}_{dB} + 3\ dB \quad \text{(A.18)}$$

A.2.4 C/N0

The C/N0 is the ratio between the received carrier power and the receiver noise density. It allows comparing the level of a desired signal to the level of the background noise power density.

$$\frac{C}{N_0} = \frac{P_{signal}}{N_0} \quad \text{(A.19)}$$

According to equations (A.8) and (A.15), C/N0 can be written according to the SNR:

$$\frac{C}{N_0} = \frac{P_{signal}}{N_0} = SNR\ B \quad \text{(A.20)}$$

Then from equation (A.14) we have:

$$\frac{C}{N_0} = \frac{Q\ R\ E_b}{A_{data}^2\ N_0}\ \frac{1}{T_s} \quad \text{(A.21)}$$

Finally:

$$\frac{C}{N_0}_{dB\ Hz} = \frac{E_b}{N_0}_{dB} + 10log_{10}(\frac{Q\ R}{A_{data}^2\ T_s}) \quad \text{(A.22)}$$

For example for GPS L1C:

$$\frac{C}{N_0}_{dB\ Hz} = \frac{E_b}{N_0}_{dB} + 23.01\ dB\ Hz \quad \text{(A.23)}$$

Annex B: Channel Coding

An information transmission is corrupted through the propagation channel which induces unwanted effects such as noise or interference. This phenomenon impacts on the received signal and can provide errors at the chain output. Channel encoding (in orange in Figure 76) adds redundancy in the information bits sequence thanks to an error-correcting code, in order to counteract the propagation channel effect.

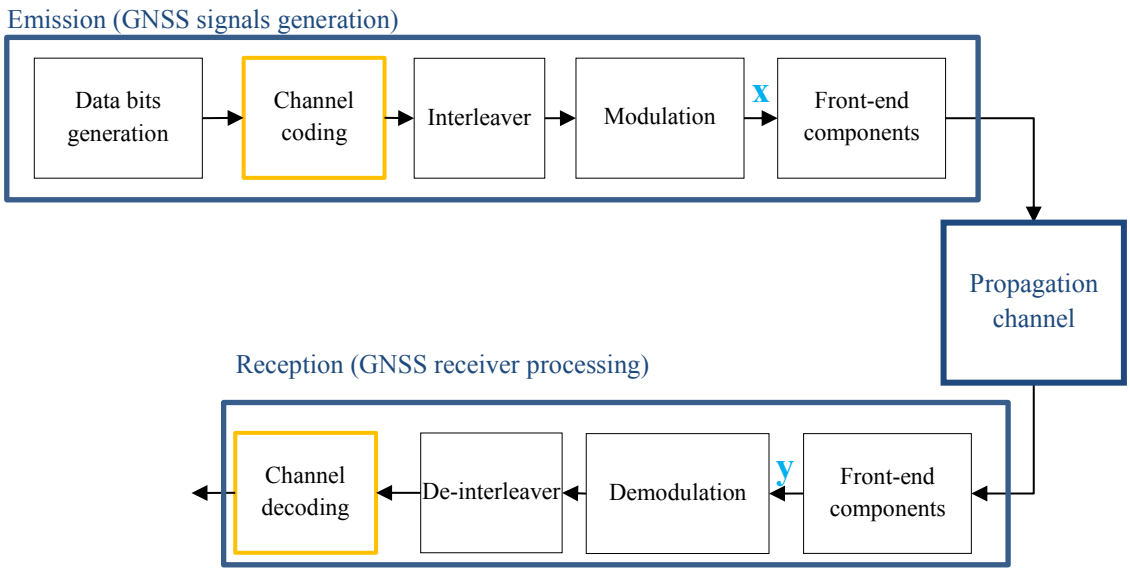

Figure 101: GNSS emission/reception chain block diagram

B.1 Code Rate

An error-correcting code provides redundancy in order to counteract the impact of errors provided by the channel. Thereby when an information sequence is composed of k bits, the encoder gives a coded sequence of n bits with $n > k$ (see Figure 102).

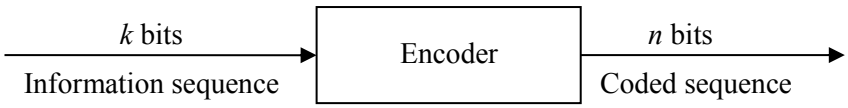

Figure 102: Code rate definition

The code rate represents thus the information transmitted per each use of the channel and is given by [25]:

$$R = \frac{k}{n} \tag{B.1}$$

where:

- R is the code rate in bits per transmission,
- k is the number of information bits, as it is described in Figure 102,
- n is the number of coded bits, called the code length.

The *k* bits are useful unless the *(n-k)* bits are redundant in order to correct errors.

B.2 Information theory

Information theory permits to quantify and qualify the amount of information present in a set of data. According to the theory of Shannon, the uncertainty measures the information. Indeed, a rare phenomenon contains more information than a phenomenon which is certain. The entropy measure *H* is used to represent an amount of information [25].

If we consider *X* as the source of the channel and *Y* as its corresponding output represented by Figure 103, the information transported from *X* to *Y* is named mutual information *I(X,Y)* and is written as [25]:

$$I(X,Y) = H(Y) - H(Y/X) \tag{B.2}$$

where:

- $I(X,Y)$ is the mutual information transported from *X* to *Y*,
- $H(Y)$ is the entropy measure of the event *Y*,
- $H(Y/X)$ is the entropy measure of the event *Y* knowing the event *X*.

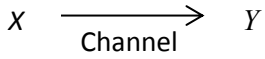

Figure 103 : Source and corresponding output through a propagation channel

A parameter called the channel capacity and noted *C* can characterize a channel. It corresponds to the measure of how much information the channel can convey, which can be compared with the capacity of a plumbing system to convey water [5]. It corresponds to the maximum mutual information between *X* and *Y* [5]:

$$C = \max_{\{p(x)\}} I(X,Y) \tag{B.3}$$

where:

- $\mathrm{p}(x)$ is the channel input probability distribution.

The unit of C is information bits/coded bits [5]. If a code possesses a code rate R for which $R < C$, it is said *achievable rates* meanings that reliable communication is achievable at these rates [5].

In contrast to classical channel codes (such as convolutional codes), modern codes (such as turbo-codes or LDPC codes) designate the new generation of error-correcting codes which are the first being able to approach the channel capacity defined above.

B.3 Channel Code Profile Impact on Performance

The channel code profile including the code rate and the block size (the information sequence length) plays an important role in the achievable performance.

B.3.1 The Code Rate

As explained in section B.2, the code rate is limited by the capacity. This capacity depends on the considered E_b/N_0. For example, Figure 104 shows this Shannon-limit performance curves for a binary-input AWGN channel for different code rates. These curves show the lowest possible E_b/N_0 required to achieve a given BER over the binary-input AWGN channel using codes of these rates [62].

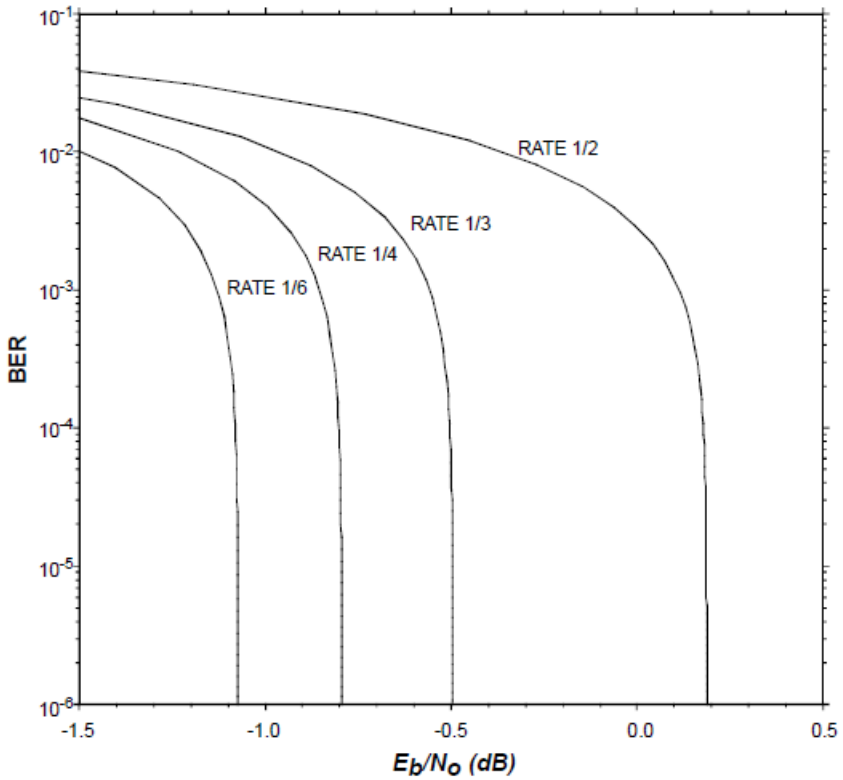

Figure 104: Capacity limits on the BER performance for codes with different rates operating over a binary input AWGN channel [62]

Logically, for the smallest values of code rates (meaning that a high number of coded bits are necessary to encode 1 information bit), you are able to achieve better BER for lower E_b/N_0 values. Nevertheless, using a high number of coded bits compared with the number of information bits to encode is poor in terms of efficiency; it requires sending a large number of bits for little useful information.

B.3.2 The Block Size

In addition, the maximum performance defined by the capacity is highly dependent on the channel code block size [62].

Figure 105 illustrates this property. Thanks to figures like Figure 104, the minimum E_b/N_0 required to achieve a given error rate (here WER equal to 10^{-4} has been considered) for an unconstrained-input channel with several values of code rates is plotted, given horizontal asymptotes labeled 'capacities'. They represent the best achievable performance. The others curves labeled 'bounds' are plotted by the same way, adding the block size dependency.

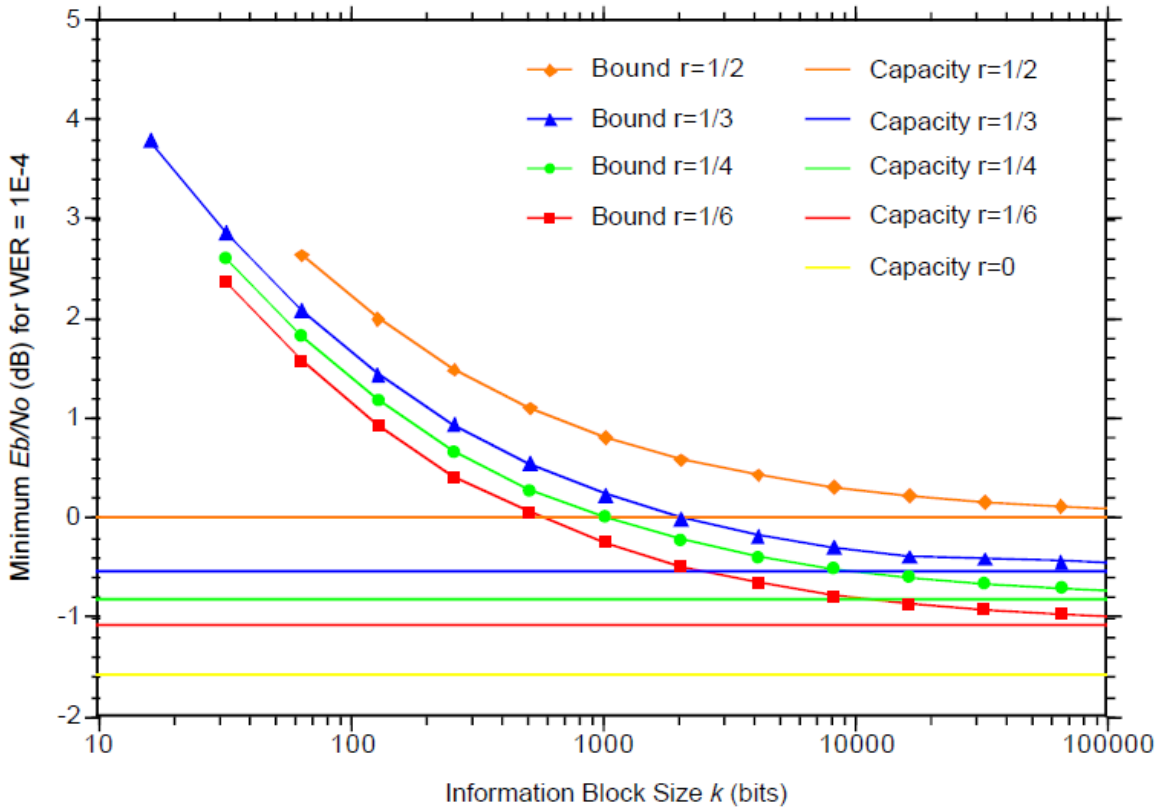

Figure 105: Shannon Sphere-Packing Lower Bounds on the WER Performance for Codes with Varying Information Block Length k and Rates 1/6, 1/4, 1/3, 1/2, Operating over an Unconstrained-Input AWGN Channel [62]

In fact, the best achievable performance is obtained considering infinite block sizes.

B.4 Concatenated Codes

Concatenated codes are error-correcting codes which are constructed from two or more simpler codes in order to achieve good performance with reasonable complexity [63]. They are derived by combining an inner code and an outer code, as it is described in Figure 106.

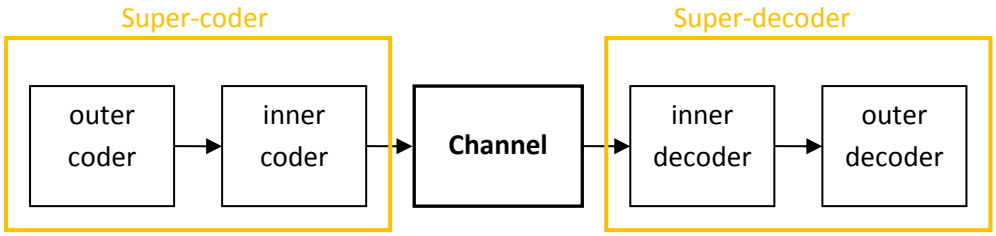

Figure 106: Concatenated code architecture

Concatenation allows building long codes from shorter ones. The problem of decoding complexity is thus reduced. Concatenated codes became widely used in space communications in the 1970s [63].

B.5 Decoding Criterion

The role of the decoder is to decide which one coded word has been emitted, thanks to the received coded word. It wants to minimize the probability of error, which is equivalent to maximize the probability of good decision. The decoding criterion can thus be written thanks to the A Posteriori Probability (APP): $p(x/y)$. Knowing the coded word y, the aim consists in maximizing the probability that x has been emitted [5].

Several strategies can be applied to do that, depending on the decoding criterion:

- The Maximum Likelihood (ML),
- The Maximum A Posteriori (MAP).

B.5.1 ML Decoding Criterion

The ML criterion considers the emitted coded word. It chooses the coded word which is the closest to the channel output y [5]. This decoder is very complex, except for very simple codes [5]. One example of ML decoding criterion algorithm is Viterbi.

B.5.2 MAP Decoding Criterion

The MAP criterion considers each emitted bit which constitutes the emitted coded word [5], instead of directly the entire coded word as for the ML decoding case. One example of MAP decoding criterion algorithm is BCJR.

The MAP decoding criterion can be written as [5]:

$$\hat{v}_q = arg \max_{v_q} p\left(b_{x_q}/y\right) \tag{B.4}$$

where:

- b_{x_q} is the q-th bit of the emitted symbol x,
- v_q is such that $b_{x_q} = (-1)^{v_q}$,
- $\hat{v}_q$ is the estimated v_q,
- y is the received symbol.

For binary channel inputs, this criterion can be written by this way:

$$If\ \ p\left(b_{x_q} = +1/y\right) > p\left(b_{x_q} = -1/y\right) \rightarrow \hat{b}_{x_q} = +1 \tag{B.5}$$

Thus:

$$If\ \ \frac{p\left(b_{x_q} = +1/y\right)}{p\left(b_{x_q} = -1/y\right)} > 1 \rightarrow \hat{b}_{x_q} = +1 \tag{B.6}$$

where:

- $\frac{p\left(b_{x_q}=+1/y\right)}{p\left(b_{x_q}=-1/y\right)}$ is called the likelihood ratio.

This criterion can again be simplified thanks to the use of the logarithm function:

$$If\ log\left(\frac{p\left(b_{x_q} = +1/y\right)}{p\left(b_{x_q} = -1/y\right)}\right) > 0 \rightarrow \hat{b}_{x_q} = +1 \tag{B.7}$$

where:

- $log\left(\frac{p\left(b_{x_q}=+1/y\right)}{p\left(b_{x_q}=-1/y\right)}\right)$ is called the Log Likelihood Ratio (LLR).

B.6 Interleaving

Interleaving consists in mixing the coded bits before the emission, in controlling the way of mixing them in order to be able to replace them in the well order after reception. This process is very efficient to counteract the multiple bursts of errors, which often occur in urban environments [5].

In order to mix the coded bits, an example of interleaver is the block interleaver, as used in GPS L1C and illustrated in Figure 107. Each coded bit is stored into the block interleaver filling in it line by line. Then, the interleaver block is read column by column. The resulting coded bit flow is thus completely different. This flow is sent through the propagation channel, bit since after reception the flow is put in the right order, the consecutive coded bits which have been impacted by bursts of errors are not consecutive anymore. Thus, instead of losing several consecutive bits due to bursts of errors, just one bit is individually affected.

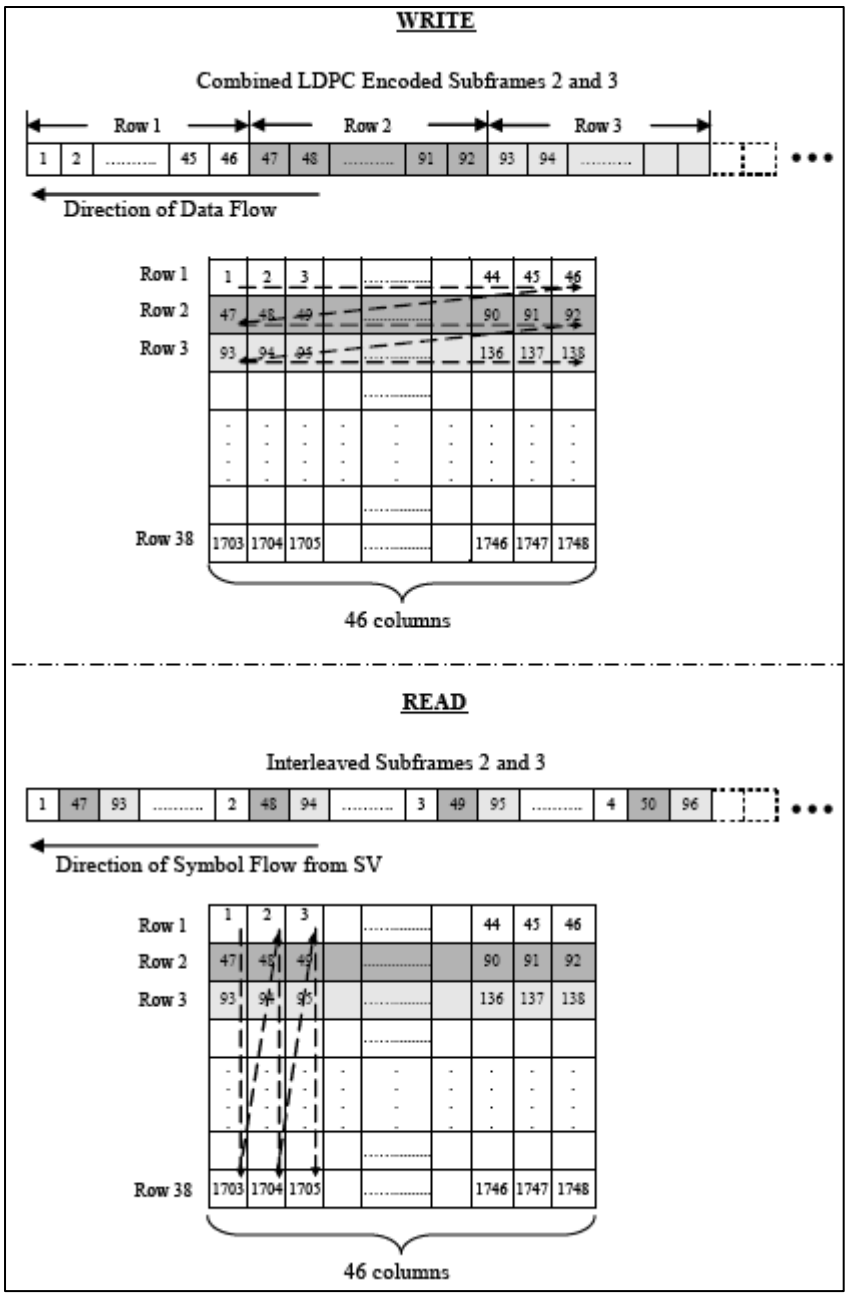

Figure 107: Conceptual Block Interleaver [19]

Nevertheless, an interleaver can just be a random vector, as it has been used to implement the partial interleavers in Chapter 6.

The interleaving depth is an important factor. It corresponds to the number of bits in each block of data. For example, the interleaving depth of Figure 108 is $I = 3$ and $I = 38$ for Figure 107.

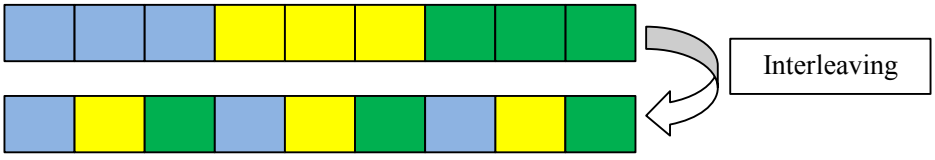

Figure 108: Interleaving depth

Figure 109 shows the impact of the interleaving depth on the performance [62]. The more the interleaving depth, the better the performance since longer bursts of errors can thus be counteracted.

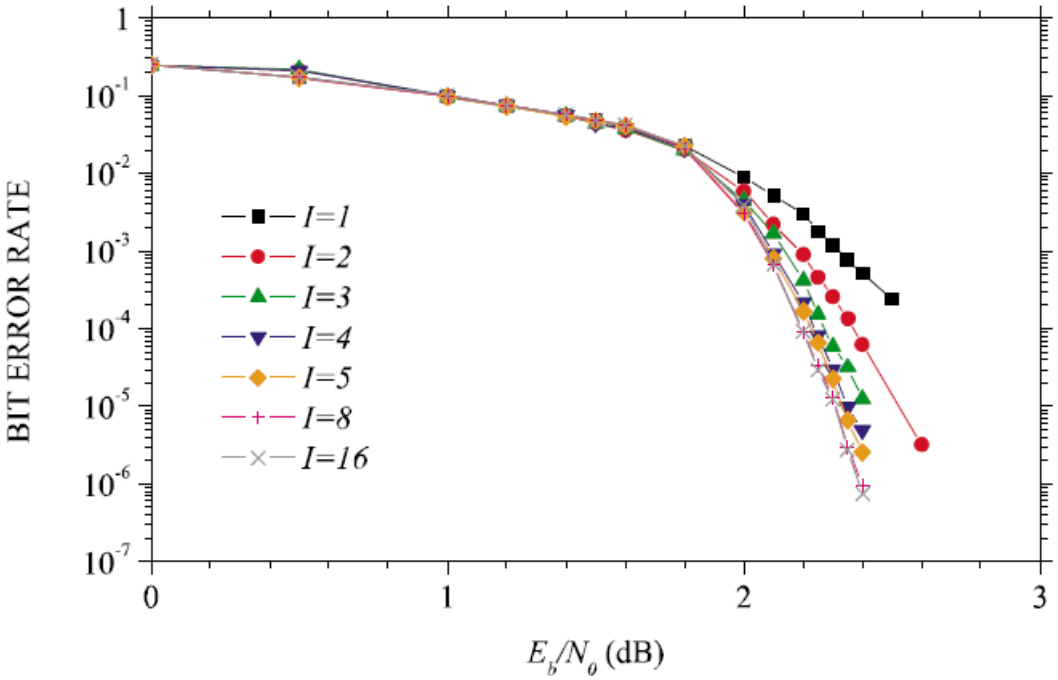

Figure 109: Bit Error Rate Simulated Performance of the CCSDS Concatenated Scheme with Outer E=16 Reed-Solomon Code (255,223) and Inner Rate-1/2 Convolutional Code as a Function of Interleaving Depth [62]

Annex C: LDPC Decoding

The SPA algorithm for the LDPC decoding has been presented in Chapter 2. This annex details the CN update and the total LLR mathematical expression given in Chapter 2. Moreover, this algorithm can be simplified in order to reduce its complexity. In this sense, the min-sum decoder will be introduced.

C.1 SPA Algorithm

The SPA algorithm has been entirely presented in Chapter 2. The purpose of this section is just to detail the CN update expression and the total LLR expression which have been firstly introduced in Chapter 2.

C.1.1 CN Update Expression

The CN update expression to be derived is:

$$L_{i\to j} = 2tanh^{-1}\left(\prod_{j'\in CN_i-\{j\}} tanh\left(\frac{1}{2}L_{j'\to i}\right)\right) \tag{C.1}$$

The MAP criterion (see Annex B) is derived for each CN. We will thus consider the coded bit c_0, for which the MAP criterion can be written as [20]:

$$\widehat{c_0} = arg \max_{c_0\in\{0,1\}} p(c_0 = 0/y, SPC) \tag{C.2}$$

From equation (2.15) which defines a LDPC code, parity check equations can be deduced, which will be used to build the Tanner graph (refer to Figure 32 of Chapter 2). According to these equations, the sum of the bits c_l belonging to the same parity check equation must be equal to 0. This constraint is equivalent to have an even number of 1s [20]. The probability in equation (C.2) is thus equal to:

$$p(c_0 = 0/y, SPC) = p(c_1, c_2, \dots, c_{d-1}\ has\ an\ even\ number\ of\ 1s/y) \tag{C.3}$$

Then, the following lemma is used.

Lemma [20]**:**
Consider a vector of d independent binary random variables $a = [a_0, a_1, \dots, a_{d-1}]$ in which $p(a_l = 1) = p_1^{(l)}$ and $p(a_l = 0) = p_0^{(l)}$. Then the probability that a contains an even number of 1s is:

$$\frac{1}{2} + \frac{1}{2}\prod_{l=0}^{d-1}\left(1 - 2p_1^{(l)}\right)$$

And the probability that a contains an odd number of 1s is:

$$\frac{1}{2} - \frac{1}{2}\prod_{l=0}^{d-1}\left(1 - 2p_1^{(l)}\right)$$

According to this lemma:

$$p(c_0 = 0/y, SPC) = 1 - p(c_0 = 1/y, SPC) = \frac{1}{2} + \frac{1}{2}\prod_{l=0}^{d-1}\left(1 - 2p(c_l = 1/y_l)\right) \quad \text{(C.4)}$$

And thus:

$$1 - 2p(c_0 = 1/y, SPC) = \prod_{l=0}^{d-1}\left(1 - 2p(c_l = 1/y_l)\right) \quad \text{(C.5)}$$

Then, we can move to the LLR representation using the relation proposed in [20], valid for binary random variable with probabilities p_1 and p_0:

$$1 - 2p_1 = tanh\left(\frac{1}{2}log\left(\frac{p_0}{p_1}\right)\right) = tanh\left(\frac{1}{2}LLR\right) \quad \text{(C.6)}$$

It gives:

$$1 - 2p(c_0 = 1/y, SPC) = tanh\left(\frac{1}{2}L(c_0/y, SPC)\right) \quad \text{(C.7)}$$

with:

- $L(c_0/y, SPC) = log\left(\frac{p(c_0=0/y,SPC)}{p(c_0=1/y,SPC)}\right)$, the LLR.

By the same way, we have:

$$\prod_{l=0}^{d-1}\left(1-2p(c_l=1/y_l)\right)=\prod_{l=0}^{d-1}tanh\left(\frac{1}{2}L(c_l/y_l)\right) \quad \text{(C.7)}$$

with:

- $L(c_l/y_l)=log\left(\frac{p(c_l=0/y_l)}{p(c_l=1/y_l)}\right)$, the LLR.

Finally:

$$tanh\left(\frac{1}{2}L(c_0/y,SPC)\right)=\prod_{l=0}^{d-1}tanh\left(\frac{1}{2}L(c_l/y_l)\right) \quad \text{(C.8)}$$

And thus:

$$L(c_0/y,SPC)=2tan^{-1}\left(\prod_{l=0}^{d-1}tanh\left(\frac{1}{2}L(c_l/y_l)\right)\right) \quad \text{(C.9)}$$

This relation can be linked to Figure 33 in Chapter 2 by adapting notations, which gives equation (C.1).

C.1.2 Total LLR Expression

The total LLR expression to be derived is:

$$L_j{}^{total}=L_j+\sum_{i\in VN_j}L_{i\to j} \quad \text{(C.10)}$$

If we replace this step into its context, the information has been firstly sent to the VN, then the CN have been updated and the information has finally been reported to the VNs. The total LLR received by one VN after one iteration is represented by this $L_j{}^{total}$.

VNs can be considered as REP codes, as it has been explained in Chapter 2. The binary coded bit c_l is transmitted k times (see Figure 95). The k coded bits $c_l\ for\ l=1,\dots,k$ correspond to the k edges connected to one VN [20]. $L_j{}^{total}$ represents the LLR associated with the c_l coded bit of one VN. Thus:

$$L_j{}^{total}=L(c_l/y)=log\left(\frac{p(c_l=0/y)}{p(c_l=1/y)}\right) \quad \text{(C.11)}$$

Thanks to the Bayes' rules, this can be written as:

$$L(c_l/y) = log\left(\frac{p(y/c_l = 0)\ \frac{p(c_l = 0)}{p(y)}}{p(y/c_l = 1)\ \frac{p(c_l = 1)}{p(y)}}\right) \tag{C.12}$$

We make the assumption that the symbols are equally distributed:

$$L(c_l/y) = log\left(\frac{p(y/c_l = 0)}{p(y/c_l = 1)}\right) \tag{C.13}$$

This simplifies as [20]:

$$L(c_l/y) = log\left(\frac{\prod_{l=0}^{k-1} p(y_l/c_l = 0)}{\prod_{l=0}^{k-1} p(y_l/c_l = 1)}\right) = \sum_{l=0}^{k-1} log\left(\frac{p(y_l/c_l = 0)}{p(y_l/c_l = 1)}\right) = \sum_{l=0}^{k-1} L(y_l/c_l) \tag{C.14}$$

This relation can be linked to Figure 33 in Chapter 2 by adapting notations, which gives equation (C.10).

C.2 Simplified SPA Algorithm

The Gallager SPA can be simplified in order to reduce its complexity.

C.2.1 Min Sum Decoder

The LLR can be written thanks to its sign and magnitude [20]:

$$L_{i\to j} = \propto_{ij}\ \beta_{ij} \tag{C.15}$$

where:

- $\propto_{ij} = sign(L_{i\to j})$,
- $\beta_{ij} = |L_{i\to j}|$.

Equation (C.1) corresponding to the CN update can thus be derived as follows:

$$L_{i\to j} = 2tan^{-1}\left(\prod_{j'\epsilon\, CN_i - \{j\}} \propto_{j'i} * \prod_{j'\epsilon\, CN_i - \{j\}} tanh\left(\frac{1}{2}\beta_{j'i}\right)\right) \tag{C.16}$$

$$L_{i\to j} = \prod_{j'\epsilon\, CN_i-\{j\}} \propto_{j'i} * 2tan^{-1}\left(\prod_{j'\epsilon\, CN_i-\{j\}} tanh\left(\frac{1}{2}\beta_{j'i}\right)\right) \tag{C.17}$$

$$L_{i\to j} = \prod_{j'\epsilon\, CN_i-\{j\}} \propto_{j'i} * 2tan^{-1}\left(log^{-1}\left(log\left(\prod_{j'\epsilon\, CN_i-\{j\}} tanh\left(\frac{1}{2}\beta_{j'i}\right)\right)\right)\right) \tag{C.18}$$

$$L_{i\to j} = \prod_{j'\epsilon\, CN_i-\{j\}} \propto_{j'i} * 2tan^{-1}\left(log^{-1}\left(\sum_{j'\epsilon\, CN_i-\{j\}} log\left(tanh\left(\frac{1}{2}\beta_{j'i}\right)\right)\right)\right) \tag{C.19}$$

We define the function ϕ such as [20]:

$$\phi(x) = -log\left(tanh\left({}^{x}/_{2}\right)\right) = log\left(\frac{e^x+1}{e^x-1}\right) \tag{C.20}$$

And use the fact that $\phi^{-1}(x) = \phi(x)$ when $x > 0$ [20]. Thus, the CN update can be written as:

$$L_{i\to j} = \prod_{j'\epsilon\, CN_i-\{j\}} \propto_{j'i} * \phi\left(\sum_{j'\epsilon\, CN_i-\{j\}} \phi\left(\beta_{j'i}\right)\right) \tag{C.21}$$

Thanks to this simplified relation, the complexity of the SPA can be reduced. From the shape of $\phi(x)$ we can note that the largest term in the sum corresponds to the smallest $\beta_{j'i}$ [20]:

$$\sum_{j'\epsilon\, CN_i-\{j\}} \phi\left(\beta_{j'i}\right) \approx \phi\left(\min_{j'\epsilon\, CN_i-\{j\}} \beta_{j'i}\right) \tag{C.22}$$

Thus:

$$\phi\left(\sum_{j'\epsilon\, CN_i-\{j\}} \phi\left(\beta_{j'i}\right)\right) \approx \phi\left(\phi\left(\min_{j'\epsilon\, CN_i-\{j\}} \beta_{j'i}\right)\right) = \min_{j'\epsilon\, CN_i-\{j\}} \beta_{j'i} \tag{C.23}$$

Thus the CN update can be simplified by:

$$L_{i\to j} = \prod_{j'\epsilon\, CN_i - \{j\}} \propto_{j'i} * \min_{j'\epsilon\, CN_i - \{j\}} \beta_{j'i} \tag{C.24}$$

Les systèmes de navigation par satellites sont de plus en plus présents dans notre vie quotidienne. De nouveaux besoins émergent, majoritairement en environnement urbain. Dans ce type d'environnement très obstrué, le signal reçu par l'utilisateur a subit des atténuations ainsi que des réfractions/diffractions, ce qui rend difficile la démodulation des données et le calcul de position de l'utilisateur. Les signaux de navigation par satellites étant initialement conçus dans un contexte d'environnement dégagé, leurs performances de démodulation sont donc généralement étudiées dans le modèle de canal de propagation AWGN associé. Or aujourd'hui ils sont utilisés aussi en environnements dégradés. Il est donc indispensable de fournir et d'étudier leurs performances de démodulation dans des modèles de canal de propagation urbain. C'est dans ce contexte que s'inscrit cette thèse, le but final étant d'améliorer les performances de démodulation des signaux GNSS en milieux urbains, en proposant un nouveau signal. Afin de pouvoir fournir et analyser les performances de démodulation des signaux de navigation par satellite en milieux urbains, un outil de simulation a été développé dans le cadre de cette thèse : SiGMeP pour « Simulator for GNSS Message Performance ». Il permet de simuler la chaine entière d'émission/réception d'un signal de navigation par satellites et de calculer ses performances de démodulation en milieu urbain. Les performances de démodulation des signaux existants et modernisés ont donc été calculées avec SiGMeP en environnement urbain. Afin de représenter au mieux ces performances pour qu'elles soient le plus réalistes possibles, une nouvelle méthode adaptée au cas urbain est proposée dans ce manuscrit. Ensuite, pour améliorer ces performances de démodulation, l'axe de recherche s'est essentiellement porté sur le « codage canal ». Pour décoder l'information utile transmise, le récepteur calcule une fonction de détection à l'entrée du décodeur. Or la fonction de détection utilisée dans les récepteurs classiques correspond à un modèle de canal AWGN. Ce manuscrit propose donc une fonction de détection avancée, qui s'adapte au canal de propagation dans lequel l'utilisateur évolue, ce qui améliore considérablement les performances de démodulation, en ne modifiant que la partie récepteur du système. Enfin, dans le but de concevoir un nouveau signal avec de meilleures performances de démodulation en environnement urbain que celles des signaux existants ou futurs, un nouveau codage canal de type LDPC a été optimisé pour une modulation CSK. En effet, la modulation CSK est une modulation prometteuse dans le monde des signaux de type spectre étalé, qui permet de se débarrasser des limitations en termes de débit de données qu'impliquent les modulations actuelles des signaux de navigation par satellites.

Global Navigation Satellite Systems (GNSS) are increasingly present in our everyday life. Further operational needs are emerging, mainly in urban environments. In these obstructed environments, the signal emitted by the satellite is severely degraded due to the many obstacles. Consequently, the data demodulation and the user position calculation are difficult. GNSS signals being initially designed in an open environment context, their demodulation performance is thus generally studied in the associated AWGN propagation channel model. But nowadays, GNSS signals are also used in degraded environments. It is thus essential to provide and study their demodulation performance in urban propagation channel models. It is in this context that this PhD thesis is related, the final goal being to improve GNSS signals demodulation performance in urban areas, proposing a new signal. In order to be able to provide and study GNSS signals demodulation performance in urban environments, a simulation tool has been developed in this PhD thesis context: SiGMeP for 'Simulator for GNSS Message Performance'. It allows simulating the entire emission/reception GNSS signal chain in urban environment. Existing and modernized signals demodulation performance has thus been computed with SiGMeP in urban environments. In order to represent this demodulation performance faithfully to reality, a new methodology adapted to urban channels is proposed in this dissertation. Then, to improve GNSS signals demodulation performance in urban environments, the research axis of this thesis has focused on the 'Channel Coding' aspect. In order to decode the transmitted useful information, the receiver computes a detection function at the decoder input. But the detection function used in classic receivers corresponds to an AWGN propagation channel. This dissertation thus proposes an advanced detection function which is adapting to the propagation channel where the user is moving. This advanced detection function computation considerably improves demodulation performance, just in modifying the receiver part of the system. Finally, in order to design a new signal with better demodulation performance in urban environments than one of existing and future signals, a new LDPC channel code has been optimized for a CSK modulation. Indeed, the CSK modulation is a promising modulation in the spread spectrum signals world, which permits to free from limitation sin terms of data rate implied by current GNSS signals modulations.